On the Structural Design Synthesis of Certifiable Aircraft Engine Pylons

Milan Stefanovic

A dissertation

submitted in partial fulfillment of the

requirements for the degree of

Doctor of Philosophy

University of Washington

2019

Reading Committee:

Eli Livne, Chair

Ramulu Mamidala

Marco Salviato

Program Authorized to Offer Degree:

William E. Boeing Department of Aeronautics and Astronautics

University of Washington

Abstract

On the Structural Design Synthesis of Certifiable Aircraft Engine Pylons

Milan Stefanovic

Chair of the Supervisory Committee:

Eli Livne

William E. Boeing Department of Aeronautics and Astronautics

The application of an integrated model based process to the design of the structure of an engine pylon at a level of detail and thoroughness that would meet certification requirements leads to significant time and cost savings as well as resulting structure with high strength to weight ratio.

Numerous technological hurdles to rapidly generate design synthesis pylon models have been cleared. Newly created modular automation platform (MAP) paves the path, implementing the multi-level sizing process, to model based design synthesis process for pylon certification driven by gradient based optimization algorithm.

The integrated model based process introduced in this work can be further extended to the entire aircraft, allowing for dramatic reductions in non-recurring costs, development times, and operational cost

Abbreviations:

MBSE – Model based system engineering

FEM – Finite Element Model

MDO – Multidisciplinary Optimization

SSD – Strength, stability, durability

DR&O – Design Requirements and Objectives

FBO – Fan blade out

FAA – Federal Aviation Administration

AR – Authorized Representative

CAD – Computer Aided Design

MAP – Modular Automation Platform

MS – Margin of safety

ULC – Number of ultimate load cases

LLC – Number of limit load cases,

SW – Switch function

COA – Center of area

Nomenclature:

P – Axial load

a, b – Panel dimensions

Nx, Ny, Nxy – Traction (load per unit length)

F_x, F_y, F_z – Cross-sectional force along x, y, and z coordinate axis respectively

A – Cross-sectional area

A_{stb} – Area of the stable part of the cross section

M_x, M_y, M_z – Cross-sectional moment around x, y, and z coordinate axis respectively

I_x, I_y, I_{xy} – Second moment of inertias

c – Distance from the neutral axis to the outermost section fiber

σ_{allow} – Allowable stress value

F_{tu} – Ultimate tensile allowable for isotropic material

t – Panel thickness

σ_{cr} – Critical stability stress

k_c – Compressive buckling constant

f_{max} – Maximum stress in the flight segment

f_{min} – Minimum stress in the flight segment

n – Number of cycles in the constant magnitude stress cycle

N – Endurance limit number of cycles for the constant magnitude stress cycle

{F} – Vector of external loads

{R} – Vectors of reaction loads

T_{kd} – Temperature correction factor

K_{pb} – Post-buckling knock down factor

k_{pb} – Post-buckling reduction factor

K_{ds} – Fastener double shear factor

F_s – Fastener calculated load

F_{su} – Fastener ultimate shear allowable, or isotropic material ultimate shear allowable

D – Fastener diameter

F_{br} – Calculated bearing stress

F_{bru} – Ultimate bearing allowable

DV – Design variable

k_{br} – Shear-bearing efficiency factor

A_{br} – Projected bearing surface

A_t – Net section area

k_t – Net tension efficiency factor

f_{bu} – Bending stress allowable

k_a – Coefficient of the fitting end

λ – Fitting factor

t_c –Thickness of the tension bolt pad area

D_w – Washer diameter

KT – Stress concentration factors

F_{sf} – Surface finish factor

F_{ft} – Fastener type factor

F_{fh} – Quality of the fastener holes drilling factor

F_{cl} – Fastener hole clearance classification factor

F_{pl} – Preload factor

g_1 – Non-FBO load cases

g_2 – FBO load cases

h_1 – Critical non-FBO load cases

h_2 – Critical FBO load cases

Contents

Table of Figures

Chapter 1: Introduction

1.1 Motivation and Goals

A Search of the aerospace literature would lead to very few technical publications on the structural design of pylons. A few reports covering safety incidents present and discuss the structural layout of the pylons involved (FSFAP1995, WO1997, ATSB2016). Very few technical publications discuss specific pylon parts (FXJ2017) or external store pylons in structural detail (CK1986, GMRG2019). The structural design synthesis of engine pylons is discussed in just a few technical papers in the public domain (ISP2003, RBFG2011, XXXT2012, CMGR2018), and in those few papers the emphasis is on studying various structural optimization methods in a conceptual way, especially topology optimization, without inclusion of the details required and the thorough analysis necessary to make the resulting design meet certification requirements.

For the structure of an engine pylon to be certified each and every component of it, regardless of how large or small, has to be substantiated using industry established analysis methods and test derived allowable values to meet all structural behavior constraints. All potential modes of failure need to be taken into consideration, including stress, buckling, fatigue, stiffness, etc. Structural optimization, based on trusted solidly-validated structural analysis, is the key to obtaining the lowest weight structural designs. Because of the statically indeterminate nature of pylon structures, the design optimization process must account for changes in internal load distributions due to changes in components and sub-components during the design process. In theory highly detailed finite element models capable of capturing all local effects and modes of failure may provide the design-oriented analysis foundation on which the optimization process would be built. But state of the art finite element models, as implemented in commercial finite element codes of today, are still not capable of capturing all potential local failures. As a result the certifying authorities still insist that the certification of pylon structures, especially those aspects of it that cover effects of highly localized nature, be based on empirical or semi-empirical data, gathered over many years by rigorous tests and test/analysis correlation studies.

The typical commercial aircraft structural design and certification process today is extremely segmented, tedious, and very slow. Adopting a highly conservative approach to safety assurance combined with a hesitance to change (or even just “tinker with”) established historic design processes, key performance metrics, such as weight or cost, seem often to be secondary in importance in the current design process. As a consequence, long design cycles may yield low performance structures that carry high price tag in both recurring and non-recurring categories.

In the nomenclature of what is known today as “model based systems engineering” (MBSE, Refs. E2007, FMS2012) the processes that are not model based are identified as document-driven processes or simply document based processes. To quote from Reference E2007: “In a nutshell, model-based engineering (MBE) is about elevating models in the engineering process to a central and governing role in the specification, design, integration, validation, and operation of a system. For many organizations, this is a paradigm shift from traditional document-based and acquisition lifecycle model approaches, many of which follow a “pure” waterfall model of system definition, system design, and design qualification. One of the biggest communication barriers that exists between the traditional engineering design disciplines (including the discipline of systems engineering) and MBE is that in a model based process, activities that support the engineering process are to be accomplished through development of increasing detailed models.”

The segmentation of the document based aircraft structural certification process stems mostly from the way that the typical structural engineering disciplines evolved and have been established through the history of the aircraft engineering. In the traditional “document-based” process internal loads are delivered to stress engineers, who then divide the structural design task to many separate tasks of designing individual components and parts. Many engineers are assigned to the many necessary structural design tasks and they typically work separately without interaction with designers of other parts of the structure using dedicated handbook empirical or semi-empirical charts and spreadsheet programs (or dedicated computer codes focused on capturing local failure effects). When the many engineers working on their tasks conclude their work, the resulting sizing results have to be assembled into updated structural loads analysis, yielding a brand new distribution of internal loads, which would, then, be sent to the stress

design engineers working on their assigned parts, and the process would be repeated. Because of the high cost in man-hours and time, it is rare to see in the case of typical engine pylon design, full convergence of the process, and the process would be stopped after no more than three iterations. To account for the lack of full convergence, a conservative margin of safety approach to the design of each part would be adopted.

In the structural and multidisciplinary design optimization (MDO) communities the term used often to describe an approach in which a single central model is used to optimize a complex system “in one shot”, covering design variables and constraints with all subsystem and overall system design considerations and freedoms, is “Integrated Design Optimization” (HG2002, LSF1990, L1999). In the case of MDO, integrated design optimizes a system simultaneously across the disciplines involved in modeling it as opposed to a sequential approach in which the system is optimized discipline by discipline with periodic exchanges of information between the separate optimization problems.

The work described here is an attempt to extend the MBSE philosophy to the process of designing and certifying aircraft structures with a level of detail and scope of modeling that would meet certification requirements. Very little has been published on the application of structural optimization technology to the structural design of real flight vehicles at levels beyond the conceptual design phase or to description of capabilities created for that (Refs. GKM2009, HHH2008). Very little has also been published on the impact of structural synthesis in realistic design environments on the cost of the resulting structures (Refs. GM2004, K2008, KZW2010). And practically nothing has been published about the impact of adopting integrated product optimization methods on the organizational restructuring that may be required and the saving in schedule and man-hours. As a matter of fact, the adoption of such methods at the level of detail that would be acceptable for certification may face organizational resistance because of its impact on traditional organizational structures.

This work will present comparisons, not available until now, between the cost and time required by current design methods and by an integrated model based design method in the case of a particular and important aerospace structural system: the engine pylon. Weight and costs of the resulting designs will also be compared. The work, therefore, covers the cost of the development process plus the cost of operating the

resulting product. It allows us for the first time to view in a quantitative way the benefits of the integrated model based approach in a highly realistic certification driven structural design case. Along the way, to build the model based integrated design optimization capability used here for this design process efficiency study, quite a number of technical innovations were necessary to make it practical and efficient. The dissertation describes those innovations too.

1.2 More on the Document Based and Model Based Structural Pylon Design and Certification Processes

The 21th century commercial aircraft marketplace cannot tolerate expensive, long, and inefficient airplane design engineering processes. In the past there might have existed certain technological hurdles that had provided some justification for such a state. However today the commercial aircraft industry is becoming rather competitive with dramatically increased number of companies competing over the limited size market. In many ways today's commercial aircraft business is starting to bear resemblance to the automotive world during the 70s' of 20th century.

Today's typical commercial aircraft structural design and certification process is extremely segmented, very tedious, and requires document based platform for its execution. The key aircraft structure design engineering disciplines are: (a) Design, (b) Loads, (c) Stress.

Not to ignore other engineering disciplines, a few other should be mentioned: testing, weights, design integration etc. However since those are not in the scope of the proposed work very few deliberations on these will be made.

The key contributors to the segmentation of the design process are the sheer volume of engineering work and analysis methods based on empirical results that are required for the aircraft manufacturer to obtain Federal Aviation Administration (FAA) certification. But mostly the segmentation has its roots in the historical shortcomings of the computational technology of the past. To be more specific, even until quite recently structural computational technology was not powerful enough to allow for practical integration of the aforementioned disciplines for the commercial aircraft certification process.

Before proceeding with the new work presented here, let us expand on the key issues that the segmentation brings:

(a) Multiple disconnected models are created. In other words, the models of loads and parts do not directly communicate with one another. A design model (CAD model) does not automatically take into account changes in the loads model (coarse finite element model - FEM), which in turn does not automatically take into account the changes in the stress model (Excel document, break-out FEM models, or any other empirical based stress tool). Often stress analysts and designers working on a particular detail of the structural design (a rivet, a bolt, a lug, a local small panel, etc.) are “blind” to the effects their changes in design would make on the rest of the structure.

(b) It requires costly and time consuming documentation that would allow various models to officially transfer information to one another;

(c) It requires data conversion between the models.

If a single mathematical model of the structure could capture its physical behavior at all levels of detail (global, local, and very local) and loading and could respond in a computationally practical way to changes in structural design variables that completely define it at all levels of detail, optimization with such a model would be straightforward and the results would meet all certification requirements. But even with the advanced finite element computational capabilities of today this is not practical because of the very large size such a model would require and because even with very fine meshes its results, regarding localized stress concentrations and other failure modes of highly localized nature, would not be trusted for certification. The day when such fully automated structural analysis capabilities will be accepted for certification will come. Meanwhile, the growing power of computer hardware and of leading structural optimization codes makes it possible to approach such a capability, and it is done in the present work by combining a fine mesh finite element model of a structure with automated numerical functions that translate handbook, data sheet, and empirical design criteria for all parts of the structure at all levels of detail into a set of subroutines and functions that communicate seamlessly with the finite element code.

The integrated-optimization idea and implementation are not new by any means and have been used in the past with some successes in the commercial aircraft industry. However the novelty of what is presented

here is the philosophy that at the center of the structural design process is a computational model that would have certification grade design synthesis capability. Such a model would contain all necessary ingredients for certification of the structural design: the design, the loads, the method of calculation, and the allowable values. The model would possess required level of detail for certification stress analysis, which typically was missing from the optimization efforts of the past, could be used for spatial integration, weight and cost tracking, systems integration, etc., and, most importantly, would be driven directly by the optimizers weight or cost objective. Such a capability will eliminate unnecessary segmentation of the structural engineering work, dramatically reduce costly documentation, and remove, today's inevitable iterative load cycles (to be discussed in more details later). The result will be an engineering process that will yield high efficiency aircraft structures in record design times and at competitive offering prices.

The most challenging aspects of building the design optimization capability for the present work include determining the sufficient level of modeling of structural details to enable this approach, internal load and loads redistribution due to design changes, section properties extraction for the sections, panels, and fastener joints, creation of mathematical formulations for the empirical stress, stability, and fatigue calculations – all as part of a single automated design-oriented model with which an optimization algorithm would work. In short, the aim is creation of a single model that contains all of the ingredients necessary for the structural certification.

Indeed, such a model has been created for this work, with the capability to shift the design process from segmented "document based" to the integrated "model based" with the following benefits:

(a) A single FEM based model that combines design, loads and stress disciplines, allowing all of the certification process to be executed within that single model
(b) Removal of the costly manual iterative scheme to arrive to certifiable design (all of the iterations are happening automatically as the part of the optimization solver)
(c) Removal of the unnecessary between-the-iterations documentation
(d) Removal of the data conversion
(e) Ability to combine FEM based direct responses with the empirical based stress calculation in a single model

(f) Ability to compare FEM based results to the empirical solutions, allowing for rapid convergence studies for the stress FE models, as well as forming the basis for qualifying FEM calculations for certification of pylon structures

(g) Ability to run sizing studies on the computing servers within a 12 hour window, which allows the sizing to be done overnight

The “iterations” mentioned above are the loads / stress distribution iterations due to the fact that when given loads are given to structural designers who then proceed to resize the structural elements they work on, that resizing of structural elements leads to redistribution of the internal loads. In a segmented process this requires, after all new sizing designs are collected from the designers, a new loads analysis, with resulting new local loads, that are then used to check and resize local structure again. The process has to be repeated a few times until convergence achieved. In practice the cost of every load / resizing step in engineering time and in schedule is so high that only a small number of such iterations is carried out, typically up to three. In the model based approach all this is automated and becomes part of a single automated optimization process.

Chapter 2: The Engine Pylon

2.1 The Pylon Structural Layout

An engine pylon is a structural member (Figure 1, and Figure 2) whose main purpose is to safely attach engines to the wing. There are a few auxiliary functions that pylons serve:

(a) Fire and fluid sealing. Protecting the wing from a potential engine fire, and protecting the engine form the moisture that can be accumulated during regular operations

(b) Mechanism for safe detachment of the nacelle from the wing during wheels-up and similar types of emergency landing maneuvers

(c) Dampener of the structural vibrations the engine may induce.

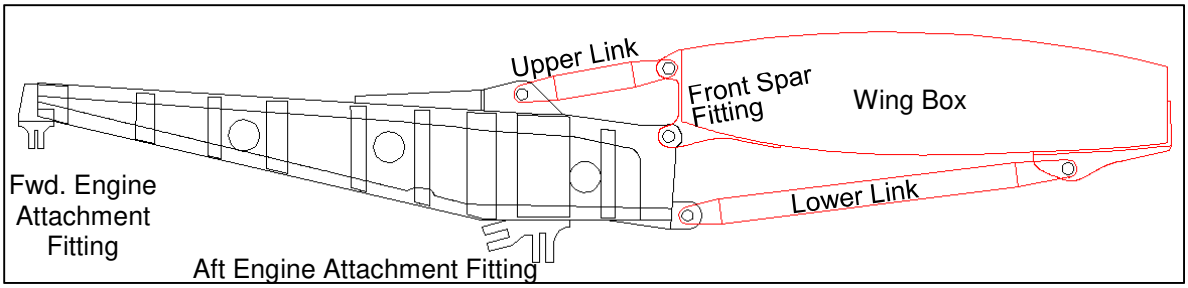

Figure 1 Side View of Pylon Attached to the Wing

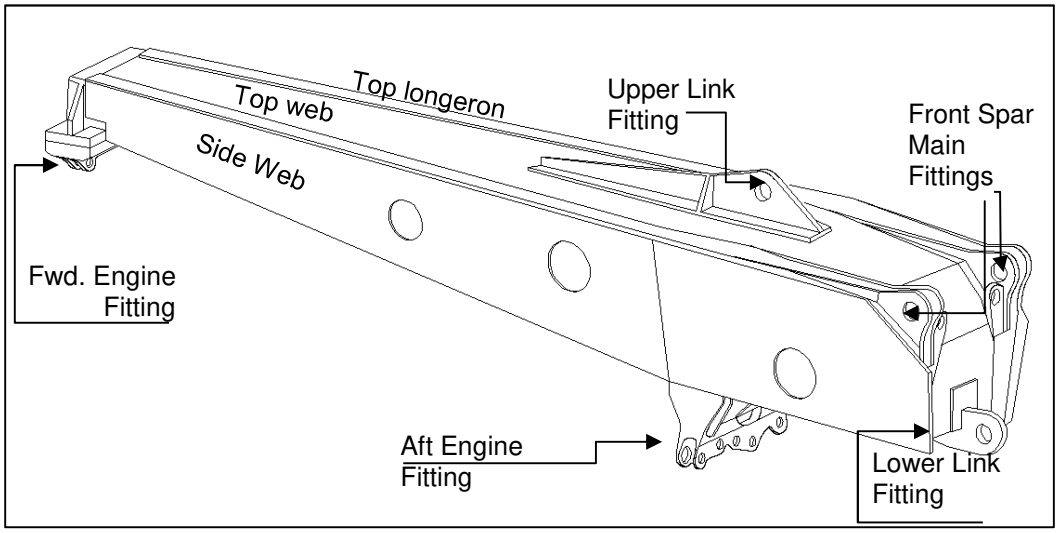

Figure 2 Isometric View of a Typical Pylon

Due to one of the functions – sealing engine fire – engine pylons are in general metallic structures. The bottom components are almost exclusively made of steel or titanium alloys because these two materials have much better fire protection properties compared to aluminum alloys.

Typical pylons are built as torque boxes (Figure 3). The top spar is comprised of a web and two longerons that end at the aft end with lugs that connect the spar to the wing front spar. The bottom spar has a very similar structural arrangement, two longerons and a web. The top and bottom webs are connected with the side webs on the outside and ribs or bulkheads on the inside.

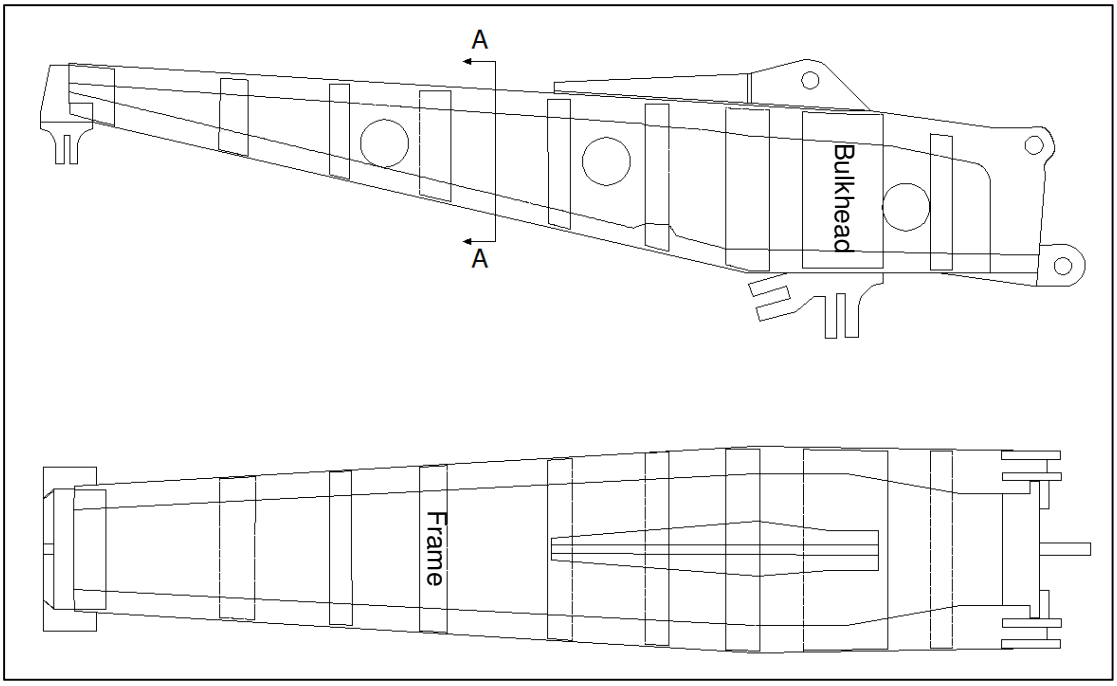

Figure 3 Side And Plan View of a Pylon

Typical cross section is shown with Figure 4.

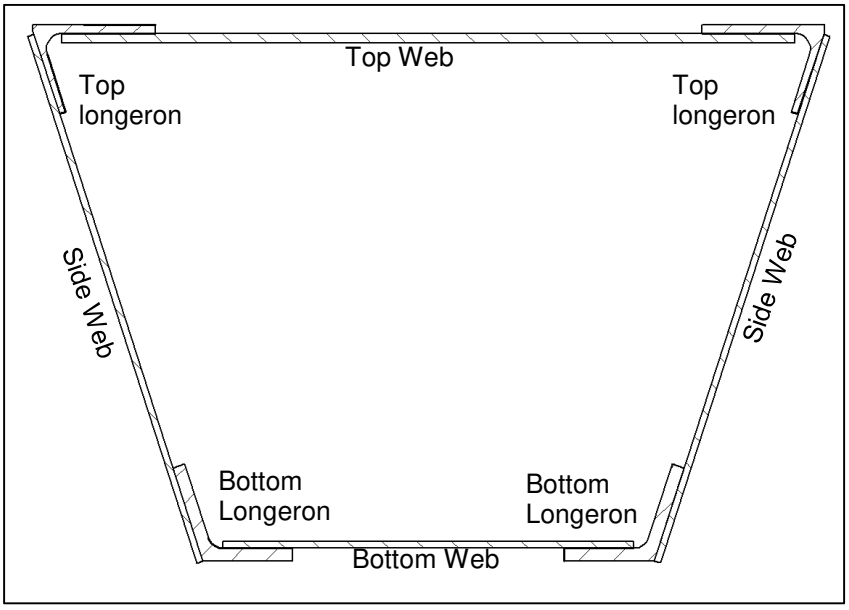

Figure 4 Section A-A of a Pylon

Frames and or bulkheads are internal components of the pylon. They are connected to all previously mentioned members. On top and bottom they connect to the top and bottom spars and on the sides they

connect to the side webs. At the corners they connect to longerons. A fairly typical bulkhead is shown in Figure 5.

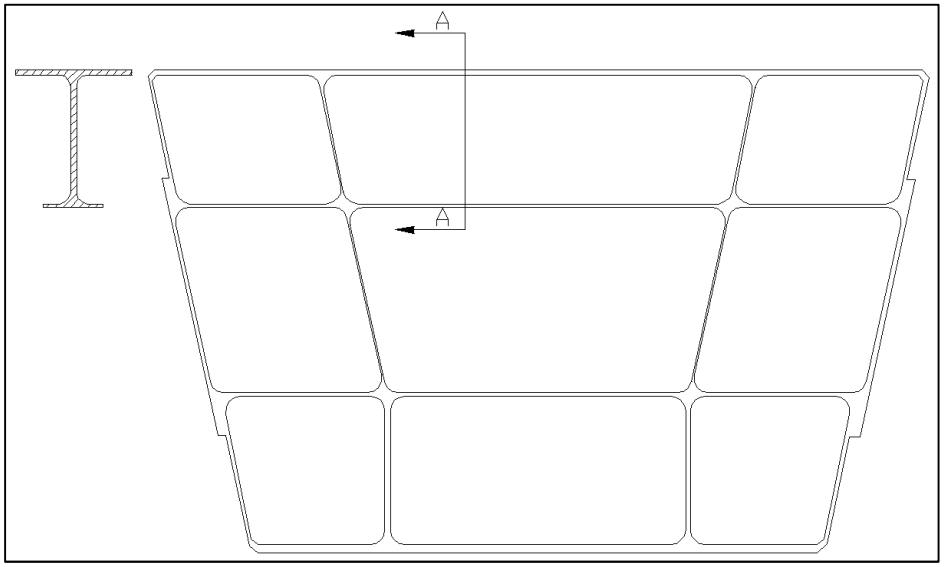

Figure 5 Typical Frame of the Pylon

2.2 Pylon Structure Certification Requirements

In order to meet the certification requirements the pylon's structural components are sized for strength, stability, and durability requirements during each of the design phases: Conceptual, Preliminary, and Final. Only the final design phase is documented for the certification purposes. However, traditionally multitude of documents are generated in the meantime to facilitate the information transfer between loads and stress engineers in the document based pylon design process.

Each of the components of the pylon has to have positive safety margins for the set of the required sizing checks. The graphical map of the required checks is shown in Figure 6. Each and every check needs to be done for the critical set of load cases in each of the design phases. Critical loads down-selection needs to be done since it would not be practical to write the margins for every single loading condition.

The types of the loading conditions for the pylon can be categorized into: (a) Design Requirements and Objective (DR&O). (b) Static maneuvers, (c) Dynamic gust, (d) Emergency Landing, (e) Fan blade out

(FBO), (f) Durability. Aeroelasticity has to be considered as well, given that the flutter requirements usually drive the overall stiffness of the pylon structure.

There are some deviations from the Figure 6 scope in the different design phases. For instance in the conceptual design phase durability is rarely considered, since the maturity of both the design and the loads is considered too preliminary.

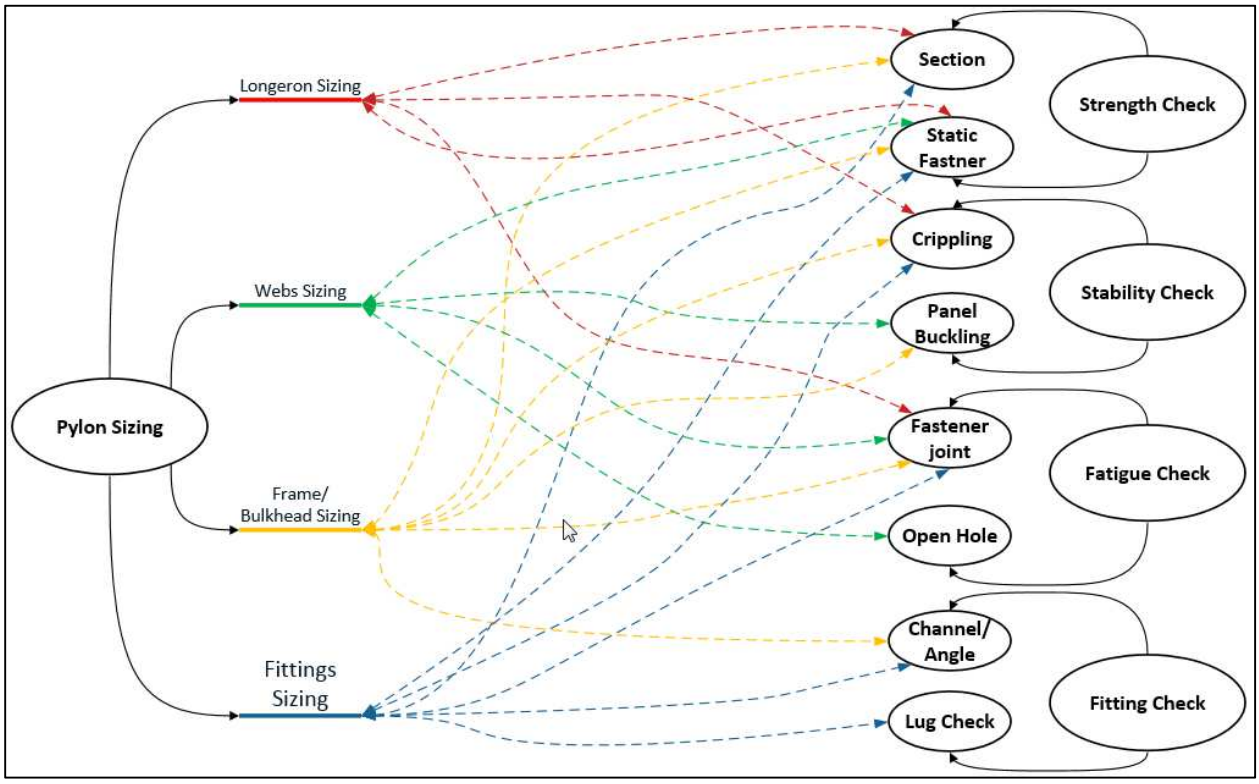

Figure 6 Pylon Structural Sizing Map

Chapter 3: The Common Document based Certification Process for Structural Certification

3.1 The Overall Sizing Procedure

The sizing process presented here is very realistic. However, since detailed design processes are not usually shared in the public domain by companies, the process used here does not replicate in detail any existing structural sizing processes known to the author.

Typically pylon structures are sized for strength and stability considerations first. After the strength /stability sizing is complete, which takes usually several cycles (to be discussed later), durability considerations are addressed.

Before any type of sizing can be performed, material allowable values must be obtained and qualified by certification authorities. In a similar fashion, the strength/stability/durability (SSD) checking methods need to be established and qualified. As described in (N1988), the bases for these SSD methods for pylon engineering are testing, theory, and empirical knowledge. These are marked with the blue dashed line box in the Figure 7 .

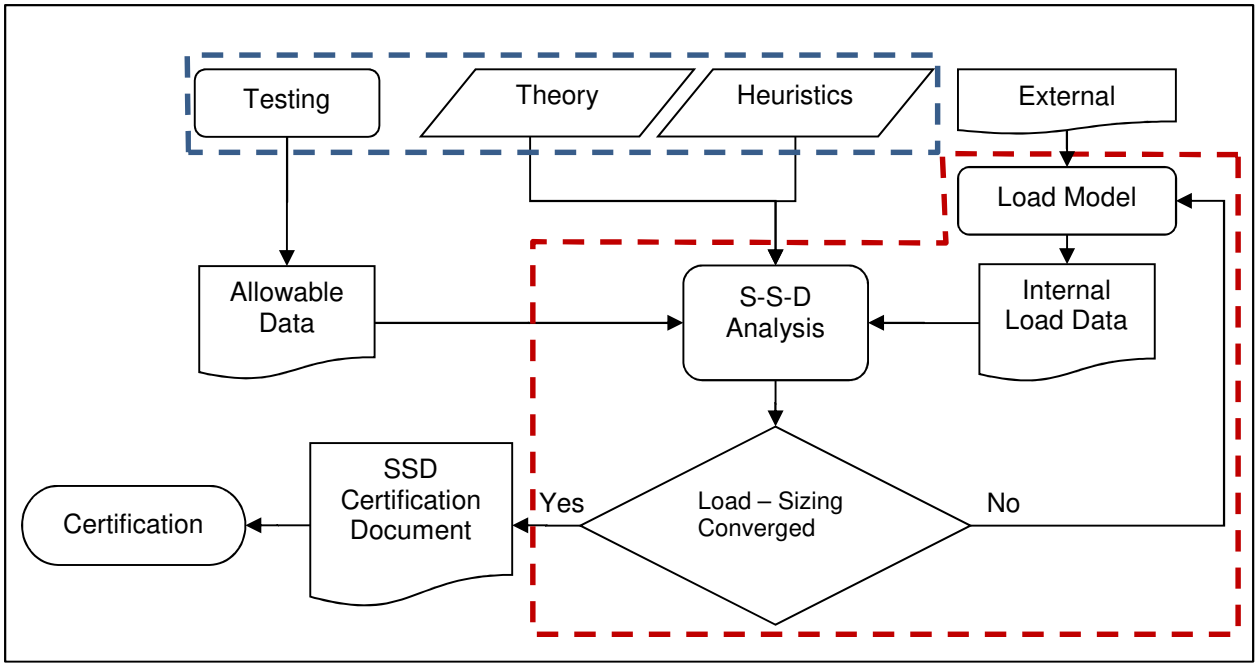

Figure 7 Document Based Pylon Analysis Certification Process

To begin with, a baseline loads FEM model needs to be established. This model has to meet basic aero-elasticity requirements and more often than not it is a modification of already established pylon structure concept, with the sizing of the major members determined by comparisons to designs of previously designed structures of such type that are scaled up or down based on some basic parameters (weight, range, maximum thrust…). Once the starting model has been developed internal load distributions can be generated. The internal load data is generated by running all loading conditions (maneuver, gust, takeoff, landing…). The SSD checking can then begin. There is structural inefficiency here, stemming from the fact that the major internal load-paths have been determined at this point by creating the loads model in this way and by not constantly updating loads distributions due to sizing changes. These design inefficiencies, relating to structural strength-to-weight ratio, development effort, and overall performance of the resulting structure will be discussed in subsequent paragraphs.

3.2 The Typical Strength/Stability Checking Process

The red dash line denoted process from the Figure 7 is shown in more detail in Figure 8.

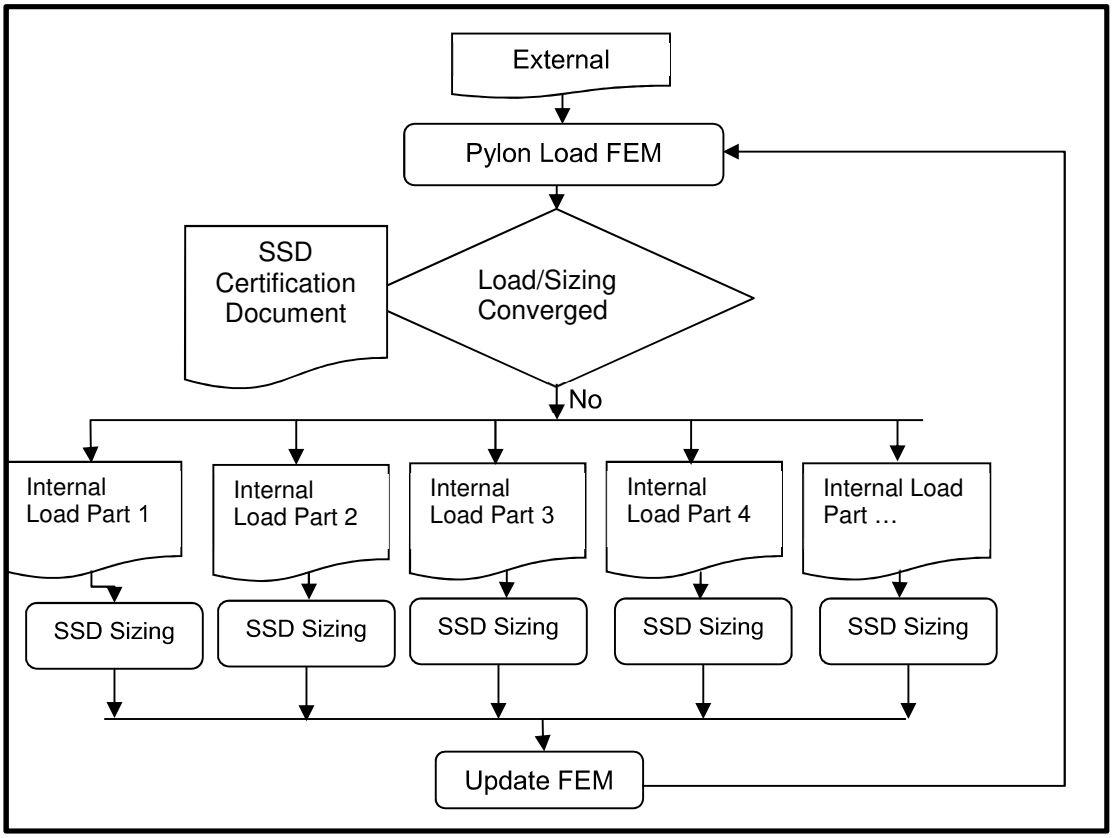

Figure 8 Document Based Structural Sizing Process

Figure 8 demonstrates the previously described segmentation issue with the document based structural sizing process. First, typical stress margins checking relies on empirical, closed-form based data sheets and equations. Second, in order to shorten the stress design process multiple engineers work to size the pylon structure, and so it only makes sense to entrust the sizing of an individual structural component to an individual engineer who would be an expert on this. The sizing of elements is done without immediately redistributing the internal loads. The major drawbacks of the described process are: (a) a need for cycles

of internal loads generation, and (b) a need for checking the convergence between the sizing and the internal loads processes.

Internal loads generation in a document based process is extremely slow and costly, mostly due to the requirement for documentation (the generation of information that would be later used for another resizing cycle of all parts), and the tedious post-processing of the FEM external loads. Note that resizing of the structure of the pylon affects not only its internal loads (which would affect the sizing of all parts) but also the way the loads would be transferred to the wing through pylon/wing attachments that are statically indeterminate.

Convergence checking takes considerable time as well. In fact, even if only one cycle of sizing is performed, at least two internal loads cycles are needed. The first one to send the set of conceptual internal loads to the individual sizing teams, and the second one after the sizing of all components is completed, and the external loads FEM is updated to check if the internal loads have changed enough to mandate the second round of sizing.

3.3 The Conceptual Design Phase

In the conceptual phase the DR&O and aeroelasticity driven stiffness requirements are considered. The durability margins are rarely computed this early. Similarly FBO and emergency landing loads are disregarded this early in the development of the structure. The following sizing is typically performed with the document based process:

(a) Fitting sizing

(b) Cross section sizing of the longerons

(c) Panel sizing for stability

Once the layout is finalized, where key design parameters are the locations of the engine fittings, and pylon to wing attachment points, the conceptual sizing of the structure can begin. The loads that the pylon is experiencing are coming from 5 major contributors:

(d) Nacelle inertia during the flight maneuvers

(e) Pressure loading coming from gusts acting on the surfaces of the nacelle

(f) Thrust from the engine itself

(g) Engine malfunction (engine seizure, fan-blade-out)

(h) Emergency landings

All but the emergency landing and fan-blade-out loads are effectively applied at the nacelle's CG location, and used for conceptual sizing of the pylon structure. According to Niu in (N1988), the structure of the pylon should be sized for the following 15 loading condition (G denotes the weight of the under-wing package, and T is engine thrust):

- 6.5 G down
- 6.5 G down + 1.5 TCruise
- 3.5 G up
- 3.5 G up + TCruise
- 3.0 G up + 1.50 Tmax
- 1.5 G down + 1.50 Tmax
- 3.0 Treverse
- 3.0 G up + 1.50 Treverse
- 3.00 G right
- 3.00 G left
- ±2.25 rad/sec2 yaw +1.5 TCruise + 1.5 G up
- ±2.25 rad/sec2 pitch +1.5 TCruise + 3.75 G up
- Engine seizure – torque that corresponds to stopping the engine's rotating mass in 0.6 seconds

A typical coordinate system used for the nacelle is shown in Figure 9.

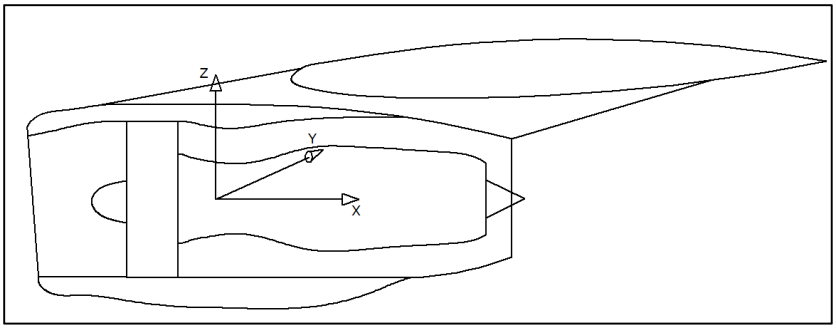

Figure 9 Nacelle Coordinate System at Center of Gravity

These 15 basic loading conditions, often called design requirements and objective (DR&O) loads, are applied to the nacelle and pylon CG (red arrows and double arrows in the Figure 10) and are used in conjunction with the aeroelasticity requirements, not only to size the pylon's structure but also to provide the loads for conceptual sizing the wing structure at the pylon attachments. Given that the pylon is connected to the wing in a redundant, statically-indeterminate, manner (it stays connected even if any single connection fails), pylon-to-wing loads change as the stiffness of the pylon changes, as mentioned above already.

A coarse Finite Element Model (FEM) representing the pylon structure needs to be created, and is used as pylon loads FEM for all phases of the pylon design. This coarse FEM will be updated repeatedly during each of the design phases as means of achieving the load-sizing convergence. Typically this is a FEM in form of a hybrid model comprised of shell, bar, and rod elements. The longerons and the frame/bulkhead flanges and stiffeners are modeled with bar elements (denoted with green lines in Figure 10). This type of model misses many important details, such as fastener connections, cut-outs, etc. Due to this incapability of the model to capture effects of highly localized structure, multiple conservative assumptions must be made during the sizing of the pylon structure.

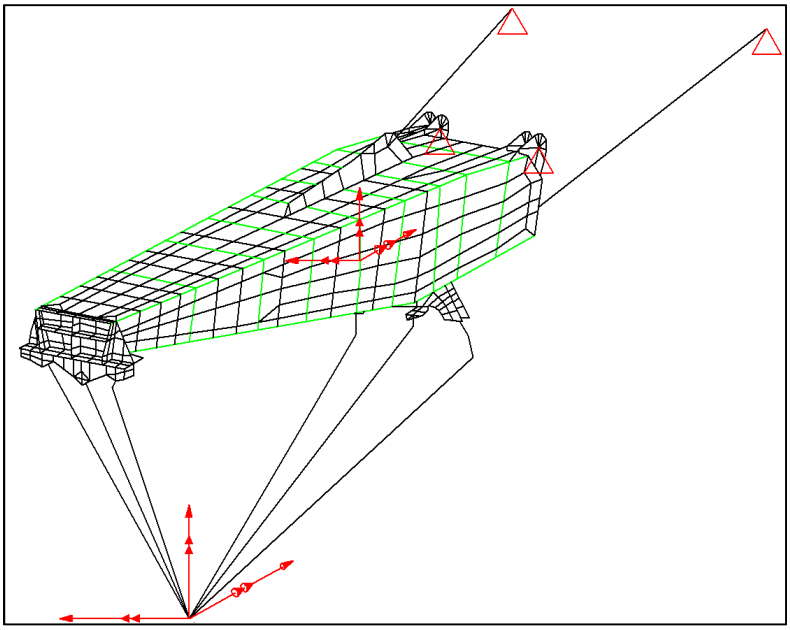

Figure 10 Coarse FEM of a Pylon

3.4 The Preliminary Design Phase

In the preliminary design phase all loading conditions, including aeroelasticity driven stiffens requirements are considered. All static and stability margins are calculated and the durability margins are computed for overall pylon layout critical design details.

In order to develop the full set of preliminary loading conditions the conceptually sized pylon properties are applied to the coarse FE model, and then pylon's coarse FEM is assembled into the complete airframe loads model. The full airframe FEM produces the pylon external loads at the nacelle center of gravity, which are now applied to the pylon during the preliminary sizing phase.

The developed loads can be categorized into:

(a) Static maneuver

(b) Dynamic gust

(c) Fan Blade Out (FBO)

(d) Fatigue

(e) Emergency Landing

3.5 Generating Break-Out FEMs for Preliminary Strength and Stability Sizing

While the airframe loads group develops the external loads for the pylon, the pylon team works on two major tasks. The pylon internal loads team updates the coarse pylon FEM with the conceptual sizing details and extracts the preliminary set of the internal loads. The pylon stress team builds refined "break-out" FEMs (FE models of sub-components) for the internal parts (frames and bulkheads), and applies the internal loads based on the free body diagrams to these refined break-out models. An example of a break-out FEM is shown with the Figure 11.

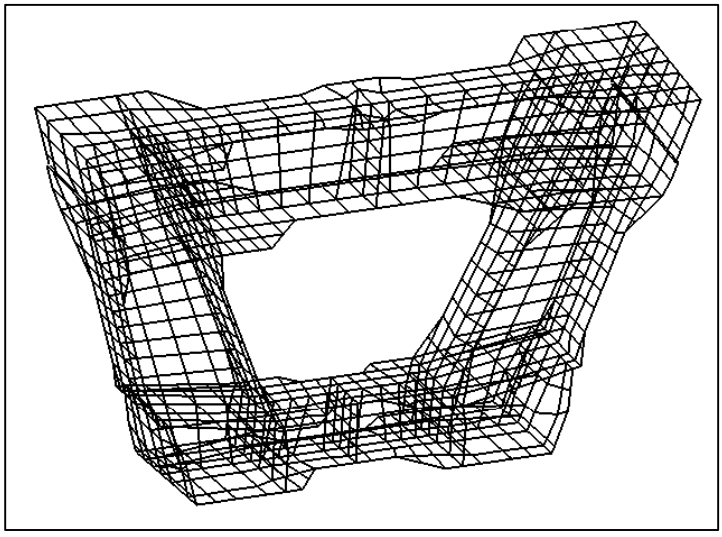

Figure 11 FEM Representing Reach Individual Part Independently

3.6 Generating, Processing, and Documenting Preliminary Internal Pylon Loads

The stress analysis team is in need of the loads that they will use to size each individual component sections and panels. Therefore the pylon internal loads team starts generating the section and panel loads for each individual component. Before these loads are developed, there is a requirement to identify the manner by which each part will be evaluated. To facilitate this the parts are categorized into their main functional groups, and based on the functional groups the loads information is extracted and communicated to the stress analysis team. For instance, the pylon longerons are treated as axial members that are reacting the vertical and lateral bending loads. The side webs and top/bottom webs are treated as shear and

tension/compression reacting panels. Frames are treated as panel breakers for the side webs and top/bottom webs. Now, based on their function and classification, the appropriate set of loads is extracted from the result files of the FEM runs by the pylon internal loads group and documented into communication sheets which, after approval and signing off, are sent to the stress analysis team for use with the stress margin calculations of each element of the structure.

Once the communication sheets are signed off and the loads sent to the stress analysis, one load cycle is complete. The entire sizing effort until the next load FEM update is performed with this set of internal loads. As the sizing is performed and the dimensions of the parts are changed to meet safety margins, the actual load distribution would change, of course. In order to take this into account for the internal loads change after several weeks of sizing, the coarse FEM model is updated with the results from the previous cycle of sizing and a new set of internal loads is distributed to the stress teams. This process is repeated until the load changes are smaller than some convergence margin policy, or, in other words, until load and sizing process has converged. The larger is the acceptable convergence criterion, the fewer are number of sizing / load iterations needed. In order to reduce the development costs, many companies would accept high convergence criterion policies, sacrificing the structural efficiency for lower development cost. Actually, enforcement of 15% margin is fairly typical during the preliminary design phase. Another major source of conservatism stems from the large number of load cases and the large number of sections/panels/fastener joints that need to be evaluated. For this reason it is fairly common that the maximum load from all the load cases across multiple sections/panels is found and documented and then that load is uniformly used to size multiple similar sections, panels.

For an example, we go back to the one of the bulkheads depicted with the Figure 5. In order to determine the loads for the shear panels of the frame the max values of the N_x, N_y and N_{xy} across all load cases are found and stored. They can be denoted N_{xmax}, N_{ymax} and N_{xymax}.

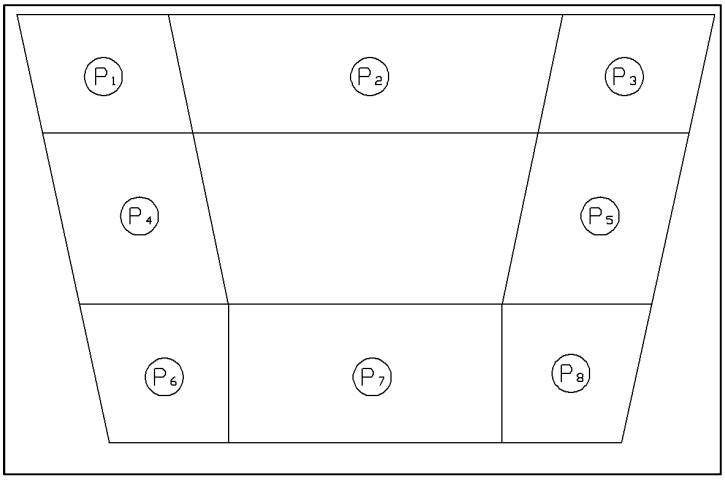

Figure 12 Panels of a Frame

$$N_{x\,max} = max\left(N_{x\,ij}\right)$$

$$N_{y\,max} = max\left(N_{y\,ij}\right) \qquad \textbf{1}$$

$$N_{xy\,max} = max\left(N_{xy\,ij}\right)$$

The index ***i*** denotes the ***i***th load case out of n load cases, and the index ***j*** denotes the ***j***th of the 8 similar panels of this particular frame.

In a similar fashion the internal loads for the sections are gathered. The maximum section loads are gathered across all of the load cases and across all of the similar structural details.

Such practice, which in its root has the need to minimize the engineering time and effort of data compilation, sorting, and documenting, creates excessively conservative loads for which sections and panels will be stress checked.

3.7 Calculating and Documenting Preliminary Stress for Strength and Stability Checks

After the loads are defined, documented and communicated, the geometrical dimensions of the sections, panels, and fasteners are documented and paired with the corresponding loads. On the other side, the allowable values are documented from the material perspective, taking into account environmental

influences on the material (temperature, corrosion…). The appropriate empirical formulas are used to calculate the actual stress value. Calculated value is compared to the allowable value; and the margin is documented. If a negative margin is encountered the sectional properties are changed until a positive margin is achieved.

For an example, Let "I" section A-A is defined on a frame (Figure 5) and be evaluated for bending stress. The bending moment is extracted from the information communication sheet, the moment of inertia is calculated and the actual stress value, and the maximum distance from the elastic axis are documented. The actual stress is compared to the allowable value, corrected for environmental factors for that material used to manufacture the frame.

$$MS = \frac{\frac{M_y \cdot c}{I_y}}{\sigma_{alloable}} - 1 \qquad \textbf{2}$$

If the margin of safety (MS) is less than the required value for this particular phase of design the sectional dimensions are adjusted until the required MS is achieved. It is clear that at that point, when the dimensions of the section are changed, they do not match the sectional properties in the FEM that is used to calculate the bending moment. As previously stated, this is one of the reasons for the conservative margin policy.

In a way similar to the conservatism coming from the internal loads, where the maximum load across the multiple load cases are assumed to act upon multiple design features (sections/panels), the source of conservatism in the stress checking comes from unification of the sections/panels to reduce the number of safety margin calculations. The edge lengths of similar panels are assumed to be identical and equal to the edge length of the most conservative from the margin calculation stand point one in the group. For example, if the edge lengths are as shown in the Figure *13*, the critical panel dimensions are chosen such that they represent the worst possible combination:

$$a_{min} = min(a_j) = a_1$$

$$b_{max} = max(b_j) = b_3 \qquad \textbf{3}$$

Where ***j*** is the panel number.

This unification also allows to have a single panel thickness across all eight panels shown by Figure 12 since it will result with a single allowable value. In the past, when the frames were built from sheet metal by riveting stiffeners and chords to the panel, this was desirable. However nowadays, when these types of parts are machined using CNC machines, there is no reason for having single thickness across all panels.

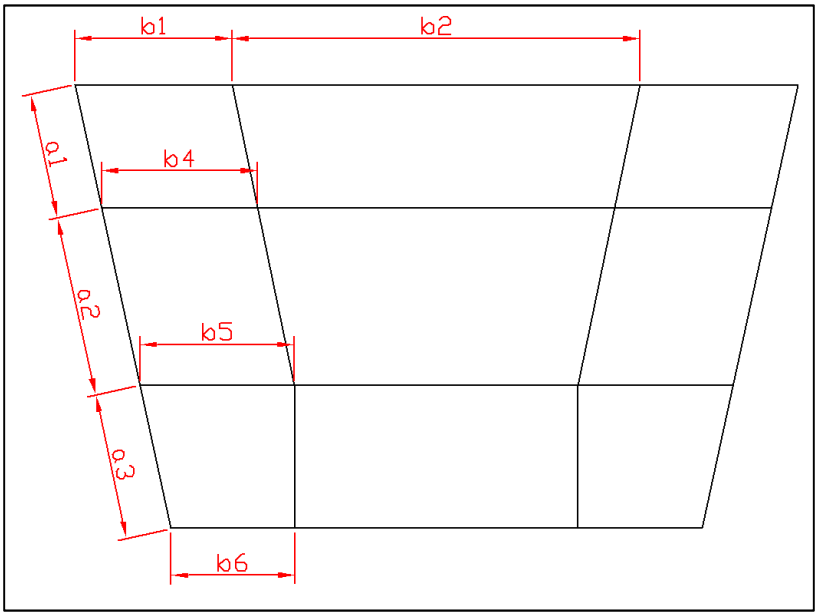

Figure 13 Panel Dimensions of a Frame

In order to more easily understand the impact of this type of unification on the safety margin calculation, let us consider buckling of flat rectangular panels under compression and shear, and its relationship to the thickness and dimensions of the panels. E. F. Bruhn (B1973) provides equations for the critical buckling stress under compression and shear. For demonstration purposes only the compression equation is provided. The shear equation has a very similar form.

$$\sigma_{cr} = \frac{\pi^2 E k_c}{12(1-\nu^2)}\left(\frac{t}{b}\right)^2 \qquad \textbf{4}$$

E, and ***ν*** are elastic constants, k_c is the compressive buckling constant that depends on the boundary conditions and aspect ratio (***a/b***) of the panel, ***t*** is the panel thickness and b is either the shorter of the two panel edges or the loaded edge length.

σ_{cr} is effectively an allowable value. If the dimension of the panel ***b*** is taken from Equation 3 and inserted into the Equation 4, the calculated allowable value will be conservative for all panels except the panel with the largest edge length. The level of conservatism depends on the ratio of edge lengths of other panels to the panel with the largest edge length. The conservatism is further amplified by the fact that ***b*** value is squared when the allowable (critical stress) value is calculated. The conservatism is further extended due to the fact that k_c is smaller value for the larger aspect rations of the panel.

3.8 The Final Design Phase

Once the preliminary sizing is complete, the changes in dimension of the geometrical features (sections, and panels) are incorporated into the coarse loads FEM. The weight changes that resulted from these changes are included in the inertia calculation for the external loads, and a new set of communication sheets are generated now, designated as the final loads. Given that the design is now further refined and deemed to be closer to the final design, the loads convergence criterion policy is relaxed and set to a range of 0-5%, depending on the types of the structure. The entire process described in the preliminary sizing section is now repeated with this detailed set of the loads. The major difference between the preliminary and detailed sizing is the fact that the durability sizing is now performed for all of the structural components. Durability sizing is a very large effort, and due to this as well as the higher level of uncertainty of the fatigue loads durability sizing is either not performed, or performed only on the critical design features, during the preliminary design phase.

3.8.1 Durability sizing

Once the detailed strength/stability sizing is complete in the detailed design phase, durability checks are required in order to finalize the design. These checks usually require significant engineering effort and therefore are only performed on a few design details, called “critical” details, during the preliminary design phase, and only after the design is close to being final. All of the joints need to be fatigue checked during the final design phase. Due to aforementioned effort and cost limitations, the durability checks are rarely performed concurrently with the strength and stability checks even in the detail sizing cycle rather, they are performed after the strength /stability sizing is complete.

Typical durability sizing process consists of the two separate but closely related checks: fatigue and damage tolerance.

3.8.2 Fatigue sizing

Given that pylons are structures that are exposed to the high level of oscillation (which comes from the fact that they are suspended from the wings that are fairly compliant and subject to gust loading) that has a cyclical nature, it is extremely important to size them for fatigue. The details that are most critical are the fastener joints, since they introduce stress concentrations into the parts that are joined. Fatigue allowable values come in form of S-N curves that define how many cycles a particular design detail (in this case fastener joint) can survive a particular cyclical load without breaking. The cyclical load is typically defined by its maximum reference stress value and the stress ratio ***R***, which if defined as quotient of the minimum, and the maximum stress of the cyclical load (R= f_{min}/ f_{max}). An example S-N curve from Ref. (DoD1998) is given with the Figure 14.

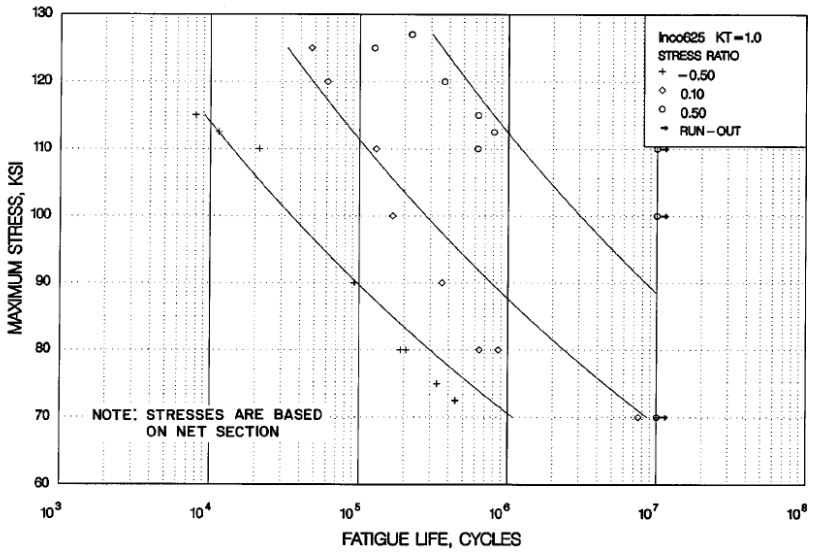

Figure 14 Sample S-N Curve for the Inconel 625

Main inputs that fatigue analysis requires are: the number of flights, the number of cycles that the pylon experiences for each of the typical flight segments, maximum (f_{max}), and minimum stress (f_{min}) during the each of the flight segments for the fatigue detail.

The actual flight spectrum, which is developed during the preliminary design phase, and is split into typical fight segments, is converted into a certain number of the constant amplitude stress cycles that would produce equivalent damage as the actual spectrum. The conversion is achieved using a “rainfall algorithm” (DS1982), either in its original form or with some modifications.

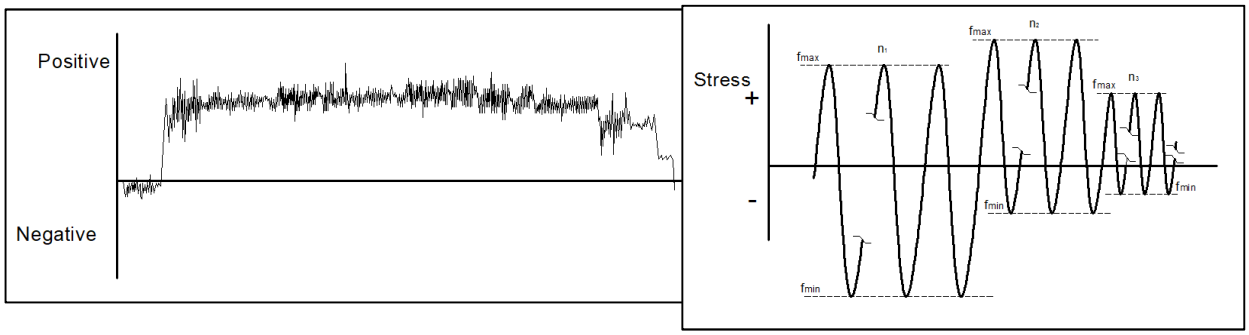

Figure 15 Original Spectrum and Equivalent Spectrum

Now, for each of the constant aplitude stress cycles, of each of the typical flight segments the damge is calcuated using the S-N curves. The actual fatigue detaiedl stress is input into the S-N curve, and the number of cycles is read (n_1, n_2, …, n_p). The damage index is then calculated for that segment by dividing the number of cycles with the endurance limit for that S-N curve (n_1/N_1, n_2/N_2, …, n_p/N_p). The cumulative damage is calculated using some variation of the Palmgren-Miner’s rule:

$$\frac{n_1}{N_1}+\frac{n_2}{N_2}+\cdots+\frac{n_p}{N_p}=\sum_{i=1}^{p}\frac{n_i}{N_i} \qquad \textbf{5}$$

$\boldsymbol{n_i}$ represent the number of cycles in the $\boldsymbol{i}^{th}$ constant magnitude stress cycle

$\boldsymbol{N_i}$ represent the endurance limit number of cycles for the $\boldsymbol{i}^{th}$ constant magnitude stress cycle

If the summation in the equation 5 yields a number greater than one, the formation of the detectable fracture may occur. Aircraft manufacturers size the structures in such a way that the structure should withstand certain number of cycles (flights) before the visible cracks appear.

3.8.3 Damage Tolerance sizing

It is necessary to show that even if a crack is formed at the certain location on the structure the crack can be detected within the planned maintenance inspections before they reach a critical crack size at which

unstable crack growth occurs. Damage tolerance is not discussed in this work. The process of its evaluation, however, can be automated in much the same way as all other margin of safety processes have been automated for this work.

3.9 Strength to Weight Inefficiencies

The strength-to-weight ratio inefficiency that is arising from the load-sizing convergence process is discussed next. Given that the tolerance has to be set for this convergence criteria, let us use nominal 10% for discussion purposes. After every sizing cycle a checking whether the loads on every independently sized component have changed by more than 10% has to be performed. If the load has changed more than prescribed 10% a new sizing cycle has to be run. If the recalculated loads are within 10% the load-sizing cycle is deemed converged. This convergence criteria has a direct impact on the sizing margins of safety. Given that there is a tolerance set on the loads convergence for all SSD requirements, then to account for that level of uncertainty, every SSD margin has to be at least 0.10 – corresponding to 10% load-sizing convergence criteria.

Other, very often overlooked, strength-to-weight inefficiency is due to the nature of the load model. The typical load model is a fairly coarse model that does not model properly neither major nor minor structural joints. Once the SSD checking cycle begins the loads going into these joints have to be approximated using free-body analysis or some other technique. Once the load distribution is to be determined on an approximately modeled joint, it is common to take conservative assumptions on the load distribution. The level of conservatism here will determine if the weight of the structural joint members will be negatively impacted.

3.10 Estimates of development effort inefficiencies

Beside the multiple iterations that need to happen when having separate load and sizing processes, which in itself would produce inefficiency, there is often a need for a more refined FEM models created to avoid making overly conservative load distribution assumptions. This refined FEM is very important for the durability assessment as well. Thus is quite necessary.

However, from the inefficiency stand point, the most dominant factor is the effort of data generation and conversion. Namely, the internal load data needs to be extracted from the load FEM results using free-body analysis, and then this data converted into a consumable format for the SSD sizing tools. The processes and documentation rigor required to perform these tasks often require entire departments of engineers, and the same process needs to be executed at every SSD sizing iteration.

The motivation for solving and overcoming all of the above listed inefficiencies lays in the potential gains possible by the change of the traditional pylon analysis certification process as pursued in this work.

3.11 Estimating the Overall Design Inefficieny of the Segmentd Document-Based Process

Let us recap all the sources of conservatism that have been introduced thus far, define if they are constant or variable, and assign some realistic value to each. The conservatism is inversely proportional to the design efficiency of the structure. Estimated design efficiency numbers are given below, based on observation of the structural design process commonly required for airframe certification.

(a) Load cycle not in phase with stress cycle (constant value, estimated conservatism 10 % - design efficiency 0.9)
(b) Unifying the loads to the max load values across multiple load-cases for similar structures (variable across different features, estimated conservatism 8 % - design efficiency 0.92)
(c) Unifying the dimensions of the sections/panels across multiple similar structural details (variable across different features, estimated conservatism 9 % - design efficiency 0.91)

An estimate of the design efficiency of the document based segmented process can be calculated, using the estimated values, by:

$$DesingEfficnency_{Total} = 0.9 \cdot 0.92 \cdot 0.91 = 0.75 \quad \textbf{6}$$

From the estimated final value of the total design efficiency it is quite clear that the current sizing process produces a structure that is fairly inefficient. The 25 percent of design inefficiency gets directly translated

into added weight of the pylon structure. In industry such as the commercial aerospace industry that regards the weight of the pylon one of the key performance parameters, such a loss seems wasteful.

Moving to the model based process depicted in Figure 16, all of these inefficiencies can be eliminated from the pylon design process.

Chapter 4: The Proposed Optimization Driven Model Based Process for Structural Certification - The Conceptual and Preliminary Design Stages

4.1 General

Progress in recent years in computing hardware and finite element (FE) codes is beginning to make an impact on the structural design process. New approaches, becoming more practical, are based on non-linear models with progressive refinement to achieve FEM stress strain prediction to a level that can be deemed a potential replacement of the physical test (MO2011). Such work, without a doubt, is extremely valuable. But during the design phase of a pylon, the building and updating such hi-fidelity models would be daunting and overly time consuming.

The process proposed here does not venture into the non-linear solid modeling domain. Yet, it changes the existing development process is a way that could be easily adopted by organizations that have long histories of engineering processes, that still use empirical sizing methods, and it enables significant efficiency gains by unifying traditionally segmented processes into a single model based process.

In order to eliminate the previously described inefficiencies with the document based structural certification method, an efficient design synthesis (optimization driven) approach is proposed. The basic idea is to replace the process outlined with the red dashed line from Figure 7 with a single process within a single design synthesis FEM based model that is supported seamlessly by functions for the evaluation of all local effects and behavior (Figure 16).

There are many challenges related to this proposal. The majority of the presented work would be to identify these challenges and to present practical solutions.

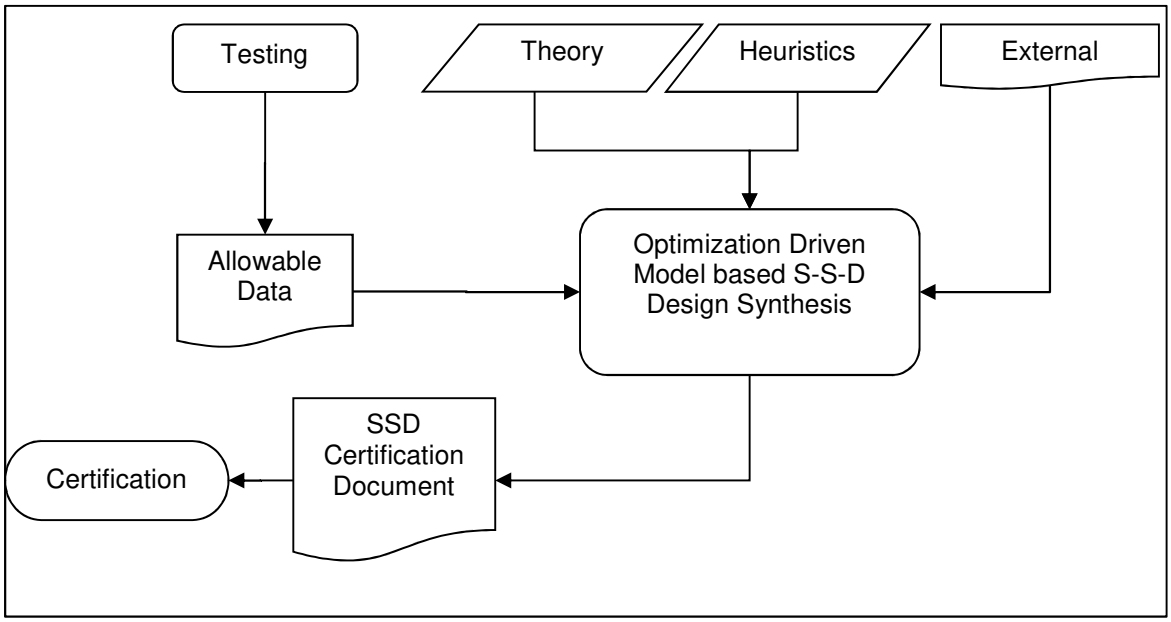

Figure 16 Optimization Driven Model Based Certification Pylon Analysis

The replacement of the document based certification method by a single model that serves as both load and stress model eliminates the following inefficiencies:

(a) Multiple load-sizing iterations

(b) Load data extraction and conversion

(c) Convergence tolerance that requires high margins of safety

In order to eliminate a few other inefficiencies from the document based certification method the model in the model based approach has to have following properties:

(a) Every major structural member needs to be modeled as a separate entity with the FEM

(b) Mesh needs to be refined enough so that the eigenvalue extraction would be within satisfactory accuracy requirements (at least eight elements across the panel)

(c) Each individual fastener joint needs to be modeled with the FEM as unique entity (details of fastener joint modeling given with Figure 17)

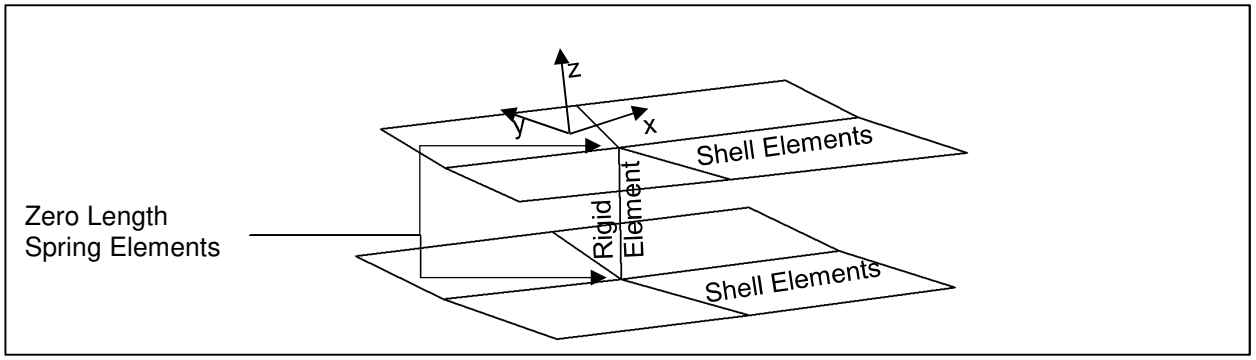

Figure 17 Detail of the Fastener Joint FEM

If the model meets these criteria following inefficiencies will be eliminated:

(a) Need for refined FEM for load extraction and durability analysis

(b) Use of conservative assumptions for load extractions at the joints

In addition to eliminating all of the inefficiencies discussed above there is another very significant potential benefit of model based approach: The model would provide the platform that would allow empirical based functional responses to be combined into the same model with the direct responses, practically creating a platform that could be used to side-by-side compare the direct response values (stress, strain, stability margins, deflections…) with the empirical based functional response values. This could, in the future, pave the way for qualifying direct responses coming from model to become basis for the pylon certification, which would dramatically reduce the development cost of the structure. That is, the model based design capability developed here can demonstrate, automatically, compliance with all empirical, analytical, and semi-analytical methods used today for the sizing and stress certification of aerospace pylon structures.

4.2 Challenges

As stated above, there are many challenges that are related to the proposed new certification method. They will be categorized into several major categories:

(a) Refined FEM model generation

(b) Load Screening

(c) Conversion of dynamic events (Fan Blade Out – FBO) loads into static loading domain

(d) Dealing with non-linear post-buckled structures within the linear domain

(e) Creation of large number of responses and constraints for the stress, and static fastener joint sizing

(f) Nonlinear (empirical driven) constraints for optimization

(g) Extraction of sectional properties, loads for sections, panels, and joints required for empirical evaluation using optimization functional responses

In the following chapters (and appendices) the design and certification of a representative commercial aircraft pylon will be taken as an example for addressing all of the challenges in detail. Practical solutions for each individual challenge will be offered, creating a platform for the proposed model based platform creation. It is emphasized here again the pylon structure used for the study here is not a pylon of any existing airplane and is just a realistic test case based on information available in the open literature..

4.3 Inserting Proposed Multi-Level Model Based Process into Multi Phase Pylon Design Process

The major elements of the typical pylon development process (conceptual, preliminary, and final) paint the background for the model based process in the same way that it does for the document based one. One of the key decisions that needs to be made with the model based approach is what type of responses will be used in each of the design phases in order to minimize the development cost.

For instance it would not make much sense to use empirical based functional responses for strength checking either during conceptual or preliminary design cycles, given that the low level of understanding which load conditions are sizing which sections/panels would require an enormously large response creation effort. Conversely, during the final design phase, which is the basis for the certification documentation, using the direct FEM-generated stress responses would not make much sense given that the FAA typically requires empirical calculation for certification (although lately Authorized Representatives – ARs have started accepting more and more FEM based results as certification basis).

The other reasoning about which types of checks are to be performed in each of the design phases can be directly applied from the document based process given that that logic is valid regardless of the overall approach.

4.4 The conceptual design phase

The inputs for the configuration layout of the pylon are the wing attachment locations and the loft (outside boundaries, usually driven by the aerodynamic requirements). The number of frames/bulkheads is driven by the locations of the major bulkheads (fwd. engine fitting, aft engine fitting and aft bulkhead). Given that the frames mostly serve the purpose of the panel breakers for the top, bottom, and side webs, their number is chosen such that it promotes the web stability.

One could argue that using the coarse FEM, typically programmatically generated, as described in the 1.2 More on the Document Based and Model Based Structural Pylon Design and Certification Process is a sufficient platform for coming up with the conceptual sizing of the major structural members of the pylon. However creation of functional responses that would work with the coarse FEM effort, compared with the effort needed to automatically create the direct stress responses, eigenvalue responses, and functional responses for the static fastener joints of the detailed FEM gives rather opposite answer. To be more specific, even though creating detailed FEM as described early in this chapter takes more time than creating the coarse FEM, the strength, stability and static fastener joint checking using detailed a FEM is dramatically more efficient than the use of the functional empirical responses required with the coarse FEM.

Due much higher level of efficiency, in addition to performing the checks that are typically done this early in the program development with the document based approach:

(a) Fitting sizing

(b) Cross section sizing of the longerons

(c) Panel sizing for stability

The following sizing is performed with the model based approach:

(a) Frames and bulkhead sizing

(b) All fastener joint sizing

The major benefits of the additional checks being done in the conceptual phase with the model based approach are the following:

(a) Fastener joint strength is such a vital part of for the pylon feasibility determination that doing it later than the conceptual phase can lead to extensive delays in the program due to the need for configuration change
(b) Sizing frames and bulkheads this early allows for accurate cost and weight numbers early in the program when the configuration change decisions can still be made based on these engineering parameters

Since at this stage it has been argued that use of the detailed (refined) FEM is the better option than using the coarse FEM, even for the conceptual design phase, it would be prudent to discuss the challenge of creation of such a FEM.

4.5 The Refined FEM Model Generation Challenge

The typical structural design team in a modern aircraft company builds three dimensional (3D) geometrical representation of the pylon using one of the commercially available computer aided design (CAD) tools. This CAD representation, coupled with modern commercially available FEM pre-processor tools, allows for rapid generation of the mid-surfaces and meshing of the pylon parts, coupled with property assignment and fastener generation. The process of building such a detailed FEM of a pylon, as it will be discussed in more detail in a later chapter, takes about one engineering week = approximately 40 engineering man hours. Based on this it is quite clear that this task thus should not represent large hurdle in the pylon development process. One could also argue that due to the constant design changes during the development phase building a new detailed FEM every time when a change in the CAD is made would result in 40 hours of engineering effort to build the brand new detailed pylon FEM. However this argument can be easily countered with the use of the mesh morphing capabilities of modern FEM pre-processors, resulting in FEM modification that take just a few hours.

4.6 The Preliminary Design Case

During the conceptual sizing the only external loads are 15 DR&O conditions. Now that the complete airframe FEM has been assembled and ran through the external load cycle, a complete set of the static maneuvers, dynamic gust, and FBO loads are received. The static maneuver and dynamic gust loads are represented in the FEM as the combination of the forces and moments applied at the CGs of the nacelle and pylon. Typically FBO loads are applied only locally at the introduction points (engine mounts and pylon to wing interfaces), but as we want to include all of the loading conditions and all of the sizing in a single model, FBO loads need to be applied in the way that all other static loads are applied. Doing so represents a significant challenge, and so a detailed section will be dedicate to solving this problem.

FBO loads aside, the first challenge that needs to be solved is load down-selection from a set of thousands of static maneuver and dynamic gust loads. To be more specific, if the aircraft is intended to have multiple variants, engines, and derivatives, and the pylon structure will be reused for all planned variants and derivatives, a separate set of loads is developed for each variant, engine, and derivative. Also, the loads are developed for both left and right side pylon (if the aircraft is equipped with two engines), or for outboard and inboard, left and right pylons (if the aircraft is equipped with four engines).

It is quite clear that the total number of loads becomes large very quickly, in fact, it is not unusual that the preliminary load list contains several thousands of loads. The loads are developed as limit loads - the maximum loads to be expected in service. Similarly to the DR&O loads, these new loads are communicated from the airframe loads team to the pylon loads team as a set of the external forces an moments acting at the center of gravity of the nacelle and the pylons. It would be unpractical to size the pylon structure for all of these loads, since such try would result in an overly large optimization model. Instead, a down-selection of loads is performed to identify a set of critical load cases for which the pylon should be designed.

In the document based process this is done by creating the large set of element loads from all of the load conditions and then down selection based on the largest values of the element loads. Such an approach would be impractical with the detailed FEM. Thus “potato-plotting” technique are used – envelopes of load combinations that cover all load cases for different points and parts in the structure.

4.7 The Loads Screening Challenge

As previously mentioned the total number of load cases (LCs) that the pylon structure needs to be designed for is very large. Once one counts all of the static maneuver and dynamic gust loading conditions the resulting number will be in thousands. The document based way of down-selecting the load cases from this long list involved very a lengthy procedure of tedious post-processing of the coarse FEM results for internal load values coming from all of the static maneuver and dynamic gust conditions. Before we go into discussion of the more efficient way of down-selection of the critical LCs that size the pylon structure, the max/min pylon to wing interface load cases have to be identified. This is achieved by recovering the reaction loads from all of the load cases, sorting, in both descending and ascending way, all of the reactions values at each of the pylon to wing interfaces. These load cases have to be included in the sizing of the pylon, since they size the pylon to wing fittings and the surrounding structure.

Once the max/min interface and FBO loads are taken from the pool of all the load cases, there is still an extremely large number of load cases that need to be considered. Instead of sorting through the max/min internal loads for each of the pylon's structure members, which is the traditional way of going about the down-selection, the more efficient process would consist of treating the pylon as a single equivalent beam structure and creating the so called "potato loads plots" that will identify the critical load cases.

In order to go into detail about this process let us first plot typical shear, moment, and torsion diagrams of a pylon structure. Based on Figure 18 it is quite clear that the pylon can be simply represented as the beam that has concentrated loads applied at the engine fittings, constrained vertically and laterally at the upper link attachment, and approximately cantilevered at the most aft attachments.

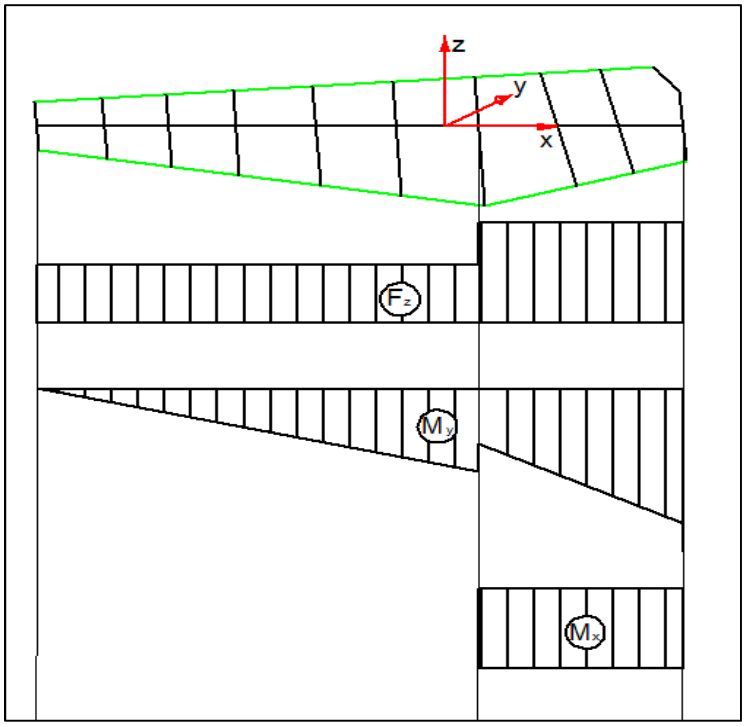

Figure 18 Simplified Plot of Pylon Sectional Forces and Moments

From the internal loads plot (vertical shear, bending moment, and torsion moment) two distinct sections of the plots can be identified, one forward of the aft engine fitting and one aft of it. The aft section experiences the torque (Mx), where the forward one does not. Similar VM plot can be made for the lateral loads, the typical segments again would be the one forward of the aft engine fitting and one aft of it. Given that there are only two representative sections for the entire pylon equivalent beam, let us extract the sectional forces at two locations. All of the force and moment components will be extracted at those two location and then three plots will be created for each of sections. F_z vs. M_y, F_y, vs. M_z, and F_x vs. M_x.

A typical “potato” plotting diagram is shown in Figure 19, as an example. The load conditions that are on the outer envelope of the plot represent the critical load case combinations, and only those loading conditions will be retained for preliminary sizing. Different types of convex shape recognition algorithms can be used to automatically select the critical load cases.

Typically for the pylon there should be 4 “potato” plots from which the critical loading conditions will be extracted:

(a) F_z vs. M_y for a representative section forward of the upper link connection

(b) F_y vs. M_z for a representative section forward of the upper link connection

(c) F_z vs. M_y for a representative section aft of the upper link connection

(d) F_y vs. M_z for a representative section aft of the upper link connection

Each plot would result in a set of critical loading conditions. A union of the four sets together with the union with the loading conditions that are producing the maximum pylon to wing interface loads would represent the preliminary non-FBO critical load set.

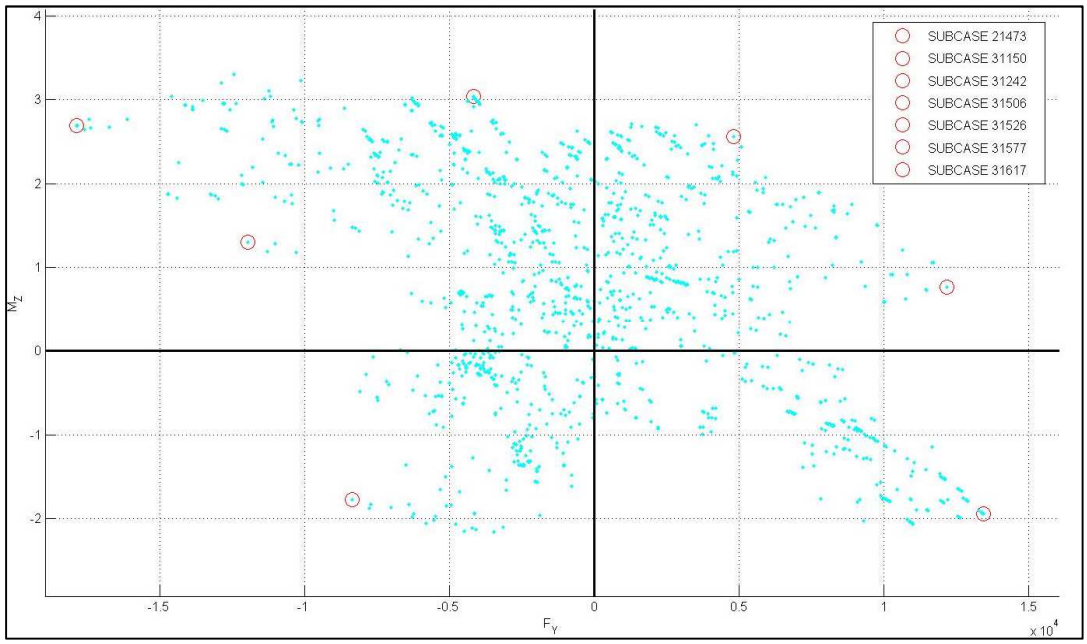

Figure 19 Potato Plotting Example

The FBO event is modeled using a dynamic solution for wing and propulsion package FEM, for various combinations of the engine RPMs, blade release angles, and fuel levels. The FBO conditions are down selected based on the maximum and minimum interface load at all of the pylon interfaces, and all of them have to be retained for the sizing, unless some other static maneuver or dynamic gust load exceeds them in magnitude at the pylon to wing interface.

The challenge lays is due to the fact that FBO loads come as discrete loads at all the pylon interfaces, both the ones that are on the nacelle/engine side and the ones that are on the wing side. If one tries to apply a

set of time correlated loads as a set of static loads to all of the interfaces the pylon would not be in the state of equilibrium, which is a basic premise of the static FEM. Given that FBO loads size quite a few parts of the pylon structure it is important to include them during the preliminary design phase sizing together with the rest of the static conditions. Thus an entire chapter of the work will be dedicated to the novel, yet practical, way of applying the FBO loads onto the model.

4.8 Including FBO Loads in the Preliminary Sizing Cycle

Note: The discussion in this section of the way consistent interface loads are generated for static FBO loads analysis to represent the most critical cases in important to the understanding of the automated model based capability derived here, but the reading of this section can be delayed to a later stage of following this dissertation. The reader may choose to skip to the next section and return to this section later.

The loads group, running a dynamic FE simulation, recovers the interface loads for a pylon and delivers a list of time stamped interface loads that are correlated with both max and min load for every single pylon interface load. If we denote the number of pylon interfaces with ***o*** the size of the matrix that is delivered is ***o*** x 2. Figure 16 gives an example of a pylon with 14 interface loads. Then ***o*** would be equal to 14, and the interface matrix would be 14 x 28 in size.

Each row in the matrix represents a separate time stamp during which one of the interface loads achieved either its maximal or minimal value.

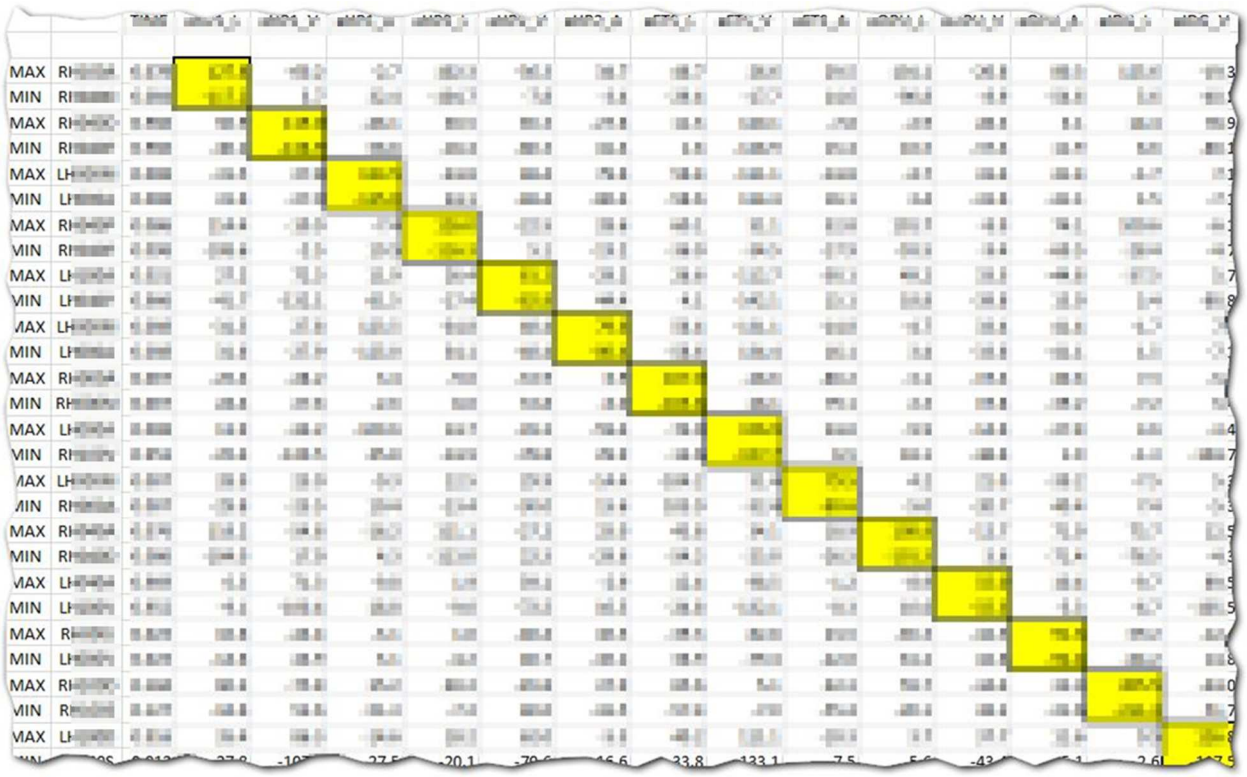

Figure 20 Example of the Dynamic Interface Load Input[1]

When converting the dynamic solution into equivalent static solution it is common to treat certain number of interface load as external loads (denoting them with the vector {***F***}), and treating the remaining set of interfaces as reactions (denoting them with {***R***}). See Figure 21. The external loads {***F***} are acting on the surface ***ΔF***, and the reaction forces {***R***} are said to be acting over the surface ***ΔR***.

Let us denote the number of reactions ***n***. If ***n*** is equal to 6 we have a statically determinate structure. If ***n***>6 we are dealing with statically indeterminate structure, which for the redundancy requirements in pylon design, is almost always the case. Similarly, let us denote the number of external forces ***m***. It is obvious that sum of ***n*** and ***m*** has to be equal to the total number of interface loads ***o***.

If one tries to simply apply {***F***}, and {***R***} to the pylon structure and pick the CG of the pylon as summation point for forces and moments a large non zero vector {***Error***} would be recovered. This is because {***F***}, and

[1] Numbers are intentionally hidden

{***R***} are generated by a dynamic simulation, with entries corresponding to different times, and thus not adhering to static equilibrium.

$$[M_F]_{6\text{xm}}\{\boldsymbol{F}\}_{\text{mx1}} + [M_R]_{6\text{xn}}\{\boldsymbol{R}\}_{\text{nx1}} = \{\boldsymbol{Error}\}_{6\text{x1}} \quad \textbf{7}$$

$[M_R]$ is matrix containing the force multipliers and moment arms to the summation point from {***R***}

$[M_F]$ is matrix containing the force multipliers and moment arms to the summation point from {***F***}

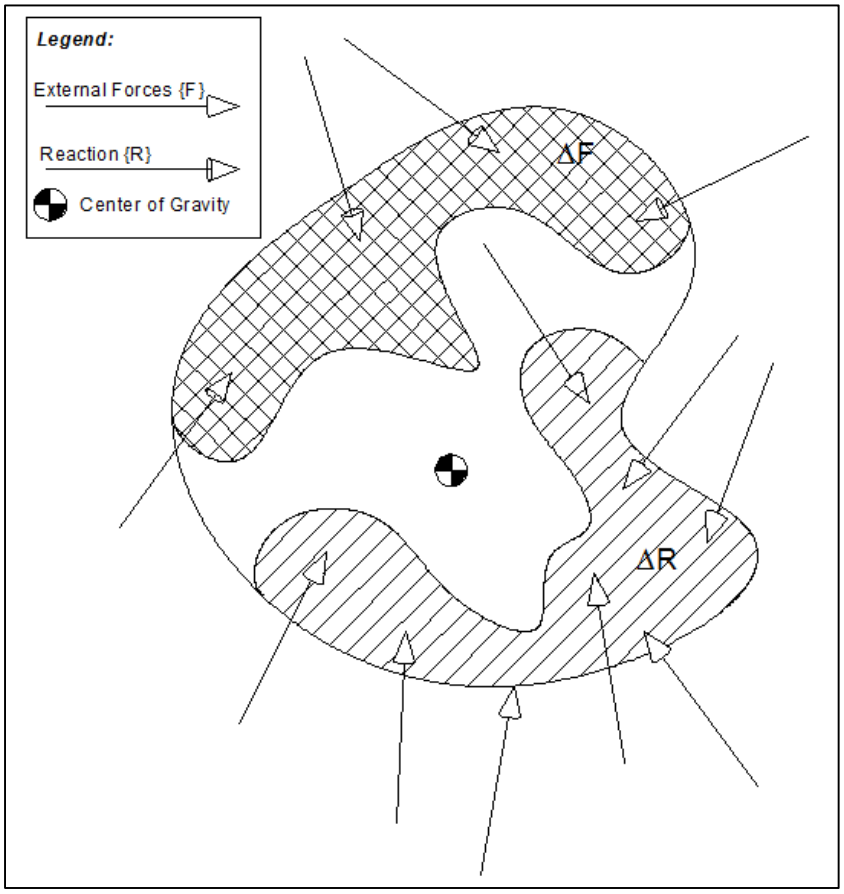

Figure 21 Interface Loads Converted to Static Forces

Now if a static solution is achieved with just the {***F***} applied to the sub-structure and reaction forces {***R****} recovered, this solution would clearly meet the equilibrium requirements, since the solution is coming from a simple static solution. However the reaction vector {***R****} will be quite different than the vector {***R***} that is coming from the dynamic solution.

$$[M_F]_{6xm}\{\boldsymbol{F}\}_{mx1} + [M_R]_{6xn}\{\boldsymbol{R}^*\}_{nx1} = \{0\}_{6x1} \quad \textbf{8}$$

Subtracting equation 8 from equation 7 leads to:

$$[M_R]_{6xn}(\{\boldsymbol{R}\}_{nx1} - \{\boldsymbol{R}^*\}_{nx1}) = \{\boldsymbol{Error}\}_{6x1} \quad \textbf{9}$$

In order to achieve static equilibrium, a supplemental set of body forces (forces in x, y, and z, and moments acting about x, y, and z axis) modeling the inertia response of the pylon to the dynamic load in the static domain need to be added, see Figure 22. These supplemental body forces/moments will be different for every time stamp coming from the dynamic solution.

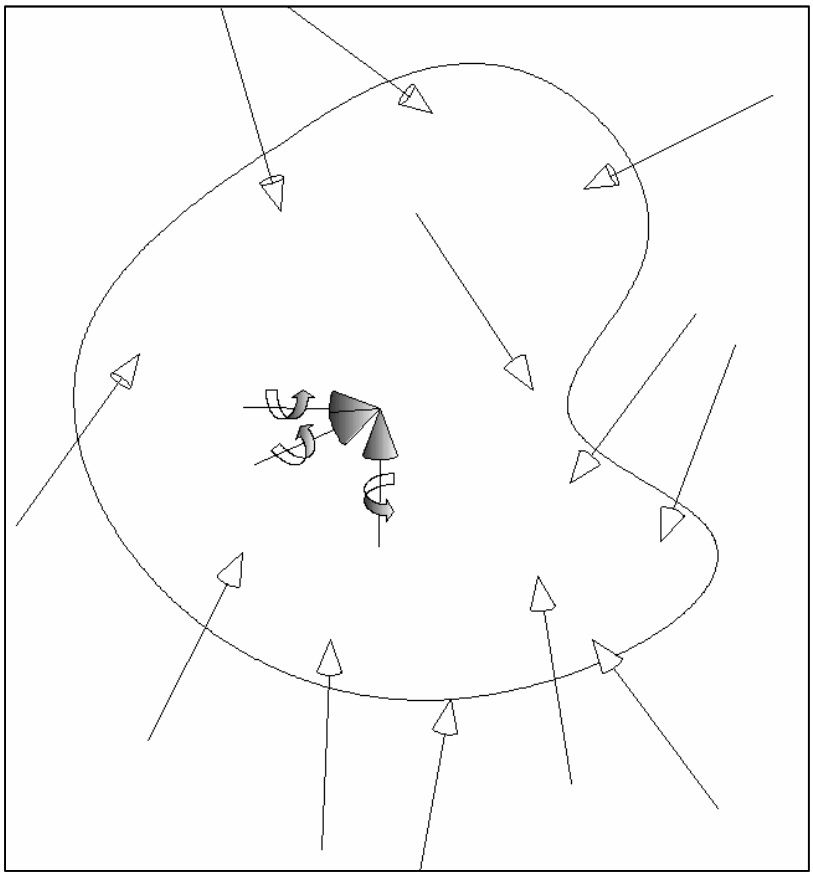

Figure 22 Supplemental Body Forces/Moments

Supplemental body forces and moments will each produce the reaction vector at each of the ***n*** reaction locations. It is necessary to understand the relationship (sensitivity) between the applied body forces/moments and the resulting reactions. This information will be generated by running six static FEM solutions, one for each of the unit body forces/moments applied at the CG of the pylon, and recovering the corresponding reaction vectors $\{\boldsymbol{R}^i\}$, where ***i*** is the body force component (i=1 for unit body force applied along x axis at the CG location, i=2 for body force applied along the y axis at the CG location, i=3 for body force applied along the z axis at the CG location, i=4 for the body moment applied about the x axis at the CG location, i=5 for the body moment applied at CG about the y axis, and finally i=6 for the body moment applied at CG about the z axis). If one takes the six obtained vectors $\{\boldsymbol{R}^i\}$, and appends them column by column into a single matrix (each $\{\boldsymbol{R}^i\}$ vector representing one column) this newly created sensitivity matrix [***S***] will contain information on how each of the unit body forces/moment influences each of the reaction loads at all ***n*** locations.

$$[\boldsymbol{S}] = [\{\boldsymbol{R}^1\} \quad \{\boldsymbol{R}^2\} \quad \{\boldsymbol{R}^3\} \quad \{\boldsymbol{R}^4\} \quad \{\boldsymbol{R}^5\} \quad \{\boldsymbol{R}^6\}]_{nx6} \qquad \textbf{10}$$

The total body force vector can be represented in the equilibrium equation as:

$$\{\boldsymbol{B}\}_{6x1} = [I]_{6x6} \cdot \{\boldsymbol{\alpha}\}_{6x1}{}^{k} \qquad \textbf{11}$$

Where the superscript ***k*** denotes that there is a distinct vector $\{\boldsymbol{\alpha}\}$ for every dynamic time stamp and thus is taking values between 1 and 2***.***

So the problem of finding the correct body force $\{\boldsymbol{B}\}$, reduces to the problem of finding the suitable vector of multipliers of the unit body forces $\{\boldsymbol{\alpha}\}$ for each and every time stamp.

The purpose of the supplemental body force is to make the error vector $\{\boldsymbol{Error}\}$ from the equilibrium equation 3 close or equal to zero. It is only possible to make it exactly zero if n is equal to 6, meaning that we have statically determinate structure. So now let us add the body force to the equation 3 and choose $\{\boldsymbol{\alpha}\}$ such that the right hand side of the new equation is equal or as close as possible to zero vector.

$$[M_R]_{6xn}(\{\boldsymbol{R}\}_{nx1} - \{\boldsymbol{R}^*\}_{nx1} - [\boldsymbol{S}]_{\mathrm{nx6}} \cdot \{\alpha\}_{6\mathrm{x1}}) = \underbrace{\{\boldsymbol{Error}\}_{6x1} - [\boldsymbol{I}] \cdot \{\alpha\}}_{\{0\}} \qquad \textbf{12}$$

The only way for the left hand side of equation 6 to satisfy equality to zero is for the expression in the bracket to be equal to zero, since matrix [M_R] is a non-zero matrix.

$$\{\boldsymbol{R}\}_{nx1} - \{\boldsymbol{R}^*\}_{nx1} = [\boldsymbol{S}]_{\mathrm{nx6}} \cdot \{\alpha\}_{6\mathrm{x1}} \qquad \textbf{13}$$

In order to be completely consistent equation 13 has to be rewritten to take into account that each time stamp has a distinct vectors {***R***} and {***R****} as well as a distinct unit body force multiplier {***α***}.

$$\{\boldsymbol{R}\}_{nx1}{}^{k} - \{\boldsymbol{R}^*\}_{nx1}{}^{k} = [\boldsymbol{S}]_{\mathrm{nx6}} \cdot \{\alpha\}_{6\mathrm{x1}}{}^{k} \qquad \textbf{14}$$

Looking at equation 14 it is clear that if ***n***=6 we can solve for the multiplier {***α***} exactly, and equation 6 will be exactly met. For the pylon structure ***n*** is actually greater than six. Thus equation 14 can be only solved approximately, such as using a least square solution. For clarity, ***n*** cannot be less than six since this would result in unconstrained pylon structure, ensuing rigid body modes in the FEM but more importantly letting the engine fly off the airplane.

The complete practical process of achieving the application of the FBO loads onto the pylon within the static domain FEM is described on the flowchart below.

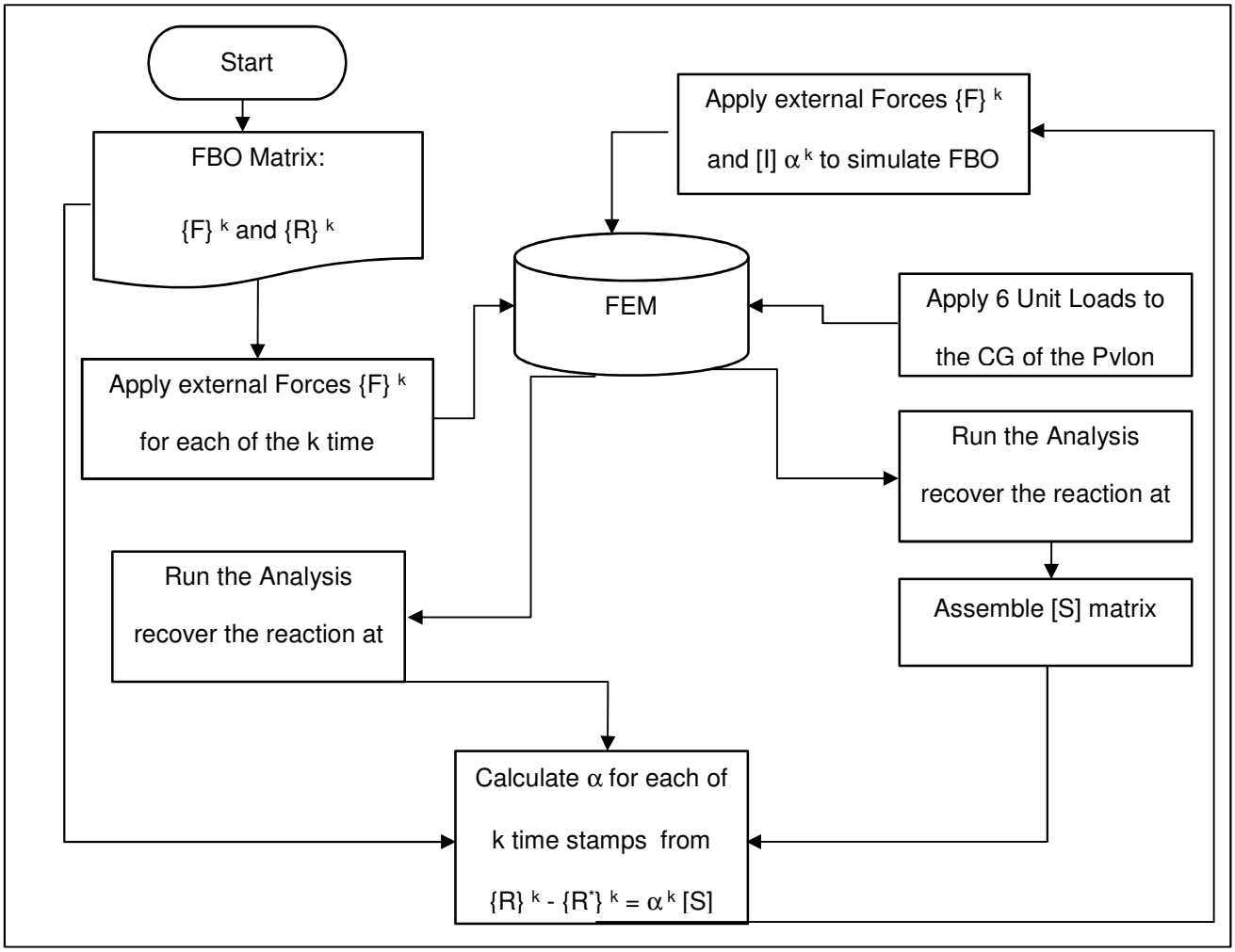

Figure 23 Supplemental Body Force Method for FBO Load Cases

It is worth mentioning here that it is typical to have the pylon to wing interface points be selected as the reaction locations and all other ones (engine fittings connections) as the force application points.

Once the set of critical load cases is assembled, the sizing of the structure can begin. All the static maneuver, dynamic gust, and FBO cases are typically available. However, the fatigue spectrum usually is still in development. For this reason, but also for expediency and cost reduction purposes, fatigue will not be considered in the preliminary design phase.

4.9 Temperature Effects and “Knock-Down” Factors

Before executing the sizing, the allowable values need to be determined. The tabular numbers for the ultimate tensile stress (Ftu) can be found in the references such as MIL-HDBK-5H (DoD1998). “knock-down” factors need to be applied to these values before they can be used for sizing the pylon structure.

A temperature knockdown factor needs to be taken into account given that the core of the engine heats up the aft engine fitting considerably and the temperature gradient is fairly high in that local area. Spatially it makes most sense to apply the temperature knockdown factors using pylon bays for the categorization. Again, finer granularity would allow for a more weight efficient design, although it would complicate the optimization sizing setup considerably.

There are usually more than a single temperature profile to be considered, but typically, given that pylon environment is not subject to great variation of temperature, usually a few typical temperature profiles are used. It is common to use one temperature profile for the limit cases and another one for the ultimate cases. For future reference let us denote these two thermal profiles as limit and ultimate thermal profile. Each property of the pylon that is supposed to be sized will have two associated temperatures. Typically these temperatures will vary from zone to zone.

The temperature-corrected allowable value is calculated as multiplying the tabular value of allowable value with the temperature correction factor (T_{kd}).

Another major challenge with regards to creation of the model based platform will end up looking as the knock-down factor. This is presented in the next sub-chapter.

4.10 Accounting for Non-Linear Post-Buckled Structural Behavior in Design Based on Linear FE Models

Special considerations have to be given to the post-buckled analysis of structural components. It is quite common in pylon structures design to allow the membrane elements to buckle under loads larger than the limit load. Now, our basis of optimization driven sizing is a model based platform that is based on a linear

detailed FEM. The load redistribution due to post-buckled states of the membrane members have account for within this framework.

Panels allowed to buckle are depicted with the red hash lines in the Figure 24.

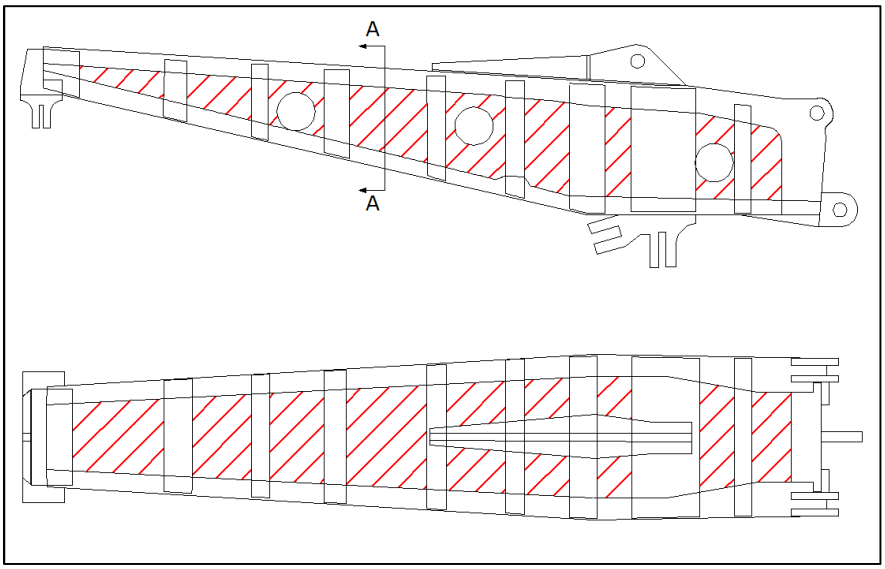

Figure 24 Panels Allowed to Buckle Over the Limit Load

Once the panels buckle under limit load, the remaining (non-buckled) structure has to carry the additional load. Most notable structural members that will be affected are the longerons and fittings. When one uses the closed form solution to size the cross section of the longeron or a fitting members the additional load would be added to the load part of the calculation. Since with the model in the preliminary load cycle we are dealing with the direct major principal stress calculation within the linear FEM, it is not feasible to increase the internal load. Some other way of taking into account the post-buckled state of membrane members has to be adopted.

Since the strength calculation is a fairly simple linear calculation that relates the load, and some geometrical property (area, moment of inertia…) to the stress, which is then compared with the allowable stress to calculate the margin of safety, it really does not matter if the post-buckled load increase for the longerons will be taken into account “on the load side” or the “allowable stress side”. Here is a simple example.

For example, if the direct compressive stress is calculated using the formula:

$$\sigma = \frac{P}{A} \quad \textbf{15}$$

And then the margin of safety is calculated as:

$$MS = \frac{F_{tu}}{\sigma} - 1 \quad \textbf{16}$$

The post-buckling knock down factor K_{pb} needs to be introduced. It will represent the amount of additional load in the longeron members due to the buckled skin panels. In order to take into account the post-bucked state of the membranes by a factor K_{pb}:

$$\sigma_{pb} = \frac{(1 + K_{pb}) \cdot P}{A} = (1 + K_{pb}) \cdot \sigma \quad \textbf{17}$$

The margin of safety can we written as:

$$MS_{pb} = \frac{F_{tu} \Big/ (1 + K_{pb})}{\sigma} - 1 \quad \textbf{18}$$

This shows that instead of increasing the internal load by the factor K_{pb} that is greater than 1, we can simply reduce the allowable stress by dividing the allowable value by that same K_{pb} factor. Now it is obvious that one can use the reduced allowable as the constraint value for the major principal stress response for the shell elements in the model.

Special attention has to be given to the K_{pb} factor determination. It is intuitive that the K_{pb} is the factor related to the cross section of the pylon. Since the pylon cross section changes from front to back (every bay has a different cross section), it only makes sense to determine this factor per bay. Ideally, K_{pb} could be calculated for every inch of the cross-section. However this would make the overall setup of the optimization problem overly complicated. The K_{pb} should be calculated as a ratio of total bay cross-sectional area to the stable part of the same section bays cross-section in the post-buckled state. Out of all possible buckled states the state with the smallest stable cross-section should be used, so that the conservatism is preserved.

An example is given for a section A-A (pylon's bay #4) from the Figure 25.

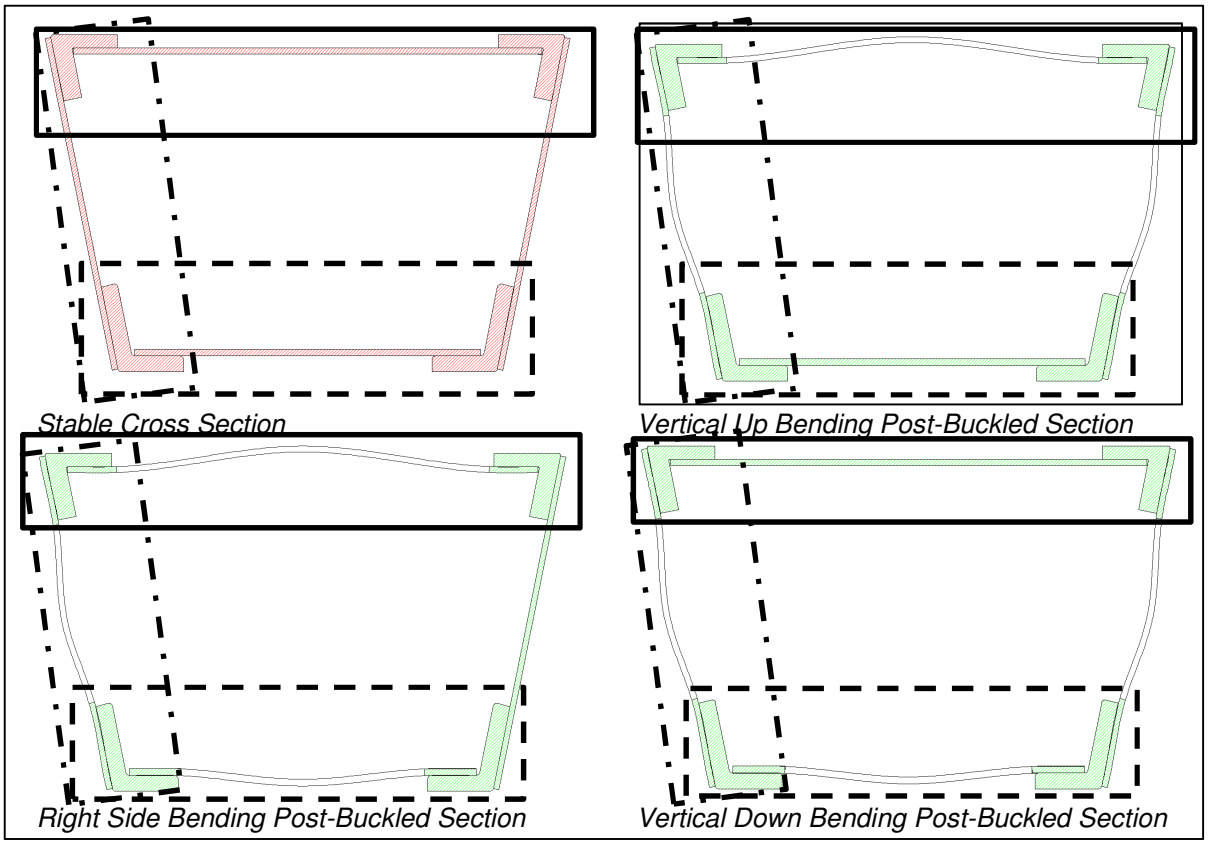

Figure 25 Stable vs. Unstable Section Areas

There are three distinct post-bucked states driven by the dominating bending load. These different post-buckled states are shown in the Figure 25. Based on the dominating loads, there are different segments of the cross-section that will carry the compressive load. These different segments are marked in Figure 25 by 3 different outlining rectangles. The solid line rectangle defines the segment of the cross-section that will be in compression under the up bending load. The dashed rectangle denotes the segment of the cross-section that will be in compression under the dominating down bending load. Lastly, dash-dotted rectangle mark the segment of the cross-section that will be in compression under the right side bending load. Assuming symmetry, the compressive segment under the left side bending is omitted from the picture.

If the area of the stable cross section (red hashed area in Figure 25) is denoted with A_{stb}^{i}, and the green hashed areas from the same figure of three possible post-bucked state sections respectively with A_{b1}^{i}, A_{b2}^{i}, and A_{b3}^{i}, the post buckled factor K_{pb}^{i} can be calculated as:

$$K_{pb}^{i} = \frac{\min(A_{b1}^{i}, A_{b2}^{i}, A_{b3}^{i})}{A_{stb}^{i}} \quad \textbf{19}$$

The superscript *i* denotes the three different compressive segments, identified by the different styles of rectangular lines.

The maximum of the three K_{pb}^{i} will be used as a uniform post-buckled coefficient.

$$K_{pb} = max(K_{pb}^{i}) \quad \textbf{20}$$

The $\boldsymbol{K_{pb}}$ represents the amount of additional load in the longeron members, thus the total load going thru the longerons can be expressed as:

$$P = P_l + P_l \cdot K_{pb} = P_l(1 + K_{pb}) \quad \textbf{21}$$

In order to resemble the temperature knocking-down of the allowable value, the lower case $\boldsymbol{k_{pb}}$ will be introduced.

$$k_{pb} = \frac{1}{(1 + K_{pb})} \quad \textbf{22}$$

With this newly introduced post-buckling reduction factor the margin of safety can be calculated as:

$$MS_{pb} = \frac{F_{tu} \cdot k_{pb}}{\sigma} - 1 \quad \textbf{23}$$

The post-buckling knockdown factor will be calculated for each bay of the pylon.

Since the sizing dimensions of the cross-section will change during the iterations, the post-buckled knockdown factor will be changing as well during the optimization iterations. To take into account this effect during the preliminary design phase would represent a significant complication to the optimization setup using the direct major principle stress. For expediency and simplicity sake, these knockdown factors are assumed to be constant during the pylon optimization driven sizing of each particular bay. However, during the final design phase the dynamic nature of these knockdown factors will be considered in an exact way.

The post-buckled knockdown factor should be applied to the longerons and because those members stay shear resistant and will see additional load.

4.11 Critical Checks for the Preliminary Design Phase

Going back to the previously made point about the types and extent of sizing that happens in each of the design phases, it is critical to identify those for the preliminary design phase. The platform for sizing is now a refined FEM which is converted to the model based platform during this design phase. The right type of responses and constraints now need to be selected. Also, it is important to understand which types of loads are available at this point of the pylon design as well as program allotted time for this particular design phase.

The following checks are to be performed during the preliminary design phase for all of the critical load cases:

(a) Strength of all structural components

(b) Stability of all structural components

(c) Static joint strength (fastener shear and bearing stress of joined parts)

(d) Major fitting checks (lug/clevis, and tension bolt fittings)

4.12 Executing Optimization Driven Sizing Checks for the Preliminary Design phase

As previously described, there needs to be a correct balance between the required checks that need to be performed in the preliminary design phase and the way those check are executed, taking into account the quality of the FEM that is available. Since the refined FEM is available, certain types of checks can be performed using the direct optimization responses. These types of checks are not sufficient for certification, however, but during the preliminary phase of design these checks provide a rapid yet accurate platform for optimization driven sizing. Table *1* describes the recommended optimization setup for each of the required checks for the preliminary design phase.

Details of each of the optimization setups will be discussed in more detail in the following paragraphs.

Strength of all structural components except major fittings	Shell elements major principal stress direct response
Stability of all structural components	Eigen value direct response
Static joint analysis	Zero length spring elements direct force responses, resultant functional response for the total in plane shear load
Major fitting checks (lug/clevis, and tension bolt fittings)	Close-form functional response that takes into account the geometry of the fitting, wall sizes as design variables, and spring element direct force responses

Table 1 Responses Related to Analysis Checks

4.13 Optimization Design Variables

Before even considering the checks in detail, the design space needs to be established. It is accepted by the preliminary design that the fastener size and number of fastener rows for each zone of the pylon are determined based on the internal load distribution of the critical loads. The fastener size drives the width of the longeron members and the frame/bulkhead landings since typically there is a prescribed minimum distance from one fastener to the next and from the fastener center to the edge of the part. So the width is predetermined by the fasteners size and number of rows, and therefore the gauges are allowed to change, and they form the design space.

In order to reduce the weight of the structure as much as possible, the recommendation is to provide the optimizer with as large of a number of design variables as possible. However, certain economic and geometric constraints have to be considered while optimizing the pylon structure. Let us consider the longeron member, for an example. The longeron spans multiple bays of the pylon and gets fastened to frames, bulkheads, and skins. The most economic design of the longeron member would be a simple L shape cross-section without any thickness variation along the longeron member's length. In terms of design space such design would constitute two dimensional space (only two design variables). One gauge variable for the side leg of the L cross-section and one gauge variable for the horizontal member of the L cross-section. If the internal load would be constant across the entire longeron length this design would not be particularly suboptimal. However, since the bending moment changes along the longeron length (see Figure 18), this approach would yield grossly suboptimal weight design because the entire length of the longeron would be sized by the largest load. On the other end of the spectrum would be a longeron whose section

is constantly changing along its length following the bending moment diagram. Even though this design could be considered optimal from the strength to weight ratio, it would not allow for easy assembly with other parts, if at all. A manufacturing constraint makes its impact here. A middle ground would represent the design of a longeron that has thickness regions that match the bay spans and the interfaces with the frames. Figure 26 shows a longeron member that spans four bays and interfaces with five frames or bulkheads would have a total number of eighteen gauge variables. Ten for the five frame/bulkhead landings, and eight for the four bays.

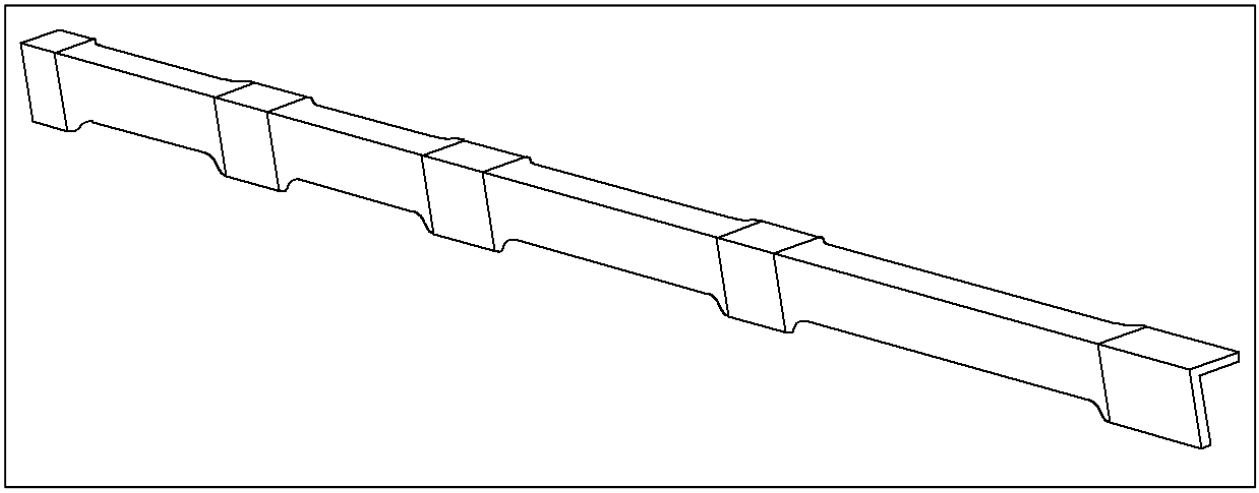

Figure 26 Longeron Spanning Four Bays

The lateral symmetry of the pylon is to be maintained, so the upper left longeron member would have the same thickness distribution as the upper right hand one. Similarly, the frames or bulkheads gauge distribution will adhere to the lateral symmetry and would have a gauge design variable for every distinct structural feature. Each chord, stiffener, and panel would be allowed to have a different thickness. For illustration purposes, if one would refer to the bulkhead in Figure 5, the number of distinct gauge variables would be twenty. Six for the panels, seven for the chords (attachments to the webs or longerons) and seven for the stiffeners. The property distribution would match the gauge zones described previously for the design variables.

4.14 Strength of All Structural Components except Major Fittings

Table *1* specifies that the recommended check for strength for all the structural components except the major fittings is direct checking of major principal stress. The reasoning behind this recommendation is that the detailed FEM is fine enough to capture the stress gradients. Checking only the major principal stress is reasonable due to the fact that are pylon structures have thin walled sections and panels, which under compression would buckle (incur instability) rather than fail under the minor principal (compressive) stress.

There is an important point to be made about the stress checking using the linear detailed FEM. Given that we are dealing with ultimate loads (50% larger than the limit loads that the pylon should ever see), the major principal stresses of all elements representing the structural member to be checked are compared to the ultimate tensile strength of the material (F_{tu}), with one exception. At the interface with the fasteners the typical strength of the material is the ultimate bearing strength (F_{bru}) that is typically significantly higher that the ultimate tensile strength of the material. Therefore, the elements attached to the spring elements that model the interface between the fastener and the structural component will be excluded from the major principal stress check. Elements that are to be excluded from the major principal stress check are shown in Figure *27*. Instead of checking these elements against the ultimate tensile strength of the material using the major principal stress, the bearing check will be performed. As it will be described in the later paragraph bearing stress will be calculated using the functional response and then will be checked against the F_{bru}.

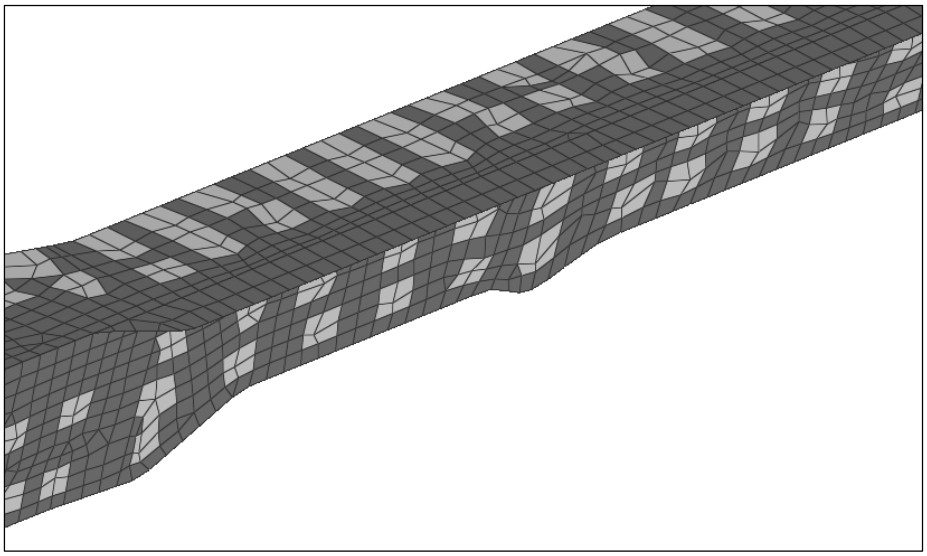

Figure 27 Light Colored Elements Excluded from Major Principal Stress Check

4.15 Execution of the Strength Constraints Creation

Considering the sheer number of the gauges (each having an independent FEM property cards assigned to them) that need to have a certain static stress strength margin, as well as the fact that each property would have a set of elements that are excluded from the stress checking, it is rather obvious that the setup of the strength constraints, if done without the automation, would represent a tedious and error prone task. Therefore some type of the automation needs to be executed to help with both shortcomings of the manual setup.

4.16 Creation of Large Number of Responses and Constraints for the Stress, and Static Fastener Joint Sizing Challenge

Table 2 shows, for an example, a few lines of the setup table. The first column would be a property ID (shell property number), the second column with the “Ftu_u” header would represent the ultimate tensile strength without any knockdowns. The third column would represent the post-buckled knock-down factor. The fourth - the temperature knock-down factor, and the fifth column with the header “Ult Load Idnt” would represent the identifier in the name of the critical load sets that would determine if a particular load case belongs to

ultimate load case set. Similar to columns one through four that contain the pertinent information for the ultimate load cases columns five through eight would represent the information required for the limit load cases. From this table one can see that the post-buckling knock-down factor is set to 1 for the limit cases given that the structure is sized to be shear resistant under limit loads. This type of the setup would also require a unique set of excluded elements in the model for each particular property. The naming of these excluded sets should relate the set name to the property is some way. For instance they can be called, “exclude_1001”, “exclude_1002”… where the first set would contain the shell elements to be excluded from the stress response for the property ID 1001.

Property id	Ftu_u	Kpb_u	Ktmp_u	Ult Load Set	Ftu_l	Kpb_l	Ktmp_l	Lim Load Set
1001	64000	0.827	0.85	1560	64000	1	0.85	2440
1002	64000	0.827	0.85	1560	64000	1	0.85	2440
1003	64000	0.827	0.85	1560	64000	1	0.85	2440
1004	64000	0.827	0.85	1560	64000	1	0.85	2440
1005	64000	0.827	0.85	1560	64000	1	0.85	2440

Table 2 Direct Stress Automation Spreadsheet

The automation algorithm is shown in Figure 28.

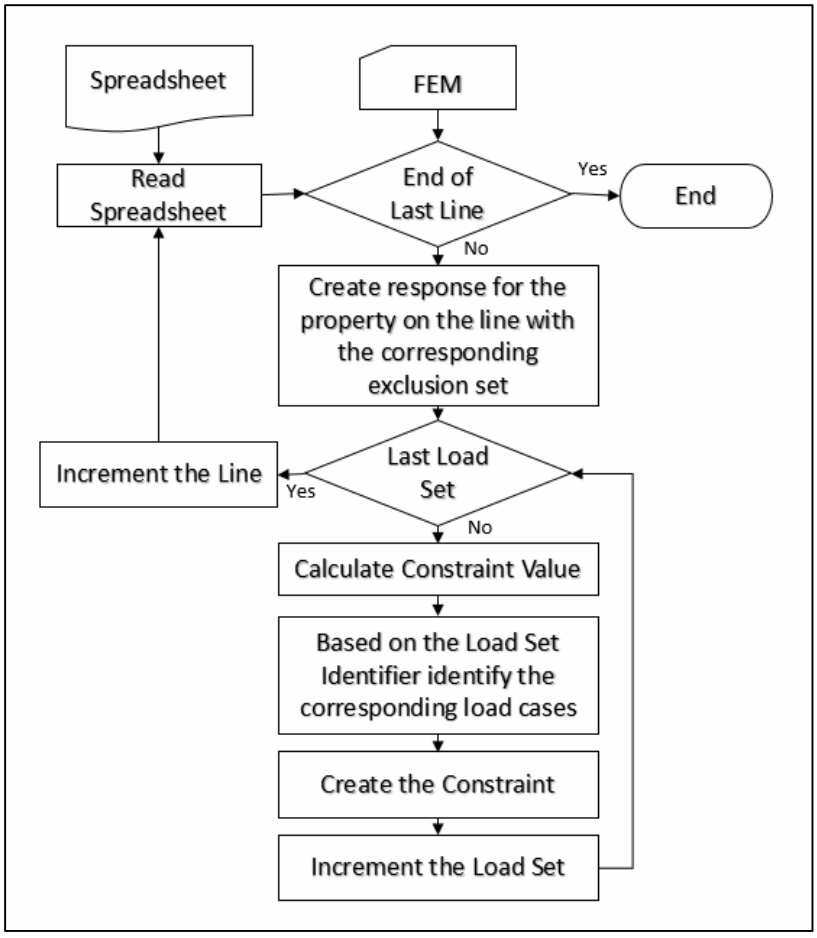

Figure 28 Direct Stress Response Automation

4.17 Static Joint Analysis

In any built-up structure the joints that hold the structure together often represent critical details of the structure and require detailed stress analysis as well; as, often, testing. An engine pylon is no exception to this. Therefore all the joints in the pylon have to be checked for both static and fatigue strength.

In the preliminary load cycle fatigue loads are often not yet available. Furthermore, the document based fatigue analysis takes many engineering hours. Thus, only the static strength of the joints will be checked during this design phase. There are two components of the static strength for which the joints need to be checked: One that relates to the fasteners (B1990) and the other that relates to the structural components that are being fastened together. The fasteners are checked against fastener shear allowable (assuming

that the structure is well designed and the fasteners are carrying the shear load). The structural components are checked against the ultimate bearing strength of the material F_{bru}.

Now, the detailed FEM is built in such a way that every fastener is represented by a combination of rigid and spring elements (see Figure 17). Thus, there is no reason to make certain assumptions about the fastener load distribution or a need to perform additional analysis to determine how much load each of the fasteners is carrying.

There are several knock-down factors that need to be considered for the joint checks. Just as any other allowable, both fastener shear and the ultimate bearing allowable have to be reduced by the temperature knock down factor T_{kd}. There are different T_{kd} values for fastener shear, based on the fastener type and material, and for ultimate bearing strength. Let us denote these with a superscript. Temperature knock-down for shear will be denoted T_{kd}^{s}, and temperature knock-down for bearing strength will be T_{kd}^{br}.

Furthermore, all the fasteners that belong to the longeron and fitting members need to be knocked-down with the post-buckling factor given that they are "seeing" additional load due to load redistribution beyond the limit loads when the panels of the webs become unstable.

When discussing the shear capability of the fasteners, the number of shear planes have to be carefully considered. Namely, for the fastener joints that connect three or more plates the inner plates are effectively putting the fastener in double shear loading. Therefore for those locations the double shear allowable should be used. The double shear strength of a fastener is typically two times larger than the single shear strength. Thus, in order to simplify the setup of the shear constraints, a double shear factor is introduced. Let us denote the double shear factor as K_{ds}. This factor will have following property:

$$K_{ds} = \begin{cases} 1.0, for\ Single\ Shear \\ 2.0, for\ Double\ Shear \end{cases} \qquad \textbf{24}$$

If the fastener shear force is denoted with Fs, and the ultimate tensile strength of the fastener is denoted with the Fsu the margin of safety is simply calculated as:

$$MS_{Fs} = \frac{F_{Su} \cdot T_{kd}^{s} \cdot k_{pb} \cdot K_{ds}}{F_s} - 1 \qquad \textbf{25}$$

Similarly, for the bearing strength of the fastened material:

$$MS_{Fbr} = \frac{F_{bru} \cdot T_{kd}^{br} \cdot k_{pb}}{F_{br}} - 1 \qquad \textbf{26}$$

Where the bearing stress is calculated directly from the shear stress using the joint details as:

$$F_{br} = \frac{F_s}{t \cdot D} \qquad \textbf{27}$$

t being the thickness of the material at the joint location, and ***D*** representing the fastener diameter.

It is important to note that for the fasteners that do not join the longerons and fitting the post-buckling knock-down factor $\boldsymbol{K_{pb}}$ will be set to 1.

In order to generate the shear load component that acts on the fastener and the structural member it is necessary to extract the direct stress responses on the spring elements. Assuming that the local spring element coordinate system is aligned such that the shaft of the fastener (represented with a rigid element, shown in Figure 17) is collinear with the z-axis, the two components that are required are the force in x and y direction. These two force components will be extracted from the direct force response, while the resultant will be calculated using the functional response using the resultant equation:

$$F_s = \sqrt{F_x^2 + F_y^2} \qquad \textbf{28}$$

This resultant force response will only have as its arguments the two direct responses $\boldsymbol{F_x}$ and $\boldsymbol{F_y}$. The bearing response will also calculated as the functional response using the bearing equation 27. The input arguments for the bearing functional response will be the gauge variable of the shell property that the spring element is attached to, a table entry or a constant for the fastener diameter, and, finally, the previously calculated resultant in-plane shear functional response.

4.18 Execution of Static Joint Analysis

The automation of the static joint response and constraint creation has greater importance than the automation of the stress responses and constraints needed for the strength sizing. The importance stems from two sources. First is the sheer number of the joints that need to be analyzed, and second is the complexity of the functional responses compared to fairly straight-forward direct responses used for the strength sizing responses.

The overall process of automation is similar to previously described direct stress response and constraint generation with the addition of the functions that need to be created for the resultant shear force and bearing stress, as well as the table entry for the fastener diameter.

There are few other differences between this automation process and the direct stress automation. The first is the format of the spreadsheet which is the starting point of the automation. Instead of using the property as the distinguishing parameter between the various fastener types and locations of the fastener joints, the element sets need to be created for the spring elements representing the interface of the fasteners and the structural members. The diameter of the fastener needs to be defined in the spreadsheet, and there are two allowable values, the fastener shear and the ultimate bearing stress. The temperature knockdown values also are different for the F_{su} and F_{bru}, and so this needs to be taken into consideration. Table 3 is a sample table for the ultimate load case set. A similar one would be created to the left of the table below for the limit load set.

Set id	D (in)	F_{su}(kips)	T_{kd}^{s}_u	F_{bru} (ksi)	K_{ds}	T_{kd}^{br}_u	K_{pb}_u	Ult Load
2148	0.375	3.85	0.827	97	1	0.85	0.78	1560
2149	0.375	3.85	0.827	97	1	0.85	0.78	1560
2150	0.375	3.85	0.827	97	1	0.85	0.78	1560
2151	0.375	3.85	0.827	97	1	0.85	0.78	1560
2152	0.375	3.85	0.827	97	2	0.85	0.78	1560

Table 3 Static Fastener Joint Shear and Bearing Automation Spreadsheet

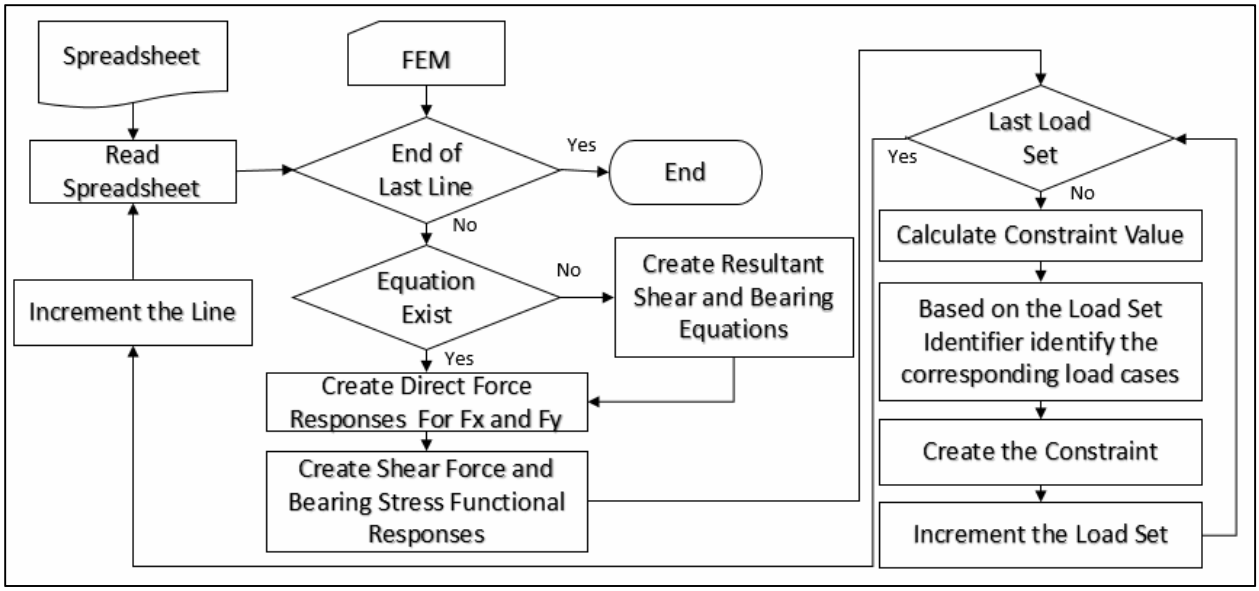

Figure 29 Fastener Constraints Creation Automation

4.19 Stability of All Structural Components

When preparing to set up the stability constraints it is very important to classify which structural components are allowed to buckle at the limit load and which need to stay stable all the way to the ultimate load. The stability of the side and upper and lower webs was discussed previously given that it directly influences the strength constraints. Let us classify the remaining parts of the pylon from the stability standpoint. Longerons and fitting need to stay stable all the way up to the ultimate load, since instability of these members would represent the collapse of the entire pylon structure. The frames and bulkheads are somewhat debatable. Since frames and bulkheads carry the vertical shear but also break the side and upper lower web panes it is obvious that the frame's chords and stiffeners need to remain stable all the way to the ultimate load, however the frames/bulkhead panels could be allowed to buckle under the ultimate load. Since the web panels of the frames and bulkheads represent a very small overall weight target, and since allowing them to buckle would represent a significant complication of the optimization sizing setup, it is generally recommended to have all the frames/bulkheads shear resistant to the ultimate load. Table 4 summarizes the stability requirements for the various components of the pylon.

Now, that the overall stability requirements are set, we can discuss how these requirements are typically executed within the optimization setup.

Component	Stability Requirement	Special Considerations
Longerons	Stable under the ultimate load	K_{pb} has to be considered for the longerons
Side Webs	Stable under the limit load	Allowed to buckle beyond the limit load value
Top/Bottom Webs	Stable under the limit load	Allowed to buckle beyond the limit load value
Fittings	Stable under the ultimate load	K_{pb} does not have to be considered for the fittings since the reactions from fittings to the wing interface should not change significantly due to the buckled webs
Frames/ Bulkheads	Stable under the ultimate load	Even though it the panels of the frames and bulkheads could be allowed to buckle the load redistribution due this would be too complicated to take into account for, thus they are required to be shear resistant to ultimate load.

Table 4 Stability Considerations

4.20 Execution of the stability requirements

Stability analysis in this phase of the design is done in a surrogate fashion using an eigenvalue buckling analysis (linear FEM eigenvalue solution of the entire pylon structure). It is required to have eigenvalue load cases created for each critical static load case. In fact, given that some structural members are being sized to be stable at the limit and some to be stable at the ultimate load values, the number of eigenvalue load cases can be greater than the number of critical static load cases. If one uses the notation ULC for to denote the number of ultimate load cases, and LLC as the number of limit load cases, the total number of eigenvalue load cases will be calculated as:

$$Number\ of\ Eigen\ Velue\ LCs = 2 \cdot ULC + LLC \qquad \textbf{29}$$

Equation 29 states that there is going to be two eigenvalue load cases for each ultimate load case, which obviously creates a larger optimization problem. However, this is really needed due to the fact that the

buckled webs are allowed in the design above the limit loads. For each ultimate load case there is going to be one that is just a regular eigenvalue extraction. This one will be used to size the webs under stability requirements. Another one will be created such that the web properties are excluded. The latter one is used to size the longerons, fittings, frames and the bulkheads under the stability requirements. For each limit load case just a regular (no excluded properties) eigenvalue load case is required.

If one assumes that the margin of safety is held at 5% during the preliminary design phase the table below describes which buckling eigenvalue constraints should be used.

Load Case	Eigen Value Constraint	Component Sized	Comments
Ultimate Eigen value load cases w/o exclusion properties	0.717	Side, upper and lower web panels	0.667 for two thirds of the ultimate case (making it limit) plus 0.05 for 5% margin
Ultimate Eigen value load cases exclusion properties	1.05	Fittings, frames and bulkheads	Panel properties of the side, upper and lower webs are excluded
Ultimate Eigen value load cases exclusion properties	1.05*Kpb	Longerons	K_{pb} has to be considered for the longerons since once the webs are buckled additional load will be distributed to the longerons
Limit Load cases' Eigen value	1.05	All components	

Table 5 Eigen Value Constraints

4.21 Major Fittings Strength Checks

Fitting are critical structural members. Pylon to wing interfaces are no exception. Thus these structural features have to the qualified using extreme care. The major fittings that will be discussed here are the pylon to wing attachments and engine fitting to pylon attachments. The common feature of both lug-clevis and tension bolt fittings is the fact that they can experience multiple types of failures, therefore for a single fitting there would be a need to have multiple strength checks done. Since there will be multiple margins of safety calculated, there is a need to collect them into a single response which will represent the minimum margin of safety of all different checks. Alternatively, some form of a cumulative constraint function may be used (HG1992, page 160).

4.21.1 Lug-Clevis Fittings

Pylon to wing fittings are most often of lug/clevis type since this type of joint design allows for relatively easy installation of the pylon to the wing. For the lug and clevis fittings there are several types of empirical analysis formulations. For all of these different certification calculations the total transverse and tension load is required to be input, load angle with respect to the lug axis, as well as the lug dimensions: thickness (t), diameter (D), width (W), and thickness in the transverse direction (a).

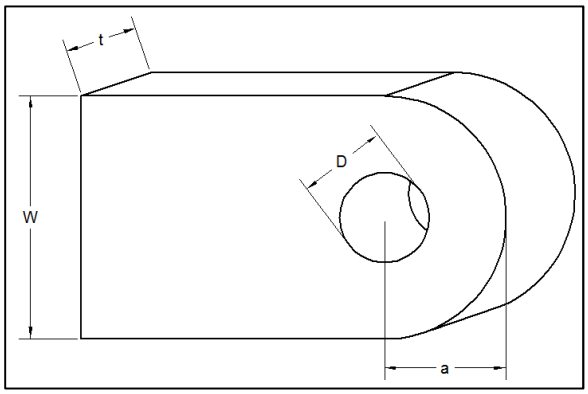

Figure 30 Typical Lug Geometry

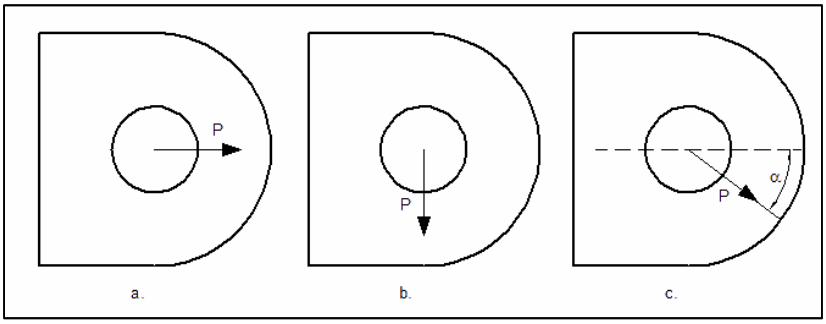

Figure 31: Three Lug Load Types a. Tension, b. Transverse, c. Oblique

The lower (aft wing spar) and upper link (front spar upper) attachments have the predetermined load direction, given that the reaction force is along the axis of the connecting rod member. The geometry of the lug for these is set such that there is only tension load. For the front spar lower attachments this is not the case, and these lugs have to be dimensioned using oblique loads (combination of the tensile and transverse) that are characterized by force and angle value. Pure tension lugs have typically three checks that they need to pass:

(a) Shear-bearing check

(b) Net tension check

(c) Yield check

The minimum margin of safety from these three checks is used as the critical margin of safety.

4.21.2 Nonlinear (Empirical Driven) Constraints for Optimization Challenge

Most of the empirical analyses use efficiency factors that are characterized by a functional curve of some sort. The geometrical parameter of the lug is used as an input to finding the efficiency factor, thus this ratio has to be automatically computed by the model as the functional response. The efficiency factors also depend on the lug material, and so that has to be taken into account. For the yield failure the yield factor needs to be computed. The yield factor curve is a discontinuous curve, which typically represents a challenge for setting up the model optimization without the use of the external responses.

An example curve is given by Figure 32. This curve is similar to the previously mentioned yield factor. Figure 33 represents generic function that will be used to explain the process of including these type of curves in the optimization setup. Figure 33 can be mathematically described with 30.

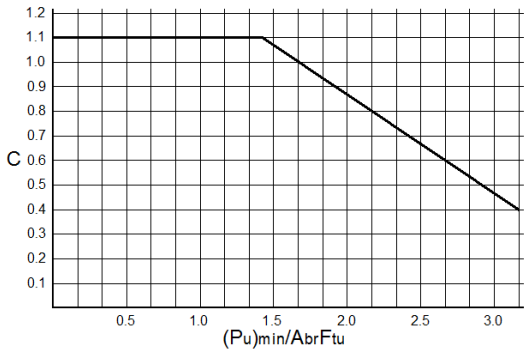

Figure 32 Example of the Discontinuous C Factor Curve

$$f(x) = \begin{cases} g(x), for\ x \geq a \\ b, for\ x \leq a \end{cases} \qquad \textbf{30}$$

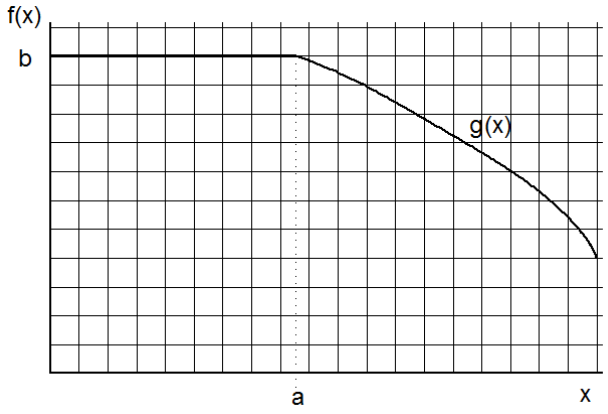

Figure 33 Generic Discontinuous Function

In a document based stress analysis this would be used by an analyst who would determine the value of the variable x, and then if the value of x is larger than a use the function g(x), and if x was less than value of "**a**" he/she would use the constant value b. If the traditional stress analysis is automated with some sort of computer based tool (could be a simple spreadsheet, or more elaborate program) the algorithm used for determining the value of f(x) would follow the logic depicted on with Figure 34.

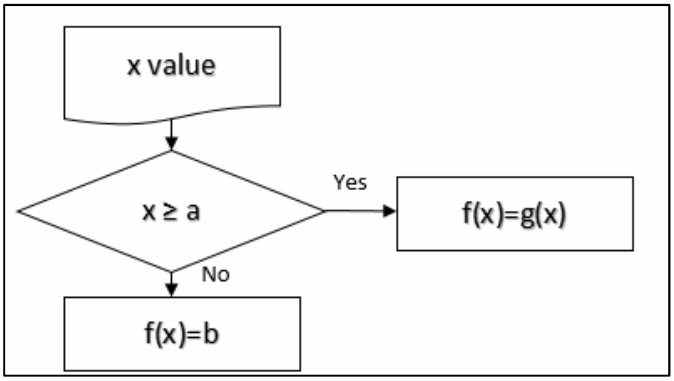

Figure 34 Discontinuous Graph Algorithm

As simple as it looks, the "if – else" statement is not available as one of the built-in functions in commercial common structural gradient based packages, such as Nastran or OptiStruct® (A-Optistruct). Therefore, if a response requiring the use of the discontinuous function needs to be used during the model setup, the typical path for creating these would be to use FORTRAN or C based external response.

Since creating external responses is not simple, and, more importantly, the since the common structural gradient based optimizers cannot create, at this time, approximate sensitivities with external responses, the approach of creating external responses is undesirable. A solution to this problem is the creation of a function that mimics the "if – else" statement using mathematical functions that are typically supported by the common structural gradient based solvers.

What one should be seeking is a function that provides a value of either one (1) or zero (0) depending on the argument value. Once this function is available, the function f(x) can be represented as a fairly simple function and does not require the use of the "if – else" logic. This binary type of the function can probably have many different mathematical formulations, but the one that will be denoted with the name "***SW***" is presented here and later used for various types of functional responses, has the form:

$$SW(x) = INT\left(\frac{MIN(x,a)}{a}\right) = \begin{cases} 1, for\ x \geq a \\ 0, for\ x \leq a \end{cases} \qquad \textbf{31}$$

This function is one of the key enablers for the optimization setup in the domain of the aerospace stress analysis, given that many allowable curves, knockdown factors, and other parameters have discontinuous nature that without function similar to SW function would require the use of the external response which would carry added complexity, and, as previously mentioned, significant time penalty related to the sensitivity calculation.

Using the above switch, the function f(x) (Figures 32 and 33) can be represented without the need for the "if-else" logics as:

$$f(x) = [1 - SW(x)] \cdot b + SW(x) \cdot g(x) \qquad \textbf{32}$$

4.21.3 Channel Angle Fittings

The front and aft engine fittings to the pylon box attachments can be typically categorized as tension fittings (of the channel or angle type). The typical configurations of the channel and angle fittings are depicted with the Figure 35.

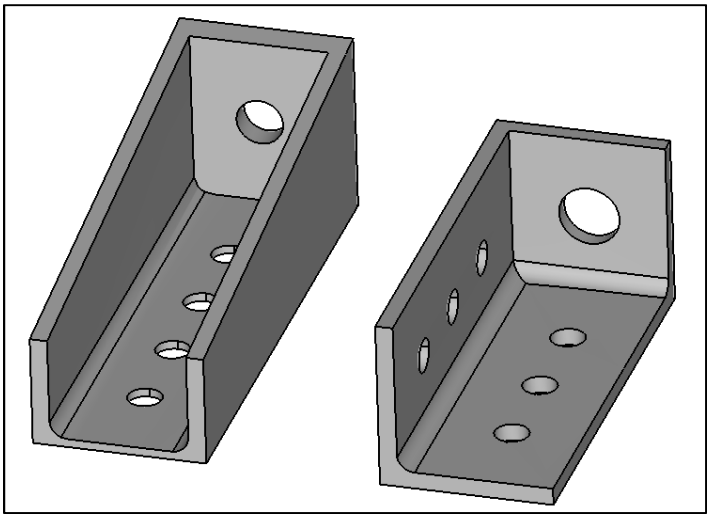

Figure 35 Channel and Angle Fitting

Qualifying these types of fittings using the model based strategy requires the extraction of the tension force coming from the tension bolt that acts on the force input hole. If that particular joint is modeled with a spring element, than the direct response measuring the tension force needs to be created. These types of fittings have recommended dimension relationships, as described in chapter nine of (N1988). For instance, the tension bolt pad height to the tension bolt hole ratio is recommended to be approximately equal to 3, and the width of the tension bolt pad to the tension bolt pad height ratio is recommended to be between 1.5 and 2.0. For this reason all of these ratios have to be calculated as functional responses communicating with the optimizer routines and the FEM. There are relationships between the thickness values themselves, thickness and diameter, thickness and wall widths/heights, and finally diameter and wall thickness/heights. These ratios need to be constrained to the recommended values (these recommended values often come from testing specimens that were used to qualify the fitting for analysis). Also some of these ratios are used to come up with the fitting factors. Given that these geometrical relationships are required to be constrained to some testing or empiric range, the functional responses related to them need to be generated. These functional responses will be functions of constant values (for instance bolt diameter), distance between nodes, and design variables (e.g. tension pad thickness).

The bolts need to be checked against the maximum ultimate tension force. This check needs to be done first, given that the diameter of the tension bolt determines the overall fitting dimensions.

The typical checks that are performed for the tension fitting walls are: (a) tension and (b) bending.

These checks will be sizing the fitting walls. The typical checks that are performed for the tension bold pad area are: (a) bending, and (b) shear thru the bolt hole. These checks will be sizing the tension bolt fitting pad.

Chapter 5: The Proposed Optimization Driven Model Based Process for Structural Certification - The Final Design Stage

5.1 The Final Design Phase

After the preliminary design phase model convergence has been achieved, the sizing values and any potential minor configuration changes need to be incorporated back into the external load FEM. Once the brand new set of loads (called final loads) are produced from the updated external load FEM these loads represent the basis for the pylon certification.

During the conceptual and preliminary design phases the optimization driven pylon sizing was using numerous FEM based responses as means of approximation of the closed form solutions. These surrogate methods still carry significant value even during the final design phase. At the end of the final design phase the government certification agencies still prefer strength, stability, and durability checks that can be documented and submitted for certification in the form of empirical based ones. Due to this fact the list of the checks needs to get amended with the empirical based optimization responses. This section will briefly discuss surrogate checks, since they still have their role. However, the focus will be on the processes of inclusion of the empirical based strength, stability and durability checks.

First let us remember which checks from the preliminary design phase are empirical based. The fastener shear and bearing checks, as well as the major fittings checks are all of the empirical type. These checks and their execution were already described during the preliminary design phase discussion, thus they will

not be further elaborated on in this section. Still, these checks will be performed during the final design now with the latest set of loads – the final loads - and with the lower margin of safety requirement.

The following strength and stability checks that were FEM based (direct responses) will have to be turned into the empirical responses:

(a) Cross sectional strength checks. The axial, bending, shear, stress as well as and stress interaction between previously mentioned stresses margin of safety need to be included into the model

(b) Cross section stability checks. Both buckling and crippling margins of safety need to be calculated, thus those have to be included into the model.

(c) Panel buckling checks

A key challenge in executing the above described checks is the generation of the functional responses that calculate the sectional and panel loads as well as the sectional properties. Since these challenges pose a significant obstacle for implementation of optimization within the aerospace engineering domain of practices, and since the detailed and practical elaboration on solution for these challenges will be provided in a special section, later on, these empirical optimization responses become a platform for comparing empirical solutions to the direct stress and stability FEM based responses.

In addition to the strength and stability checks in closed form, the fatigue check needs to be added during the final design phase. Determining the fatigue stress at the critical fatigue details poses a significant challenge. For the fastener joint details, the key challenge is how to determine the fatigue stress value given that due to the way the joint is modeled there is not enough detail for achieving correct stress extraction from the FEM. Similarly, for the open hole, the insufficient refinement of the FEM mesh does not allow for correct stress extraction out of the FEM. The solution for both of these challenges will be presented in the following sections. The solution makes it possible to effectively and quickly set up the fatigue based optimization for every single fastener joint and open hole in the pylon.

5.2 Extraction of Sectional Properties, Loads For Sections, Panels, and Joints Required for Empirical Evaluation Using Optimization Functional Response

5.2.1 The automation Platform for Certification Grade Stress/Stability Optimization Checks

Empirical based, certification grade, stress or stability margin calculations require two distinct scalar entities for the stress calculation. One is the sectional or panel defining geometric scalar entity such as area, moment of inertia, torsional constant, and etc. for a section, or panel dimensions and thickness for a panel. The other is the load component, such as axial force, shear force, bending moment, and etc. for the section and in-plane force traction for the panel. Extracting these types of the scalars from the coarse FEM is rather simple, and thus this type of the FEM has had major role in the pylon stress analysis for decades. However extracting these scalar entities from the detailed FEM represents a significant challenge. As previously mentioned, the detailed FEM possesses numerous advantages over the coarse FEM, including correct eigenvalue buckling predictions and direct access to fastener loads to name few. However the disadvantage of the detailed FEM lays in the complicated process of extraction of the load as well as section/panel geometrical feature entities (sectional forces, moments, area, and moments of inertia).

The proposed solution is to create a software automation platform that allows a stress analyst to easily generate large numbers of direct and functional responses required for optimizer to access sectional/panel geometrical and force components scalar entities. Effectively the tool that has been developed for this purpose produces all required responses to enable use of the closed form stress checks directly on top of the detailed FEM, effectively creating an integrated FEM / empirical- detail model that can obtain the sizing solution for the pylon structure using both direct responses, such as eigenvalues or principal stresses, as well as their empirical counterparts such as the Euler-Johnson buckling margin or Euler beam bending stresses. This type of the solution has many advantages over the other potential solutions of using the external responses for the empirical stress/stability responses.

The presented software package needs to be modular both in terms of types of the geometrical/functional features that it can process (sections, panels, fasteners, fittings), and the types of the checks that can be executed on these geometrical/functional entities.

Figure 36 shows how the modularity works. Each of the functional entities will be discussed in detail at later sections.

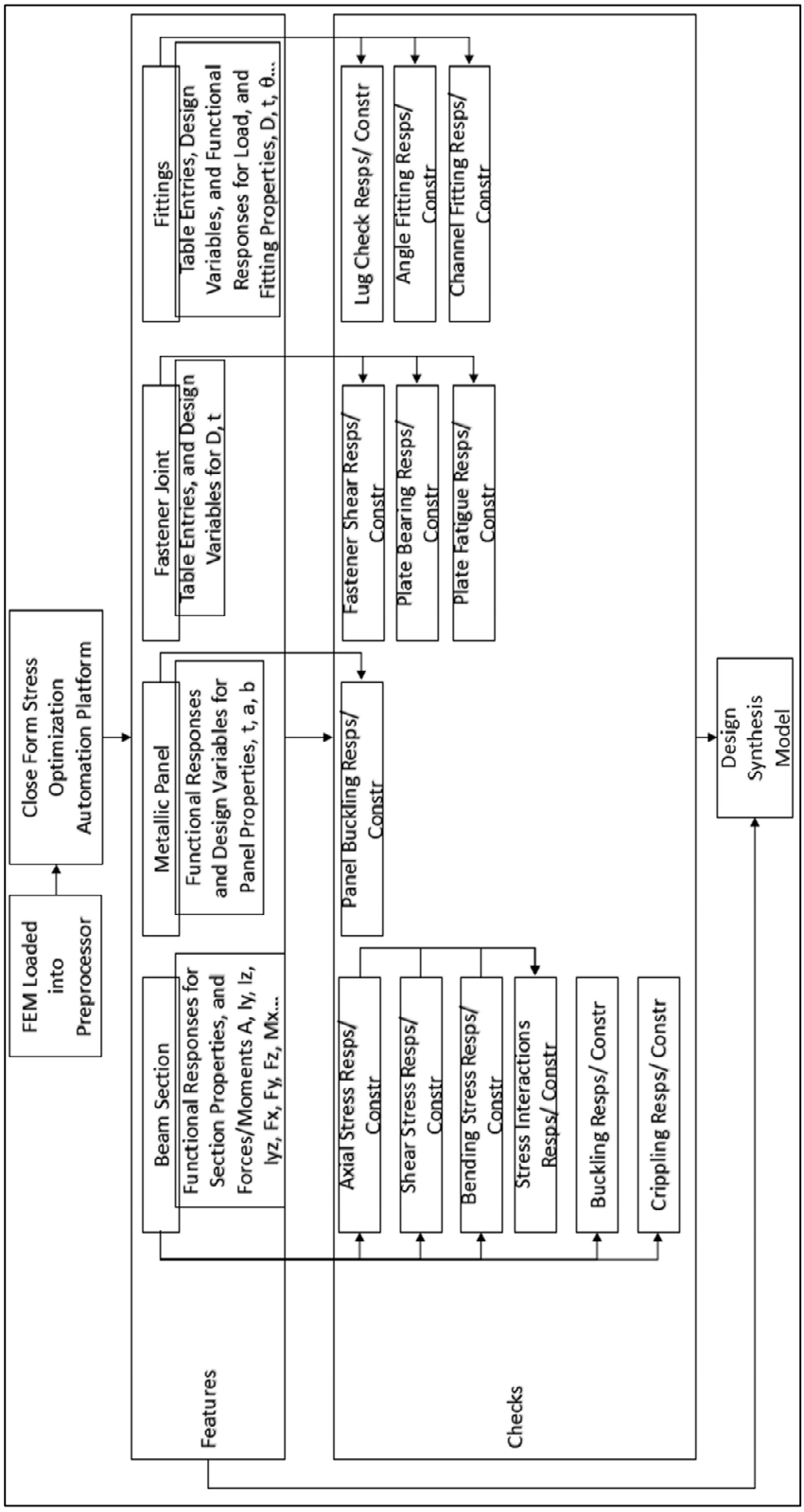

Figure 36 Modular Automation Platform (MAP)

5.2.2 Beam Section Feature

One of the often overlooked problem of structural model generation for design (but a FEM problem in general) is reducing the fidelity of the model, since this process requires certain assumptions to be made. The problem at hand is generating the section properties needed for the empirical stress calculation starting with the detailed FEM. But there is one additional level of complexity: Not only do the section properties need to be calculated once, they need to be submitted to the stress analysis as variables that depend on the shape of the section as well as the gauges of the section segments. Thus the section properties are inserted into the model as functional responses of the distances between the nodes that comprise the section and of the gauge design variables of the section segments, all referenced to the local coordinate system that is aligned with the beam axis. Schematics bellow will provide the basis for further discussion of the problems that exist when starting with the detailed FEM. One is to generate the functional responses of the scalar geometrical properties such as Area (A), first moment of area (Q), second order of inertias (I_y, I_z, I_{yz}), etc.

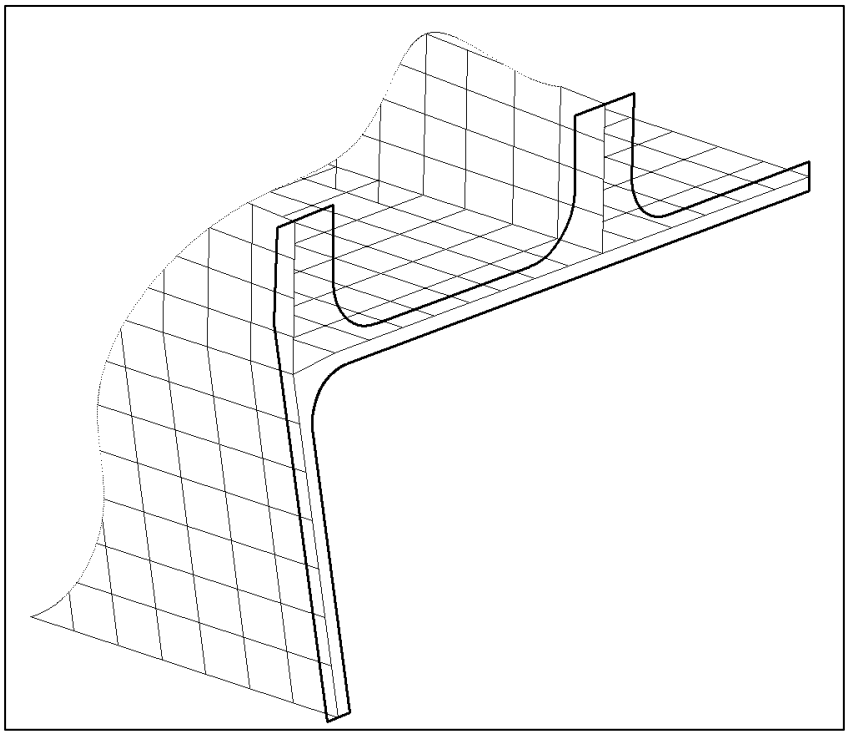

Figure 37 Geometrical Section in relation to detailed FEM

In Figure 37 the heavy line represents the actual geometry of the part that is modeled with the detailed FEM, there the mesh lines are represented by the lower thickness solid lines. In order to generate the sectional properties starting with the detailed FEM the section entities have to be identified. To do so, a set of nodes and elements needs to be defined. These are shown in Figure 38.

The nodal set required for the response creation is identified with the heavy dots, and the element set is shaded.

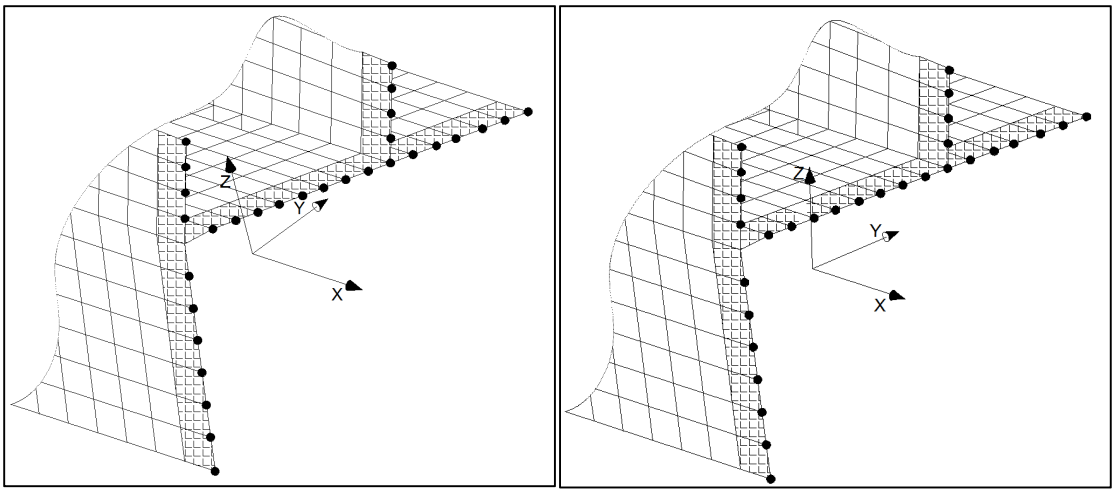

Figure 38 Nodal and Elemental Set

The complete algorithm required to build the sectional functional responses required for the closed form stress optimization will be provided later. Before that is done, however, a few important steps are required. First, a local coordinate system needs to be built. This system is going to be used as a reference for all of the response creation. The crucial property of this system is the alignment with the beam axis. The local coordinate system x axis needs to be aligned with the beam axis, thus the cross section itself will be residing in the y-z plane. The best way place the origin is in the geometrical centroid of the section, and it is practical to set the angle that the y axis forms with one of the major section segment to zero. The automation software platform can easily perform the system alignment. Two versions of the sectional coordinate system are shown in Figure 38. The image on the left shows the system not aligned with a sectional segment, and the one on the right shows the systems y axis aligned with the upper flange. As long as the x axis alignment is

correct and all of the responses are referenced to the same system each local systems should work for performing the downstream functional responses based optimization driven sizing.

5.2.3 Determining the Connectivity

For various types of beam checks different geometrical features are critical. All of these have to be taken into account in order to build sufficient information and fidelity into the functional responses. The different considerations are given in the list below:

(a) For bending check the outer-most fibers locations have to be checked for stress. Thus these locations have to be identified. Typically these locations are either on the junctions between the crippling segments or at the free edges of the part. These nodal locations need to be checked for the bending stress

(b) For shear stress the middle location of the shear web needs to be selected since the shear stress has parabolic distribution across the shear web and the maximum occurs at the middle of the web.

(c) For the crippling check it is necessary to determine the crippling segments, as well as whether the segment has free edges.

In order to better visually describe the algorithm for creating all of the necessary direct and functional responses required for the beam section checks let us number the nodes and elements of the example section. Later during the algorithm description these numbers will be useful for understanding the process.

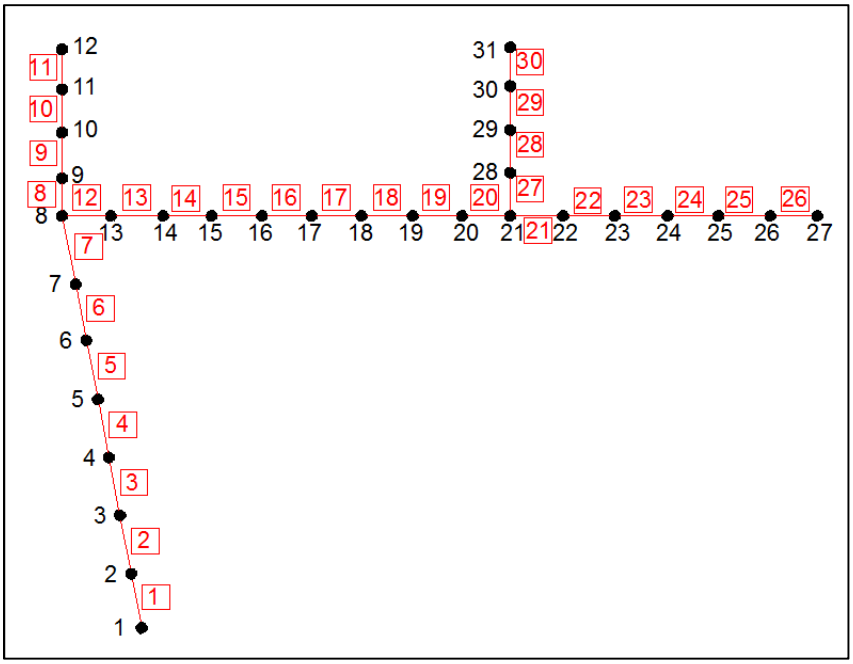

Figure 39 Example Section Node and Element Identification Numbers

The starting point for the response creation is a list of nodes and elements. At this point nodes and element lists are not related to one another, and that is the first thing that needs to be taken care of. Using the built in functions in the preprocessor the relationship between the nodes and elements is established using the connectivity functions. For instance node 1 has only one element from the element list (element 1) attached to it. In the ordered hash list the relationship will be denoted as {1} {1}, node 2 has two elements attached to it (elements 1 and 2), so the hash list would look like {2} {1 2}, continuing with this process the following hash table can be assembled.

{1} {1}	{7} {6 7}	{13} {12 13}	{19} {18 19}	{25} {24 25}	{31} {30 }
{2} {1 2}	{8} {7 8 12 }	{14} {13 14}	{20} {19 20}	{26} {25 26}	
{3} {2 3}	{9} {8 9}	{15} {14 15}	{21} {20 21 27}	{27} {26 }	
{4} {3 4}	{10} {9 10}	{16} {15 16}	{22} {21 22}	{28} {27 28}	
{5} {4 5}	{11} {10 11 }	{17} {16 17}	{23} {22 23}	{29} {28 29}	
{6} {5 6}	{12} {11 }	{18} {17 18}	{24} {23 24}	{30} {29 30}	

Table 6 Node to Element Connectivity Hash

It is obvious that based on the number of elements attached to a node certain conclusions can be made, even without knowledge of the actual section geometry. For instance the nodes that have only one element attached are the free edge nodes (nodes 1, 12, 27, and 31). The nodes that have more than 2 elements

attached represent the section junction nodes (nodes 8 and 21). Lastly the nodes that have exactly 2 elements attached to them represent web segment nodes.

If a reverse process is followed, a hash list formed by looking at the nodes attached to each individual element the result is nowhere as insightful, since each element will have exactly two nodes from the node set related to them, however this hash list is still very useful.

{1} {1 2}	{8} {7 8 }	{13} {13 14}	{19} {19 20}	{25} {25 26}
{2} {2 3}	{8} {8 9}	{14} {14 15}	{20} {20 21}	{26} {26 27}
{3} {3 4}	{9} {9 10}	{15} {15 16}	{21} {21 22}	{27} {21 28}
{4} {4 5}	{10} {10 11}	{16} {16 17}	{22} {22 23}	{28} {28 29}
{5} {5 6}	{11} {11 12}	{17} {17 18}	{23} {23 24}	{29} {29 30}
{6} {6 7}	{12} {8 13}	{18} {18 19}	{24} {24 25}	{30} {30 31}

Table 7 Element to Node Connectivity Hash

This list relates an element whose design variable defines the thickness of that element to the distance between two nodes. This list, then, relates the width of the rectangle to the height of that same rectangle, where a rectangle is a single element. This forms the basis for area calculation.

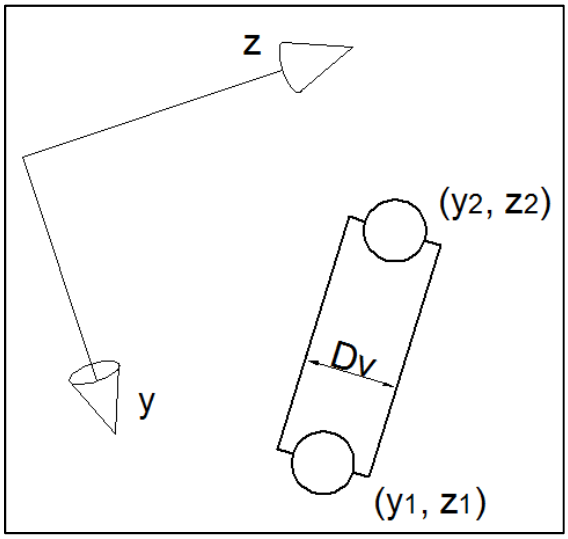

Figure 40 i^{th} Element Area Calculation

Looking at Figure 40 it is clear that the area of the i^{th} element in the cross section can be calculated using the formula:

$$A_i = dv_i\sqrt{\left(y_{2_i} - y_{1_i}\right)^2 + \left(z_{2_i} - z_{1_i}\right)^2} \qquad \textbf{33}$$

Where $\boldsymbol{dv_i}$ is the thickness design variable.

Now that we have the function for calculating the area of the single element, the area of the entire section area calculation becomes a simple summation of the individual elements' areas.

$$\mathrm{A} = \sum_{\mathrm{i}} \mathrm{A_i} \qquad \textbf{34}$$

The moment of inertia calculation is not that simple, since one needs to take into account both the parallel axis theorem and inclined axis second moments of inertia calculation.

Let us first address the inclined axis. In the Figure 41, a basic coordinate system for $\boldsymbol{i}^{\text{th}}$ rectangular segment of the section is identified. The Greek letters ψ, and ζ are used for denoting the basic segment coordinate system at the centroid of the segment.

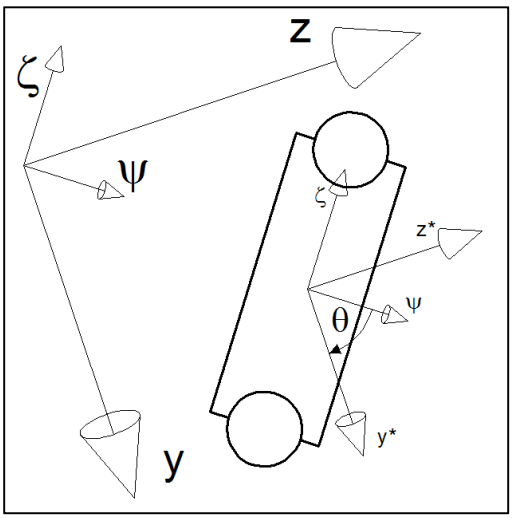

Figure 41 Basic Segment System With Respect to Sectional System

Given that each segment is always a rectangle, the moments of inertia about the segmental axis can be written as:

$$I_{\zeta_i} = \sqrt{\left(y_{2_i} - y_{1_i}\right)^2 + \left(z_{2_i} - z_{1_i}\right)^2} \cdot \frac{{dv_i}^3}{12}$$

$$I_{\psi_i} = dv_i \cdot \frac{\sqrt{\left(y_{2_i} - y_{1_i}\right)^2 + \left(z_{2_i} - z_{1_i}\right)^2}^3}{12} \qquad \textbf{35}$$

$$I_{\psi\zeta_i} = 0$$

Now, if θ is the angle between the ψ and y axis the moments of inertia of the ***i***th segment in the system parallel to the sectional coordinate system (system y*z*) can be written as:

$$I_{y^*_i} = I_{\psi_i} cos^2(\theta_i) + I_{\zeta_i} sin^2(\theta_i)$$

$$I_{z^*_i} = I_{\psi_i} sin^2(\theta_i) + I_{\zeta_i} cos^2(\theta_i) \qquad \textbf{36}$$

$$I_{y^*z^*_i} = \frac{\left(I_{\psi_i} - I_{\zeta_i}\right)}{2} \cdot \sin(2\theta_i)$$

In terms of the coordinates of the segment the q angle can be represented as:

$$A\theta_i = arctan\left(\frac{z_{2_i} - z_{1_i}}{y_{2_i} - y_{1_i}}\right) \qquad \textbf{37}$$

Now there is still a need to calculate the second moments of inertia correction for the distance between the center of area (COA) of the segment and the sectional coordinate system origin. To do so, first the COA location needs to be calculated. Using Figure 41 it is clear that the y coordinate of the COA of the ***i***th segment is just an average of the y coordinates of the nodal coordinates at the segment ends. Similarly, z coordinate of the COA of the ***i***th segment is the average of the z coordinates of the segment ends.

$$y_{COA_i} = \frac{y_{2_i} + y_{1_i}}{2}$$

$$z_{COA_i} = \frac{z_{2_i} + z_{1_i}}{2} \qquad \textbf{38}$$

Finally, the segmental second moments of inertia can be calculated using the parallel axes theorem as:

$$I_{y_i} = I_{y^*_i} + A_i \cdot {z_{COA_i}}^2$$

$$I_{z_i} = I_{z*_i} + A_i \cdot {y_{COA}}_i^2 \qquad \textbf{39}$$

$$I_{yz_i} = I_{y*z*_i} + A_i \cdot y_{COA_i} \cdot z_{COA_i}$$

To express the second moments of inertia of each individual segment exclusively as functions of grid locations and the design variables assigned to the shell elements, we now substitute all the above formulas into a single formula for each of the moments of inertia:

$$I_{y_i} = dv_i \cdot \frac{\sqrt{\left(y_{2_i} - y_{1_i}\right)^2 + \left(z_{2_i} - z_{1_i}\right)^2}^3}{12} \cdot cos^2\left[arctan\left(\frac{z_{2_i} - z_{1_i}}{y_{2_i} - y_{1_i}}\right)\right] + \sqrt{\left(y_{2_i} - y_{1_i}\right)^2 + \left(z_{2_i} - z_{1_i}\right)^2} \cdot \frac{{dv_i}^3}{12} \cdot sin^2\left[arctan\left(\frac{z_{2_i} - z_{1_i}}{y_{2_i} - y_{1_i}}\right)\right] + dv_i \cdot \sqrt{\left(y_{2_i} - y_{1_i}\right)^2 + \left(z_{2_i} - z_{1_i}\right)^2} \cdot \left(\frac{z_{2_i} + z_{1_i}}{2}\right)^2$$

$$I_{z_i} = dv_i \cdot \frac{\sqrt{\left(y_{2_i} - y_{1_i}\right)^2 + \left(z_{2_i} - z_{1_i}\right)^2}^3}{12} \cdot sin^2\left[arctan\left(\frac{z_{2_i} - z_{1_i}}{y_{2_i} - y_{1_i}}\right)\right] + \sqrt{\left(y_{2_i} - y_{1_i}\right)^2 + \left(z_{2_i} - z_{1_i}\right)^2} \cdot \frac{{dv_i}^3}{12} \cdot cos^2\left[arctan\left(\frac{z_{2_i} - z_{1_i}}{y_{2_i} - y_{1_i}}\right)\right] + dv_i \cdot \sqrt{\left(y_{2_i} - y_{1_i}\right)^2 + \left(z_{2_i} - z_{1_i}\right)^2} \cdot \left(\frac{y_{2_i} + y_{1_i}}{2}\right)^2 \qquad \textbf{40}$$

$$I_{yz_i} = dv_i \cdot \sqrt{\left(y_{2_i} - y_{1_i}\right)^2 + \left(z_{2_i} - z_{1_i}\right)^2} \cdot \left\{\frac{\left(y_{2_i} - y_{1_i}\right)^2 + \left(z_{2_i} - z_{1_i}\right)^2 - {dv_i}^2}{24} \cdot \sin\left[2 \cdot arctan\left(\frac{z_{2_i} - z_{1_i}}{y_{2_i} - y_{1_i}}\right)\right] + \left(\frac{y_{2_i} + y_{1_i}}{2}\right) \cdot \left(\frac{z_{2_i} + z_{1_i}}{2}\right)\right\}$$

The sectional second moments of inertia are the summation of the segmental moments of inertia across all of the segments:

$$I_y = \sum_i I_{y_i}$$

$$I_z = \sum_i I_{z_i} \qquad \textbf{41}$$

$$I_{yz} = \sum_i I_{yz_i}$$

Except for the area and moments of inertia of equivalent beam elements, in order to carry out the crippling calculations, crippling segments must be determined as well as boundary conditions (whether any of the segments has free edges). In order to determine the segments, it is necessary to survey the topology of the section and an algorithm needs to be developed that would execute this type of the section topology determination. Figure 42 shows the algorithm developed for the tool needed for this purpose.

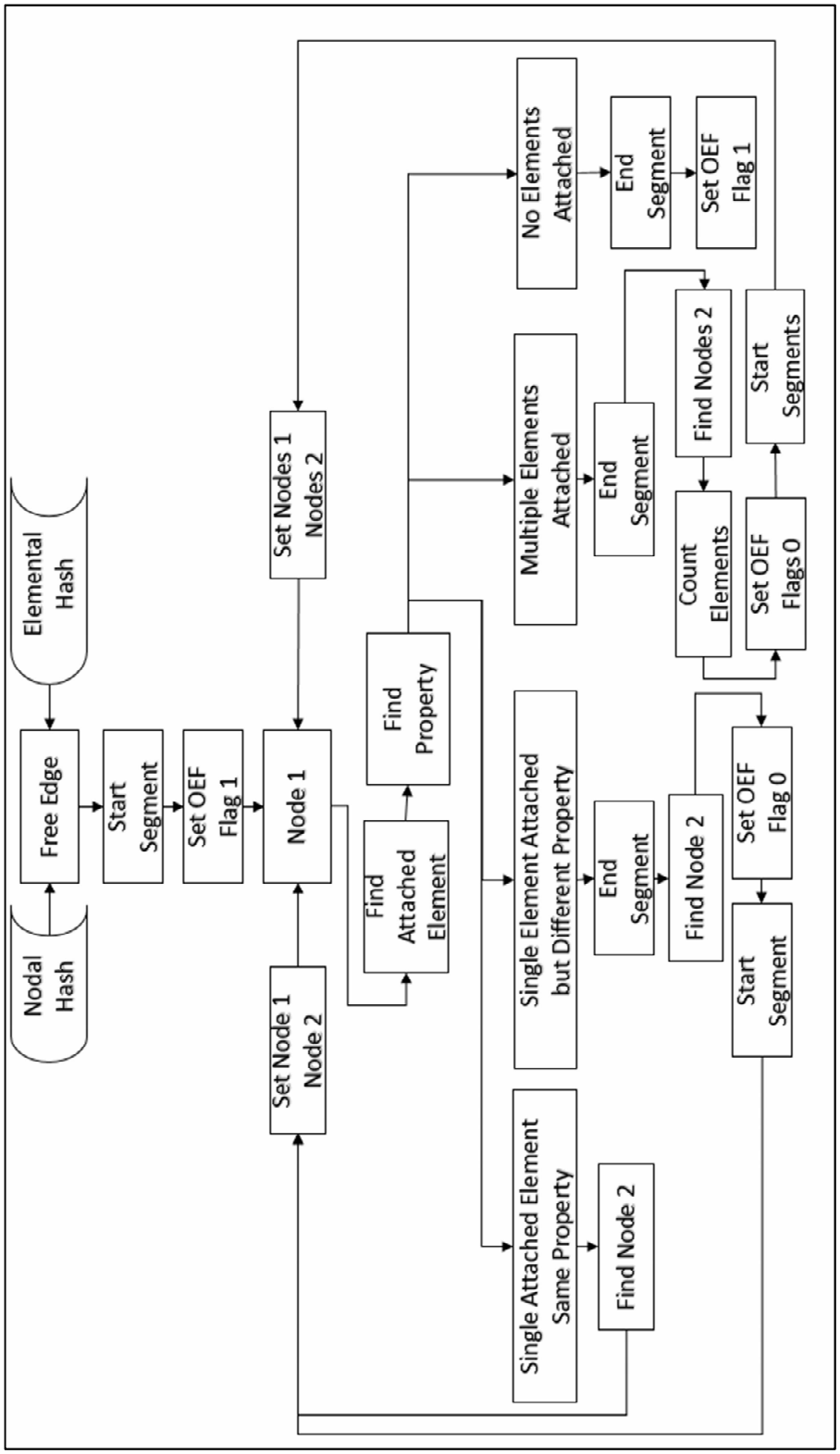

Figure 42 Crippling Segment Determination Algorithm

Some modern FEM / optimization solvers such as Altair's OptiStruct® (A-Optistruct) have built-in direct responses for the sectional forces an moments. These will be used in this work. However, since such responses are still unavailable for quite a few FE/optimization platforms, the functions required to calculate the sectional forces and moments as functional responses will be presented here.

From the section property calculation formulas it is rather clear that we need to have the nodal coordinates in the local sectional coordinate system available as direct responses. These will be used here to calculate the moment arms for each individual nodal force, but also to calculate the center of area of the section. The nodal forces will be required as well, and it is very important to create these direct responses in the local coordinate system to avoid any potential force vector transformation.

Nodal forces and moments serve as input for the sectional forces and moments calculation. Their summation should be done across the nodes while the sectional property summation was performed over the segments. Let us denote the nodes with the letter ***j***. In Figure 43 a segment with 2 nodes is shown, and for simplicity nodes 1 and 2 are shown. The force summation is simple and the sum over all j nodes gives the total force for three directions.

$$F_x = \sum_j F_{x_j}$$

$$F_y = \sum_j F_{y_j} \qquad \textbf{42}$$

$$F_z = \sum_j F_{z_j}$$

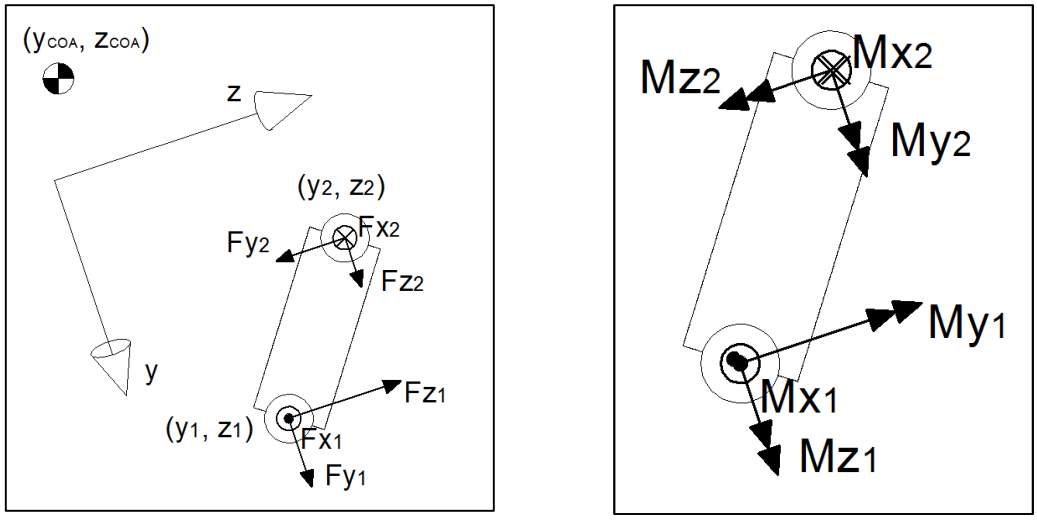

Figure 43 Nodal Forces/Moments for a Single Segment

The moment summation is somewhat more complicated. The three components of the moment from of the ***j***th node can be calculated as:

$$M_{x_j}^{Total} = M_{x_j} + F_{y_j} \cdot (z_j - z_{COA}) + F_{z_j} \cdot (y_j - y_{COA})$$

$$M_{y_j}^{Total} = M_{y_j} + F_{x_j} \cdot (z_j - z_{COA}) \qquad \textbf{43}$$

$$M_{z_j}^{Total} = M_{z_j} + F_{x_j} \cdot (y_j - y_{COA})$$

It is interesting to note that due to the fact that the x coordinate of all of the ***j*** nodes in a section is zero and the x_{COA} is zero, there are no contributions to the M_y and M_z from the F_z and F_y respectively.

Similar to the total force vector components, the sectional moment components are simple summation of the nodal contributions:

$$M_x = \sum_j M_{x_j}^{Total}$$

$$M_y = \sum_j M_{y_j}^{Total} \qquad \textbf{44}$$

$$M_z = \sum_j M_{z_j}^{Total}$$

5.2.4 Metallic Panel Feature

In a detailed FEM the panel would typically consist of multiple elements, and this poses a challenge in terms of extracting the panel stress values that are required for the empirical buckling prediction. In a coarse FEM one panel is typically represented by a single shell element, and in such a case values of the tractions Nx, Ny, and Nxy can be extracted, converted to stresses, and then compared to the critical compressive and shear stresses. The comparable approach for the detailed FEM would be to average the Nx, Ny, and Nxy values and then create the buckling margin calculation in the similar fashion.

In order to create all of the necessary responses required for panel buckling estimation, both the stress extraction as well as the identification of panel dimensions need to be executed automatically. From the selection of elements (represented as the interior of the dashed line in Figure 44) the corner nodes (represented with a circle in Figure 44) can either inferred or the nodes can be explicitly selected. Note that the x-y axes now are in the plane of the panel.

The design variable that is assigned to the panel property shell thickness is required both for the critical stress calculation as well as the true panel stress. Young's modus, and Poisson's ratio need to be extracted from the material card referenced by the shell property, and table entries need to be created for them. The minimal and maximal panel dimensions have to be calculated as a functional response, since if shape optimization is employed these could change during the optimization iterations (shape optimization is nor pursued here). The equations for the functional responses would be the simple minimum or maximum of four dimensions of the panel.

$$b = \min(A_1, B_1, A_2, B_2)$$

$$a = \max(A_1, B_1, A_2, B_2) \qquad \textbf{\textit{45}}$$

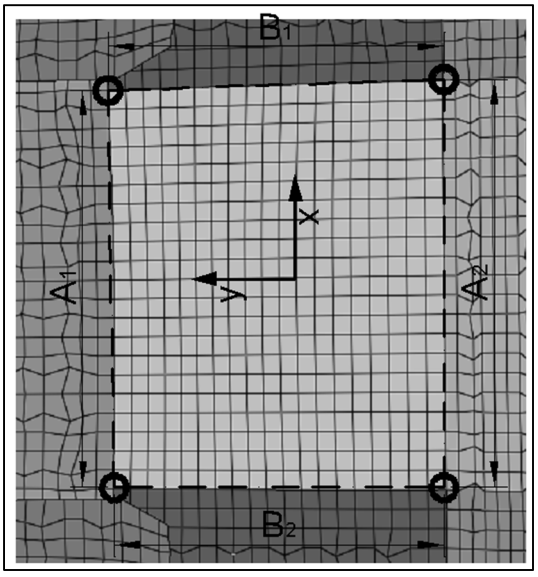

Figure 44 Panel Feature Selections and Orientation

The critical stress (allowable buckling stress) is calculated using the following equation (B1973):

$$\sigma_{cr} = \frac{\pi^2 E k_c}{12(1-\nu^2)}\left(\frac{t}{b}\right)^2$$

$$\tau_{cr} = \frac{\pi^2 E k_s}{12(1-\nu^2)}\left(\frac{t}{b}\right)^2 \qquad \textbf{46}$$

One of the responses that need to be calculated is the compressive and/or shear buckling coefficient (***k_c***, and/or ***k_s***). A sample graph for this coefficient can be found in Figure 45. The edge rotational restraint should not change during the optimization and needs to be chosen either based on previous experience or based on testing results. Once we have the right buckling failure curve selected based on the applicable rotational restraints the buckling coefficient needs to be calculated as the functional response. The automation of this process is also important if future shape optimization is carried out because during shape optimization the

aspect ratio of the panel (***a/b***) can change and the buckling failure coefficient would vary during the optimization.

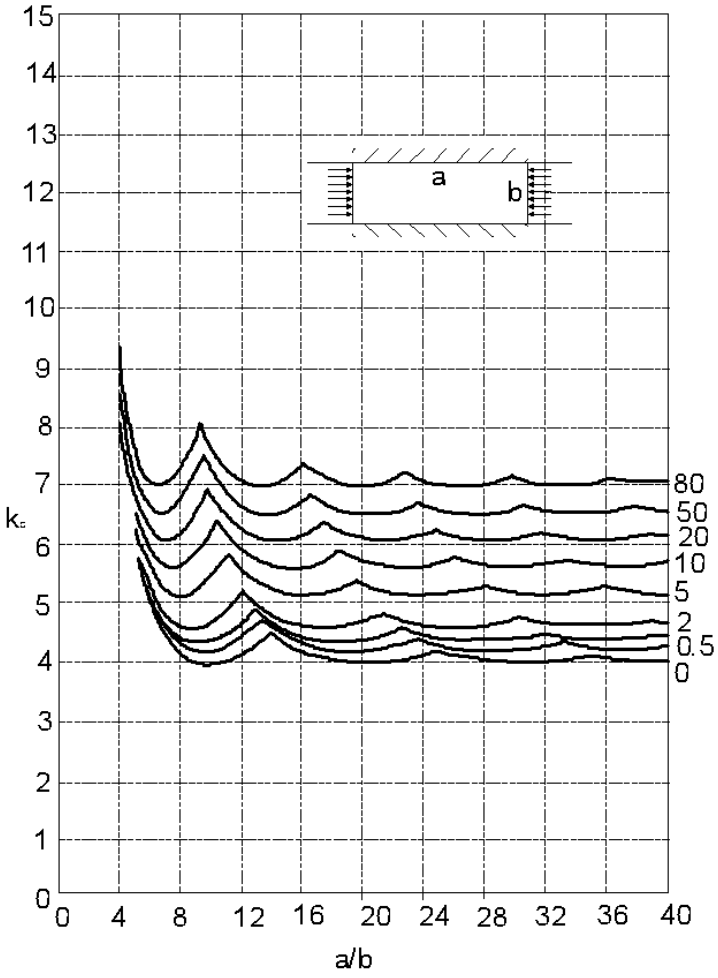

Figure 45 Compressive Buckling Stress coefficient of plates as a function of aspect ratio (a/b) for various amount of the edge rotational restraint (From (B1973))

Previously a switch function was described that allowed inclusion in the optimization process certain behavior functions that had a switch between one behavior and another. This can be used for the buckling Ks or Kc curves. Looking at Fig. 46, for example, the first part of the curve (first cusp) can be approximated with a second order polynomial $f_1(a/b)$, while the next cusps is significantly less pronounced and can be approximated with a log function $f_2(a/b)$.

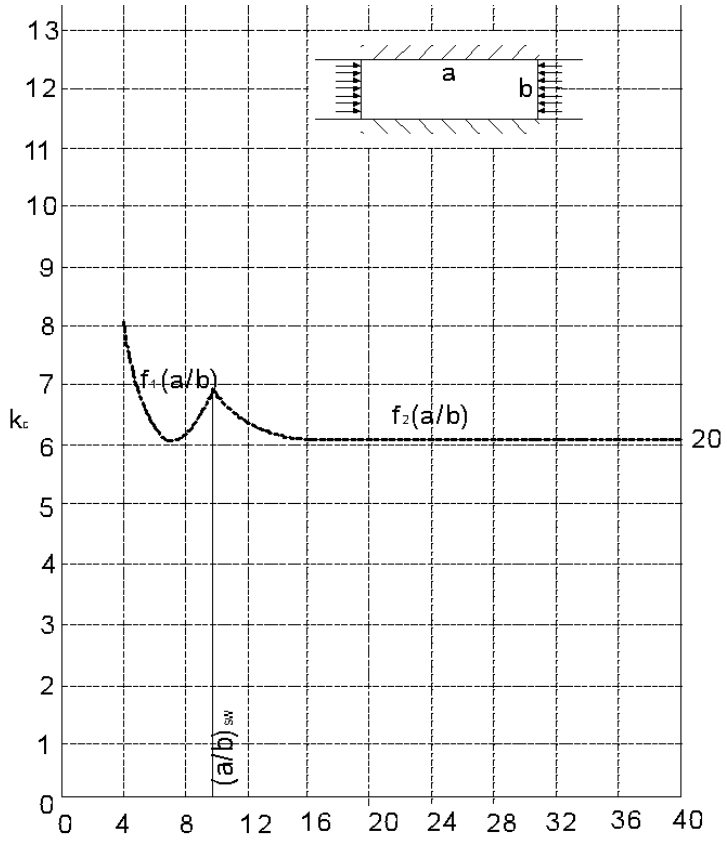

Figure 46 Simplified Version of the Compressive Buckling coefficient

For the response generation, the following functions can be used.

$$SW\left(\frac{a}{b}\right) = INT\left(\frac{MIN\left(\frac{a}{b}, \left(\frac{a}{b}\right)_{sw}\right)}{\left(\frac{a}{b}\right)_{sw}}\right) = \begin{cases} 1, for\ \frac{a}{b} \geq \left(\frac{a}{b}\right)_{sw} \\ 0, for\ \frac{a}{b} \leq \left(\frac{a}{b}\right)_{sw} \end{cases}$$

$$k_c\left(\frac{a}{b}\right) = \left[1 - SW\left(\frac{a}{b}\right)\right] \cdot f_1\left(\frac{a}{b}\right) + SW\left(\frac{a}{b}\right) \cdot f_2\left(\frac{a}{b}\right) \qquad \textbf{47}$$

All the required values needed for the allowable calculation are now in place, so the remaining response needed for the margin calculation is the actual panel stress.

Following what typically would be done with the coarse load FE model, extracting the traction values from the shell element representing the panel (N_x, N_y, and N_{xy}), and dividing them with the thickness, the actual panel stress can be calculated as the average of traction values from the elements defining the panel

divided by the panel thickness. Note that we have an opportunity here to use more or less conservatism by selecting the stresses used in the optimization to be higher or lower than the average stress.

$$\sigma_{act} = \frac{Avg(Nx)}{t}$$

$$\tau_{act} = \frac{Avg(Nxy)}{t} \qquad \textbf{48}$$

5.3 Fastener Joint Feature

Two checks are necessary to substantiate the static strength of every fastener joint in the pylon structure:

(a) Fastener shear and axial strength

(b) Bearing stress of the attached plates

As previously described, the detailed FEM needs to have the fastener joint modeled with the combination of rigid and spring elements. Other, a bit more sophisticated, models of fastener joints can be used as well, as long as the discrete element exist from which the load information can be extracted by the optimization responses.

The following are the formulas needed to substantiate the fastener joint.

Fastener shear:

$$MS_{Fs} = \frac{F_{Su} \cdot T_{kd}^{s} \cdot k_{pb} \cdot K_{ds}}{F_s} - 1 \qquad \textbf{49}$$

F_{su} is the shear allowable for the fastener, $T_{kd}^{s}$is thermal knockdown factor, and $\boldsymbol{k_{pb}}$ is the post-buckling knock-down factor, and double shear factor is defined as:

$$K_{ds} = \begin{cases} 1.0, for\ Single\ Shear \\ 2.0, for\ Double\ Shear \end{cases} \qquad \textbf{50}$$

Shear force $\boldsymbol{F_s}$, has to be calculated as the functional response using the simple square root of the in-plane force ($\boldsymbol{F_x}$ and $\boldsymbol{F_y}$ direct responses) squared.

$$F_s = \sqrt{F_x^2 + F_y^2} \quad \textbf{51}$$

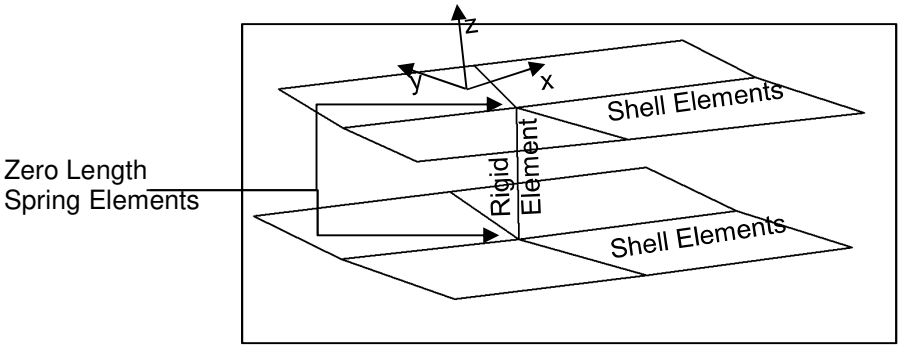

Figure 47 Fastener Joint FEM Representation

Fastener axial check margin is going to be calculated using the functional response with the following function:

$$MS_{FA} = \frac{F_{Au} \cdot T_{kd}^{A} \cdot k_{pb}}{F_z} - 1 \quad \textbf{52}$$

$\boldsymbol{F_{Au}}$ is the axial allowable for the fastener, $T_{kd}^{A}$is thermal knockdown factor, and $\boldsymbol{k_{pb}}$ is the post-buckling knock-down factor. $\boldsymbol{F_z}$ is a direct response from the spring element defining the interface between the fastener and the fastened plate.

Bearing margin needs to be calculated as the functional response using the following function:

$$MS_{Fbr} = \frac{F_{bru} \cdot T_{kd}^{br} \cdot k_{pb}}{F_{br}} - 1 \quad \textbf{53}$$

$\boldsymbol{F_{bru}}$ is the plate specific bearing allowable, $T_{kd}^{br}$is thermal knockdown factor, and $\boldsymbol{k_{pb}}$ is the post-buckling knock-down factor. $\boldsymbol{F_{br}}$ is a functional response calculated as:

$$F_{br} = \frac{F_s}{t \cdot D} \quad \textbf{54}$$

where the plate thickness (***t***) is coming from the design variable, and ***D*** is the fastener diameter and is input into the functional response and the table value since it has a constant value for a given fastener joint configuration.

It is worth mentioning here is that the bearing margin needs to be calculated for each plate that is connected with the fastener joint. So for instance, if two plates are connected there should be two bearing margins calculated.

5.4 Fitting Features

Typical fittings that need to be sized in a pylon are lugs, angle, and channel (also known as “bathtub”) fittings.

5.4.1 Lugs

Typical pylon lug analysis is based on the empirical method. That is, physical testing is performed for various lug geometries, materials, and loading conditions, the failure loads are recorded, and then curve fitting is used to prepare efficiency coefficient plots. For brevity, only lug axial load analysis conversion for the optimization process will be described here, based on the information from (N1988) the transverse and oblique loading optimization cases are very similar.

Two failure modes dominate the axially loaded lug analysis: Tension and shear failure. These two failure modes are shown in Figure 48.

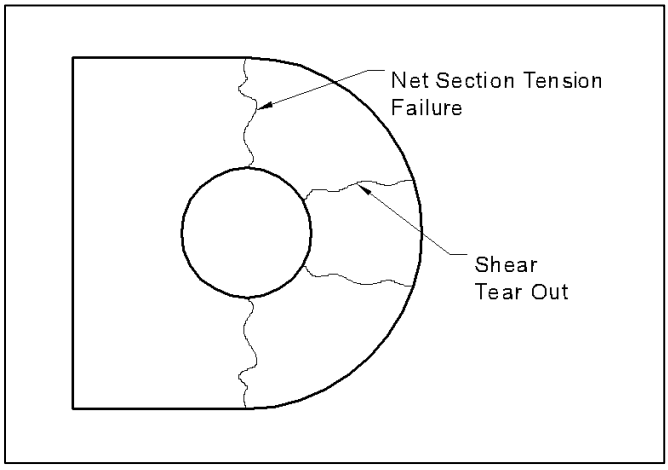

Figure 48 Axially Loaded Lug Failure Modes

The shear tear-out failure margin:

The shear tear out allowable load is calculated as a functional response using the following formula:

$$P_{bru} = k_{br} \cdot F_{tux} \cdot A_{br} \qquad \textbf{55}$$

F_{tux} represents the ultimate tensile strength of the material in the loading direction, and $\boldsymbol{A_{br}}$ is the projected bearing surface (***D*t***). There is not much to note about these values, except, maybe, that $\boldsymbol{F_{tux}}$ is a temperature dependent constant, D is a true constant and the thickness (***t***) would be a design variable in the optimization setup. What is worth discussing is the $\boldsymbol{k_{br}}$ which is the shear-bearing efficiency factor and is typically provided in the literature in graphical form.

Example from (N1988) is given in Figure 49. It can be seen that the $\boldsymbol{k_{br}}$, and thus the allowable load is the function of the design variables of the lug, namely the ***D/t*** and ***a/D*** ratios. Therefore, this allowable will be created as the functional response. The typical difficulty with these types of the allowable values is the fact that the testing values are only provided for discrete values of the ***D/t***. And so if this ratio changes the value (and it does since the thickness – ***t*** is typically the design variable) the allowable related to the efficiency factor needs to "jump" from one to the next curve, or, even worse, there might not be a curve in the graph that corresponds to every possible ratio of D/t that an optimizer can generate and for a response is needed.

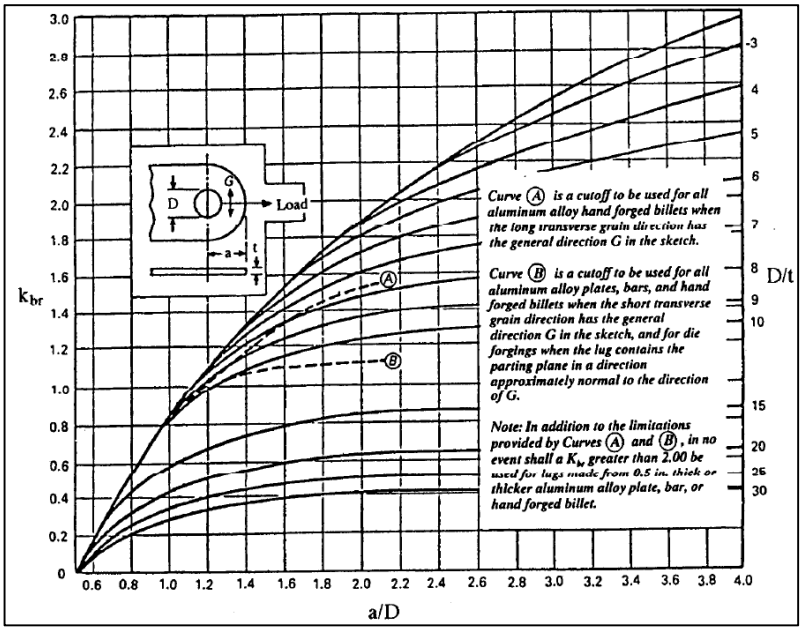

Figure 49 Example Shear Bearing Efficiency Factor for an aluminum alloy (from (N1988))

These types of graphs often represent significant challenge for the certification grade optimization setup. The following few paragraphs will describe an effective and practical way of solving this problem.

It is a fair assumption that every curve on the Figure 49, or any similar type of graph can be represented with a polynomial. For simplicity, only few curves from Figure 49 are considered for describing the solution. However the same general principle can be used with any number of curves. Figure 50 has only 5 curves pulled from the Figure 49.

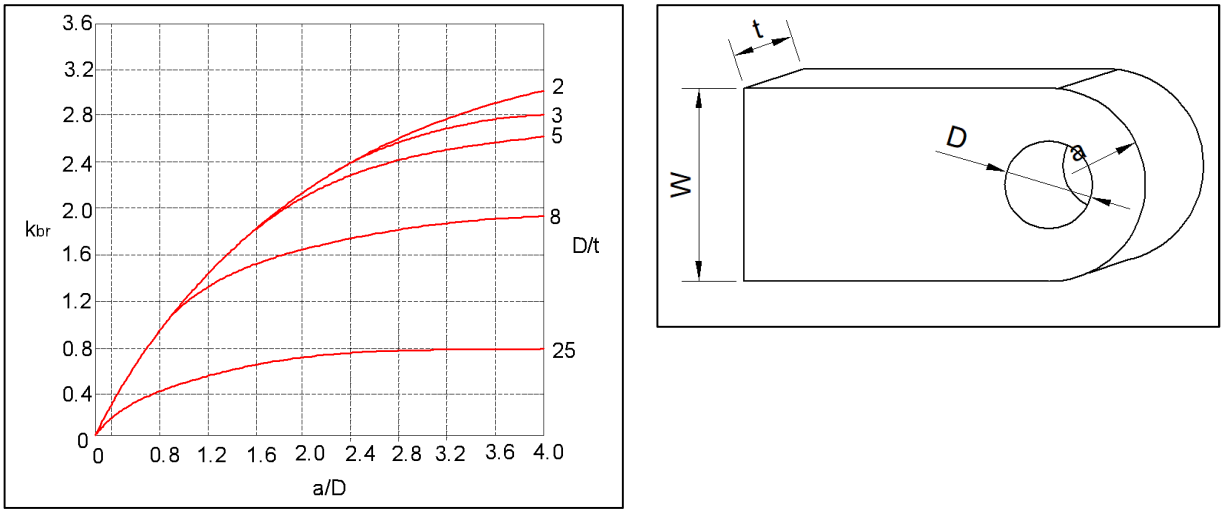

Figure 50 Few representative curves form the Shear Bearing Efficiency Factor

Figure 51 shows the result of fitting polynomials to example curves.

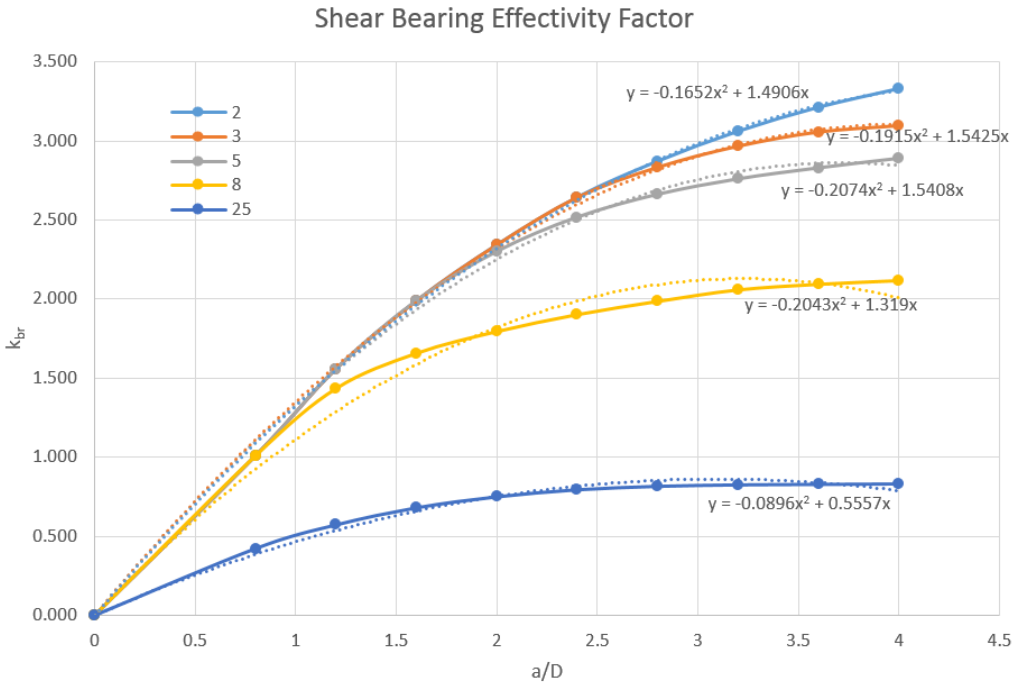

Figure 51 Trend Lines and Corresponding Second Order Polynomial Functions

Now if one collects the polynomial factors (a_1 and a_2) for the D/t ratios with Table 8 .

D/t	a_2	a_1
2	-0.1652	1.4906
3	-0.1915	1.5425
5	-0.2074	1.5408
8	-0.2043	1.319
25	-0.0896	0.5557

Table 8 Polynomial Factors

Linear interpolation is now used across the (D/t) range for the a1 and a2 coefficients. The resulting linear functions represent the basis for predicting the polynomial factors for any potential value of the D/t ratio:

$$a_1 = -0.044 \cdot \left({}^{D}/_{t}\right) + 1.6677 \qquad \textbf{56}$$

$$a_2 = 0.0044 \cdot \left({}^{D}/_{t}\right) - 0.2092$$

Using these equations every curve from the Figure 51 can be represented with the following equation:

$$k_{br} = \left(0.0044 \cdot \left({}^{D}/_{t}\right) - 0.2092\right) \cdot \left(\frac{a}{D}\right)^2 + \left(-0.044 \cdot \left({}^{D}/_{t}\right) + 1.6677\right) \cdot \frac{a}{D} \qquad \textbf{57}$$

Now that we have all of the necessary functions, constants, and design variables defined and/or identified, the remaining part is to recover the actual load that the lug experiences so that the margin calculation can be performed. This is achieved by modeling the lug interface with a spring element as shown in Figure 52.

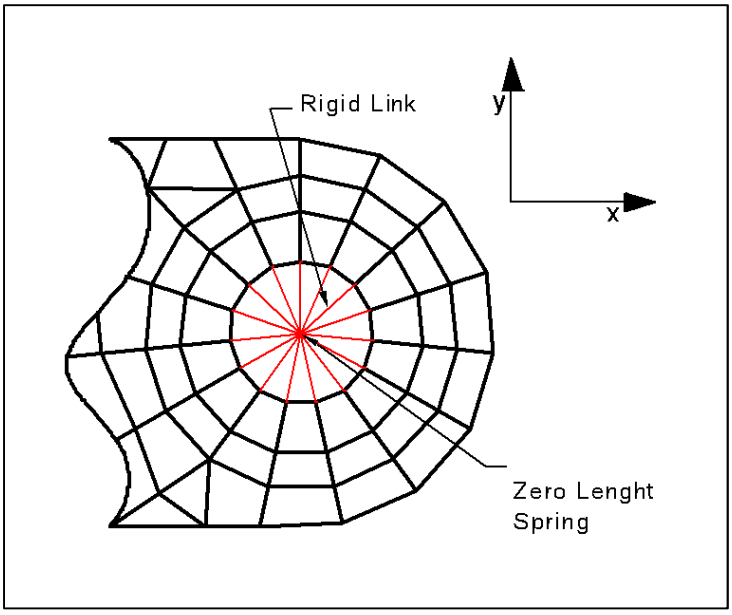

Figure 52 FEM Lug Modeling for Force Extraction

The direct response measuring the F_x force from the zero length spring element needs to be created. With that response the margin of safety calculation for the lug shear tear out failure becomes another functional response using the following function.

$$MS_{TearOut} = \frac{P_{bru}}{F_x} - 1 \qquad \textbf{58}$$

Net Section Tension Margin:

Similar to the shear tear out failure margin calculation, the net section tension allowable value is calculated:

$$P_{tu} = k_t \cdot F_{tux} \cdot A_t \qquad \textbf{59}$$

F_{tux} represents the ultimate tensile strength of the material in the loading direction, and A_t is the net section area calculated as:

$$A_t = (W - D) \cdot t \qquad \textbf{60}$$

The net tension efficiency factor (k_t) is determined by the curve from the Figure 53.

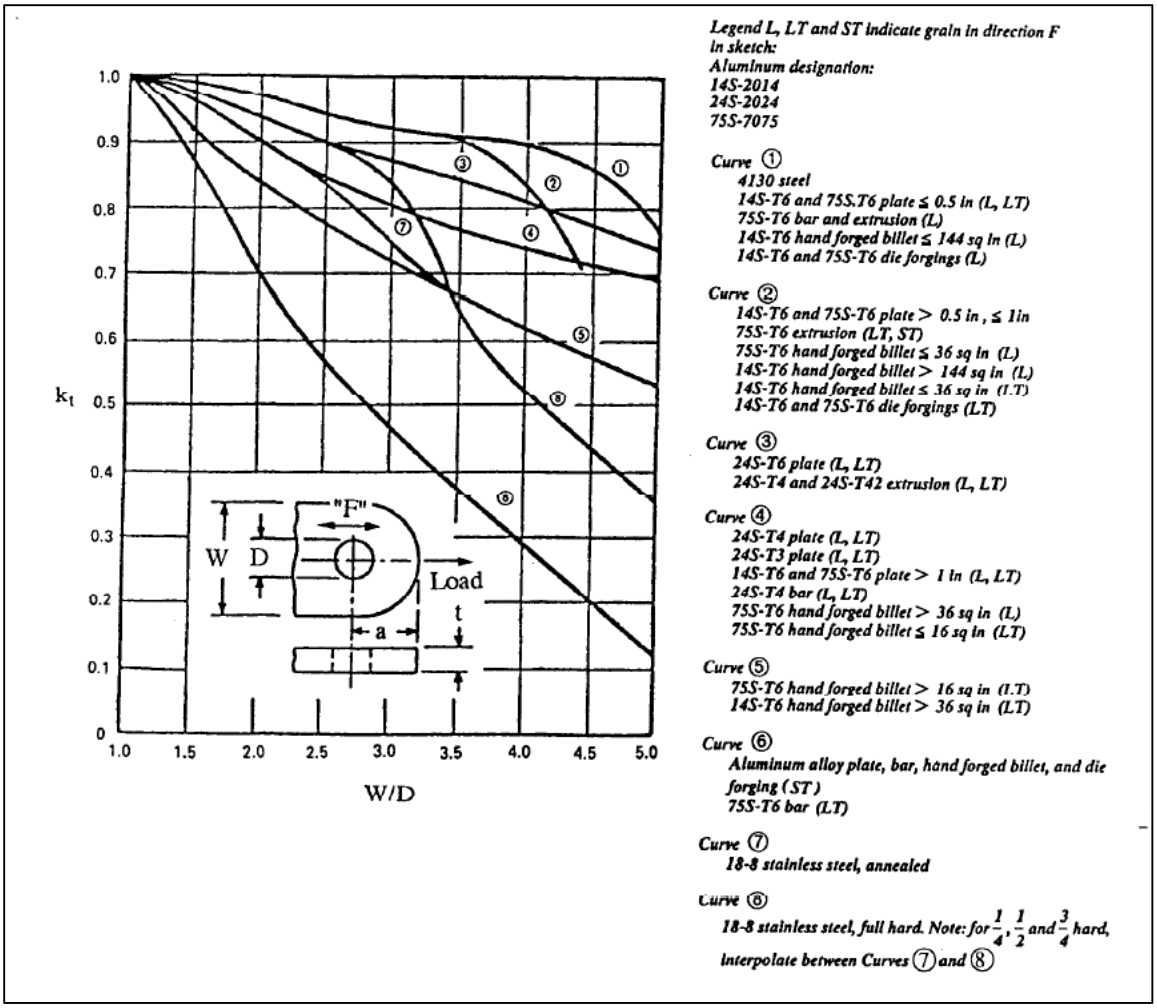

Figure 53 Net Tension Efficiency Factor (N1988)

The net tension efficiency factor is the function of the material and the W/D ratio, which is typically constant. Therefore this factor in the optimization setup can be inserted as a table value (there is no need to calculate it as a functional response).

Finally the margin of safety for the net section tension failure can be setup as a functional response using the formula:

$$MS_{NetTension} = \frac{P_{tu}}{F_x} - 1 \qquad \textbf{61}$$

5.4.2 Angle / Channel Fittings:

Angle and channel fitting analyses are very similar, so for the brevity, only the angle fitting optimization sizing setup will be described. The strength analysis formulas are taken from Chapter 9 of (N1988).

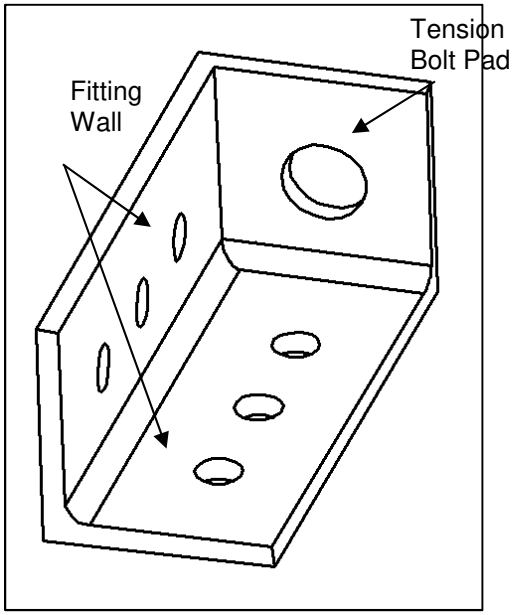

Figure 54 Angle Fitting Features

The typical checks that are performed for the tension fitting walls are tension and bending.

This check, per (N1988), is performed as a section check of the fitting walls (see Fig. 55)). The section feature described previously is used.

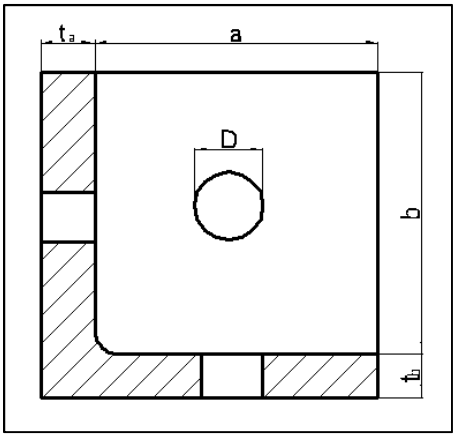

Figure 55 Fitting Wall Section Evaluated using Cross Section Feature

The typical checks that are performed for the tension bold pad area are bending and shear thru the bolt-hole.

For the bending stress allowable functional response the following equation is used:

$$f_{bu} = \frac{k_a \cdot P}{t_c^2} \qquad \textbf{62}$$

Where the k_a is coefficient of the fitting end that is available from the graph shown in Figure 56, which is either a constant if shape optimization is not employed and used as a table value, or calculated as the functional response if shape optimization is used.

P is the direct response from the zero length spring element that is placed in the FEM to represent the interface for the load application. This is done exactly in the same way as it was described for the lug analysis. t_c is the thickness of the tension bolt pad area.

The margin calculation is a functional response using the following equation:

$$MS_{Bend} = \frac{F_{tu}}{\lambda \cdot f_{bu}} - 1 \qquad \textbf{63}$$

Where λ is the fitting factor and is typically set to 1.15.

Shear stress allowable for the tension bolt pad is calculated as a functional response using the following equation:

$$f_{su} = \frac{P}{0.6 \cdot \pi \cdot D_w \cdot t_c} \qquad \textbf{64}$$

Where D_w is the washer diameter, and the factor 0.6 is used to represent 60% effectiveness of the shear area.

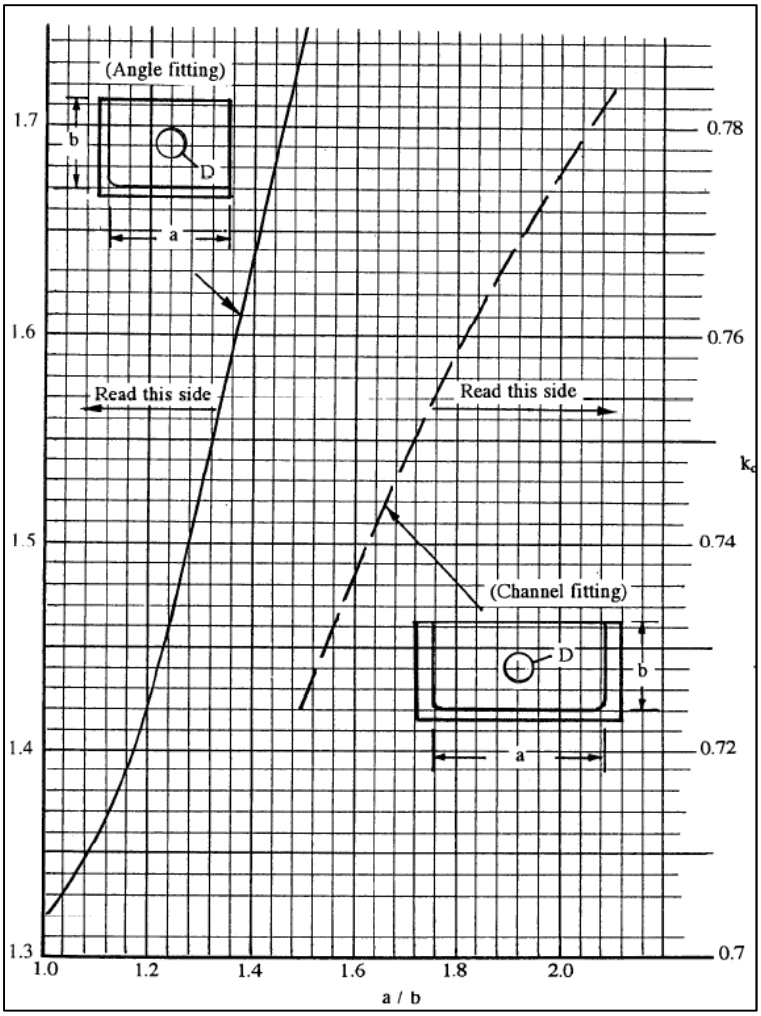

Figure 56 Coefficient of Fitting End (N1988)

The margin calculation for shear stress of the bolt tension pad is a functional response using the following equation:

$$MS_{shear} = \frac{F_{su}}{\lambda \cdot f_{su}} - 1 \qquad \textbf{65}$$

A fitting factor of 1.15 is still recommended, and F_{su} is the shear ultimate strength of the material.

5.5 Fatigue Checks

Now that stress/stability in the detailed design phase have been completed, fatigue checks need to be performed. As previously described, the main inputs for the fatigue margin calculation of the joint details

are: the number of cycles (flights), maximum tensile (f_{max}) and R ratio (R ratio being the ratio between the max tensile and max compressive stress) during the typical flight for the critical detail, and the number of cycles for each flight.

It is safe to assume that for each typical flight segment (taxi, take-off, initial climb...) the entire pylon as the part of the under-the-wing package will experience same flight excitation spectrum. Knowing this and extracting the maximum and minimum stress for each flight segment, the fatigue margin can be calculated using the rainfall algorithm, appropriate S-N curves, and Palmgren-Miner's rule.

The key challenge with this process is automated stress extraction. This section describes how the fatigue process can be included into the optimization driven model based model.

The extreme external load condition of each flight segment needs to modeled with a consistent equivalent static external load applied at both pylon and nacelle CGs. The total number of loading conditions can be significant, depending on level of detail each flight segment is broken into. As previously described, for the fatigue analysis the key hurdle is determining the fatigue stress at the fastener joints, given that due to the way the joint is modeled with FEM there is no sufficient detail for achieving correct stress extraction directly from the FEM.

The approach used here is to recover stresses (sometimes called far filed stresses) for each fastener joint in two orthogonal direction and use the resultant of the maximums in both directions as the reference stress. The actual stress is then calculated using the appropriate stress intensity factor for the fastener joint.

There are certain modeling requirements that need to be fulfilled:

(a) There should be exactly 4 quad shell elements around the zero length spring element that models the interface between the fastener joint and the plate being fastened
(b) The shell elements material orientation matches the orientation of the zero length spring element

For each of the four quad elements N_x and N_y direct responses need to created. Next, two functional responses calculating the average N_x values need to be created. One average is calculated for the negative and one for the positive side of the zero length spring elements.

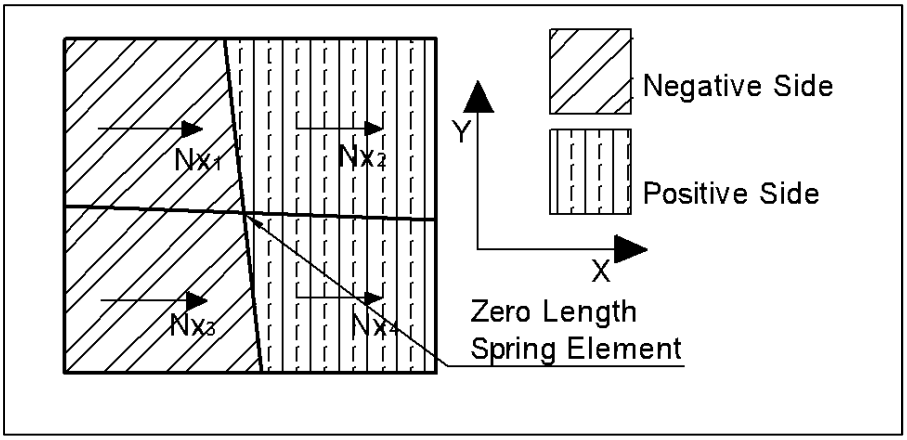

Figure 57 Average N_x Functional Response Explanation

Similarly the average N_y average functional responses need to be created.

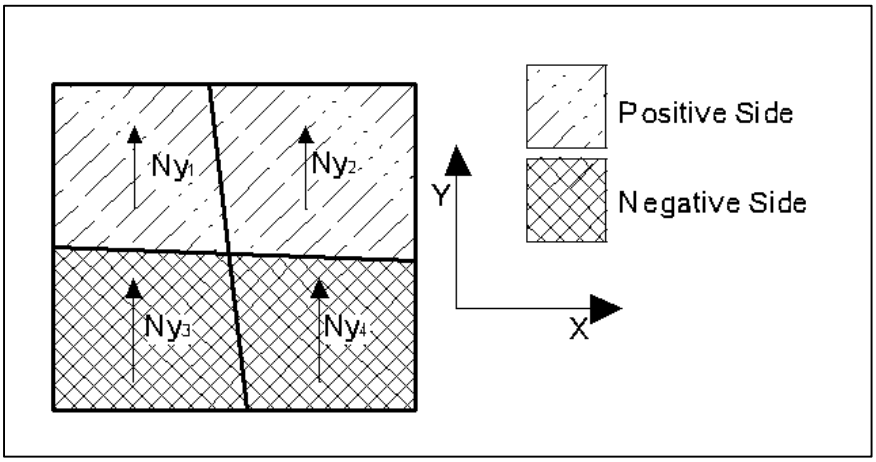

Figure 58 Average N_y Functional Response Explanation

If one denotes the average responses N_x^+, and N_x^- for the traction values related to the x-direction, then the functional average response, based on the Figure 57 elements arrangement, would be calculated as:

$$N_x^+ = \frac{N_{x2} + N_{x4}}{2} \qquad \textbf{66}$$

$$N_x^- = \frac{N_{x1} + N_{x4}}{2}$$

Similarly for the tractions in the y-direction based on the Figure 58:

$$N_y^+ = \frac{N_{y1} + N_{y2}}{2} \quad \textbf{67}$$

$$N_y^- = \frac{N_{y3} + N_{y4}}{2}$$

The reference stress would be calculated as the square root of the maximum traction values for both directions, divided by the thickness to obtain the stress units.

$$f_{ref} = \frac{\sqrt{\max(N_x^+, N_x^-)^2 + \max\left(N_y^+, N_y^-\right)^2}}{t} \quad \textbf{68}$$

Now that the reference stress is calculated, the actual stress that the fastened plate "sees" can be calculated using the stress concentration for the open hole:

$$f_{act} = f_{ref} \cdot K_T \quad \textbf{69}$$

The actual stress is now used to read the number of the cycles that the fastener detail can take under the given cyclic load (n_1). Comparing this number to the number of cycles that is calculated based on the planned service life of the airplane (N_1) one gets the damage index that a particular segment of flight inflicts on this particular joint.

This process is now repeated for all of the constant amplitude loads segments that the actual flight spectrum is broken down into (using the rain-fall algorithm), effectively calculating all of the damage index values that are then combined into the summation per the Palmgren-Miner's rule equation 5.

Chapter 6: The Test-Case Pylon Used for Comparing the Document Based and Model Based Sizing Processes

6.1 The Test Case Pylon and the Design Problem

The test-case engine pylon used for the comparing the document based sizing process and the newly proposed model based approach is shown with Figure 59. The key dimensions are driven by the integration requirement for the full propulsion package, where the aerodynamic requirements are the most important ones. The gauges and cross-sectional dimensions of all structural components as well as the number of fasteners and their diameters, are estimated by the design team based on engineering experience and past designs. The work here focuses on sizing type optimization that has to be tackled and fully understood first before proceeding to shape and topology optimization.

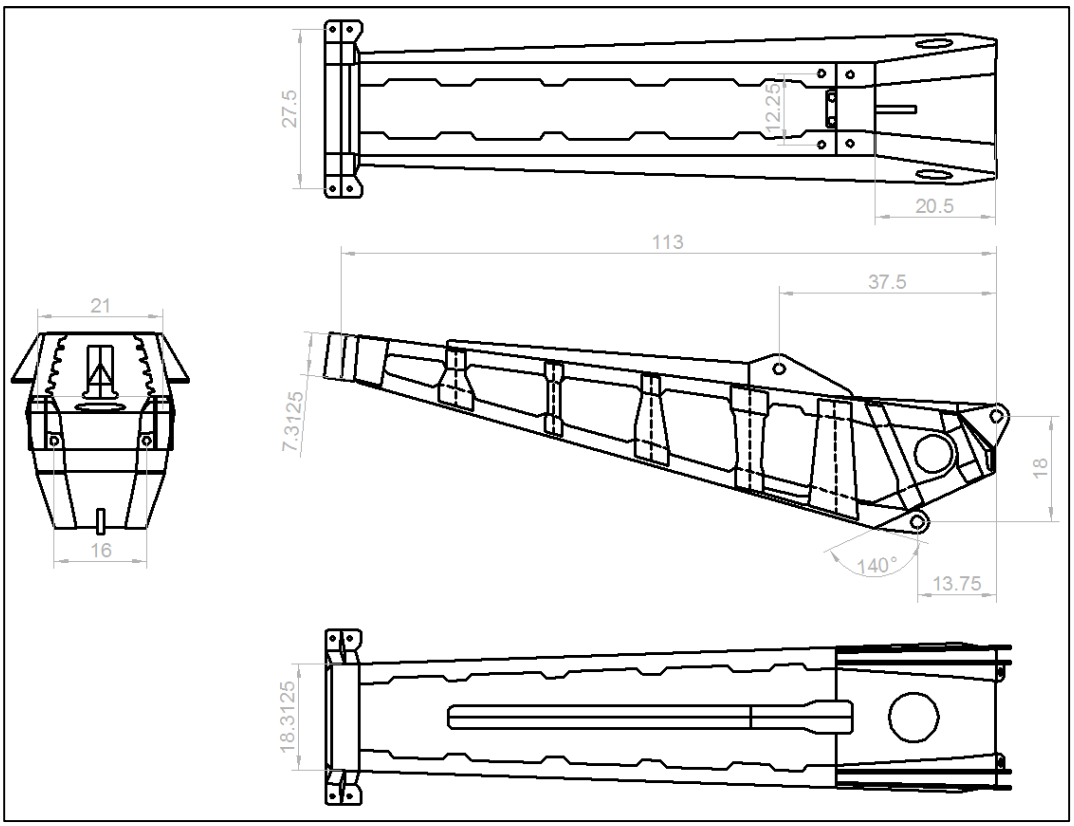

Figure 59 The Test-Case Pylon (Key Dimensions are in Inches)

The preliminary set of load cases that the test-case pylon will be evaluated for is given with Table 10. It is worth noting is that beside the set of load cases that correspond to the ultimate flight conditions when the pylon is intact, it is necessary to evaluate the pylon for each of the wing attachment failure conditions.

The list of materials is given with the Table 9, this table also cross-references to the Figure 60.

Components	Name	Material
1	RH_Upr_Longeron	Ti-6Al-4V
2	LH_Upr_Longeron	Ti-6Al-4V
3	Upper_Web	Al 7075
4	Aft_Upper_Web	Al 7075
5	RH_Lwr_Longeron	Steel 17-4PH
6	LH_Lwr_Longeron	Steel 17-4PH
7	Lower_Web	Steel 17-4PH
8	Fwd_Eng_Fitt_Bulkhead	Ti-6Al-4V
9	Frame_1	Al 7075
10	Frame_2	Al 7075
11	Frame_3	Al 7075
12	Frame_4	Ti-6Al-4V
13	Aft_Eng_Fitt_Bulkhead	Ti-6Al-4V
14	Frame_5	Ti-6Al-4V
15	Frame_6	Ti-6Al-4V
16	Aft_Bulkhead	Ti-6Al-4V
17	Upper_Link_Fitting	Ti-6Al-4V
18	RH_Front_Spar_Fitting	Ti-6Al-4V
19	LH_Front_Spar_Fitting	Ti-6Al-4V
20	Lwr_Link_Fitting	Ti-6Al-4V
21	RH_Side_Web	Al 7075
22	LH_Side_Web	Al 7075

Table 9 List of Materials

1	6.5 G down	301	4.33 G down + LH Frnt Spar Fitt Failed
2	3.5 G up	302	2.33 G up + LH Frnt Spar Fitt Failed
3	3.0 G up + 1.10 T_{max}	303	2.0 G up + 0.733 Tmax + LH Frnt Spar Fitt Failed
4	1.5 T_{max}	304	1.0 Tmax + LH Frnt Spar Fitt Failed
5	3.0 G up + 1.50 T_{max}	305	2.0 G up + 1.0 Tmax + LH Frnt Spar Fitt Failed
6	4.85 G down + 1.65 G right	306	3.23 G down + 1.1 G right + LH Frnt Spar Fitt Failed
7	4.85 G down + 1.65 G left	307	3.23 G down + 1.1 G left + LH Frnt Spar Fitt Failed
8	3.00 G right	308	2.0 G right + LH Frnt Spar Fitt Failed
9	3.00 G left	309	2.0 G left + LH Frnt Spar Fitt Failed
10	2.25 rad/sec^2 yaw +1.5 T_{Cruise}	310	1.5 rad/sec2 yaw + 1.0 Tcruise + LH Frnt Spar Fitt Failed
11	-2.25 rad/sec^2 yaw +1.5 T_{cruise}	311	-1.5 rad/sec2 yaw + 1.0 Tcruise +LH Frnt Spar Fitt Failed
12	Engine seizure	312	0.667 Engine seizure + LH Frnt Spar Fitt Failed
101	4.33 G down + Upper Link Failed	401	4.33 G down + RH Frnt Spar Fitt Failed
102	2.33 G up + Upper Link Failed	402	2.33 G up + RH Frnt Spar Fitt Failed
103	2.0 G up + 0.733 Tmax + Upper Link Failed	403	2.0 G up + 0.733 Tmax + RH Frnt Spar Fitt Failed
104	1.0 Tmax + Upper Link Failed	404	1.0 Tmax + RH Frnt Spar Fitt Failed
105	2.0 G up + 1.0 Tmax + Upper Link Failed	405	2.0 G up + 1.0 Tmax + RH Frnt Spar Fitt Failed
106	3.23 G down + 1.1 G right + Upper Link Failed	406	3.23 G down + 1.1 G right + RH Frnt Spar Fitt Failed
107	3.23 G down + 1.1 G left + Upper Link Failed	407	3.23 G down + 1.1 G left + RH Frnt Spar Fitt Failed
108	2.0 G right + Upper Link Failed	408	2.0 G right + RH Frnt Spar Fitt Failed
109	2.0 G left + Upper Link Failed	409	2.0 G left + RH Frnt Spar Fitt Failed
110	1.5 rad/sec2 yaw + 1.0 Tcruise + Upper Link Failed	410	1.5 rad/sec2 yaw + 1.0 Tcruise + RH Frnt Spar Fitt Failed
111	-1.5 rad/sec2 yaw + 1.0 Tcruise + Upper Link Failed	411	-1.5 rad/sec2 yaw + 1.0 Tcruise + RH Frnt Spar Fitt Failed
112	0.667 Engine seizure + Upper Link Failed	412	0.667 Engine seizure + RH Frnt Spar Fitt Failed
201	4.33 G down + Lower Link Failed		
202	2.33 G up + Lower Link Failed		
203	2.0 G up + 0.733 Tmax + Lower Link Failed		
204	1.0 Tmax + Lower Link Failed		
205	2.0 G up + 1.0 Tmax + Lower Link Failed		
206	3.23 G down + 1.1 G right + Lower Link Failed		
207	3.23 G down + 1.1 G left + Lower Link Failed		
208	2.0 G right + Lower Link Failed		
209	2.0 G left + Lower Link Failed		
210	1.5 rad/sec2 yaw + 1.0 Tcruise + Lower Link Failed		
211	-1.5 rad/sec2 yaw + 1.0 Tcruise + Lower Link Failed		
212	0.667 Engine seizure + Lower Link Failed		

Table 10 Preliminary Set of Load Cases

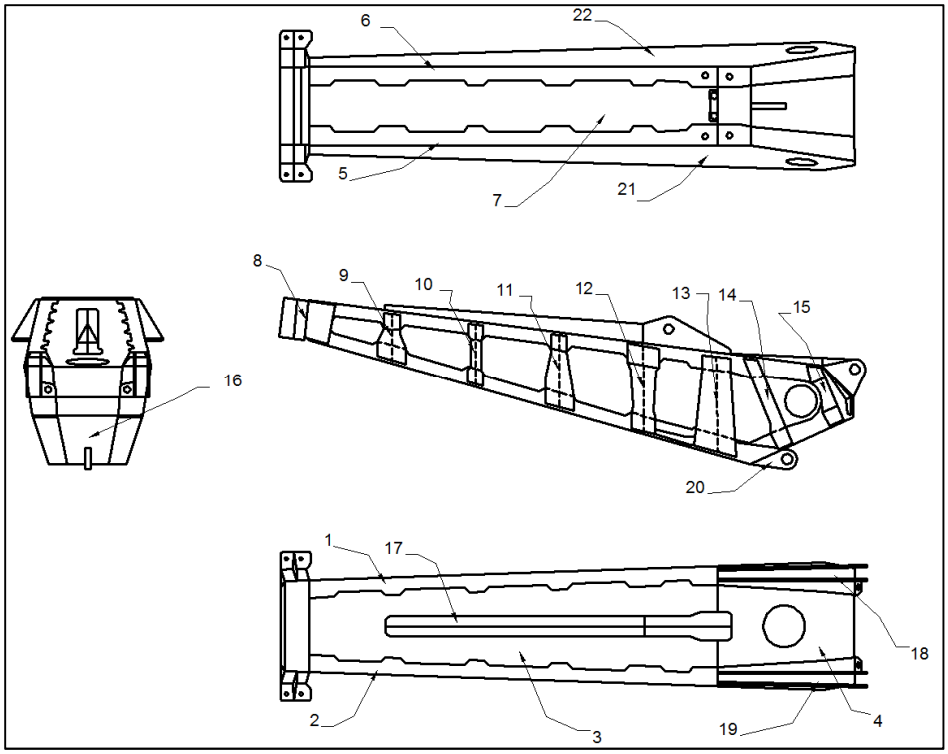

Figure 60 Study Pylon Part Definition for Bill of Materials

Before we get to the actual calculations it is useful to gather and lay out all the checks that need to be performed in order to structurally substantiate (or, in other words, perform all necessary checks to meet certification requirements) a typical pylon structure. Color coded Figure 61 shows the breakdown of the all required checks by the part type and by check type.

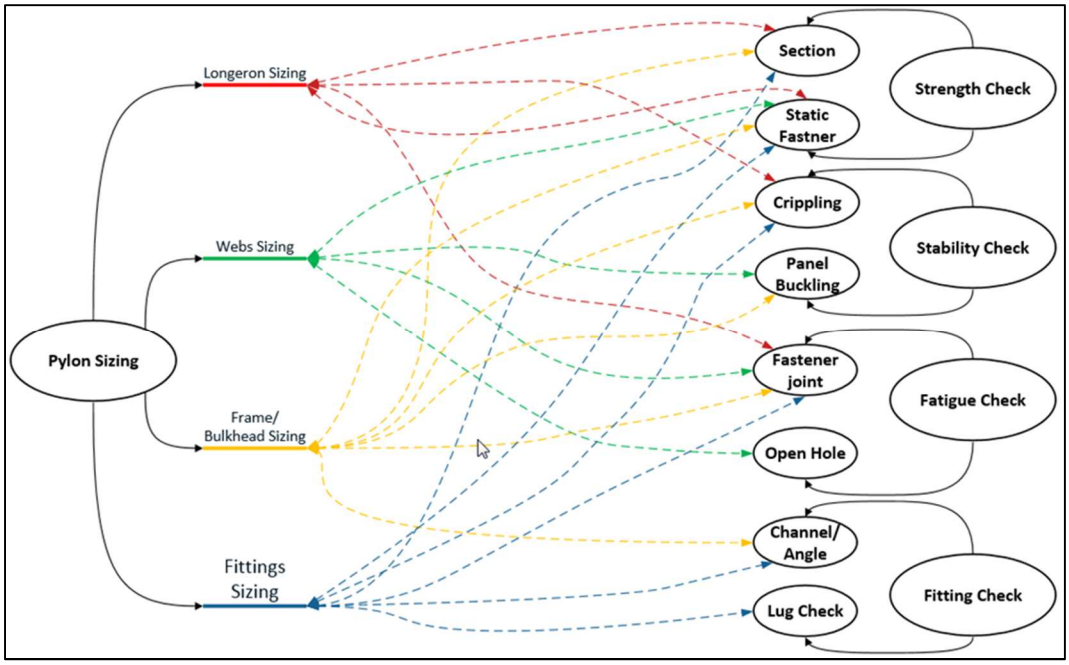

Figure 61 Pylon Sizing Effort

6.2 The Study

The previous chapters laid out in details all of the model based tools and process enablers required for the design optimization of metallic jet engine pylons to meet certification requirements. The sizing and substantiation effort and the engineering time reduction possible have to be carefully executed so that the actual value of the proposed paradigm shift from segmented document based to integrated model based can be measured. We are interested here not only in the quality and performance of the designs obtained each way but also in the engineering effort and schedule costs of each process.

To study the engineering management aspect of the work, and the impact of integrated model based design on development cost and schedule, both engineering efforts, one using the traditional document based platform, and the other, using the newly proposed model based platform, were executed for one load cycle of the pylon structural design. The results were then compared and extrapolated to the typical 3 load cycles of the document based design. The results as well as final remarks and conclusions will be presented in the following sections.

Before calculating the engineering hours required for two processes, the following assumptions are made to remove any possible unfair advantage of one process over the other:

A single load cycle is used for the experiment.

For the sizing effort and critical load comparison the conceptual load cycle is used since it does not require presenting any proprietary information and it provides for simple side by side comparisons.

For the internal load development effort the preliminary load cycle is used since conceptual loads have too few load cases, all of them critical (the conceptual load cycle does not allow for the loads development engineering effort comparison).

For the document based process in an established aerospace company a certain level of automation of the engineering processes does exist.

The model based optimization platform tool is available for the experiment, as described by Figure 36.

All the elements for the design experiment based on the traditional document based structural sizing were taken into account when logging the engineering time required:

(a) Coarse FEM development
(b) Internal loads development for critical loads down-selection, and documentation of critical load set from the coarse FEM
(c) Refined (stress) FEM development, and coarse FEM load application to the refined FEM
(d) Extraction of loads from the refined (stress) FEM
(e) building and using the stress templates
(f) refined FEM loads data transformation into the stress templates
(g) calculation of the margins
(h) documentation of necessary changes to the design either to achieve positive margin or to reduce excessive margin
(i) loads model update
(j) load/stress convergence check
(k) documentation of the final margins

It is also required to record any potential repetition of the described process due to lack of loads/stress convergence.

On the other track of the experiment all of the efforts related to the model based structural sizing were considered when calculating the engineering effort time:

(a) Building of the single FEM

(b) Loads' down-selection

(c) Creation of the optimization responses and constraints using the model base platform

(d) Documentation of the margins

The engineering design process was discussed in previous chapters. Here a detailed map of the engineering effort required to structurally size and qualify a pylon structure was developed with the aim of creating a mathematical formulation needed for comparing the engineering effort and cost.

Pylons can greatly vary in size and complexity based on the weight, thrust, geometry of the engine they are attaching to the wing, as well as the possible airplane missions. To evaluate the complexity, and associated design challenge, of different pylons, a size generalization table is created, using size factors that effectively lead to a sensible mathematical form. Table 11 lays out all of the pertinent size factors, as well as certain constants that are required for assessing the costs of engineering effort.

g	Total number of load cases	h	Number of critical load cases
i	Number of Bays	i+1	Number of Frames/Bulkheads
j	Average number of longeron fasteners per bay	k	Average number of frame/bulkhead to longeron fastener connections
4	Number of Webs (2 side, upper and lower)	l	Average number of cutouts per web
m	Average number of frame/bulkhead to web fastener connections	n	Average Number of Panels within the Frame/Bulkhead
$8*\sqrt{n}$	Average Number of Stiffeners in a Frame/Bulkhead	8	Number of angle fittings
8	Number of channel fittings	12	Number of tension bolts
6	Number of lugs	o	Number of all fitting/lug/tension bolt interfaces
p	Coarse FEM number of elements per bay	q	Number of bays that are not connected with the upper link fitting
r	Number of bays that are connected with the lower link fitting	s	Number of bays that connected with the front Spar fitting
t	Number of convergence loops within a single load cycle	u	Number of pylon to wing fittings

Table 11 Size Factors Explanation

Now that the generic size factors have been introduced let's create the table of the size factors specific to the study pylon depicted by the Figure 59.

Number of critical load cases	47
number of bays	7
Number of frames/bulkheads	8
Average number of longeron fasteners per bay	15
Average number of frame/bulkhead to longeron fastener connections	4
Average number of cutouts per web	2
Number of Webs (2 side, upper and lower)	4
Number of Longerons	4
Average number of frame/bulkhead to web fastener connections	8
Average Number of Panels within the Frame/Bulkhead	9
Average Number of Stiffeners in a Frame/Bulkhead	24
Number of angle fittings	8
Number of channel fittings	8
Number of tension bolts	12
Number of lugs	6
Number of all fitting/lug/tension bolt interfaces	8
Number of bays that are connected with the upper link fitting	4
Number of bays that are connected with the lower link fitting	2
Number of bays that are connected with the front Spar fitting	3
Number of convergence loops within a single load cycle	3

Table 12 Study Pylon Size Parameters

Chapter 7: The Test Document Based Process

7.1 Cost of the Engineering Development of the Coarse FEM

Typically in an established commercial aircraft company fairly high level of automation of the coarse FEM model creation exists. Therefore generating the nodes, elements, properties, and material definitions, together with the boundary conditions (loads and constraints) of a structure such as the pylon studied here does not require much of the engineering effort. However, a significant amount of engineering effort is required to fine-tune the initial model to the expected airplane performance level during the conceptual design phase of the pylon development, or to translate existing geometrical (CAD) definitions into such a coarse model, since there is no one-to-one mapping between CAD and coarse models of pylons. In other words, the coarse FEM has to have reasonable stiffness and mass characteristics that would assure that full airplane level model has expected natural frequency and modes that relate to the under-the-wing package. The engineering effort of creating the coarse FEM and fine-tuning it to meet stiffness requirements typically takes 85 hours: 80 hours (2 one man engineering working weeks) for model fine-tuning and 5 hours for the initial coarse model generation.

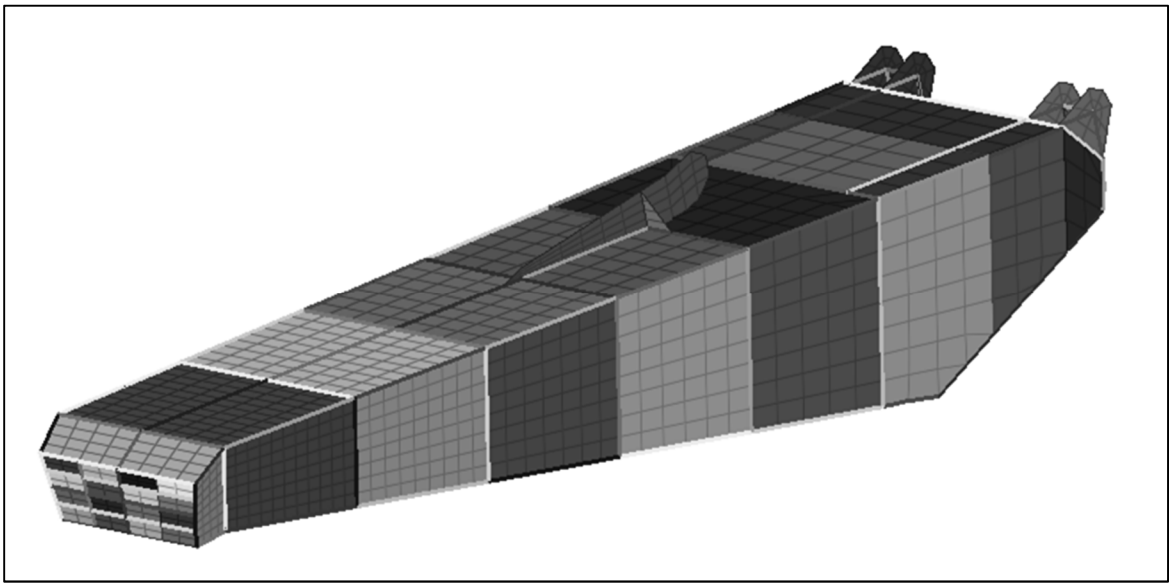

Figure 62 Coarse FEM used for the Document Based Process

7.2 Internal Loads Development for Loads' Down-Selection, And Documentation of Critical Load Set from the Coarse FEM

For effort-tracking purposes let us denote the total number of maneuver and the gust loading conditions g_1 and the number of FBO event loading conditions that relate to the pylon sizing g_2. The total number of loading conditions will be equal to:

$$g = g_1 + g_2 \qquad 70$$

The coarse FEM generation includes the effort of creating all of the g_1 load cases. This set of load-cases contains all of the intact and fail-safe conditions that relate to the maneuver and gust conditions. The FBO loads will be discussed separately since they are developed using a different solution sequence compared to the maneuver and gust loading conditions.

The FEM run files are organized such that the nodes, elements, materials, and properties belong to one textual FEM file whereas the boundary conditions (constraints and loads) are in kept in another, separate, textual file. Each of the g_1 load cases are run separately by combining the two textual FEM files, and a total of g_1 resulting output files are created.

The critical set of load cases, the ones that are enveloping the set of g_1 load cases is denoted h_1. Selecting the set of the critical load cases for all of the structural members of the pylon in a typical, documents based fashion is a tedious process. It consist of writing out into the textual results files the forces and moments for all of the pylon's coarse FEM bar and spring elements, writing all the tractions of the shell elements into the g_1 textual output files, and then sorting them for minimum and maximum values. For instance in order to calculate the required longeron cross sections of the pylon, the max and min values of the axial load, and shear forces need to be output for each bay and for each of the longeron bays. Typically, some sort of software exists that allows for the textual output file data extraction and sorting. However due to the sheer volume of data that needs to be extracted and sorted as well as the large number of the output files this is a sizable effort. For each combination of bay (or frame/bulkhead), element type (bar vs. shell), load type (axial vs. shear), and loading condition there will be two load cases identified (one min and one max). Every

subset of the critical load case will be denoted with h_{ab} where the index a represents the type of the load extraction (such as longeron axial force, web shear traction, etc.), and the index b represent either the bay or frame/fitting number. Figure 63, although incomplete for the brevity, shows how these subsets are formed.

Based on the created subsets, the final set of critical load cases - h_1 coming from the subset of all non-FBO loading conditions g_1 is created as a union of all the h_{ab} subsets.

$$h_1 = h_{11} \cup h_{12} \cup \ldots \cup h_{1i} \cup h_{21} \cup h_{22} \cup \ldots h_{2i} \cup h_{31} \cup h_{32} \cup \ldots \cup h_{3i-1} \cup h_{41} \cup h_{42} \cup \ldots \cup h_{4o} \quad (71)$$

The effort of selecting the critical load set h_1 using the coarse FEM is dependent on the number of total non-FBO loading conditions g_1, number of bays, number of pylon interfaces, and type of the structural members in the coarse FEM. The entire engineering effort of determining the h_1 set of critical load cases for an averaged sized pylon typically takes 160 hours (4 engineering work weeks). The documentation of the critical set of load cases and the signing of the released documents takes another 80 hours.

Now that all of the non-FBO related load cases have been down selected, let us discuss the process of the FBO loads for pylon development. The solution sequence that is typically used to determine the pylon max/min interface loads is an implicit non-linear solution. The pylon coarse FEM is integrated with the fairly detailed FEM of the engine. Then a design of experiment type analysis is performed. Namely the model is run for various blade angle releases, various wing weights (levels of fuel in the wing fuel tank), as well as left vs. right wing mounting scheme. There are g_2 such runs. From all of these runs the min/max interface loads are sorted, looking at the time history of the interface load, and then the time correlated loads are documented in the table similar to the one shown with Figure 20.

There are h_2 of these load cases. The entire engineering effort of determining the FBO h_2 set of critical load cases for an average sized pylon typically take 180 hours (4.5 engineering work weeks). The documentation of the critical set of load cases and the appropriate signing takes another 20 hours. The total number of critical load cases is:

$$h = h_1 + h_2$$ 72

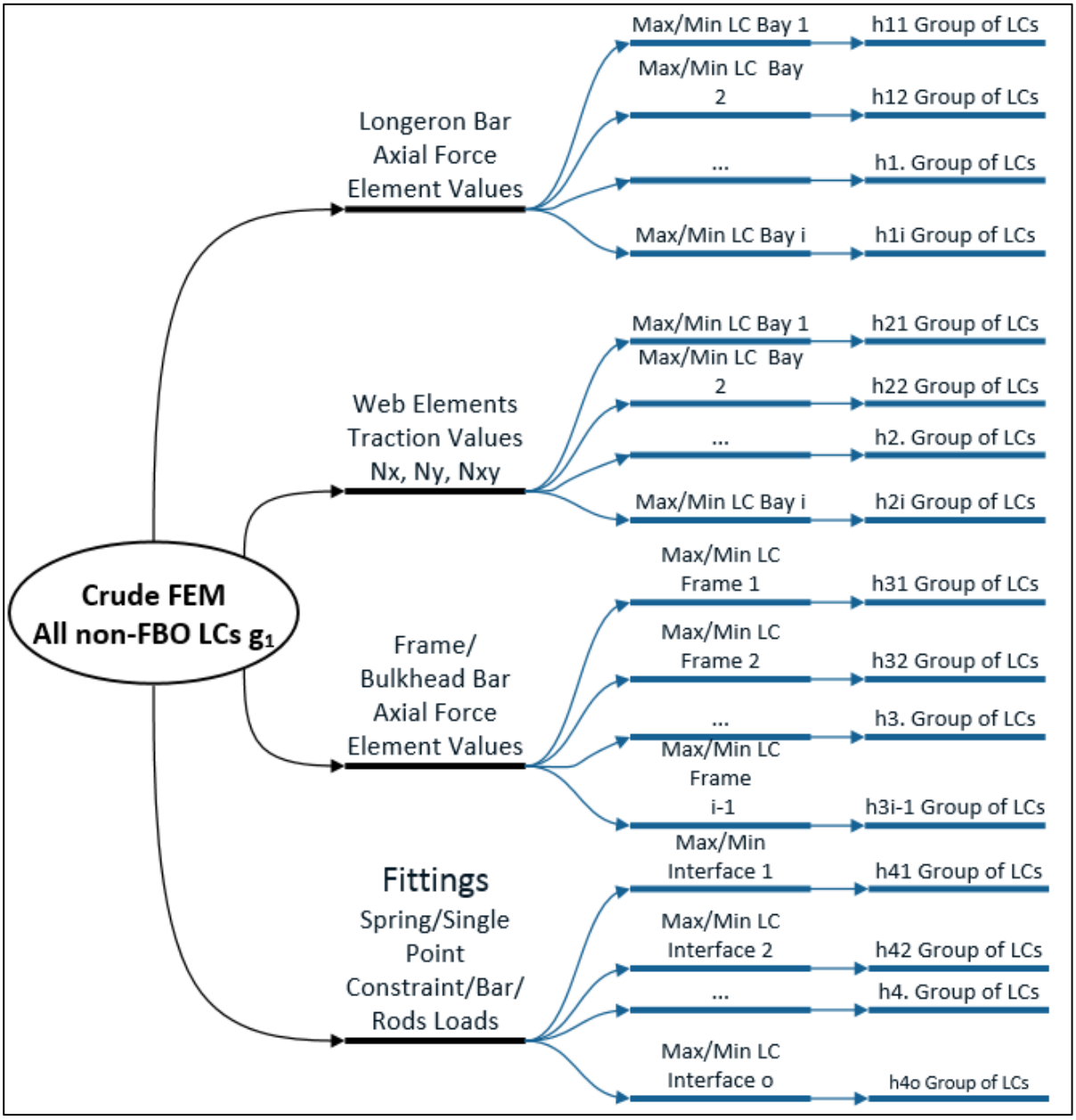

Figure 63 Subsets of Critical Load Cases

At this point the loads team has finished one load cycle, and the effort measured in the engineering hours is equal to:

$$T^{D}_{Loads} = 85 + 160 + 180 + 20 = 445 \quad \textbf{73}$$

7.3 Refined (Stress) FEM Development, And Coarse FEM Load Application onto Refined FEM, And Extraction of Loads from the Refined (Stress) FEM

To calculate the number of engineering hours that are required to create the refined stress FEM it is crucial to understand which parts require the refined FEM. Typically longerons and fittings do not require the refined FEM. Frames and bulkheads do. The reason for building the refined FEM is that only the outside stiffener loads are typically extracted from the coarse FEM, and the distribution of the loads within the internal stiffeners and the typical frame or bulkhead, depicted with the Figure 5, need to be calculated. Figure 11 represents well the refined FEM.

The engineering effort of creating the FEM typically take 4 hours, and application of each load case additional 0.2h which includes the data for coarse FEM data conversion and spreading the overall load (from the coarse FEM) onto the fine FEM. Extracting the stiffener and panel loads takes another 0.016h for each stiffener/panel.

Thus the total engineering effort for creating the stress FEM, applying the coarse FEM loads, and extracting the stiffener/panel internal loads is estimated as

$$T^{D}_{FEM} = (i + 1) \cdot [4 + h \cdot (0.2 + 0.16)] \quad \textbf{74}$$

Individual fastener loads also need to be calculated since the coarse FEM only provides the total load that any given fastener pattern takes. For static fastener strength and bearing stress this might not be that important since the assumption can be made that under the ultimate loads the fastener loads are equally distributed amongst each of the fasteners within the fastener pattern. However for fatigue evaluation it is absolutely critical to calculate the correctly the individual fastener load.

The total number of fastener patterns that exist in a pylon can be calculated as:

$$\underbrace{8 \cdot (2 \cdot i + 1)}_{\substack{Longerons\ to\ webs \\ and \\ Frames/Bulkheads}} + \underbrace{(2 \cdot q + 1)}_{Upper\ Link\ Fitting} + \underbrace{(2 \cdot r + 1)}_{Lower\ Link\ Fitting} + \underbrace{(2 \cdot s + 1)}_{Front\ Spar\ Fitting} + \underbrace{4}_{Aft\ Bulkhead} \quad \textbf{75}$$

Assuming symmetry, this number can be divided by two, and so upon simplification and division the total number of fastener patterns that need to have individual fastener loads calculated is:

$$8i + q + r + s + \frac{23}{2} \quad \textbf{76}$$

With a fair level of automation that is assumed to exist this task takes 0.166 hours for each of the fastener patters. This has to be repeated for all of the critical load cases, and the total number of hours that the stress team spends on this task can be calculated as:

$$T^{D}_{Fast\_Load} = h \cdot \left[8i + q + r + s + \frac{23}{2}\right] \cdot 0.166 \quad \textbf{77}$$

7.4 Building And Use of the Stress Templates, Refined FEM Loads Data Transformation into the Stress Templates, And Calculation of the Margins

From Figure 61 8 different types of checks that need to be performed emerge. For each of the check types Table 13 provides the typical engineering time for execution:

Check Type	Typical Execution Time (hours)
Section check	0.166
Static Fastener check (fastener shear and plate bearing)	0.05
Crippling	0.166
Panel Buckling	0.083
Fastener joint fatigue	0.25
Open hole fatigue	0.5
Channel/Angle fitting check	0.333
Lug Checks	0.166
Tension Bolt Check	0.05

Table 13 Check Execution Time

It is assumed that some sort of template for calculating these checks already exist in an established commercial aircraft company, so it is assumed that template creating does not take any time. However, the use of the templates for margin calculation needs to be executed for each part type:

(a) Longeron

(b) Web

(c) Frame/Bulkhead

(d) Fitting

Figure 64, Figure 65, Figure 66, and Figure 67 show the scope of the sizing effort for each of the part types. Multiplication of the scope numbers with the number of the check types and required engineering time for execution of the checks yields the total number of engineering hours that are spent on checking all of the parts of the pylon.

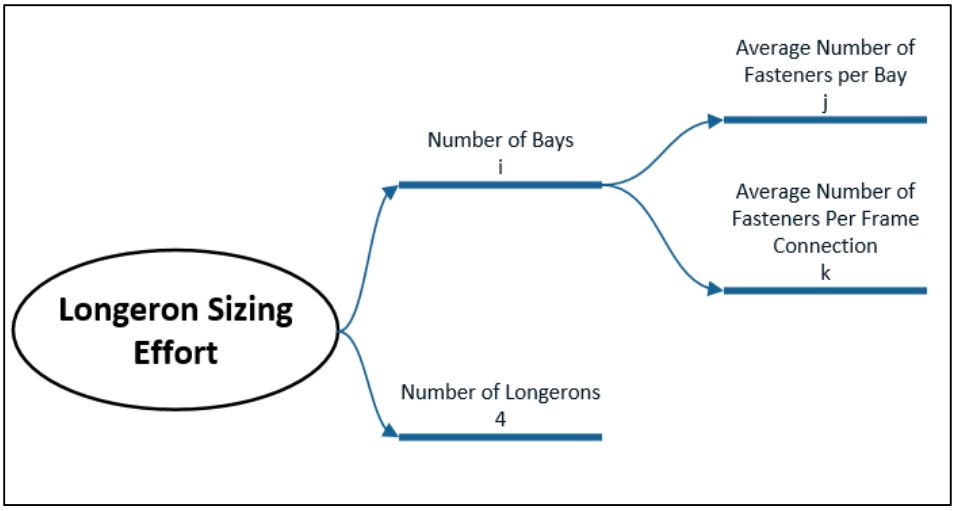

Figure 64 Longeron Sizing Scope

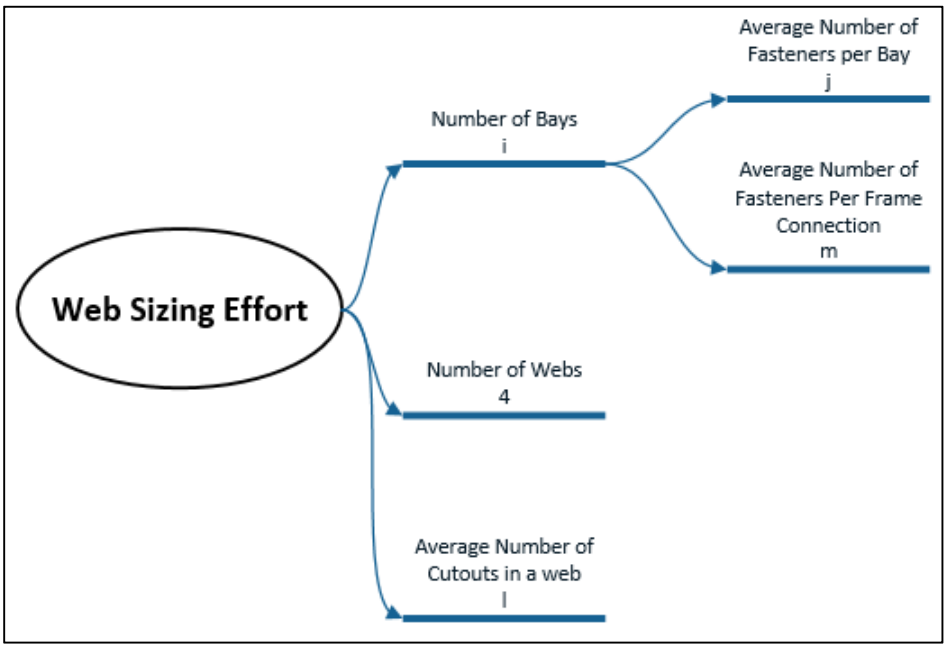

Figure 65 Web Sizing Scope

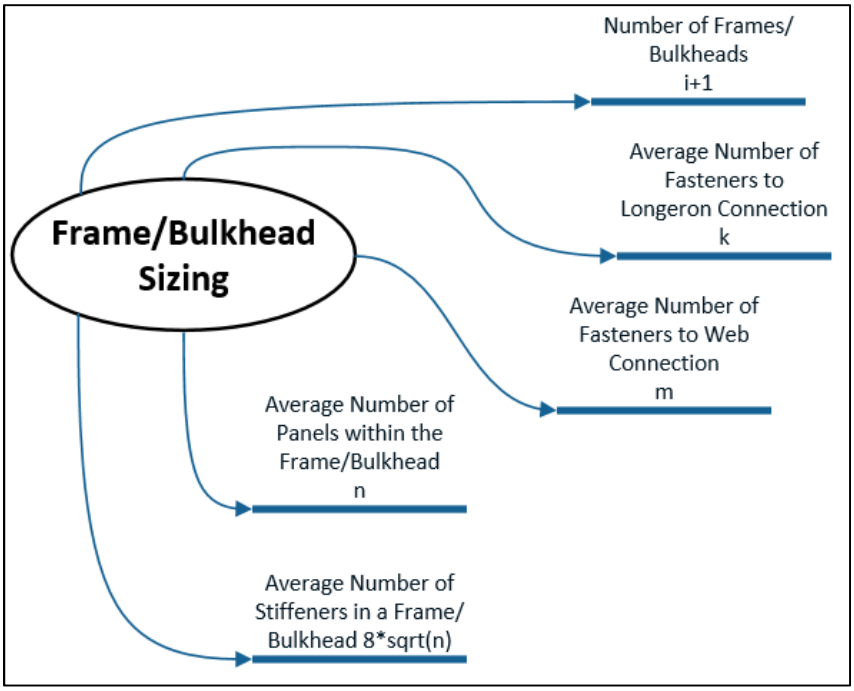

Figure 66 Frame/Bulkhead Sizing Scope

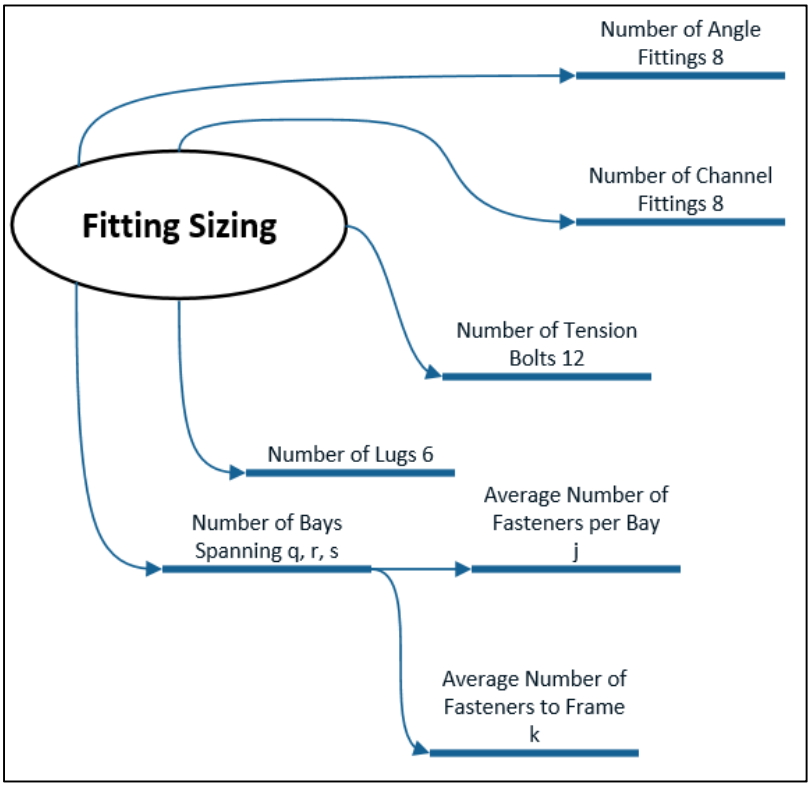

Figure 67 Fitting Sizing Scope

7.5 Engineering Time Required To Size Longerons Using the Document Based Process

From the Figure 61 we can see that the following checks need to be performed on to substantiate the longeron:

(a) Section strength check

(b) Crippling

(c) Static Fastener Joints

(d) Fatigue Fastener Joints

From the Figure 64 the number of checks for each category can be determined. Combining this with the hours required for each check from Table 13, the number of engineering hours required to substantiate the longerons of the pylon for one convergence loop of a single load cycle, assuming longeron symmetry, and only first row of fasteners checked for each bay, can be calculated by:

$$T_{Long}^{D} = 4/2 \cdot \left[i \cdot \left(\underbrace{0.166}_{Section} + \underbrace{0.166}_{Crippling} + \left(\underbrace{0.05}_{Stat\ Fast.} + \underbrace{0.166}_{Fatigue\ Fast.} \right) \cdot 4 \right) + (i+1) \cdot (0.05 + 0.166) \cdot k \right] \quad \textbf{78}$$

7.6 Engineering Time Required to Size Webs Using the Document Based Process

From Figure 61 the following checks need to be performed to substantiate each of the webs:

(a) Panel Buckling

(b) Static Fastener Joints

(c) Fatigue Fastener Joints

(d) Open Hole Fatigue

From Figure 65 the number of checks for each category can be determined. Combining this with the hours required for each check from Table 13, the number of engineering hours required to substantiate the webs of the pylon for one convergence loop of a single load cycle, with only first row of fasteners checked for each bay and each frame, can be calculated using:

$$T^{D}_{Webs} = 4 \cdot \left[i \cdot \left(\underbrace{0.083}_{Panel\ Buck.} + \left(\underbrace{0.05}_{Stat\ Fast.} + \underbrace{0.166}_{Fatigue\ Fast.} \right) \cdot 4 \cdot 2 \right) + (i+1) \cdot (0.05 + 0.166) \cdot (2 \cdot k + 4) + l \cdot \underbrace{0.5}_{open\ hole\ fatigue} \right] \quad \textbf{79}$$

The lower and upper webs are not symmetric. However, it is worth mentioning that the symmetry between the left hand and right hand webs cannot be assumed either due to the different cutout patterns in them. Also, each web is attached to two longerons and therefore the factor of two has to be included in the formula above to take this into account.

7.7 Engineering Time Required To Size Frames/Bulkheads Using the Document Based Process

From Figure 61 the following checks need to be performed to substantiate the Frame/Bulkhead:

(a) Section check

(b) Crippling

(c) Static Fastener Joints

(d) Fatigue Fastener Joints

(e) Panel Buckling

(f) Channel/Angle Fitting (Bulkheads that connect to engine fittings, and for frame under the upper link fitting)

From Figure 66 the number of checks for each category can be determined. Combining this with the hours required for each check from Table 13, the number of engineering hours required to substantiate the frames

or bulkheads of the pylon for one convergence loop of a single load cycle, assuming frame/bulkhead symmetry, and only first row of fasteners checked for each bay, can be calculated using:

$$T^{D}_{Fr/Blk} = (i+1)\cdot\left(\frac{8\cdot\sqrt{n}}{2}\cdot\left(\underbrace{0.166}_{Section}+\underbrace{0.166}_{Crippling}\right)+\frac{n}{2}\cdot\underbrace{0.083}_{Panel\ Buck.}\right.$$
$$\left.+\left(\underbrace{0.05}_{Stat\ Fast.}+\underbrace{0.166}_{Fatigue\ Fast.}\right)\cdot(16+k)\right)+6\cdot\underbrace{0.333}_{Ch-Ang.\ Fitting} \quad \textbf{80}$$

7.8 Engineering Time Required To Size Fittings the Document Using Based Process

From Figure 61 the following checks need to be performed to substantiate the fittings:

(a) Section check

(b) Crippling

(c) Static Fastener Joints

(d) Fatigue Fastener Joints

(e) Channel/Angle Fitting (only for upper Link Fitting)

(f) Lug Checks

$$T^{D}_{Fitt} = (q+r+s)\cdot\left[\left(\underbrace{0.166}_{Section}+\underbrace{0.166}_{Crippling}\right)+\left(\underbrace{0.05}_{Stat\ Fast.}+\underbrace{0.166}_{Fatigue\ Fast.}\right)\cdot 4\right]+(q+r+s+3)$$
$$\cdot\left(\underbrace{0.05}_{Stat\ Fast.}+\underbrace{0.166}_{Fatigue\ Fast.}\right)\cdot 4+2\cdot\underbrace{0.333}_{Ch-Ang.\ Fitting}+6\cdot\underbrace{0.166}_{Lug} \quad \textbf{81}$$

Due to the significant number of margins calculated that can be negative or excessively large, the number of the above calculations will be repeated. In order to take into account the repeated calculation, a “repeat factor” will be introduced. The repeat factor represents the percentage of repeated calculations compared to all of the calculations. It is pretty conservative to assume that the repeat factor would be 0.33 first time thru the load/sizing convergence loop. Given that with every loads/stress convergence loop there should be a decaying number of repeated calculation another factor, “repeat decay factor” is introduced. Let us

say that for every additional load/sizing convergence loop the repeat decay factor is cut by factor of 2. For example for the first load/sizing loop it is assumed to be 1, for second 0.5, for third 0.25, etc. So the total time of the sizing effort will be multiplied with these two factors. The formula for the engineering time related to the refined (stress) FEM development, coarse FEM load application onto refined FEM, extraction of loads from the refined (stress) FEM, building and use of the stress templates, refined FEM loads data transformation into the stress templates and calculation of the margins can be written as:

$$T^D_{Sizing} = \sum_{g=1}^{g=t} \left(1 + \underbrace{0.33}_{repeat\ fac.} \cdot \underbrace{\frac{1}{g}}_{repeat\ decay\ fac.} \right) \cdot \left(T^D_{Long} + T^D_{Webs} + T^D_{Fr/Blk} + T^D_{Fitt} \right) \qquad \textbf{82}$$

Where ***g*** denotes the convergence loop. From the formula above, every time that the sizing loop is repeated fewer operation less time is spent on the sizing effort.

7.9 Documentation of Necessary Changes to the Design Either Achieve Positive Margin or to Reduce Excessive Margin, Loads Model Update, and Load/Stress Convergence Check

Communication between the sizing, load, and design models within the document based structural engineering process needs to happen at every design change. This is one of the largest drawbacks of the document based engineering process compared to the model based engineering process proposed in this work. In order to quantify total engineering effort required to execute these tasks we break down the effort into 3 categories:

(a) Documentation and communication of changes

(b) Load (coarse FEM) model update

(c) Load/Stress Convergence check

The number of hours of documentation is typically 25 hours per pylon bay. Documentation has direct relationship to the pylon size, and given that the number of bays is the parameter that best describes the pylon overall size the engineering effort for documentation will be calculated as:

$$T^{D}_{Docum} = i \cdot 25 \qquad \textbf{83}$$

Using the previously introduced “repeat factor” as a measure of the engineering effort used for necessary margin recalculation (either due to the negative or excessive margin) as well as typical 60 hours for coarse FEM updates, the engineering effort of the update can be calculated as:

$$T^{D}_{Load_{upd.}} = 0.33 \cdot \frac{1}{g} \cdot 60; where\ g = 1{,}2 \ldots Sizng\ Loop \qquad \textbf{84}$$

Checking for convergence of the loads is a big effort since it consists of comparison of internal loads for all of the ***h*** critical load cases from previous loop to the current. For the sake of safety it has to be done for all of the internal loads. Typically high level of automation exists for this task due to its size and complexity. Thus the overall number of engineering hours spent on this task is not overwhelming. Typical engineering time spent on each load case is on average 1 hour.

$$T^{D}_{Load_{Converg}} = h \cdot 1 \qquad \textbf{85}$$

The total engineering effort for the tasks documentation of necessary changes to the design that either achieve positive margin or if there is a need to reduce excessive margin, the loads model update and the load/stress convergence check can be calculated as:

$$T^{D}_{Update/conv} = \sum_{g=1}^{s} (g-1) \cdot \left[i \cdot 25 + 0.33 \cdot \frac{1}{g} \cdot 60 + h \cdot 1 \right] \qquad \textbf{86}$$

7.10 Actual Engineering Hours Required to Size Study Pylon Using the Document Based Approach

Inserting values from Table 12, and Table 13 into the formulas 73 to 77 produces the engineering hours/weeks required to execute the loads development.

T^D_{Loads}	T^D_{FEM}	$T^D_{Fast\_Load}$	Sum (hours)
445	167.36	596.85	1209.21
		Sum (weeks)	30.23

Table 14 Loads Development Engineering Hours for Document Based Process

Inserting values from Table 12, and Table 13 into the formulas 78 to 82 produces the calculation of the engineering hours/weeks required to execute the sizing of the study pylon.

T^D_{Long}	T^D_{Webs}	$FT^D_{Fr/Blk}$	T^D_{Fitt}	$T^D_{Long} + T^D_{Webs} + T^D_{Fr/Blk} + T^D_{Fitt}$	Loop1	Loop2	Loop3	Sum (hours)
28.378	161.844	71.418	22.794	284.434	378.29	331.36	315.72	1025.38
							Sum (weeks)	25.63

Table 15 Pylon Component Sizing Engineering Hours for Document Based Process

Inserting values from Table 12, and Table 13 into the formulas 83 to 86 produces the engineering hours/weeks required to execute the documentation and updates of the loads and stress sizing of the study pylon.

	Loop1	Loop 2	Update
T^D_{Docum}	175	175	350
T^D_{Update}	19.8	9.9	29.7
T^D_{conv}	47	47	94
		Sum (hours)	473.7
		Sum (weeks)	11.84

Table 16 Documentation, Updating, and Convergence Engineering Hours for Document Based Process

Table 17 summarizes the engineering time required for one cycle of pylon sizing done by single engineer

	Engineering hours (weeks)
Loads Development	30.23
Sizing	25.63
Documentation/Updating/Convergence	11.84
Sum	68

Table 17 Total Engineering Hours for Document Based Process

7.11 Sizing the Test-Case Pylon using the Document Based Approach

Typically the pylon is sized in two major phases: (a) Static and Stability Sizing, and (b) Fatigue Sizing. Static sizing is typically done per component, whereas the fatigue size is done per bay. The static sizing process for each component is performed independently using the algorithm shown in Figure 7, starting with the initial pylon design as the baseline, and evolving through multiple load/sizing iterations. Typically, in current processes used by the industry, there are three load/sizing iterations.

The Initial design is based on the pylon designer's knowledge of past pylons and basic information of currently developed pylon's loads. Table 18 provides the weight summary of the initial design.

Component	Weight(lbs.)
Aft_Bulkhead	23.200
Aft_Eng_Fitt_Bulkhead	61.302
Aft_Upper_Web	10.457
Frame_1	8.914
Frame_2	4.915
Frame_3	12.034
Frame_4	30.689
Frame_5	17.955
Frame_6	8.276
Fwd_Eng_Fitt_Bulkhead	65.883
LH_Front_Spar_Fitting	58.951
LH_Lwr_Longeron	24.726
LH_Side_Web	35.588
LH_Upr_Longeron	13.262
Lower_Web	70.032
Lwr_Link_Fitting	26.296
RH_Front_Spar_Fitting	58.854
RH_Lwr_Longeron	24.725
RH_Side_Web	35.587
RH_Upr_Longeron	13.262
Upper_Link_Fitting	25.102
Upper_Web	31.423
Total:	661.431

Table 18 Initial (before sizing) Component's Weights

The key input for the wing design are the maximum envelope loads at the pylon to wing interfaces. These are provided in18. Besides being key input parameter for the wing design, these values are used to show the equivalence between the coarse FEM used in this chapter for document based sizing and the detailed FEM used later in the integrated model based sizing.

	Fx(kips)	Fy(kips)	Fz(kips)	Fres(kips)
Max LH_FS_Diag	0	39.017	102.95	110.0955
Max RH_FS_Diag	0	38.563	102.95	110.0955
Max Upper_Link	261.94	0	136.12	295.1969
Max LH_FS_Main	302.97	0	206.35	366.5667
Max RH_FS_Main	302.97	0	206.35	366.5667
Max Lower_Link	311.64	0	59.857	379.2477

Table 19 Coarse FEM Initial Design Pylon to Wing Reaction Forces

Before the sizing can be started the allowable values need to be determined for each part. The allowable values need to be knocked down by the temperature correction coefficient. The list of the allowable values, operating temperatures, related temperature knock-down factors, and margin factors (for the 5% margin policy) are listed with the Table 20.

The temperature knock-down factors and the allowable values are taken from Ref. (DoD1998).

Material	Component	Operating Temp	Tkd	Margin Factor (5% margin)	Ftu	Allowable
Ti-6Al-4V AMS 4911	RH_Upr_Longeron	185.2	0.925	0.9524	134000	117719.4
Ti-6Al-4V AMS 4911	LH_Upr_Longeron	185.2	0.925	0.9524	134000	117719.4
Al 7075 AMS 4044	Upper_Web	235	0.845	0.9524	74000	59407.38
Al 7075 AMS 4044	Aft_Upper_Web	236	0.844	0.9524	74000	59344.7
Steel 15-5PH AMS 5659 H925	RH_Lwr_Longeron	365	0.898	0.9524	170000	145011.1
Steel 15-5PH AMS 5659 H925	LH_Lwr_Longeron	365	0.898	0.9524	170000	145011.1
Steel 15-5PH AMS 5862	Lower_Web	362	0.899	0.9524	154000	131467.3
Ti-6Al-4V AMS 4911	Fwd_Eng_Fitt_Bulkhead	165	0.939	0.9524	134000	119571.7
Al 7075 AMS 4126	Frame_1	175	0.890	0.9524	75000	63417.18
Al 7075 AMS 4126	Frame_2	204	0.869	0.9524	75000	61947.96
Al 7075 AMS 4126	Frame_3	275	0.801	0.9524	75000	57044.75
Ti-6Al-4V AMS 4911	Frame_4	305	0.844	0.9524	134000	107425.7
Ti-6Al-4V AMS 4911	Aft_Eng_Fitt_Bulkhead	325	0.832	0.9524	134000	105916.2
Ti-6Al-4V AMS 4911	Frame_5	312	0.840	0.9524	134000	106888.6
Ti-6Al-4V AMS 4911	Frame_6	285	0.856	0.9524	134000	109009.2
Ti-6Al-4V AMS 4911	Aft_Bulkhead	199	0.915	0.9524	134000	116461.4
Ti-6Al-4V AMS 4911	Upper_Link_Fitting	185.2	0.925	0.9524	134000	117719.4
Ti-6Al-4V AMS 4911	RH_Front_Spar_Fitting	236	0.889	0.9524	134000	113152.1
Ti-6Al-4V AMS 4911	LH_Front_Spar_Fitting	236	0.889	0.9524	134000	113152.1
Ti-6Al-4V AMS 4911	Lwr_Link_Fitting	346	0.820	0.9524	134000	104417.7
Al 7075 AMS 4044	RH_Side_Web	340	0.824	0.9524	74000	57894.74
Al 7075 AMS 4044	LH_Side_Web	340	0.824	0.9524	74000	57894.74

Table 20 Allowable Values for the Model Based Sizing

Before the per component weight results are presented for the static and stability sizing, a few key points need to be made:

(a) In order to allow for the best comparison between the document and model based approaches the same margin policy is to be used (5% margin for static strength and stability)[2]

(b) During the document based sizing there is no effort of weight saving. The only objective is to achieve a certifiable design by increasing the gauges once negative margins are discovered

The fastener shear strength values (F_{su}) are used from the Fastener Design Manual (B1990) and the bearing allowable values are used from (DoD1998). See Table 43 in appendix A.

Table 20 is a component weight table after the strength and stability sizing which includes:

(a) Section static strength

(b) Section stability (crippling)

(c) Panel stability

(d) Static fastener joint strength

(e) Channel/angle fitting and lug strength[3]

Component	Weight(lbs.)
Aft_Bulkhead	26.66
Aft_Eng_Fitt_Bulkhead	80.48
Aft_Upper_Web	22.25
Frame_1	8.96
Frame_2	4.93
Frame_3	12.84
Frame_4	32.23
Frame_5	36.58
Frame_6	9.05
Fwd_Eng_Fitt_Bulkhead	71.99
LH_Front_Spar_Fitting	74.36
LH_Lwr_Longeron	37.92
LH_Side_Web	50.62
LH_Upr_Longeron	14.56
Lower_Web	93.59
Lwr_Link_Fitting	48.48
RH_Front_Spar_Fitting	74.25

[2] Typically for document based approach a 15% margin is used

[3] Table 55 to Table 64

RH_Lwr_Longeron	37.92
RH_Side_Web	50.62
RH_Upr_Longeron	14.56
Upper_Link_Fitting	46.42
Upper_Web	45.87
	895.15

Table 21 Static Strength and Stability Sizing Completed Component's Weight

It is interesting to study the results. The weight increase due to the static sizing seems rather large (895.15-661.432=233.718 lbs.). However considering that to begin with there were:

(a) 54 unique tension sections that were violating the stress margins (only the top 4 components violations are documented with Table 44)

(b) 36 section crippling and/or panel stability violations, top ones detailed with

(c) Table 45

(d) 153 static fastener margin violations, top violations detailed with Table 46

The weight increase would be typically well justifiable.

Proceeding to fatigue sizing - Fatigue sizing shows positive margins everywhere. Thus, with the document based approach in the test case studied here there is no need to gauge up any of the components to achieve positive fatigue margins.

Table 47 to Table 54 (see Appendix) provide the list of lowest fatigue margins for the document based sizing fatigue work.

Chapter 8: The Test Case by the Model Based Process

8.1 Optimization Strategy and Tool

The entire model based sizing process is executed using the method of feasible directions (MFD) algorithm implemented within the OptiStruct® solver (A-Optistruct). The constraint screening and sensitivity approximation routines are all used with their respective default settings.

8.2 Cost of the Engineering Effort

8.2.1 The Building of the Single FEM

Todays' commercial FEM preprocessing software platforms contain most if not all of the required tools that enable extremely rapid automated detailed FEM modeling. Starting with the 3D solid parts representations that come from the CAD package, together with the lines that model fastener locations, the detailed FEM of the pylon can be built in approximately one engineering week – 40 engineering man hours.

Comparing this process to the coarse FEM built for the document based approach, there is one crucial difference. With the detailed FEM there is no need for calibration of the FEM, since each part is represented in FEM by its original shape and form. The same applies to fasteners. Every fastener is represented in the model. Conversely, with the coarse FEM, most of the time building the FEM is spent on the calibration of the coarse FEM to the desired mass and stiffness of the overall detailed model.

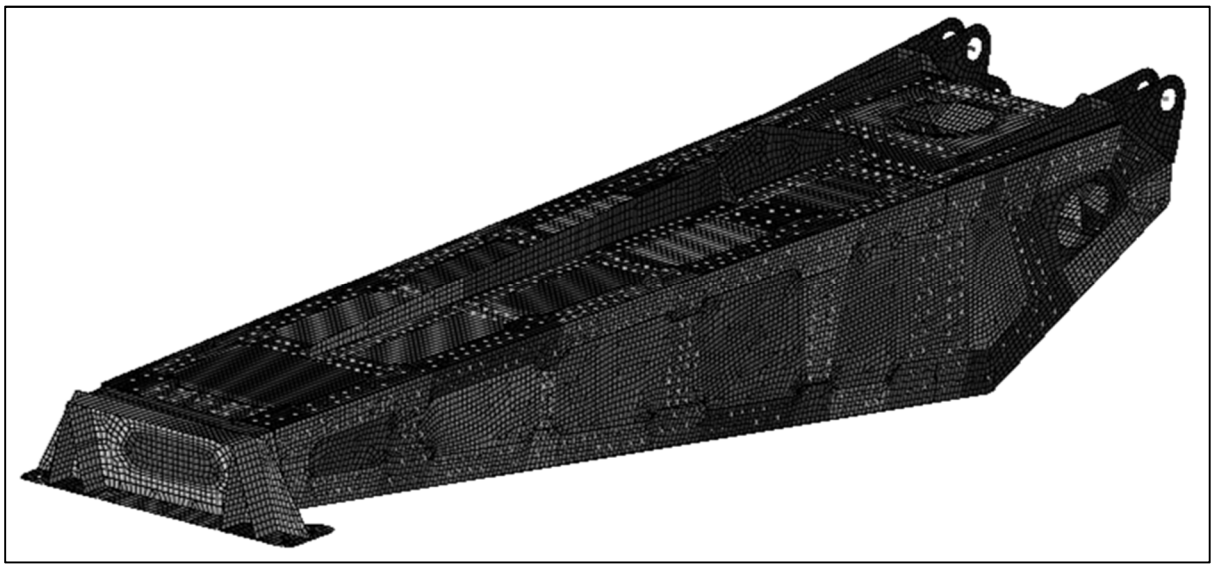

Figure 68 Detailed FEM of the Pylon for the Model Based Process

8.2.2 Loads Down-Select

In contrast to the document base process where the critical loads are found by sifting through the output files seeking the worst min/max loading for each element representing the particular physical component,

the model based approach is much simpler and quicker. As described in Section 4.6, if the pylon model is treated as an equivalent beam and the two representative sections are created from the FEM using the automated model based platform, one forward of the upper link, and one aft of it, and once the internal loads/moments F_x, F_y, F_z, M_x, M_y, and M_z are extracted for all of the maneuver and gust load cases, then for each of the two representative pylon cross-sections a total of three potato loads plots F_z vs. M_y, F_y vs. M_z, and F_x vs. M_x need to be plotted. From each plot now only the load cases that reside on the outside boundary are chosen for pylon sizing. The engineering effort of selecting the $\boldsymbol{h_1}$ (non-FBO) critical load cases using the automated potato-plotting platform is 20 hours.

There are two important considerations at this point. First, the down selection of the critical load cases using the potato load envelope plotting technique produces the same set of critical load cases $\boldsymbol{h_1}$ if the process is started from the same full set of maneuver and gust load cases $\boldsymbol{g_1}$. Second, the document based process provides the information on which particular load case from the $\boldsymbol{h_1}$ load cases is critical for each structural component and each section/panel/fastener within the pylon, whereas the automated potato-loads plotting approach does not. It only provides the information on which load cases are critical for the pylon in the global sense.

The question is: Isn't this a deficiency of the loads potato plotting approach?

The answer: Downstream within the model based optimization driven sizing process the sizing is done for all of the components at the same time with all of the critical load cases. The automated constraint screening that is part of every modern gradient based optimization algorithm eliminates the very large number of addressing all load case constraints.

Regarding FBO loads, since the FBO loads come from the integrated under-the-wing package simulation the model based approach does not differ in this segment form the document based process, thus the engineering effort for determining the $\boldsymbol{h_2}$ FBO based critical load cases is 180 hours, with the need for the 20 hour long process of documenting FBO loads.

8.2.3 Level One Sizing Engineering Effort

There are two spreadsheets and two automation scripts that are required for the level-one sizing effort. The algorithms for the automations are outlined with Figure 28, and Figure 29. The sample spreadsheets are given by Table 2, and Table 3 . The direct stress automation spread-sheet is relatively simple to build. However due to the sheer number of fastener joints in the pylon the static fastener joint strength check automation spreadsheet take much more time.

It takes typically 4 hours to build the direct stress automation spreadsheet and 24 hours for the static fastener joint strength one. Once the spreadsheets are available the generation of the optimization responses and constraints that relate to them takes just a few minutes, since the automation of this task is trivial and the scripts are part of the model based platform.

The only remaining set of responses needed for the constraint set is the buckling responses. The creation of these response and relating constraint is so simple that it really does not require any automation. This task takes a few minutes of engineer's time working with modern pre-processor. The engineering effort of creating the responses and constraints needed to run level one optimization sizing is about 1 hour.

8.2.4 Level Two Sizing Engineering Effort

The S-N curves can be provided for various stress concentration factors ***KT***, and the ones appropriate to the actual use of the fatigue detail that is being evaluated should be used. The S-N curves are typically provided for the surface polished samples of the material, with the ideal cyclical loading. However in the real production level airplane hardware there are no such cases as ideally polished parts subject to ideal cyclical load. Thus most of the aircraft companies introduce stress modification factors that take into account the surface finish (F_{sf}), types of the fasteners used (F_{ft}), quality of the fastener holes drilling (F_{fh}), fastener hole clearance classification (F_{cl}) , amount of preload (F_{pl}), etc.

In order to take into account the complexity that fatigue stress calculation is subject to, with all of the modification factors, a spreadsheet similar to the one created for the fastener joint static joint strength needs to be created.

Set id	D (in)	F_{sf}	F_{ft}	F_{pl}	F_{cl}	F_{fh}
2148	0.375	1.1	1.0	1.0	1.07	1.05
2149	0.375	1.0	1.0	1.0	1.07	1.05
2150	0.375	1.12	1.0	1.0	1.07	1.05
2151	0.375	1.0	1.0	1.0	1.07	1.05
2152	0.375	1.0	1.0	1.0	1.07	1.05

Table 22 Sample of the Spreadsheet Containing Modification Factors for Fatigue Calculation

Starting with the detailed FEM model with all possible load cases related to the fatigue of the pylon (down-bending, up-bending, left lateral bending, right lateral bending, etc.) and the automated process (similar to the one portrayed with Figure 29) that takes the fatigue specific parameters defined with Table 22, the very complex functional response is created for each fastener joint detail. The response calculates the failure index by combining the calculated reference stress with all of the appropriate modification factors, the pertinent S-N curve, and the Palmgren-Miner's rule given by the equation 5. Similar to the static fastener joint spreadsheet, it takes 24 hours for a fastener joint fatigue strength one to be created. The automated script that uses the aforementioned spreadsheet takes about 15 minutes to run (0.25 hours). Once the model contains all the fatigue failure index responses, the input file is output from the pre-processor and the job is submitted for solution.

The process for the open-hole fatigue case is very similar, with the exception that the spreadsheet is not required since there are no modification factors to worry about. The "reader elements" required for this type of optimization setup are rod elements with the miniscule area at the edge of the holes, checked for the fatigue. The automated script, upon the selection of all of the reader elements, creates the same type of response that is generated for the fastener joint fatigue details without the modification factors, since the direct stress values from the detailed model are directly input to the appropriate S-N curve. The functional response for each of the reader elements calculates the failure index with the same fatigue spectrum used for the fastener joint fatigue evaluation. The complete engineering effort of creating of the open-hole fatigue failure index responses takes 1 hour.

8.2.5 Level Three Sizing Engineering Effort

After the first two levels of the sizing effort are done, the final third phase requires the effort of running empirical style optimization responses for the static and stability (buckling/crippling) checks so that the pylon structure can be certified in the typical way. Even though the type of the analysis that is sufficient for substantiation of the sections and panels is a discretion of the designated authorized certification agency representative (AR), it is safe to assume that the empirically based equations that show actual stress calculation using the math formula relating the applied load to the appropriate geometrical and material characteristics of the section/panel are required.

For the level three sizing effort Fig, 36 is employed. Similar to the traditional-based sizing effort, checks needed to be performed to substantiate the longeron, fitting, and frames stiffener sections:

(a) Section strength check

(b) Crippling

(c) Column buckling

The use of the MAP is broken down into two sub tasks: one is creating the features. In this case the beam sections on the longerons, fittings and frames. The other: creating the actual checks (strength, crippling, and column buckling).

In order to quantify the required engineering hours for creating the complete set of features and checks for the beam sections, let us break it down to the engineering hours required to create the features and engineering hours required to create the actual checks. The process of creating the beam section features consists of selecting the elements and the nodes that define the sections. It takes about 0.083 hours to create each of the beam section features.

$$T^{M}_{BeamSecFeat} = \left[\frac{4}{2}\cdot i + (i+1)\cdot\left(\frac{8\cdot\sqrt{n}}{2}\right) + (q+r+s)\right]\cdot 0.083 \qquad \textbf{87}$$

Using MAP checks can be generated for multiple features. However given that the allowable values are related to the manufacturing material, one need to create checks for each individual part (longeron, frame/bulkhead/fitting) independently. So the total effort related to creating the checks using the MAP is

directly related to the number of the components in the pylon (the symmetry needs to be accounted for). There are 4 longerons (but half used for symmetry), ***u*** of the pylon to wing fittings, and (***i+1***) frames bulkheads. If one check takes 0.083 hours, the total engineering effort of creating the checks can be calculated as:

$$T^{M}_{BeamSecChecks} = \left[\frac{4}{2} + (i+1) + u\right] \cdot 0.083 \qquad \textbf{88}$$

In order to substantiate the panel stability requirements, the panel features and then panel buckling checks are to be created using the MAP. The panel feature-creating consists of selecting all of the elements that belong to a given panel. The engineering effort of creating a single panel feature is 0.033 hours. However there is a significant number of panels in the pylon model. Thus, the total engineering effort of crating the panel features can be calculated as:

$$T^{M}_{PanelFeat} = \left[4 \cdot i + (i+1) \cdot \frac{n}{2}\right] \cdot 0.033 \qquad \textbf{89}$$

Creating the check for all of the panel features is a trivial task since it can be done in few clicks for all of the created panel features. The allowable value is identical for all of the panel features. Total engineering time for panel checks is 1 hour.

The only remaining checks that are required for the level 3 sizing effort are the lug and angle/channel fitting checks. The engineering effort for creating the angle/channel fitting feature, and lug feature are 0.166 and 0.083 hours respectively. For total of 16 angle/channel fitting features and 6 lugs the total engineering time for the feature creating can be calculated as:

$$T^{M}_{FittingsLugsFeat} = 16 \cdot 0.166 + 6 \cdot 0.083 = 3.154 hours \qquad \textbf{90}$$

Finally one needs to create the angle/channel fitting and lug allowable checks. Typically the actual allowable values are not straightforward and require some effort to create. The engineering hours for each of the checks is 0.25 hours. So with 22 total features the total engineering effort is equal to:

$$T^{M}_{FittingsLugsCheck} = 22 \cdot 0.25 = 5.5 hours \qquad \textbf{91}$$

8.2.6 Documentation of the Final Margins

Final documentation of the margins with the model based approach is not any different from the document based process. Still, the number of hours of documentation is typically 25 hours per pylon bay. Documentation has direct relationship to the pylon size, and since the number of bays is the parameter that best describes the pylon overall size, the engineering effort for documentation will be calculated as:

$$T^{D}_{Docum} = i \cdot 25 \qquad \textbf{92}$$

8.2.7 Actual Engineering Hours Required to Size Study Pylon Using the Model Based Approach

The total engineering hours required to generate the loads for the model based approach are summarized in Table 23.

	Load Development
Hours	260
Weeks	6.5

Table 23 Loads Development Engineering Hours for Model Based Process

The results of the calculation of the engineering hours/weeks required to execute the sizing of the test-case pylon using the model based approach are shown with Table 24.

Sizing Tasks	Engineering Hours
Level One Setup Spreadsheets	32
Level One Response/Constraint	1
Level Two Spreadsheet	24
Level Two Response/Constraint	2
Level Three section features	9.88
Level Three section checks	1.08
Level Three Panel features	5.31
Level Three Panel check	1
Level Three fitting/lugs features	3.15
Level Three fitting/lugs checks	5.5
Sum	84.92
Sum (weeks)	2.12

Table 24 Pylon Component Sizing Engineering Hours for Model Based Process

The documentation effort is shown in Table 25.

	Engineering Hours	Engineering Weeks
Documentation	175	4.375

Table 25 Documentation Engineering Hours for Model Based Process

Table 26 summarizes the engineering time required for one cycle of pylon sizing done by single engineer.

	Engineering hours (weeks)
Loads Development	6.5
Sizing	2.12
Documentation	4.375
Sum	13

Table 26 Total Engineering Hours for Model Based Process

8.3 Sizing the Study Pylon Using the Model Based Approach

8.3.1 The Model Based Multi-Level Sizing Platform

The multi-level strength, stability and durability sizing is carried out with the model based approach. This means that a combination of the surrogate checks (FEM stresses for strength, and eigenvalue for stability), and empirical based checks are done for the static joint analysis, as the first level of the sizing. Once the structure is approximately sized using the first level, the results of that sizing are applied to the pylon FEM and a single critical load case is determined for each structural component as well as the particular section/panel/fastener pattern on the component. The second level of optimization consists of the fatigue checks for each fastener joint and open hole. During the second level optimization sizing using the automated fatigue model based tool the design variables are allowed to only increase from the results achieved by the first level sizing. Fatigue typically sizes only a limited number of fastener joint locations (since each fastener is previously sized using the static fatigue check during the first level sizing optimization) and web cutouts. This validates the assumption that the results of the static, stability and static fastener checks, done during the first level sizing are still valid. Finally, the third level of optimization, uses the information from the level one sizing optimization about a single critical load case for each structural

component as well as the particular section or panel on the component to apply empirical checks for the sections, panels, and fittings using the model based automated response and constraint generating platform (Figure 36).

8.3.2 Initial pylon design

As with any gradient based optimization approaches and design evolution in general, the initial design is important. In a typical commercial aircraft development program the initial design gets created by the design team starting with the overall, newly designed, aircraft parameters as well as past program pylon designs. The detailed FEM, the basis for the model based sizing approach, has to be built based on this initial design, and the weights for each individual pylon component recorded into the table.

The starting test-case pylon design weights are recorded in Table 27.

The key input for the wing design are the maximum envelope loads at the pylon to wing interfaces. These are provided in Table 28. Except for being key input parameters for the wing design, these values are used to show the equivalence between the coarse FEM used for the document based sizing and the detailed FEM used for the model based sizing approach.

8.3.3 Level-One Sizing Results

The allowable values used in the model based approach are the same ones that were previously used with the document based approach (see Table 20). The strength check responses and constraints are applied to the model using Table 20 and the process described in Section 4.14 Strength of All Structural Components except Major Fittings.

Component	Weight(lbs.)
Aft_Bulkhead	23.200
Aft_Eng_Fitt_Bulkhead	61.302
Aft_Upper_Web	10.457
Frame_1	8.914
Frame_2	4.915
Frame_3	12.034
Frame_4	30.689
Frame_5	17.955
Frame_6	8.276
Fwd_Eng_Fitt_Bulkhead	65.883
LH_Front_Spar_Fitting	58.951
LH_Lwr_Longeron	24.726
LH_Side_Web	35.588
LH_Upr_Longeron	13.262
Lower_Web	70.032
Lwr_Link_Fitting	26.296
RH_Front_Spar_Fitting	58.854
RH_Lwr_Longeron	24.725
RH_Side_Web	35.587
RH_Upr_Longeron	13.262
Upper_Link_Fitting	25.102
Upper_Web	31.423
Total:	661.431

Table 27 Initial (before sizing) Component's Weights

	Fx(kips)	Fy(kips)	Fz(kips)	Fres(kips)
Max LH_FS_Diag	0.18525	39.05	103.05	110.2009
Max RH_FS_Diag	0.18514	38.571	102.99	110.1363
Max Upper_Link	257.57	0	133.85	290.2725
Max LH_FS_Main	303	0	206.36	366.5971
Max RH_FS_Main	303.11	0	206.34	366.6851
Max Lower_Link	312.31	0	59.931	380.0295

Table 28 Detailed FEM Initial Design Pylon to Wing Reaction Forces

During the first level of model based sizing the pylon structure is sized for stability using the eigenvalue buckling solution and therefore the related direct response is constrained with the lower bound to the value of 1.05 (effectively 5% margin). The fastener checks are implemented using the empirical method described earlier. The checks are applied to the model using the process described Section 4.15. Table 43 that is used to generate all the static fastener joint checks can be found in Appendix A. The fastener shear strength values (Fsu) are used from (B1990), and the bearing allowable values are used from (DoD1998).

It is recommended to run sizing for strength first, then add the stability requirements (buckling and crippling), and then finally to the pylon sized for strength and stability add the static fastener joint checks. If the level one sizing is run in such a way, the knowledge about the design is elevated and could be used for future initial designs decision making.

After level one strength sizing, using the direct principal stress constraints the following results were obtained:

Component	Weight(lbs.)
Aft_Bulkhead	18.634
Aft_Eng_Fitt_Bulkhead	44.376
Aft_Upper_Web	8.405
Frame_1	6.374
Frame_2	4.088
Frame_3	8.951
Frame_4	19.875
Frame_5	10.859
Frame_6	6.814
Fwd_Eng_Fitt_Bulkhead	60.356
LH_Front_Spar_Fitting	41.281
LH_Lwr_Longeron	15.559
LH_Side_Web	31.888
LH_Upr_Longeron	8.027
Lower_Web	30.786
Lwr_Link_Fitting	33.541
RH_Front_Spar_Fitting	41.249
RH_Lwr_Longeron	15.559
RH_Side_Web	31.888
RH_Upr_Longeron	8.027
Upper_Link_Fitting	25.366
Upper_Web	24.787
	496.690

Table 29 Level 1 Strength Sizing Only Component's Weight

Since the starting weights, given by the Table 27, were an educated guess by the design team, it does not add much to discussion the weight difference before and after strength sizing. However it is worth mentioning that even at the much higher weight compared to the strength sized solution (661 lbs. vs. 476 lbs.) the initial design had some extremely high negative margins. The first twenty worst margins in the initial design are provided in Table 30.

Response	Load Case	Measured	Allowed	Margin
304 STRES PStr_100	1	3.43E+05	1.18E+05	-0.66
304 STRES PStr_100	1	3.41E+05	1.18E+05	-0.65
177 STRES PStr_130	1	1.62E+05	5.70E+04	-0.65
243 STRES PStr_513	12	2.93E+05	1.06E+05	-0.64
243 STRES PStr_513	12	2.86E+05	1.06E+05	-0.63
177 STRES PStr_130	1	1.50E+05	5.70E+04	-0.62
303 STRES PStr_100	1	3.04E+05	1.18E+05	-0.61
303 STRES PStr_100	1	3.04E+05	1.18E+05	-0.61
232 STRES PStr_513	12	2.58E+05	1.06E+05	-0.59
232 STRES PStr_513	12	2.58E+05	1.06E+05	-0.59
304 STRES PStr_100	3	2.86E+05	1.18E+05	-0.59
304 STRES PStr_100	3	2.85E+05	1.18E+05	-0.59
304 STRES PStr_100	201	2.84E+05	1.18E+05	-0.59
304 STRES PStr_100	201	2.82E+05	1.18E+05	-0.58
177 STRES PStr_130	201	1.30E+05	5.70E+04	-0.56
177 STRES PStr_130	3	1.29E+05	5.70E+04	-0.56
344 STRES PStr_201	103	2.34E+05	1.04E+05	-0.55
344 STRES PStr_201	103	2.34E+05	1.04E+05	-0.55
303 STRES PStr_100	201	2.53E+05	1.18E+05	-0.54
303 STRES PStr_100	201	2.53E+05	1.18E+05	-0.53

Table 30 Initial Design before Sizing Twenty Worst Negative Margins

After adding the stability requirements to the sizing optimization run (Buckling eigenvalue greater or equal to the 1.05 for all of the load cases) the process converges to the solution. This solution is described by the weights in the Table 31.

There are some important points that can be made based on Table 31 results. First, the results seem to make sense. The components that feature panels (all of the webs) as well as the long and slender components (longerons) have been up-gauged. But maybe more important is the fact that the optimization driven model based sizing takes advantage of all weight opportunities. Even though the additional requirement is placed on the design (that it needs to be stable under the prescribed set of loads) weight is removed from certain components. This is not due to the fact that these components were oversized. They were not, since they were sized previously by the strength driven optimization simulation. Rather this is due to the fact that once webs and longerons are sized-up to meet the stability requirement, other components picked up less load, and thus they could be down-gauged.

Component	Streght Only	Streght + Stability	Delta
Aft_Bulkhead	18.634	17.552	-1.082
Aft_Eng_Fitt_Bulkhead	44.376	43.573	-0.803
Aft_Upper_Web	8.405	10.153	1.748
Frame_1	6.374	6.196	-0.178
Frame_2	4.088	4.562	0.474
Frame_3	8.951	8.871	-0.080
Frame_4	19.875	19.369	-0.506
Frame_5	10.859	10.886	0.027
Frame_6	6.814	6.800	-0.014
Fwd_Eng_Fitt_Bulkhead	60.356	60.666	0.310
LH_Front_Spar_Fitting	41.281	40.062	-1.219
LH_Lwr_Longeron	15.559	23.129	7.570
LH_Side_Web	31.888	42.475	10.587
LH_Upr_Longeron	8.027	9.995	1.968
Lower_Web	30.786	58.620	27.834
Lwr_Link_Fitting	33.541	31.300	-2.241
RH_Front_Spar_Fitting	41.249	40.036	-1.213
RH_Lwr_Longeron	15.559	23.129	7.570
RH_Side_Web	31.888	42.474	10.586
RH_Upr_Longeron	8.027	9.995	1.968
Upper_Link_Fitting	25.366	26.608	1.242
Upper_Web	24.787	33.037	8.250
	496.69	569.488	72.798

Table 31 Component Weight Table after Strength and Stability Sizing

The final part of the level one model based sizing process adds the static fastener joint constraints to the strength and stability sized pylon. The results in terms of the component weights after the optimization with strength, stability and static fastener joint checks converges is given by Table 32.

Once the level-one sizing is complete, the model based approach provides visibility regarding the minimum margins (Figure 69).

Component	Streght + Stability	Streght + Stability + Static Joint Strengh	Delta
Aft_Bulkhead	17.552	18.005	0.453
Aft_Eng_Fitt_Bulkhead	43.573	44.230	0.657
Aft_Upper_Web	10.153	10.217	0.064
Frame_1	6.196	6.218	0.022
Frame_2	4.562	4.546	-0.016
Frame_3	8.871	8.849	-0.022
Frame_4	19.369	19.612	0.243
Frame_5	10.886	10.904	0.018
Frame_6	6.8	6.800	0.000
Fwd_Eng_Fitt_Bulkhead	60.666	61.478	0.812
LH_Front_Spar_Fitting	40.062	40.740	0.678
LH_Lwr_Longeron	23.129	24.435	1.306
LH_Side_Web	42.475	45.036	2.561
LH_Upr_Longeron	9.995	10.183	0.188
Lower_Web	58.62	59.686	1.066
Lwr_Link_Fitting	31.3	32.188	0.888
RH_Front_Spar_Fitting	40.036	40.714	0.678
RH_Lwr_Longeron	23.129	24.434	1.305
RH_Side_Web	42.474	45.035	2.561
RH_Upr_Longeron	9.995	10.183	0.188
Upper_Link_Fitting	26.608	26.503	-0.105
Upper_Web	33.037	32.928	-0.109
	569.488	582.922	13.434

Table 32 Component Weight Table after Strength, Stability and Static Fastener Strength Sizing

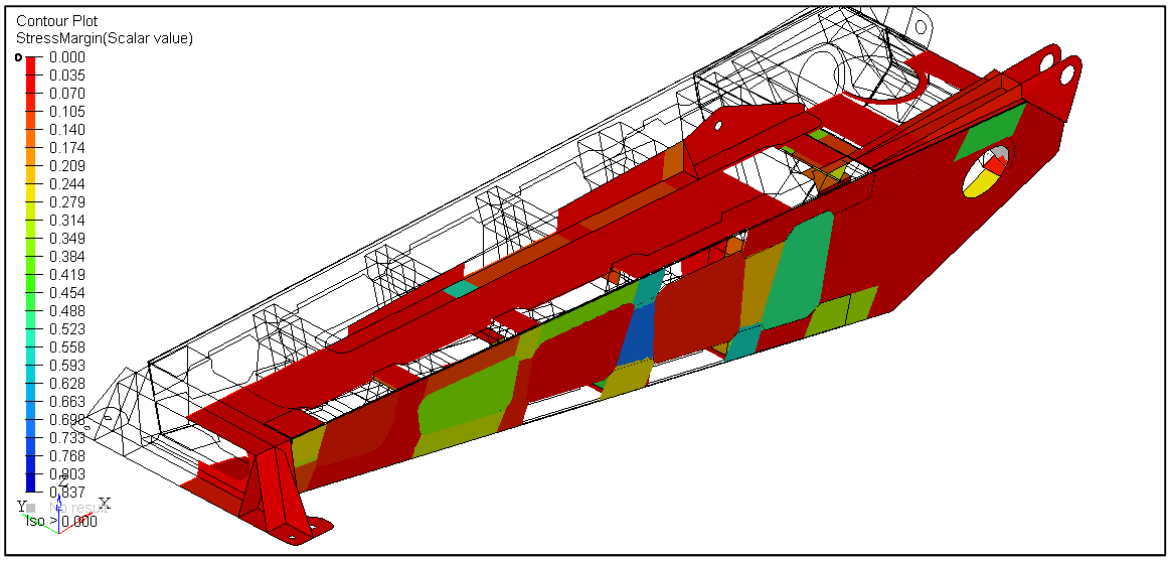

Figure 69 Minimum Strength Margin Contour Plot

Except for plotting the minimum margins, it is critical to understand from the certification stand point which parts of the pylon are sized by which load. The model based platform provides easy visualization in the form of contour plots (Figure 70).

The plot here is shown for the visualization purposes. Table 65 in Appendix A contains part by part contour plots that will be used during the level 3 sizing for guidance to where and which the certification grade checks need to be carried out.

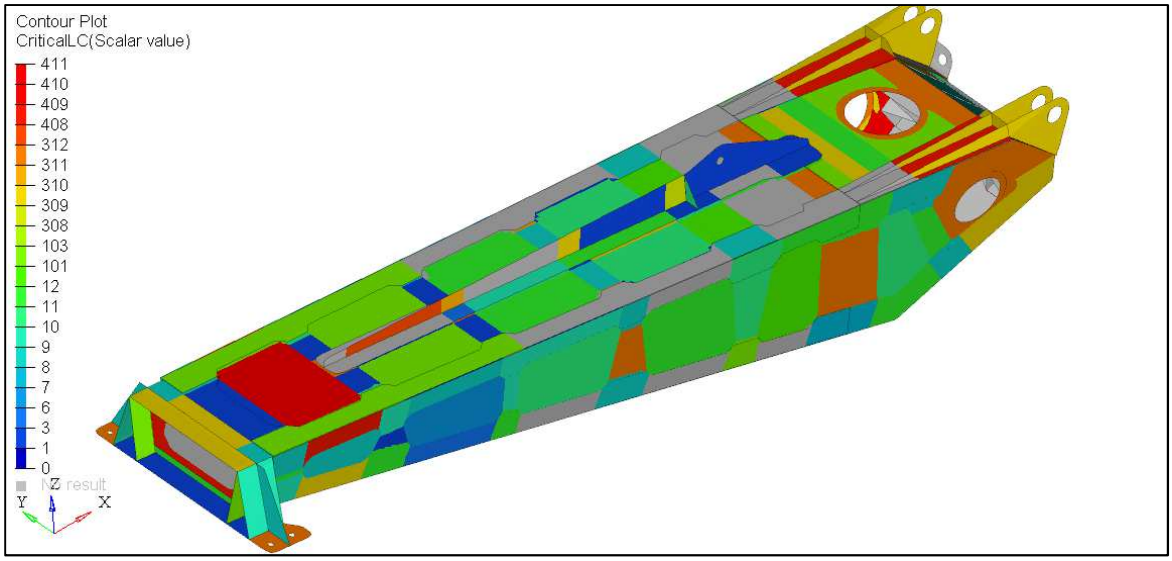

Figure 70 Critical Strength Margins' Load Cases

Similar to the strength sizing plots the model based platform provides insight into the entire stability solution. The final sizing iteration gives the summary of the lowest stability margins. Table 33 shows the lowest stability margins, and Table 66 in Appendix A shows the buckling eigenvectors for these stability critical load cases.

Load Case	Eigen Value	Allowable	Margin	Load Case	Eigen Value	Allowable	Margin
91	1.046292	1.05	-0.004	9203	1.352215	1.05	0.288
93	1.148021	1.05	0.093	9301	1.52754	1.05	0.455
96	1.314667	1.05	0.252	9307	1.560476	1.05	0.486
97	1.315394	1.05	0.253	9308	1.184207	1.05	0.128
98	1.076371	1.05	0.025	9309	1.336257	1.05	0.273
99	1.113979	1.05	0.061	9310	1.140029	1.05	0.086
910	1.055102	1.05	0.005	9311	1.222245	1.05	0.164
911	1.054125	1.05	0.004	9401	1.527688	1.05	0.455
912	1.074368	1.05	0.023	9406	1.553722	1.05	0.480
9101	1.056819	1.05	0.006	9408	1.352687	1.05	0.288
9102	1.542928	1.05	0.469	9409	1.187845	1.05	0.131
9103	1.06836	1.05	0.017	9410	1.239079	1.05	0.180
9106	1.442047	1.05	0.373	9411	1.144882	1.05	0.090
9107	1.44909	1.05	0.380	9412	1.315287	1.05	0.253
9110	1.493139	1.05	0.422				
9111	1.493993	1.05	0.423				
9201	1.22748	1.05	0.169				

Table 33 Lowest Stability Margins

The model based platform also allows the engineer to visually inspect the minimum margins of the static fastener joint checks, both for bearing and the fastener shear margins. Figure 71, and Figure 72 show the bearing and fastener shear margins, and Table 67, and Table 68 report the components affected by the minimal static fastener joint margins.

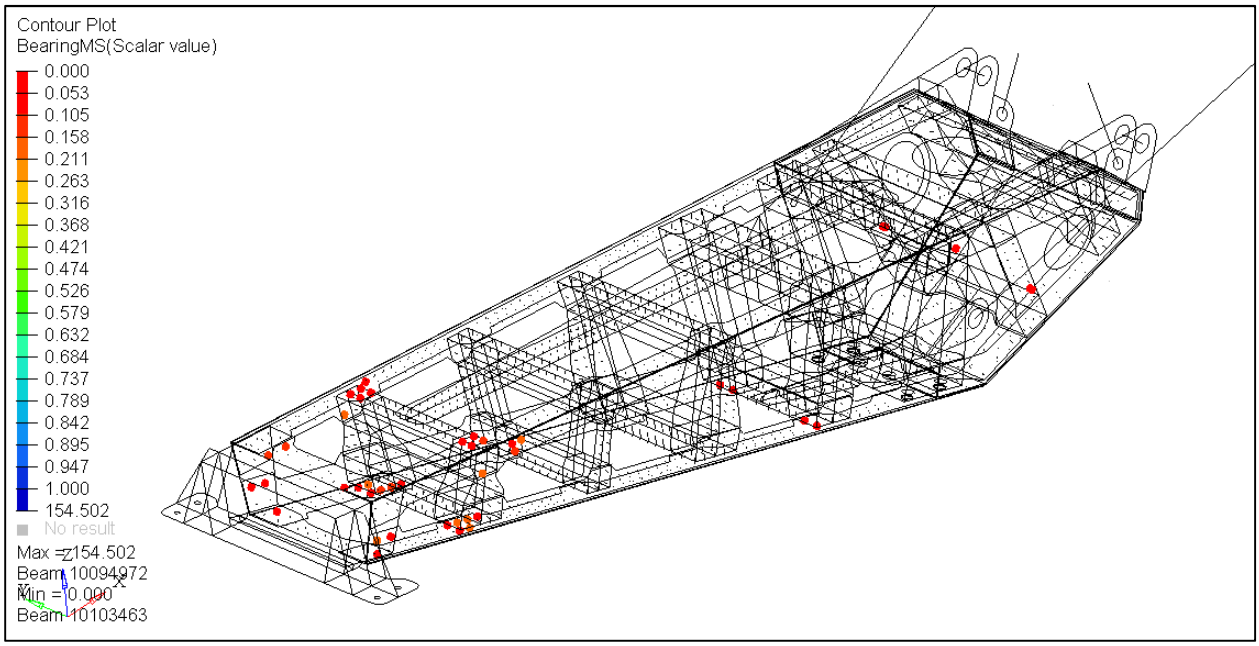

Figure 71 Minimum Bearing Margins

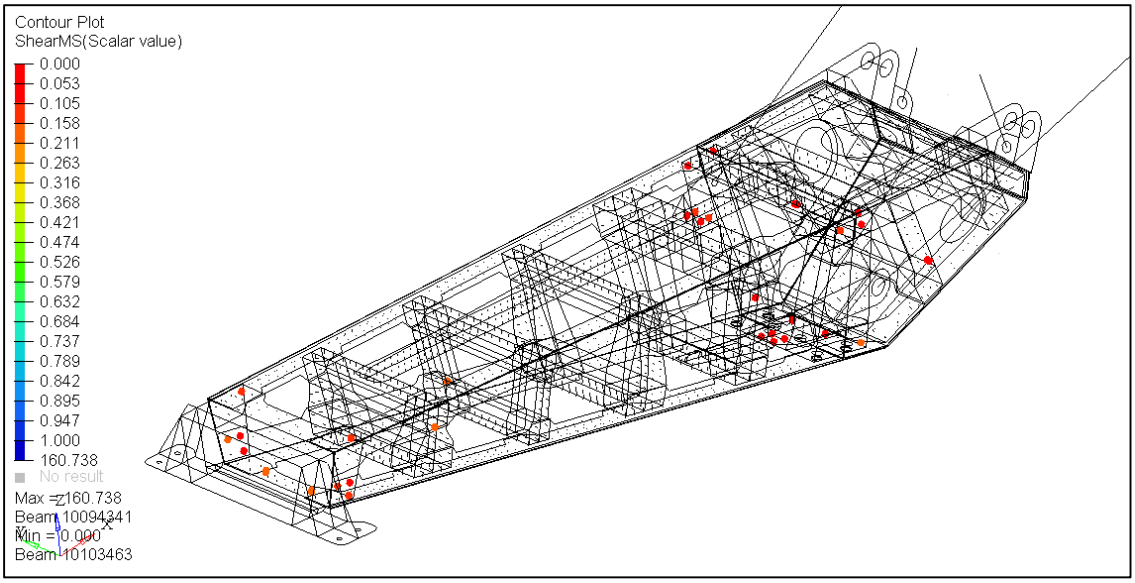

Figure 72 Minimum Fastener Shear Margins

8.3.4 Level-Two Results

After level-one optimization is complete, the level two fatigue sizing phase begins. Typically, after phase one sizing is complete, and if all of the static fastener margins are calculated for each individual fastener, the sizing for fastener joint margins does not increase the overall weight of the pylon box significantly. Table 34 proves this point, showing that the overall pylon box weight after fatigue sizing has increased by merely 4.87 lbs, or less than one percent. The detailed margin values for the fatigue joint analysis are provided with Table 69 to

Table 76 in Appendix A.

Component	Level One Sizing Complete	Level Two (Fatigue)	Delta
Aft_Bulkhead	18.005	18.005	0.000
Aft_Eng_Fitt_Bulkhead	44.23	44.229	0.000
Aft_Upper_Web	10.217	10.217	0.000
Frame_1	6.218	6.218	0.000
Frame_2	4.546	5.110	0.564
Frame_3	8.849	8.849	0.000
Frame_4	19.612	21.212	1.600
Frame_5	10.904	11.895	0.991
Frame_6	6.8	6.800	0.000
Fwd_Eng_Fitt_Bulkhead	61.478	61.478	0.000
LH_Front_Spar_Fitting	40.74	40.740	0.000
LH_Lwr_Longeron	24.435	24.435	0.000
LH_Side_Web	45.036	45.893	0.857
LH_Upr_Longeron	10.183	10.183	0.000
Lower_Web	59.686	59.686	0.000
Lwr_Link_Fitting	32.188	32.192	0.000
RH_Front_Spar_Fitting	40.714	40.714	0.000
RH_Lwr_Longeron	24.434	24.434	0.000
RH_Side_Web	45.035	45.892	0.857
RH_Upr_Longeron	10.183	10.183	0.000
Upper_Link_Fitting	26.503	26.503	0.000
Upper_Web	32.928	32.928	0.000
	582.922	587.795724	4.869

Table 34 Component Weight Table after Fatigue Sizing

8.3.5 Level-Three Sizing

The level three sizing needs to be executed in order to meet the requirements of certification grade analysis. The panel buckling (eigenvalue solutions) and the fastener analysis done with level one and two are certification grade, and so neither panel buckling nor fastener joint analysis need to be considered with the level three analysis. However the following checks need to be performed, as per Figure 6:

(a) Longeron, fitting and frame section net tension and crippling checks

(b) Fitting lug checks

(c) Bulkhead/Frame, fitting angle/channel fitting

Longeron, fitting, and frame section net tension and crippling checks: Figure 70, as well as the Table 65 show which load cases are critical for each of the parts. Thus, the net tension and crippling checks will be executed only for these load cases.

After the net tension and crippling section checks are complete there are just lower longeron sections that require thickness update in order to meet the allowable values. This section is shown in Figure 73 .

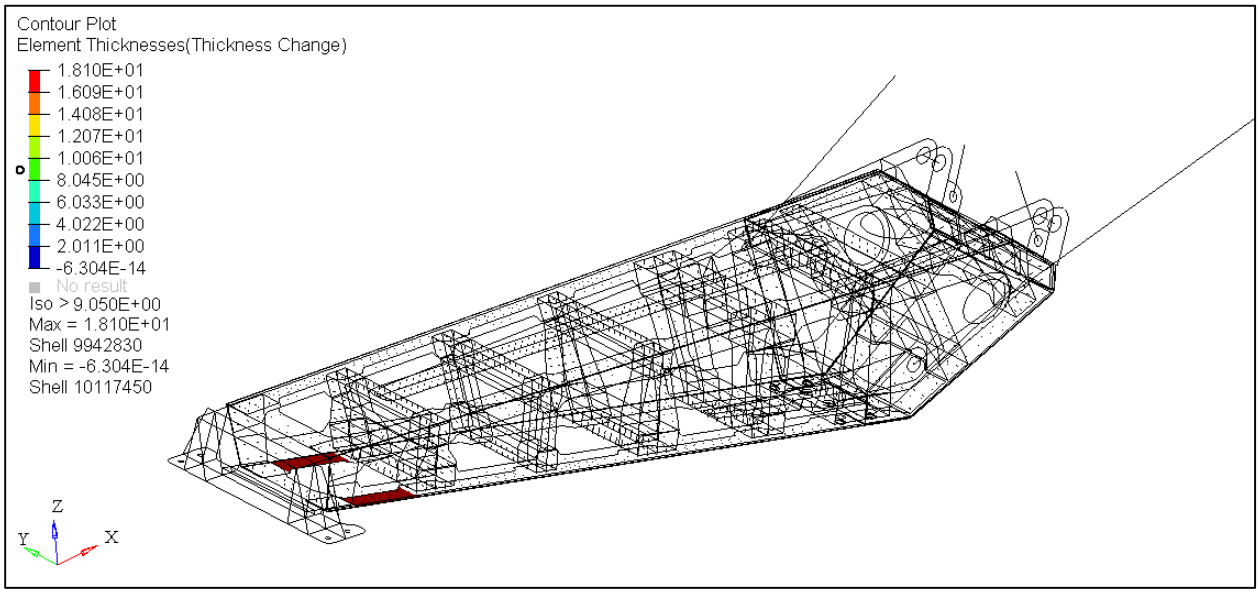

Figure 73 Thickness Increase due to the Net Tension and Crippling Checks

The weight increase is minimal, broken down by the component in the Table 35.

Component	Level Two Sizing Complete	Level Three (Section Checks Only) Complete	Delta
Aft_Bulkhead	18.005	18.005	0.000
Aft_Eng_Fitt_Bulkhead	44.229	44.229	0.000
Aft_Upper_Web	10.217	10.217	0.000
Frame_1	6.218	6.218	0.000
Frame_2	5.110	5.110	0.000
Frame_3	8.849	8.849	0.000
Frame_4	21.212	21.212	0.000
Frame_5	11.895	11.895	0.000
Frame_6	6.800	6.800	0.000
Fwd_Eng_Fitt_Bulkhead	61.478	61.478	0.000
LH_Front_Spar_Fitting	40.740	40.740	0.000
LH_Lwr_Longeron	24.435	24.664	0.229
LH_Side_Web	45.893	45.893	0.000
LH_Upr_Longeron	10.183	10.183	0.000
Lower_Web	59.686	59.686	0.000
Lwr_Link_Fitting	32.192	32.192	0.000
RH_Front_Spar_Fitting	40.714	40.714	0.000
RH_Lwr_Longeron	24.434	24.664	0.230
RH_Side_Web	45.892	45.892	0.000
RH_Upr_Longeron	10.183	10.183	0.000
Upper_Link_Fitting	26.503	26.503	0.000
Upper_Web	32.928	32.928	0.000
	587.796	588.254	0.458

Table 35 Weight Summary after the Level Three Section Sizing

Fitting lug checks

In order to calculate the margins of safety of the pylon to wing lugs the summary of critical loading conditions has to be created. Table 36 provides the summary of the critical loading as well as the angle of the load with respect to the horizontal plane.

	Fx (lbs.)	Fy (lbs.)	Fz (lbs.)	Fres (lbs.)	Angle(deg.)	Load Case
Lateral Front Spar Fitting	185	39050	103050	110201	69.25	411
Lower Link	312110	0	59893	379683	10.86	101
Main Front Spar Fitting	303110	0	206340	366685	34.24	310
Upper Link	257300	0	133710	289968	27.46	1

Table 36 Critical Lug Loading

Table 55 through Table 58 provide the details of the lug sizing analysis. These results are identical between the document and model based sizing approach since the loads, geometry, allowable values, and method are identical.

The required minimum margin of safety is 5% as it is for the rest of analyses. Table 37 details the component weights and the weight increase due to the lug analysis. From the data it is apparent that level one sizing for lugs significantly under sizes the lugs.

Component	Level Three (Section Checks Only) Complete	Level Three (Section and Lug Analysis) Complete	Delta
Aft_Bulkhead	18.005	18.005	0.000
Aft_Eng_Fitt_Bulkhead	44.229	44.229	0.000
Aft_Upper_Web	10.217	10.217	0.000
Frame_1	6.218	6.218	0.000
Frame_2	5.110	5.110	0.000
Frame_3	8.849	8.849	0.000
Frame_4	21.212	21.212	0.000
Frame_5	11.895	11.895	0.000
Frame_6	6.800	6.800	0.000
Fwd_Eng_Fitt_Bulkhead	61.478	61.478	0.000
LH_Front_Spar_Fitting	40.740	42.981	2.241
LH_Lwr_Longeron	24.664	24.664	0.000
LH_Side_Web	45.893	45.893	0.000
LH_Upr_Longeron	10.183	10.183	0.000
Lower_Web	59.686	59.686	0.000
Lwr_Link_Fitting	32.192	32.676	0.484
RH_Front_Spar_Fitting	40.714	42.955	2.241
RH_Lwr_Longeron	24.664	24.664	0.000
RH_Side_Web	45.892	45.892	0.000
RH_Upr_Longeron	10.183	10.183	0.000
Upper_Link_Fitting	26.503	33.234	6.731
Upper_Web	32.928	32.928	0.000
	588.255	599.952	11.697

Table 37 Weight Summary after Level Three Lug Analysis

Bulkhead/Frame, Fitting Angle/Channel Fitting

Appendix A, in Table 59 to Table 64, detail the sizing of the angle and channel fittings. The weight increase (2.73 lbs.) due to these checks is fairly minimal. The forward engine fitting bulkhead required gauging up the angle fitting walls due to the slightly negative wall bending checks. The aft engine fitting bulkhead had all positive margins. However, in order to meet the check requirements (two bending walls need to have same thickness) detailed in (N1988), a small up-gauging was required. Finally, the upper link fitting required small up-gauging of the end pad to meet the end pad shear requirement.

The summary of weight increase is provided in Table 38.

Component	Level Three (Section and Lug Analysis) Complete	Level Three Complete	Delta
Aft_Bulkhead	18.005	18.005	0
Aft_Eng_Fitt_Bulkhead	44.229	45.368	1.139
Aft_Upper_Web	10.217	10.217	0
Frame_1	6.218	6.218	0
Frame_2	5.11	5.11	0
Frame_3	8.849	8.849	0
Frame_4	21.212	21.212	0
Frame_5	11.895	11.895	0
Frame_6	6.8	6.8	0
Fwd_Eng_Fitt_Bulkhead	61.478	62.984	1.506
LH_Front_Spar_Fitting	42.981	42.981	0
LH_Lwr_Longeron	24.664	24.664	0
LH_Side_Web	45.893	45.893	0
LH_Upr_Longeron	10.183	10.183	0
Lower_Web	59.686	59.686	0
Lwr_Link_Fitting	32.676	32.676	0
RH_Front_Spar_Fitting	42.955	42.955	0
RH_Lwr_Longeron	24.664	24.664	0
RH_Side_Web	45.892	45.892	0
RH_Upr_Longeron	10.183	10.183	0
Upper_Link_Fitting	33.234	33.322	0.088
Upper_Web	32.928	32.928	0
	599.952	602.685	2.733

Table 38 Weight Summary after Level Three Sizing

Chapter 9: The Model Based Process Compared to Document Based Process

9.1 Cost of the Engineering Effort Comparison

9.1.1 Loads Development Time and Cost Comparison

Comparing the values from the Table 14 and Table 23 – approximately 30 vs. 6.5 weeks - the advantage of the model based over the document based process is obvious. Percentage wise the adoption of the model based engineering platform for the pylon certification process would result in reduction of 78.5% in engineering weeks required for loads development for pylon certification. Load development cost savings, given that the present date engineering hour costs approximately $250.00 (taking in account the base pay, and all of the benefits), would equate to $237,300.

This staggering time and engineering cost savings that comes from the model based approach adoption can be attributed to these major differences:

(a) Elimination of the internal load extraction

(b) Elimination of the load/sizing convergence checks

(c) Elimination of the additional load cycles due to the non-converged solution

9.1.2 Structural Sizing Time and Cost Comparison

Comparing the values from Table 15 and Table 24 – approximately 25 vs. 2 weeks - the advantage of the model based over the document based process is obvious. Percentage-wise, the adoption of the model based engineering platform for the pylon certification process would result in reduction of almost 92% in engineering weeks required for structural sizing of the pylon. Structural sizing cost savings (assuming same cost of $250 per engineering hour) would equate to $235,100.

High time and engineering cost savings that results from the model based approach adoption should be attributed to these major differences:

(a) Elimination of multiple models, rather use of a single model that contains all the pertinent information about the design

(b) Elimination of the part by part checking philosophy typical for the document based process

(c) Elimination of the additional load cycles due to the non-converged solution

9.1.3 Documentation Time and Cost Comparison

Comparing the values from Table 16 and Table 25 – approximately 12 vs. 4.375 weeks - the advantage of the model based over the document based process is obvious. Percentagewise, the adoption of the model based engineering platform for the pylon certification process would result in reduction of approximately 63% in engineering weeks required for documentation. Documentation cost savings (still assuming cost of $250 per engineering hour) would equate to $74,650.

These significant time and engineering cost savings that results from the model based approach adoption should be attributed to these major differences:

(a) Elimination of the documentation of the internal loads

(b) Elimination the data transfer, and data conversion that is required with the document based approach

(c) Elimination of the additional load cycles due to the non-converged solution

9.1.4 Overall Time and Cost Comparison

Table 39 provides the full summary of the comparison of the engineering cost and effort between the document and model based approach.

	Document Based	Model Based	Difference	Percentage Difference	Cost Difference
Loads	30.23	6.5	-23.73	-78.50%	-$237,300
Sizing	25.63	2.12	-23.51	-91.73%	-$235,100
Documentation	11.84	4.375	-7.465	-63.05%	-$74,650
		Sum:	-54.705	Sum:	-$547,050

Table 39 Engineering Effort and Cost Comparison

Taking into account that this comparison captures only one out of typically three load cycles of the pylon development, the cost savings that model based approach provides are even more significant. For three load cycles the non-recurring (engineering) cost savings for a single program would be close to 1.5 million dollars. As much as the cost savings is significant, in the competitive market place the reduction in the development time might be even more significant. For three load cycles the total engineering time that can be saved using the model based approach is 3.15 engineering years. This, off course, does not directly translate into shortening engineering development by full 3.15 years since the engineering workload is spread across multiple engineers with document based process. Nevertheless, it represents a very relevant reference number on the advantage that the model based engineering platform has over the document based one.

9.2 Sizing Results Comparison

Before getting into the detailed comparison of numbers, it very important to reiterate that the two resulting designs, one coming from following the document based approach and the other coming from following the model based approach, started from the same exact initial design (approximately 661 lbs.). Equally important is the fact that both designs are capable of meeting the same structural requirements using exactly the same allowable values.

9.2.1 Overall Weight Comparison

Comparison of the final values from the Table 21 and Table 38 – 895.15 lbs. vs. approximately 602.7 lbs. - shows a significant weight advantage of the model based approach. The weight difference of approximately 292 pounds represents a reduction in weight of 32.67% when the model based approach is used. Realistically, the document based pylon sizing process typically is followed by a post-design optimization effort that on average removes 5-10% of weight. However, it adds to the non-recurring

engineering cost of the document base process[4]. This manual optimization effort has not been carried out as part of this work. Nevertheless, assuming the highest (based on experience) common weight savings coming from the post-design optimization work (10%) with the document based process, the resulting weight would be approximately 805 lbs. Comparing this number to the model based development approach weight of 602.7 lbs. the weight difference of approximately 203 lbs. would still represent approximately 25% weight difference between the two approaches. Interestingly, this 25% weight savings correlates extremely well with the initial predictions provided by Equation 6 that describes the design inefficiency of the document based approach.

[4] The document based optimization, done in component by component fashion, is typically very limited, due to requirement that the interface loads (loads between the components) remain unchanged. The cause for applying such limitation to the weight-savings optimization comes from the fact that running additional load-sizing iterations take significant time and effort and thus is very costly.

9.2.2 Component by Component Weight Comparison

Let us first examine the initial pylon design and compare it to the document based process sized design.

	Initial Design	Document Based Design	Difference (lbs.)	Percentage Difference
Aft_Bulkhead	23.2	26.66	3.46	14.91%
Aft_Eng_Fitt_Bulkhead	61.302	80.48	19.178	31.28%
Aft_Upper_Web	10.457	22.25	11.793	112.78%
Frame_1	8.914	8.96	0.046	0.52%
Frame_2	4.915	4.93	0.015	0.31%
Frame_3	12.034	12.84	0.806	6.70%
Frame_4	30.689	32.23	1.541	5.02%
Frame_5	17.955	36.58	18.625	103.73%
Frame_6	8.276	9.05	0.774	9.35%
Fwd_Eng_Fitt_Bulkhead	65.883	71.99	6.107	9.27%
LH_Front_Spar_Fitting	58.951	74.36	15.409	26.14%
LH_Lwr_Longeron	24.726	37.92	13.194	53.36%
LH_Side_Web	35.588	50.62	15.032	42.24%
LH_Upr_Longeron	13.262	14.56	1.298	9.79%
Lower_Web	70.032	93.59	23.558	33.64%
Lwr_Link_Fitting	26.296	48.48	22.184	84.36%
RH_Front_Spar_Fitting	58.854	74.25	15.396	26.16%
RH_Lwr_Longeron	24.725	37.92	13.195	53.37%
RH_Side_Web	35.587	50.62	15.033	42.24%
RH_Upr_Longeron	13.262	14.56	1.298	9.79%
Upper_Link_Fitting	25.102	46.42	21.318	84.93%
Upper_Web	31.423	45.87	14.447	45.98%
	661.431	895.15	233.719	Avg: 35.34%

Table 40 Initial Design Component vs. Document Based Design Weights

Table 40 shows that most of the components, except Frames 1, and 2, experienced significant weight increases. Considering that the initial design was grossly violating the structural requirements (see Table 44 to Table 46) as previously said, the conclusion is that the weight increase is well justified. Frames 1 and 2 did not underwent weight increase and for these two components it seems that they were properly sized.

Now let us evaluate the initial pylon design in comparison to the model based process sized design, bearing in mind that exactly same structural margin violations of the initial design were noted with the model based approach as they were with the document based approach.

	Initial Design	Model Based	Difference	Percentage Difference
Aft_Bulkhead	23.2	18.005	-5.195	-22.39%
Aft_Eng_Fitt_Bulkhead	61.302	45.368	-15.934	-25.99%
Aft_Upper_Web	10.457	10.217	-0.24	-2.30%
Frame_1	8.914	6.218	-2.696	-30.24%
Frame_2	4.915	5.11	0.195	3.97%
Frame_3	12.034	8.849	-3.185	-26.47%
Frame_4	30.689	21.212	-9.477	-30.88%
Frame_5	17.955	11.895	-6.06	-33.75%
Frame_6	8.276	6.8	-1.476	-17.83%
Fwd_Eng_Fitt_Bulkhead	65.883	62.984	-2.899	-4.40%
LH_Front_Spar_Fitting	58.951	42.981	-15.97	-27.09%
LH_Lwr_Longeron	24.726	24.664	-0.062	-0.25%
LH_Side_Web	35.588	45.893	10.305	28.96%
LH_Upr_Longeron	13.262	10.183	-3.079	-23.22%
Lower_Web	70.032	59.686	-10.346	-14.77%
Lwr_Link_Fitting	26.296	32.676	6.38	24.26%
RH_Front_Spar_Fitting	58.854	42.955	-15.899	-27.01%
RH_Lwr_Longeron	24.725	24.664	-0.061	-0.25%
RH_Side_Web	35.587	45.892	10.305	28.96%
RH_Upr_Longeron	13.262	10.183	-3.079	-23.22%
Upper_Link_Fitting	25.102	33.322	8.22	32.75%
Upper_Web	31.423	32.928	1.505	4.79%
	661.431	602.685	-58.748	Avg: -8.47%

Table 41 Initial Design Component vs. Model Based Design Weights

Table 41 values represent maybe the biggest difficulty for the engineering communities that are used to document based process to accept optimization driven model based platform results. The fact that the weight of the final design is lower than the weight of the initial design, while the initial design is infeasible, seems counter-intuitive. Intuition based on the document based segmented process may suggest that additional material, and, hence, more weight, are required to make the initial infeasible design feasible.

The integrated model based approach, however, can lead to weight reduction in a structure that initially violates constraints because the entire pylon margins are calculated within the same model and the optimizer takes advantage of the load redistribution. The document based approach, due to its segmentation, misses on this opportunity.

Finally, let us compare the document based process-sized design to the model based process-sized design.

	Document Based	Model Based	Difference	Percentage Difference
Aft_Bulkhead	26.66	18.005	-8.655	-32.46%
Aft_Eng_Fitt_Bulkhead	80.48	45.368	-35.112	-43.63%
Aft_Upper_Web	22.25	10.217	-12.033	-54.08%
Frame_1	8.96	6.218	-2.742	-30.60%
Frame_2	4.93	5.11	0.18	3.65%
Frame_3	12.84	8.849	-3.991	-31.08%
Frame_4	32.23	21.212	-11.018	-34.19%
Frame_5	36.58	11.895	-24.685	-67.48%
Frame_6	9.05	6.8	-2.25	-24.86%
Fwd_Eng_Fitt_Bulkhead	71.99	62.984	-9.006	-12.51%
LH_Front_Spar_Fitting	74.36	42.981	-31.379	-42.20%
LH_Lwr_Longeron	37.92	24.664	-13.256	-34.96%
LH_Side_Web	50.62	45.893	-4.727	-9.34%
LH_Upr_Longeron	14.56	10.183	-4.377	-30.06%
Lower_Web	93.59	59.686	-33.904	-36.23%
Lwr_Link_Fitting	48.48	32.676	-15.804	-32.60%
RH_Front_Spar_Fitting	74.25	42.955	-31.295	-42.15%
RH_Lwr_Longeron	37.92	24.664	-13.256	-34.96%
RH_Side_Web	50.62	45.892	-4.728	-9.34%
RH_Upr_Longeron	14.56	10.183	-4.377	-30.06%
Upper_Link_Fitting	46.42	33.322	-13.098	-28.22%
Upper_Web	45.87	32.928	-12.942	-28.21%
	895.15	602.685	-292.455	Avg: -31.16%

Table 42 Document Based Design vs. Model Based Design Component Weights

Except for Frame 2, whose weight has been discussed already and deemed to be initially pretty well sized, the only two components that have relatively small weight differences between the designs arrived by the document and model based processes are the side webs. These components are the components that are tasked mostly with the shear load transfer from the engine input loads to the wing reaction loads and their gauges are almost exclusively driven by the shear stability requirements.

It seems that the only components that are similarly sized by the document and model based processes are the ones that are predominantly sized by the shear stability requirement and whose internal load are not dramatically influenced by the design changes.

Chapter 10: Model Based Design Based Exclusively on Direct Response

10.1 Introduction

Examining the weight numbers in Table 29 to Table 38 of the model based pylon sizing results, one question begs asking: “Given that the functional responses are adding fairly small amount of weight over the sizing done with the direct response driven sizing, is it possible to perform certification grade sizing of a pylon structure using exclusively FE based direct responses available in a modern gradient based commercial of-the-shelf software package?”.

Only the first two sizing optimization simulations, whose results are provided in Table 29 and Table 31 are in their entirety done using the direct optimization responses. A few very important observations at this point need to be made:

(a) These responses size the structure away from joints (fastener, lugs, fitting)

(b) The weight of the structure after these two sizing runs is 569.488 lbs. which represents a weight that is only 5.5 percent smaller than the final 602.685 lbs. weight number.

10.2 Static Fastener Joint Sizing Direct Vs. Functional Responses

The static fastener joint checks added relatively a small amount of the weight: 13.434 lbs. (the difference between the weights from Table 32 and Table 31) to the structure. Looking at the weight difference, one can lead to the conclusion that the direct stress responses due to their comprehensiveness (checking the stress at every element except for the elements immediately next to the spring elements defining the interface of the fasteners to the components under every load case) provide a fairly good approximation to the static joint analysis.

However there is a crucial point that can be missed here: Even though the bearing stress check might be approximated by the direct principle stress check, the static shear strength of the fastener itself cannot be

approximated in this fashion simply due to the fact that the static shear strength of the fastener is not captured with the direct stress responses. For example, if the two components are joined with the pattern of ¼" fasteners and the two components are sized adequately by the optimizer using the direct principal stress constraints under the tension load and with eigenvalue constraints under the compression load, there is potential that the individual fasteners are experiencing loads that exceed ¼" fastener shear carrying capability.

10.3 Fatigue Fastener Joint Sizing Direct Vs. Functional Responses

Comparing just the weight numbers from Table 34, and Table 32 that show the relatively small weight increase with the fatigue (level two model based) sizing (4.869 lbs.), one could make an erroneous conclusion that the level-one sizing approximates the fatigue sizing fairly well, and from there make the further conclusion that the direct stress and eigenvalue direct responses that dominate the level-one model based sizing could be used in lieu of the full fatigue evaluation. The major flaw of such conclusion would be due to the fact that the details are neglected. Namely, by looking at the weight number, one would could miss a poor fatigue detail that could rip open the entire pylon due to the fatigue crack propagation. Due to the shape functions of the typical FEM shell element formulations, the direct stress responses at the shell element with the discrete load input (such as the fastener detail represented with the Figure 17) are incorrect due to the singularity involved. For that reason the far field stress for the fatigue details is measured in the way that was described earlier. Clearly, the functional responses that are used for far field stress recovery at the fastener joint details are necessary, and without dramatically changing the fastener modeling (to a refined fastener hole with the fastener shank contact modeling) it would be impossible to extract the far fields stress values using the direct responses

10.4 Sectional Strength Sizing Direct Vs. Functional Responses

Based on the miniscule weight increase shown by Table 35 and the fact that direct principal stress and eigenvalue responses target the same type of checks away from the joints as the functional section stress

responses, one could state with the confidence that the sectional stress checks done with the very first part of the level three model based sizing could be replaced by the direct FE based responses.

10.5 Lug and Fitting Checks Direct Vs. Functional Responses

Both lug and the angle/channel fitting areas of the pylon have been assigned to the direct stress responses of the level one model based sizing domains. Nevertheless, Table 37, and Table 38 weight increases (11.697, and 2.733 lbs. respectively) clearly show that the direct stress responses, in combination with the eigenvalue responses and related constraints do not size these details adequately. There are two major reasons for this fact:

(a) Lug interface modeling shown in Figure 52, which does not represent the lug load transfer correctly (transfers the load in both tension and compression, whereas the lug only can carry compressive load)

(b) Inaccurate shell finite elements stress calculation when the load introduction point is at one of the shell elements' nodes

Chapter 11: Conclusion and Recommendation

11.1 Cost Savings of the Model Based Approach

Comparing the weight and the engineering effort (non-recurring cost) of the traditional document based design and the newly proposed model based approaches we can see the significant advantages that model based approach offers.

Non-recurring cost savings, estimated at 1.5 million dollars for the pylon development engineering effort, present a very significant value to a typical commercial aircraft company. These savings are direct result of the eliminations of the design process inefficiencies. The model based approach completely eliminates the segmentation of the engineering work and repetitive sizing-loads iterations, effectively removing the need for additional load cycles stemming from sizing-load non-convergence.

To take, for our estimation effort, as little credit for the model based approach, the weight of the document based approach sized test-case pylon is further reduced by 10% to account for post processing additional optimization of the document based design. Even with this additional weight savings of 10 percent the document based approach arrives at a test-case pylon structural weight of 805 lbs. Compared to the weight of the model based platform sized pylon of approximately 603 lbs. the weight delta is very significant – 202 lbs. per pylon, or 404 lbs. per airplane.

At this point it would be useful to quantify the weight difference in terms of service costs. Based on (K2008) the lifetime fuel cost per kilogram gross weight is €1500-2000/kg, or if translated to $ per pound (at the 2019 exchange rate between € and $ of 1.14), $3766-5022/lbs. Using the lower of the estimated costs per pound of weight, the 404 lbs. of weight savings would translate into 1.52 million dollars.

11.2 Technical Advancements Enabling the Model Based Approach

Clearly, the model based process outshines the document based one in both cost and weight. However, it should be stated that several technological advancements described in Section 4.2 needed to be engineered and programmed so that the model based platform could be established. These technological challenges and the development of the three level approach to the pylon sizing using the model based approach provide the engineering community with a basis for building knowledge based design approaches for airframe structural design. If the model based sizing is executed using such a layered approach, the database of the weight attributed to each sizing step can be established. From there, using the trend lines, very precise predictions can be made about the weights of any future pylon design, which is a very important step during the early design phase of the aircraft.

The creation of the design synthesis FE based model that contains all of the critical design detail, is loaded exclusively with critical load cases (including the non-linear ones such as the fan blade out loads), with the capability to extract the loads and sectional properties and to handle the post-buckled structure, as well as using general non-linear design constraints that capture empirical and semi-empirical criteria, requires model based platform (Figure 36) that took several years of development.

The design synthesis models that get generated by the aforementioned platform have an extremely important property. Each of the design synthesis simulations when submitted to the computation server for solution run within the 12 hours. This allows the engineers to set up their simulations using the model based platform during the work hours, and then, on the following work day, post-process and document the results that were computed overnight. Such work efficiency enables streamlining of the work flow of the pylon design.

11.3 Using Exclusively Direst Responses in the Model Based Approach

Chapter 10**: Model Based Design Based Exclusively on Direct Response** examines the possibility of using exclusively direct stress responses for the creation of the design synthesis models. The conclusion is that due to the desired level of fastener modeling idealization that is required for the simulations to run over-night on current computing servers the full direct response design synthesis models are not practical at the present time. To enable such approach, fastener modeling would need to evolve into a very detailed hole and shank contact interaction model that would require much finer shell meshes of the pylon components as well as solid mesh modeling of each fastener. Such models would take much more time to build and to solve. Therefore, for practical application this approach would need to wait for some time until computing power and modeling platforms advance sufficiently.

11.4 Extending the Model Based Approach to the Remainder of the Aircraft Structure

The model based pylon design approach that was introduced in this work can and should be extended to the entire airframe. There are few important enablers for such a scenario: (a) The structure would need to be modeled with a fine mesh, (b) Every fastener needs to be explicitly modeled, (c) The loads have to be applied externally to the structure being sized

What would be the impact of such a development? An engine pylon which was taken as an example structure to study the model based approach advantages over the traditional document based approach is a small structure compared to the full airframe of an aircraft. It typically represents less than 5% of the

aircraft empty weight. Extending the non-recurring cost savings to the rest of the aircraft structure would yield significant savings (estimated at 28.5 million dollars based on the pylon studies here) and similar levels savings for the operational cost.

Based on these significant savings extending the model based integrated structural design and certification process to the entire airframe is recommended, based on the technical solutions presented in this work that eliminate all potential road-blocks for such an implementation.

APPENDIX A

Table 43 Fastener Sets Allowable Values

Fastener set	Diam (in)	Type	Sh F.	Fbru (psi)	Fsu (psi)
Fwd_Eng_Fitt_Bulkhead_LH_Lwr_Longeron_LH_Side_Web	0.4375	St 160Ksi	1	260000	17780
LH_Lwr_Longeron_Fwd_Eng_Fitt_Bulkhead_LH_Side_Web	0.4375	St 160Ksi	2	332000	17780
LH_Side_Web_Fwd_Eng_Fitt_Bulkhead_LH_Lwr_Longeron	0.4375	St 160Ksi	1	142000	17780
Fwd_Eng_Fitt_Bulkhead_RH_Lwr_Longeron_RH_Side_Web	0.4375	St 160Ksi	1	260000	17780
RH_Lwr_Longeron_Fwd_Eng_Fitt_Bulkhead_RH_Side_Web	0.4375	St 160Ksi	2	332000	17780
RH_Side_Web_Fwd_Eng_Fitt_Bulkhead_RH_Lwr_Longeron	0.4375	St 160Ksi	1	142000	17780
Fwd_Eng_Fitt_Bulkhead_Lower_Web_LH_Lwr_Longeron	0.4375	St 140Ksi	1	260000	15560
Lower_Web_Fwd_Eng_Fitt_Bulkhead_LH_Lwr_Longeron	0.4375	St 140Ksi	2	246000	15560
LH_Lwr_Longeron_Fwd_Eng_Fitt_Bulkhead_Lower_Web	0.4375	St 140Ksi	1	332000	15560
Fwd_Eng_Fitt_Bulkhead_Lower_Web_RH_Lwr_Longeron	0.4375	St 140Ksi	1	260000	15560
Lower_Web_Fwd_Eng_Fitt_Bulkhead_RH_Lwr_Longeron	0.4375	St 140Ksi	2	246000	15560
RH_Lwr_Longeron_Fwd_Eng_Fitt_Bulkhead_Lower_Web	0.4375	St 140Ksi	1	332000	15560
Aft_Eng_Fitt_Bulkhead_LH_Lwr_Longeron_LH_Side_Web	0.4375	St 140Ksi	1	260000	15560
LH_Lwr_Longeron_Aft_Eng_Fitt_Bulkhead_LH_Side_Web	0.4375	St 140Ksi	2	332000	15560
LH_Side_Web_Aft_Eng_Fitt_Bulkhead_LH_Lwr_Longeron	0.4375	St 140Ksi	1	142000	15560
Aft_Eng_Fitt_Bulkhead_RH_Lwr_Longeron_RH_Side_Web	0.4375	St 140Ksi	1	260000	15560
RH_Lwr_Longeron_Aft_Eng_Fitt_Bulkhead_RH_Side_Web	0.4375	St 140Ksi	2	332000	15560
RH_Side_Web_Aft_Eng_Fitt_Bulkhead_RH_Lwr_Longeron	0.4375	St 140Ksi	1	142000	15560
Aft_Eng_Fitt_Bulkhead_LH_Front_Spar_Fitting_LH_Side_Web	0.4375	St 140Ksi	1	260000	15560
LH_Front_Spar_Fitting_Aft_Eng_Fitt_Bulkhead_LH_Side_Web	0.4375	St 140Ksi	2	260000	15560
LH_Side_Web_Aft_Eng_Fitt_Bulkhead_LH_Front_Spar_Fitting	0.4375	St 140Ksi	1	142000	15560
RH_Side_Web_RH_Front_Spar_Fitting_Aft_Eng_Fitt_Bulkhead	0.4375	St 140Ksi	1	142000	15560
RH_Front_Spar_Fitting_RH_Side_Web_Aft_Eng_Fitt_Bulkhead	0.4375	St 140Ksi	2	260000	15560
Aft_Eng_Fitt_Bulkhead_RH_Side_Web_RH_Front_Spar_Fitting	0.4375	St 140Ksi	1	260000	15560
LH_Side_Web_LH_Front_Spar_Fitting_7_16	0.4375	St 140Ksi	1	142000	15560
LH_Front_Spar_Fitting_LH_Side_Web_7_16	0.4375	St 140Ksi	1	260000	15560
RH_Side_Web_RH_Front_Spar_Fitting_7_16	0.4375	St 140Ksi	1	142000	15560
RH_Front_Spar_Fitting_RH_Side_Web_7_16	0.4375	St 140Ksi	1	260000	15560
Lwr_Link_Fitting_Aft_Bulkhead_RH_Front_Spar_Fitting	0.4375	St 140Ksi	1	260000	15560
Aft_Bulkhead_Lwr_Link_Fitting_RH_Front_Spar_Fitting	0.4375	St 140Ksi	2	276000	15560
RH_Front_Spar_Fitting_Lwr_Link_Fitting_Aft_Bulkhead	0.4375	St 140Ksi	1	260000	15560
LH_Front_Spar_Fitting_Aft_Bulkhead	0.4375	St 140Ksi	1	260000	15560
Aft_Bulkhead_LH_Front_Spar_Fitting	0.4375	St 140Ksi	1	276000	15560
RH_Front_Spar_Fitting_Aft_Bulkhead	0.4375	St 140Ksi	1	260000	15560
Aft_Bulkhead_RH_Front_Spar_Fitting	0.4375	St 140Ksi	1	276000	15560
Aft_Upper_Web_Aft_Bulkhead_LH_Front_Spar_Fitting	0.4375	St 140Ksi	1	142000	15560
Aft_Bulkhead_Aft_Upper_Web_LH_Front_Spar_Fitting	0.4375	St 140Ksi	2	276000	15560
LH_Front_Spar_Fitting_Aft_Upper_Web_Aft_Bulkhead	0.4375	St 140Ksi	1	260000	15560

Aft_Upper_Web_Aft_Bulkhead_RH_Front_Spar_Fitting	0.4375	St 140Ksi	1	142000	15560
Aft_Bulkhead_Aft_Upper_Web_RH_Front_Spar_Fitting	0.4375	St 140Ksi	2	276000	15560
RH_Front_Spar_Fitting_Aft_Upper_Web_Aft_Bulkhead	0.4375	St 140Ksi	1	260000	15560
Aft_Upper_Web_Aft_Bulkhead	0.4375	St 140Ksi	1	142000	15560
Aft_Bulkhead_Aft_Upper_Web	0.4375	St 140Ksi	1	276000	15560
Lwr_Link_Fitting_Aft_Bulkhead_LH_Front_Spar_Fitting	0.4375	St 140Ksi	1	260000	15560
Aft_Bulkhead_Lwr_Link_Fitting_LH_Front_Spar_Fitting	0.4375	St 140Ksi	2	276000	15560
LH_Front_Spar_Fitting_Lwr_Link_Fitting_Aft_Bulkhead	0.4375	St 140Ksi	1	260000	15560
Fwd_Eng_Fitt_Bulkhead_LH_Upr_Longeron_LH_Side_Web	0.375	St 140Ksi	1	260000	11540
LH_Upr_Longeron_Fwd_Eng_Fitt_Bulkhead_LH_Side_Web	0.375	St 140Ksi	2	262000	11540
LH_Side_Web_Fwd_Eng_Fitt_Bulkhead_LH_Upr_Longeron	0.375	St 140Ksi	1	142000	11540
Fwd_Eng_Fitt_Bulkhead_RH_Upr_Longeron_RH_Side_Web	0.375	St 140Ksi	1	260000	11540
RH_Upr_Longeron_Fwd_Eng_Fitt_Bulkhead_RH_Side_Web	0.375	St 140Ksi	2	262000	11540
RH_Side_Web_Fwd_Eng_Fitt_Bulkhead_RH_Upr_Longeron	0.375	St 140Ksi	1	142000	11540
LH_Upr_Longeron_Upper_Web_Fwd_Eng_Fitt_Bulkhead	0.375	St 140Ksi	1	262000	11540
Upper_Web_LH_Upr_Longeron_Fwd_Eng_Fitt_Bulkhead	0.375	St 140Ksi	2	142000	11540
Fwd_Eng_Fitt_Bulkhead_LH_Upr_Longeron_Upper_Web	0.375	St 140Ksi	1	260000	11540
RH_Upr_Longeron_Upper_Web_Fwd_Eng_Fitt_Bulkhead	0.375	St 140Ksi	1	262000	11540
Upper_Web_RH_Upr_Longeron_Fwd_Eng_Fitt_Bulkhead	0.375	St 140Ksi	2	142000	11540
Fwd_Eng_Fitt_Bulkhead_RH_Upr_Longeron_Upper_Web	0.375	St 140Ksi	1	260000	11540
Frame_1_LH_Lwr_Longeron_LH_Side_Web	0.375	St 140Ksi	1	129000	11540
LH_Lwr_Longeron_Frame_1_LH_Side_Web	0.375	St 140Ksi	2	332000	11540
LH_Side_Web_Frame_1_LH_Lwr_Longeron	0.375	St 140Ksi	1	142000	11540
RH_Side_Web_RH_Lwr_Longeron_Frame_1	0.375	St 140Ksi	1	142000	11540
RH_Lwr_Longeron_RH_Side_Web_Frame_1	0.375	St 140Ksi	2	332000	11540
Frame_1_RH_Side_Web_RH_Lwr_Longeron	0.375	St 140Ksi	1	129000	11540
Frame_1_Lower_Web_LH_Lwr_Longeron	0.375	St 140Ksi	1	129000	11540
Lower_Web_Frame_1_LH_Lwr_Longeron	0.375	St 140Ksi	2	246000	11540
LH_Lwr_Longeron_Frame_1_Lower_Web	0.375	St 140Ksi	2	332000	11540
Frame_1_Lower_Web_RH_Lwr_Longeron	0.375	St 140Ksi	1	129000	11540
Lower_Web_Frame_1_RH_Lwr_Longeron	0.375	St 140Ksi	2	246000	11540
RH_Lwr_Longeron_Frame_1_Lower_Web	0.375	St 140Ksi	2	332000	11540
Frame_2_LH_Lwr_Longeron_LH_Side_Web	0.375	St 140Ksi	1	129000	11540
LH_Lwr_Longeron_Frame_2_LH_Side_Web	0.375	St 140Ksi	2	332000	11540
LH_Side_Web_Frame_2_LH_Lwr_Longeron	0.375	St 140Ksi	1	142000	11540
Frame_2_RH_Lwr_Longeron	0.375	St 140Ksi	1	129000	11540
RH_Lwr_Longeron_Frame_2	0.375	St 140Ksi	2	332000	11540
Frame_2_Lower_Web_LH_Lwr_Longeron	0.375	St 140Ksi	1	129000	11540
Lower_Web_Frame_2_LH_Lwr_Longeron	0.375	St 140Ksi	2	246000	11540
LH_Lwr_Longeron_Frame_2_Lower_Web	0.375	St 140Ksi	2	332000	11540
Frame_2_Lower_Web_RH_Lwr_Longeron	0.375	St 140Ksi	1	129000	11540
Lower_Web_Frame_2_RH_Lwr_Longeron	0.375	St 140Ksi	2	246000	11540

RH_Lwr_Longeron_Frame_2_Lower_Web	0.375	St 140Ksi	2	332000	11540
Frame_3_Lower_Web_LH_Lwr_Longeron	0.375	St 140Ksi	1	129000	11540
Lower_Web_Frame_3_LH_Lwr_Longeron	0.375	St 140Ksi	2	246000	11540
LH_Lwr_Longeron_Frame_3_Lower_Web	0.375	St 140Ksi	2	332000	11540
Frame_3_Lower_Web_RH_Lwr_Longeron	0.375	St 140Ksi	1	129000	11540
Lower_Web_Frame_3_RH_Lwr_Longeron	0.375	St 140Ksi	2	246000	11540
RH_Lwr_Longeron_Frame_3_Lower_Web	0.375	St 140Ksi	2	332000	11540
Frame_4_LH_Upr_Longeron_LH_Side_Web	0.375	St 140Ksi	1	260000	11540
LH_Upr_Longeron_Frame_4_LH_Side_Web	0.375	St 140Ksi	2	262000	11540
LH_Side_Web_Frame_4_LH_Upr_Longeron	0.375	St 140Ksi	1	142000	11540
Frame_4_RH_Upr_Longeron_RH_Side_Web	0.375	St 140Ksi	1	260000	11540
RH_Upr_Longeron_Frame_4_RH_Side_Web	0.375	St 140Ksi	2	262000	11540
RH_Side_Web_Frame_4_RH_Upr_Longeron	0.375	St 140Ksi	1	142000	11540
Frame_4_Upper_Web_LH_Upr_Longeron	0.375	St 140Ksi	1	260000	11540
Upper_Web_Frame_4_LH_Upr_Longeron	0.375	St 140Ksi	2	142000	11540
LH_Upr_Longeron_Frame_4_Upper_Web	0.375	St 140Ksi	2	262000	11540
Frame_4_Upper_Web_RH_Upr_Longeron	0.375	St 140Ksi	1	260000	11540
Upper_Web_Frame_4_RH_Upr_Longeron	0.375	St 140Ksi	2	142000	11540
RH_Upr_Longeron_Frame_4_Upper_Web	0.375	St 140Ksi	2	262000	11540
Frame_4_LH_Lwr_Longeron_LH_Side_Web	0.375	St 140Ksi	1	260000	11540
LH_Lwr_Longeron_Frame_4_LH_Side_Web	0.375	St 140Ksi	2	332000	11540
LH_Side_Web_Frame_4_LH_Lwr_Longeron	0.375	St 140Ksi	1	142000	11540
Frame_4_RH_Lwr_Longeron_RH_Side_Web	0.375	St 140Ksi	1	260000	11540
RH_Lwr_Longeron_Frame_4_RH_Side_Web	0.375	St 140Ksi	2	332000	11540
RH_Side_Web_Frame_4_RH_Lwr_Longeron	0.375	St 140Ksi	1	142000	11540
Frame_4_Lower_Web_LH_Lwr_Longeron	0.375	St 140Ksi	1	260000	11540
Lower_Web_Frame_4_LH_Lwr_Longeron	0.375	St 140Ksi	2	246000	11540
LH_Lwr_Longeron_Frame_4_Lower_Web	0.375	St 140Ksi	2	332000	11540
Frame_4_Lower_Web_RH_Lwr_Longeron	0.375	St 140Ksi	1	260000	11540
Lower_Web_Frame_4_RH_Lwr_Longeron	0.375	St 140Ksi	2	246000	11540
RH_Lwr_Longeron_Frame_4_Lower_Web	0.375	St 140Ksi	2	332000	11540
Lower_Web_Aft_Eng_Fitt_Bulkhead_Lwr_Link_Fitting	0.4375	St 140Ksi	1	246000	15560
Aft_Eng_Fitt_Bulkhead_Lower_Web_Lwr_Link_Fitting	0.4375	St 140Ksi	1	260000	15560
Lwr_Link_Fitting_Lower_Web_Aft_Eng_Fitt_Bulkhead	0.4375	St 140Ksi	1	260000	15560
Aft_Bulkhead_Aft_Eng_Fitt_Bulkhead_Lwr_Link_Fitting	0.375	St 140Ksi	1	276000	11540
Aft_Eng_Fitt_Bulkhead_Aft_Bulkhead_Lwr_Link_Fitting	0.375	St 140Ksi	1	260000	11540
Lwr_Link_Fitting_Aft_Bulkhead_Aft_Eng_Fitt_Bulkhead	0.375	St 140Ksi	1	260000	11540
LH_Side_Web_Aft_Eng_Fitt_Bulkhead	0.375	St 140Ksi	1	142000	11540
Aft_Eng_Fitt_Bulkhead_LH_Side_Web	0.375	St 140Ksi	1	260000	11540
Aft_Eng_Fitt_Bulkhead_RH_Side_Web	0.375	St 140Ksi	1	260000	11540
RH_Side_Web_Aft_Eng_Fitt_Bulkhead	0.375	St 140Ksi	1	142000	11540
LH_Side_Web_LH_Front_Spar_Fitting_Aft_Eng_Fitt_Bulkhead	0.375	St 140Ksi	1	142000	11540

LH_Front_Spar_Fitting_LH_Side_Web_Aft_Eng_Fitt_Bulkhead	0.375	St 140Ksi	2	260000	11540
Aft_Eng_Fitt_Bulkhead_LH_Side_Web_LH_Front_Spar_Fitting	0.375	St 140Ksi	1	260000	11540
LH_Side_Web_LH_Front_Spar_Fitting	0.375	St 140Ksi	1	142000	11540
LH_Front_Spar_Fitting_LH_Side_Web	0.375	St 140Ksi	1	260000	11540
RH_Side_Web_RH_Front_Spar_Fitting	0.375	St 140Ksi	1	142000	11540
RH_Front_Spar_Fitting_RH_Side_Web	0.375	St 140Ksi	1	260000	11540
LH_Side_Web_LH_Front_Spar_Fitting_Frame_5	0.375	St 140Ksi	1	142000	11540
LH_Front_Spar_Fitting_LH_Side_Web_Frame_5	0.375	St 140Ksi	2	260000	11540
Frame_5_LH_Side_Web_LH_Front_Spar_Fitting	0.375	St 140Ksi	1	260000	11540
Frame_5_RH_Front_Spar_Fitting_RH_Side_Web	0.375	St 140Ksi	1	260000	11540
RH_Front_Spar_Fitting_Frame_5_RH_Side_Web	0.375	St 140Ksi	2	260000	11540
RH_Side_Web_Frame_5_RH_Front_Spar_Fitting	0.375	St 140Ksi	1	142000	11540
Aft_Bulkhead_Lwr_Link_Fitting_3_8	0.4375	St 140Ksi	1	276000	15560
Aft_Bulkhead_Lwr_Link_Fitting_3_8	0.4375	St 140Ksi	1	260000	15560
Frame_5_Aft_Bulkhead_LH_Front_Spar_Fitting	0.375	St 140Ksi	1	260000	11540
Aft_Bulkhead_Frame_5_LH_Front_Spar_Fitting	0.375	St 140Ksi	2	276000	11540
LH_Front_Spar_Fitting_Frame_5_Aft_Bulkhead	0.375	St 140Ksi	1	260000	11540
Frame_5_Aft_Bulkhead_RH_Front_Spar_Fitting	0.375	St 140Ksi	1	260000	11540
Aft_Bulkhead_Frame_5_RH_Front_Spar_Fitting	0.375	St 140Ksi	2	276000	11540
RH_Front_Spar_Fitting_Frame_5_Aft_Bulkhead	0.375	St 140Ksi	1	260000	11540
LH_Front_Spar_Fitting_Aft_Bulkhead_Frame_6	0.375	St 140Ksi	1	260000	11540
Aft_Bulkhead_LH_Front_Spar_Fitting_Frame_6	0.375	St 140Ksi	2	276000	11540
Frame_6_LH_Front_Spar_Fitting_Aft_Bulkhead	0.375	St 140Ksi	1	260000	11540
RH_Front_Spar_Fitting_Aft_Bulkhead_Frame_6	0.375	St 140Ksi	1	260000	11540
Aft_Bulkhead_RH_Front_Spar_Fitting_Frame_6	0.375	St 140Ksi	2	276000	11540
Frame_6_RH_Front_Spar_Fitting_Aft_Bulkhead	0.375	St 140Ksi	1	260000	11540
Upper_Web_Fwd_Eng_Fitt_Bulkhead	0.3125	St 140Ksi	1	142000	7510
Fwd_Eng_Fitt_Bulkhead_Upper_Web	0.3125	St 140Ksi	1	260000	7510
Fwd_Eng_Fitt_Bulkhead_Lower_Web	0.3125	St 140Ksi	1	260000	7510
Lower_Web_Fwd_Eng_Fitt_Bulkhead	0.3125	St 140Ksi	1	246000	7510
Frame_1_LH_Upr_Longeron_LH_Side_Web	0.3125	St 140Ksi	1	129000	7510
LH_Upr_Longeron_Frame_1_LH_Side_Web	0.3125	St 140Ksi	2	262000	7510
LH_Side_Web_Frame_1_LH_Upr_Longeron	0.3125	St 140Ksi	1	142000	7510
Frame_1_RH_Upr_Longeron_RH_Side_Web	0.3125	St 140Ksi	1	129000	7510
RH_Upr_Longeron_Frame_1_RH_Side_Web	0.3125	St 140Ksi	2	262000	7510
RH_Side_Web_Frame_1_RH_Upr_Longeron	0.3125	St 140Ksi	1	142000	7510
Frame_1_Upper_Web_LH_Upr_Longeron	0.3125	St 140Ksi	1	129000	7510
Upper_Web_Frame_1_LH_Upr_Longeron	0.3125	St 140Ksi	2	142000	7510
LH_Upr_Longeron_Frame_1_Upper_Web	0.3125	St 140Ksi	2	262000	7510
Frame_1_Upper_Web_RH_Upr_Longeron	0.3125	St 140Ksi	1	129000	7510
Upper_Web_Frame_1_RH_Upr_Longeron	0.3125	St 140Ksi	2	142000	7510
RH_Upr_Longeron_Frame_1_Upper_Web	0.3125	St 140Ksi	2	262000	7510

Frame_2_LH_Upr_Longeron_LH_Side_Web	0.3125	St 140Ksi	1	129000	7510
LH_Upr_Longeron_Frame_2_LH_Side_Web	0.3125	St 140Ksi	2	262000	7510
LH_Side_Web_Frame_2_LH_Upr_Longeron	0.3125	St 140Ksi	1	142000	7510
Frame_2_RH_Upr_Longeron_RH_Side_Web	0.3125	St 140Ksi	1	129000	7510
RH_Upr_Longeron_Frame_2_RH_Side_Web	0.3125	St 140Ksi	2	262000	7510
RH_Side_Web_Frame_2_RH_Upr_Longeron	0.3125	St 140Ksi	1	142000	7510
Frame_2_Upper_Web_LH_Upr_Longeron	0.3125	St 140Ksi	1	129000	7510
Upper_Web_Frame_2_LH_Upr_Longeron	0.3125	St 140Ksi	2	142000	7510
LH_Upr_Longeron_Frame_2_Upper_Web	0.3125	St 140Ksi	2	262000	7510
Frame_2_Upper_Web_RH_Upr_Longeron	0.3125	St 140Ksi	1	129000	7510
Upper_Web_Frame_2_RH_Upr_Longeron	0.3125	St 140Ksi	2	142000	7510
RH_Upr_Longeron_Frame_2_Upper_Web	0.3125	St 140Ksi	2	262000	7510
Frame_3_LH_Upr_Longeron_LH_Side_Web	0.3125	St 140Ksi	1	129000	7510
LH_Upr_Longeron_Frame_3_LH_Side_Web	0.3125	St 140Ksi	2	262000	7510
LH_Side_Web_Frame_3_LH_Upr_Longeron	0.3125	St 140Ksi	1	142000	7510
Frame_3_RH_Upr_Longeron_RH_Side_Web	0.3125	St 140Ksi	1	129000	7510
RH_Upr_Longeron_Frame_3_RH_Side_Web	0.3125	St 140Ksi	2	262000	7510
RH_Side_Web_Frame_3_RH_Upr_Longeron	0.3125	St 140Ksi	1	142000	7510
Frame_3_Upper_Web_LH_Upr_Longeron	0.3125	St 140Ksi	1	129000	7510
Upper_Web_Frame_3_LH_Upr_Longeron	0.3125	St 140Ksi	2	142000	7510
LH_Upr_Longeron_Frame_3_Upper_Web	0.3125	St 140Ksi	2	262000	7510
Frame_3_Upper_Web_RH_Upr_Longeron	0.3125	St 140Ksi	1	129000	7510
Upper_Web_Frame_3_RH_Upr_Longeron	0.3125	St 140Ksi	2	142000	7510
RH_Upr_Longeron_Frame_3_Upper_Web	0.3125	St 140Ksi	2	262000	7510
Frame_3_LH_Lwr_Longeron_LH_Side_Web	0.3125	St 140Ksi	1	129000	7510
LH_Lwr_Longeron_Frame_3_LH_Side_Web	0.3125	St 140Ksi	2	332000	7510
LH_Side_Web_Frame_3_LH_Lwr_Longeron	0.3125	St 140Ksi	1	142000	7510
Frame_3_RH_Lwr_Longeron_RH_Side_Web	0.3125	St 140Ksi	1	129000	7510
RH_Lwr_Longeron_Frame_3_RH_Side_Web	0.3125	St 140Ksi	2	332000	7510
RH_Side_Web_Frame_3_RH_Lwr_Longeron	0.3125	St 140Ksi	1	142000	7510
Upper_Web_Frame_4	0.3125	St 140Ksi	1	142000	7510
Frame_4_Upper_Web	0.3125	St 140Ksi	1	260000	7510
LH_Side_Web_Frame_4	0.3125	St 140Ksi	1	142000	7510
Frame_4_LH_Side_Web	0.3125	St 140Ksi	1	260000	7510
RH_Side_Web_Frame_4	0.3125	St 140Ksi	1	142000	7510
Frame_4_RH_Side_Web	0.3125	St 140Ksi	1	260000	7510
Frame_4_Upper_Web_Upper_Link_Fitting	0.3125	St 140Ksi	1	260000	7510
Upper_Web_Frame_4_Upper_Link_Fitting	0.3125	St 140Ksi	2	142000	7510
Upper_Link_Fitting_Frame_4_Upper_Web	0.3125	St 140Ksi	1	260000	7510
Aft_Eng_Fitt_Bulkhead_LH_Upr_Longeron_LH_Side_Web	0.3125	St 160Ksi	1	260000	8590
LH_Upr_Longeron_Aft_Eng_Fitt_Bulkhead_LH_Side_Web	0.3125	St 160Ksi	2	262000	8590
LH_Side_Web_Aft_Eng_Fitt_Bulkhead_LH_Upr_Longeron	0.3125	St 160Ksi	1	142000	8590

Aft_Eng_Fitt_Bulkhead_RH_Upr_Longeron_RH_Side_Web	0.3125	St 160Ksi	1	260000	8590
RH_Upr_Longeron_Aft_Eng_Fitt_Bulkhead_RH_Side_Web	0.3125	St 160Ksi	2	262000	8590
RH_Side_Web_Aft_Eng_Fitt_Bulkhead_RH_Upr_Longeron	0.3125	St 160Ksi	1	142000	8590
Lower_Web_Lwr_Link_Fitting	0.3125	St 140Ksi	1	246000	7510
Lwr_Link_Fitting_Lower_Web	0.3125	St 140Ksi	1	260000	7510
Aft_Eng_Fitt_Bulkhead_Upper_Web_LH_Upr_Longeron	0.3125	St 140Ksi	1	260000	7510
Upper_Web_Aft_Eng_Fitt_Bulkhead_LH_Upr_Longeron	0.3125	St 140Ksi	2	142000	7510
LH_Upr_Longeron_Aft_Eng_Fitt_Bulkhead_Upper_Web	0.3125	St 140Ksi	1	262000	7510
Aft_Eng_Fitt_Bulkhead_Upper_Web_RH_Upr_Longeron	0.3125	St 140Ksi	1	260000	7510
Upper_Web_Aft_Eng_Fitt_Bulkhead_RH_Upr_Longeron	0.3125	St 140Ksi	2	142000	7510
RH_Upr_Longeron_Aft_Eng_Fitt_Bulkhead_Upper_Web	0.3125	St 140Ksi	1	262000	7510
Aft_Eng_Fitt_Bulkhead_Upper_Web	0.3125	St 140Ksi	1	260000	7510
Upper_Web_Aft_Eng_Fitt_Bulkhead	0.3125	St 140Ksi	1	142000	7510
Aft_Eng_Fitt_Bulkhead_Aft_Upper_Web_Upper_Link_Fitting	0.3125	St 140Ksi	1	260000	7510
Aft_Upper_Web_Aft_Eng_Fitt_Bulkhead_Upper_Link_Fitting	0.3125	St 140Ksi	2	142000	7510
Upper_Link_Fitting_Aft_Eng_Fitt_Bulkhead_Aft_Upper_Web	0.3125	St 140Ksi	1	260000	7510
Aft_Bulkhead_Lwr_Link_Fitting_5_16	0.3125	St 140Ksi	1	276000	7510
Lwr_Link_Fitting_Aft_Bulkhead_5_16	0.3125	St 140Ksi	1	260000	7510
Frame_5_Aft_Upper_Web_LH_Front_Spar_Fitting_5_16	0.3125	St 140Ksi	1	260000	7510
Aft_Upper_Web_Frame_5_LH_Front_Spar_Fitting_5_16	0.3125	St 140Ksi	2	142000	7510
LH_Front_Spar_Fitting_Frame_5_Aft_Upper_Web_5_16	0.3125	St 140Ksi	1	260000	7510
Frame_5_Aft_Upper_Web_RH_Front_Spar_Fitting_5_16	0.3125	St 140Ksi	1	260000	7510
Aft_Upper_Web_Frame_5_RH_Front_Spar_Fitting_5_16	0.3125	St 140Ksi	2	142000	7510
RH_Front_Spar_Fitting_Frame_5_Aft_Upper_Web_5_16	0.3125	St 140Ksi	1	260000	7510
Aft_Upper_Web_Frame_5	0.3125	St 140Ksi	1	142000	7510
Frame_5_Aft_Upper_Web	0.3125	St 140Ksi	1	260000	7510
LH_Side_Web_Frame_5	0.3125	St 140Ksi	1	142000	7510
Frame_5_LH_Side_Web	0.3125	St 140Ksi	1	260000	7510
RH_Side_Web_Frame_5	0.3125	St 140Ksi	1	142000	7510
Frame_5_RH_Side_Web	0.3125	St 140Ksi	1	260000	7510
Aft_Bulkhead_Frame_5	0.3125	St 140Ksi	1	276000	7510
Frame_5_Aft_Bulkhead	0.3125	St 140Ksi	1	260000	7510
Aft_Upper_Web_LH_Front_Spar_Fitting_Upper_Deck	0.3125	St 140Ksi	1	142000	7510
LH_Front_Spar_Fitting_Aft_Upper_Web_Upper_Deck	0.3125	St 140Ksi	1	260000	7510
RH_Front_Spar_Fitting_Aft_Upper_Web_Upper_Deck	0.3125	St 140Ksi	1	260000	7510
Aft_Upper_Web_RH_Front_Spar_Fitting_Upper_Deck	0.3125	St 140Ksi	1	142000	7510
Frame_6_Aft_Upper_Web_LH_Front_Spar_Fitting	0.3125	St 140Ksi	1	260000	7510
Aft_Upper_Web_Frame_6_LH_Front_Spar_Fitting	0.3125	St 140Ksi	2	142000	7510
LH_Front_Spar_Fitting_Frame_6_Aft_Upper_Web	0.3125	St 140Ksi	1	260000	7510
Frame_6_Aft_Upper_Web_RH_Front_Spar_Fitting	0.3125	St 140Ksi	1	260000	7510
Aft_Upper_Web_Frame_6_RH_Front_Spar_Fitting	0.3125	St 140Ksi	2	142000	7510
RH_Front_Spar_Fitting_Frame_6_Aft_Upper_Web	0.3125	St 140Ksi	1	260000	7510

Aft_Upper_Web_Frame_6_5_16	0.3125	St 140Ksi	1	142000	7510
Frame_6_Aft_Upper_Web_5_16	0.3125	St 140Ksi	1	260000	7510
Aft_Bulkhead_Frame_6_5_16	0.3125	St 140Ksi	1	276000	7510
Frame_6_Aft_Bulkhead_5_16	0.3125	St 140Ksi	1	260000	7510
LH_Side_Web_LH_Upr_Longeron	0.3125	St 140Ksi	1	142000	7510
LH_Upr_Longeron_LH_Side_Web	0.3125	St 140Ksi	1	262000	7510
RH_Upr_Longeron_RH_Side_Web	0.3125	St 140Ksi	1	262000	7510
RH_Side_Web_RH_Upr_Longeron	0.3125	St 140Ksi	1	142000	7510
Upper_Web_LH_Upr_Longeron	0.3125	St 140Ksi	1	142000	7510
LH_Upr_Longeron_Upper_Web	0.3125	St 140Ksi	1	262000	7510
RH_Upr_Longeron_Upper_Web	0.3125	St 140Ksi	1	262000	7510
Upper_Web_RH_Upr_Longeron	0.3125	St 140Ksi	1	142000	7510
LH_Lwr_Longeron_LH_Side_Web	0.3125	St 140Ksi	1	332000	7510
LH_Side_Web_LH_Lwr_Longeron	0.3125	St 140Ksi	1	142000	7510
RH_Side_Web_RH_Lwr_Longeron	0.3125	St 140Ksi	1	142000	7510
RH_Lwr_Longeron_RH_Side_Web	0.3125	St 140Ksi	1	332000	7510
LH_Lwr_Longeron_Lower_Web	0.3125	St 140Ksi	1	332000	7510
Lower_Web_LH_Lwr_Longeron	0.3125	St 140Ksi	1	246000	7510
Lower_Web_RH_Lwr_Longeron	0.3125	St 140Ksi	1	246000	7510
RH_Lwr_Longeron_Lower_Web	0.3125	St 140Ksi	1	332000	7510
Aft_Upper_Web_LH_Front_Spar_Fitting_5_16	0.3125	St 140Ksi	1	142000	7510
LH_Front_Spar_Fitting_Aft_Upper_Web_5_16	0.3125	St 140Ksi	1	260000	7510
Aft_Upper_Web_RH_Front_Spar_Fitting_5_16	0.3125	St 140Ksi	1	142000	7510
RH_Front_Spar_Fitting_Aft_Upper_Web_5_16	0.3125	St 140Ksi	1	260000	7510
Frame_1_Upper_Web	0.25	St 140Ksi	1	129000	4680
Upper_Web_Frame_1	0.25	St 140Ksi	1	142000	4680
LH_Side_Web_Frame_1	0.25	St 140Ksi	1	142000	4680
Frame_1_LH_Side_Web	0.25	St 140Ksi	1	129000	4680
RH_Side_Web_Frame_1	0.25	St 140Ksi	1	142000	4680
Frame_1_RH_Side_Web	0.25	St 140Ksi	1	129000	4680
Frame_1_Lower_Web	0.25	St 140Ksi	1	129000	4680
Lower_Web_Frame_1	0.25	St 140Ksi	1	246000	4680
Frame_1_Upper_Web_Upper_Link_Fitting	0.25	St 140Ksi	1	129000	4680
Upper_Web_Frame_1_Upper_Link_Fitting	0.25	St 140Ksi	2	142000	4680
Upper_Link_Fitting_Frame_1_Upper_Web	0.25	St 140Ksi	1	260000	4680
Upper_Web_Frame_2	0.25	St 140Ksi	1	142000	4680
Frame_2_Upper_Web	0.25	St 140Ksi	1	129000	4680
LH_Side_Web_Frame_2	0.25	St 140Ksi	1	142000	4680
Frame_2_LH_Side_Web	0.25	St 140Ksi	1	129000	4680
RH_Side_Web_Frame_2	0.25	St 140Ksi	1	142000	4680
Frame_2_RH_Side_Web	0.25	St 140Ksi	1	129000	4680
Frame_2_Lower_Web	0.25	St 140Ksi	1	129000	4680

Lower_Web_Frame_2	0.25	St 140Ksi	1	246000	4680
Frame_2_Upper_Web_Upper_Link_Fitting	0.25	St 140Ksi	1	129000	4680
Upper_Web_Frame_2_Upper_Link_Fitting	0.25	St 140Ksi	2	142000	4680
Upper_Link_Fitting_Frame_2_Upper_Web	0.25	St 140Ksi	1	260000	4680
Upper_Web_Frame_3	0.25	St 140Ksi	1	142000	4680
Frame_3_Upper_Web	0.25	St 140Ksi	1	129000	4680
LH_Side_Web_Frame_3	0.25	St 140Ksi	1	142000	4680
Frame_3_LH_Side_Web	0.25	St 140Ksi	1	129000	4680
RH_Side_Web_Frame_3	0.25	St 140Ksi	1	142000	4680
Frame_3_RH_Side_Web	0.25	St 140Ksi	1	129000	4680
Lower_Web_Frame_3	0.25	St 140Ksi	1	246000	4680
Frame_3_Lower_Web	0.25	St 140Ksi	1	129000	4680
Frame_3_Upper_Web_Upper_Link_Fitting	0.25	St 140Ksi	1	129000	4680
Upper_Web_Frame_3_Upper_Link_Fitting	0.25	St 140Ksi	2	142000	4680
Upper_Link_Fitting_Frame_3_Upper_Web	0.25	St 140Ksi	1	260000	4680
Frame_4_Lower_Web	0.25	St 140Ksi	1	260000	4680
Lower_Web_Frame_4	0.25	St 140Ksi	1	246000	4680
Lower_Web_Frame_4_Lwr_Link_Fitting	0.25	St 140Ksi	2	246000	4680
Frame_4_Lower_Web_Lwr_Link_Fitting	0.25	St 140Ksi	1	260000	4680
Lwr_Link_Fitting_Lower_Web_Frame_4	0.25	St 140Ksi	1	260000	4680
Aft_Eng_Fitt_Bulkhead_Aft_Upper_Web_LH_Front_Spar_Fitting	0.25	St 180Ksi	1	260000	6010
Aft_Upper_Web_Aft_Eng_Fitt_Bulkhead_LH_Front_Spar_Fitting	0.25	St 180Ksi	2	142000	6010
LH_Front_Spar_Fitting_Aft_Eng_Fitt_Bulkhead_Aft_Upper_Web	0.25	St 180Ksi	1	260000	6010
Aft_Eng_Fitt_Bulkhead_Aft_Upper_Web_RH_Front_Spar_Fitting	0.25	St 180Ksi	1	260000	6010
Aft_Upper_Web_Aft_Eng_Fitt_Bulkhead_RH_Front_Spar_Fitting	0.25	St 180Ksi	2	142000	6010
RH_Front_Spar_Fitting_Aft_Eng_Fitt_Bulkhead_Aft_Upper_Web	0.25	St 180Ksi	1	260000	6010
Frame_5_Aft_Upper_Web_LH_Front_Spar_Fitting	0.25	St 140Ksi	1	260000	4680
Aft_Upper_Web_Frame_5_LH_Front_Spar_Fitting	0.25	St 140Ksi	2	142000	4680
LH_Front_Spar_Fitting_Frame_5_Aft_Upper_Web	0.25	St 140Ksi	1	260000	4680
Frame_5_Aft_Upper_Web_RH_Front_Spar_Fitting	0.25	St 140Ksi	1	260000	4680
Aft_Upper_Web_Frame_5_RH_Front_Spar_Fitting	0.25	St 140Ksi	2	142000	4680
RH_Front_Spar_Fitting_Frame_5_Aft_Upper_Web	0.25	St 140Ksi	1	260000	4680
Aft_Upper_Web_LH_Front_Spar_Fitting	0.25	St 140Ksi	1	142000	4680
LH_Front_Spar_Fitting_Aft_Upper_Web	0.25	St 140Ksi	1	260000	4680
Aft_Upper_Web_RH_Front_Spar_Fitting	0.25	St 140Ksi	1	142000	4680
RH_Front_Spar_Fitting_Aft_Upper_Web	0.25	St 140Ksi	1	260000	4680
Aft_Upper_Web_Frame_6	0.25	St 140Ksi	1	142000	4680
Frame_6_Aft_Upper_Web	0.25	St 140Ksi	1	260000	4680
Upper_Web_Upper_Link_Fitting	0.25	St 140Ksi	1	142000	4680
Upper_Link_Fitting_Upper_Web	0.25	St 140Ksi	1	260000	4680

Table 44 Initial Design Largest Violations of Tension Stress

Component	Load Case	Tension	Allowable	Margin
Upper_Link_Fitting Frame 4 Fwd Attachment	1	343000	118000	-0.656
Upper_Link_Fitting Frame 4 Fwd Attachment	3	286000	118000	-0.587
Upper_Link_Fitting Frame 4 Fwd Attachment	201	284000	118000	-0.585
Upper_Link_Fitting Frame 4 Fwd Attachment	203	245000	118000	-0.518
Upper_Link_Fitting Frame 4 Aft Attachment	1	304000	118000	-0.612
Upper_Link_Fitting Frame 4 Aft Attachment	201	253000	118000	-0.534
Upper_Link_Fitting Frame 4 Aft Attachment	3	244000	118000	-0.516
Frame3 Uflange	1	162000	57000	-0.648
Frame3 Uflange	201	130000	57000	-0.562
Frame3 Uflange	3	129000	57000	-0.558
Aft_Eng_Fitt_Bulkhead Bott Side Flange	12	293000	106000	-0.638
Aft_Eng_Fitt_Bulkhead Bott Side Flange	12	293000	106000	-0.638
Aft_Eng_Fitt_Bulkhead Bott Side Flange	12	286000	106000	-0.629
Aft_Eng_Fitt_Bulkhead Bott Side Flange	12	286000	106000	-0.629
Aft_Eng_Fitt_Bulkhead Tension Bolt Pad	12	258000	106000	-0.589
Lwr_Link_Fitting ASB Connection	103	2.34E+05	1.04E+05	-0.556

Table 45 Initial Design Stability of Sections and Panels Largest Margin Violations

Load Case	Min Margin	Load Case	Min Margin
912	-0.66819	9111	-0.386
9103	-0.59829	9210	-0.38571
9310	-0.5959	9110	-0.38505
9411	-0.59352	93	-0.36362
911	-0.59105	9201	-0.35286
910	-0.59038	9309	-0.31457
9308	-0.55867	9109	-0.31305
9409	-0.556	9209	-0.31305
99	-0.542	9408	-0.31295
9412	-0.54181	9108	-0.31133
98	-0.54086	9208	-0.31133
9112	-0.50229	97	-0.26276
9212	-0.50229	96	-0.26162
9312	-0.45581	91	-0.18743
9102	-0.43571	9306	-0.10448
9311	-0.38771	9407	-0.09981
9410	-0.38686	92	-0.09086
9211	-0.38667	9203	-0.04876

Table 46 Largest Static Joint Margin Violations of Baseline Design

Element	Check	Load Case	Shear Stress	Shear Allowable	Margin
15136	Fastener Shear	310	9.31E+03	6.01E+03	-0.35467
15068	Fastener Shear	411	9.19E+03	6.01E+03	-0.34567
15136	Fastener Shear	309	8.80E+03	6.01E+03	-0.3172
15136	Fastener Shear	308	8.80E+03	6.01E+03	-0.3172
15140	Fastener Shear	310	8.73E+03	6.01E+03	-0.31173
15068	Fastener Shear	409	8.67E+03	6.01E+03	-0.30712
15068	Fastener Shear	408	8.67E+03	6.01E+03	-0.30712
15064	Fastener Shear	411	8.60E+03	6.01E+03	-0.301
15184	Fastener Shear	310	8.43E+03	6.01E+03	-0.28682
15116	Fastener Shear	411	8.32E+03	6.01E+03	-0.2773
15136	Fastener Shear	311	8.29E+03	6.01E+03	-0.27529
15140	Fastener Shear	309	8.21E+03	6.01E+03	-0.26823
15140	Fastener Shear	308	8.21E+03	6.01E+03	-0.26823
15068	Fastener Shear	410	8.17E+03	6.01E+03	-0.26402
15064	Fastener Shear	409	8.08E+03	6.01E+03	-0.25619
15064	Fastener Shear	408	8.08E+03	6.01E+03	-0.25619
15188	Fastener Shear	310	7.95E+03	6.01E+03	-0.24422
15184	Fastener Shear	309	7.95E+03	6.01E+03	-0.24403
15184	Fastener Shear	308	7.95E+03	6.01E+03	-0.24403
6136	Fastener Shear	310	1.13E+04	8.59E+03	-0.2425

Table 47 Forward Engine Fitting Bulkhead and Connecting Parts Lowes Fatigue Margins

Detail Name	Fx	Fy	Fs	t	d	Sigma allowable	Sigma fatigue	Fatigue Margin
c_3_n_99269372_A_90_Ctr	1.08	7.644	2.2	0.338	0.375	9.8248	7.644	0.29
c_8_n_99268725_A_0_Otr	0.713	2.841	2.919	0.556	0.4375	4.1902	2.919	0.44
c_8_n_99268740_A_0_Otr	1.555	3.232	3.764	0.556	0.4375	5.5866	3.764	0.48
c_8_n_99268735_A_90_Otr	0.289	6.063	4.697	0.556	0.4375	4.6233	2.888	0.6
c_3_n_99269397_A_90_Ctr	1.25	6.821	2.799	0.338	0.375	11.545	6.821	0.69
c_3_n_99269377_A_90_Ctr	0.531	5.355	1.714	0.338	0.375	9.4999	5.355	0.77
c_8_n_99268715_A_0_Otr	2.385	3.394	4.46	0.2703	0.4375	9.7933	4.46	1.2
c_8_n_99268705_A_0_Otr	2.55	3.828	6.903	0.2703	0.4375	15.4252	6.903	1.23
c_3_n_99269392_A_90_Ctr	0.511	4.729	2.414	0.338	0.375	10.8821	4.729	1.3
c_22_n_99268708_A_90_Otr	0.304	3.04	3.224	0.1503	0.4375	7.9311	3.224	1.46

Table 48 Frame 1 and Connecting Parts Lowes Fatigue Margins

Detail Name	Fx	Fy	Fs	t	d	Sigma allowable	Sigma fatigue	Fatigue Margin
c_22_n_99269872_A_90_Otr	0.846	4.153	4.967	0.2042	0.375	9.6727	4.967	0.95
c_22_n_99269867_A_90_Otr	0.602	3.996	4.658	0.2042	0.375	9.4904	4.658	1.04
c_22_n_99269887_A_90_Otr	0.526	3.877	4.381	0.2042	0.375	9.1544	4.381	1.09
c_3_n_99273220_A_90_Ctr	0.419	7.449	2.229	0.202	0.3125	15.6813	7.449	1.11
c_22_n_99273234_A_90_Otr	0.281	6.041	2.222	0.2053	0.3125	13.0728	6.041	1.16
c_22_n_99273244_A_90_Otr	0.363	5.412	3.865	0.2053	0.3125	11.6773	5.412	1.16
c_3_n_99274758_A_90_Ctr	0.339	8.671	1.959	0.1628	0.25	18.8343	8.671	1.17
c_3_n_99274753_A_90_Ctr	0.333	8.624	1.938	0.1628	0.25	18.8202	8.624	1.18
c_3_n_99274763_A_90_Ctr	0.393	8.344	2.644	0.1628	0.25	18.6734	8.344	1.24
c_3_n_99274773_A_90_Ctr	0.191	8.115	2.709	0.1628	0.25	18.5919	8.115	1.29

Table 49 Frame 2 and Connecting Parts Lowes Fatigue Margins

Detail Name	Fx	Fy	Fs	t	d	Sigma allowable	Sigma fatigue	Fatigue Margin
c_22_n_99273354_A_90_Otr	0.073	8.569	0.869	0.222	0.3125	13.5541	8.569	0.58
c_22_n_99273349_A_90_Otr	0.117	8.403	0.689	0.222	0.3125	13.434	8.403	0.6
c_22_n_99273364_A_90_Otr	0.193	6.736	1.714	0.222	0.3125	12.6984	6.736	0.89
c_22_n_99273359_A_90_Otr	0.233	6.26	1.36	0.222	0.3125	12.5108	6.26	1
c_3_n_99273335_A_90_Ctr	0.044	6.556	1.386	0.1913	0.3125	16.4315	6.556	1.51
c_3_n_99275261_A_90_Ctr	0.23	7.299	2.91	0.2076	0.25	18.6982	7.299	1.56
c_3_n_99275256_A_90_Ctr	0.231	7.16	1.596	0.2076	0.25	18.7363	7.16	1.62
c_3_n_99275251_A_90_Ctr	0.426	7.091	3.021	0.2076	0.25	18.6421	7.091	1.63
c_3_n_99275226_A_90_Ctr	0.238	7.122	1.816	0.2076	0.25	18.811	7.122	1.64
c_3_n_99275231_A_90_Ctr	0.224	7.132	1.562	0.2076	0.25	18.8197	7.132	1.64

Table 50 Frame 3 and Connecting Parts Lowes Fatigue Margins

Detail Name	Fx	Fy	Fs	t	d	Sigma allowable	Sigma fatigue	Fatigue Margin
c_17_n_99275691_A_90_Otr	-0.146	24.049	3.248	0.2279	0.25	39.269	24.049	0.63
c_17_n_99275696_A_90_Otr	-0.146	24.002	3.266	0.2279	0.25	39.3627	24.002	0.64
c_17_n_99275716_A_90_Otr	-0.069	22.792	5.686	0.2279	0.25	38.2507	22.792	0.68
c_17_n_99275706_A_90_Otr	-0.059	22.752	5.66	0.2279	0.25	38.3798	22.752	0.69
c_17_n_99275681_A_90_Otr	-0.022	22.217	2.168	0.2279	0.25	39.7922	22.217	0.79
c_22_n_99273389_A_90_Otr	0.132	8.068	0.983	0.222	0.3125	14.6417	8.068	0.81
c_22_n_99273394_A_90_Otr	0.123	8.068	0.707	0.222	0.3125	14.6329	8.068	0.81
c_17_n_99275701_A_90_Otr	-0.022	22.004	2.186	0.2279	0.25	39.9019	22.004	0.81
c_17_n_99275711_A_90_Otr	0.1	20.579	2.718	0.2279	0.25	39.9678	20.579	0.94
c_17_n_99275686_A_90_Otr	0.1	20.368	2.723	0.2279	0.25	40.1358	20.368	0.97

Table 51 Frame 4 and Connecting Parts Lowes Fatigue Margins

Detail Name	Fx	Fy	Fs	t	d	Sigma allowable	Sigma fatigue	Fatigue Margin
c_22_n_99269611_A_90_Otr	0.844	17.957	2.059	0.5	0.375	-2.4085	-1.495	0.61
c_22_n_99269491_A_90_Otr	1.237	7.691	1.834	0.2503	0.375	13.2807	7.691	0.73
c_22_n_99269616_A_90_Otr	0.154	19.175	3.942	0.5	0.375	-2.4379	-1.383	0.76
c_22_n_99269486_A_90_Otr	1.077	7.646	1.636	0.2503	0.375	13.5723	7.646	0.78
c_17_n_99273775_A_90_Otr	-0.09	22.208	7.383	0.73	0.3125	-5.0555	-2.833	0.78
c_22_n_99269481_A_90_Otr	0.937	7.737	1.133	0.2503	0.375	13.8864	7.737	0.79
c_22_n_99269476_A_90_Otr	0.965	7.689	1.396	0.2503	0.375	13.8084	7.689	0.8
c_22_n_99269621_A_90_Otr	0.549	16.557	2.516	0.5	0.375	-2.771	-1.51	0.84
c_22_n_99269626_A_90_Otr	0.08	18.239	4.589	0.5	0.375	-2.4394	-1.315	0.86
c_17_n_99273750_A_90_Otr	-0.01	20.573	7.244	0.73	0.3125	-3.2533	-1.731	0.88

Table 52 Frame 5 and Connecting Parts Lowes Fatigue Margins

Detail Name	Fx	Fy	Fs	t	d	Sigma allowable	Sigma fatigue	Fatigue Margin
c_22_n_99270357_A_90_Otr	0.315	6.656	2.881	0.5	0.375	5.3906	4.81	0.12
c_19_n_99270368_A_90_Ctr	0.732	13.807	7.208	0.4102	0.375	1.7232	1.435	0.2
c_22_n_99270362_A_90_Otr	0.397	6.788	5.031	0.5	0.375	4.6638	3.82	0.22
c_19_n_99274540_A_90_Otr	0.058	7.865	1.151	1.2802	0.3125	3.4432	2.631	0.31
c_19_n_99270358_A_90_Ctr	0.247	6.433	6.011	0.6142	0.375	9.0754	6.433	0.41
c_19_n_99270373_A_90_Ctr	0.343	13.363	5.995	0.4102	0.375	1.7021	1.136	0.5
c_19_n_99276691_A_90_Otr	0.157	9.141	2.774	1.2802	0.25	2.2319	1.45	0.54
c_19_n_99274535_A_90_Otr	0.042	6.049	1.149	1.2802	0.3125	3.0966	1.995	0.55
c_19_n_99276696_A_90_Otr	0.238	7.991	2.547	1.2802	0.25	2.0056	1.185	0.69
c_19_n_99276701_A_90_Otr	0.167	6.677	2.54	1.2802	0.25	1.7234	0.897	0.92

Table 53 Frame 6 and Connecting Parts Lowes Fatigue Margins

Detail Name	Fx	Fy	Fs	t	d	Sigma allowable	Sigma fatigue	Fatigue Margin
c_19_n_99270433_A_90_Ctr	2.509	13.175	9.997	0.7748	0.375	4.0801	3.391	0.2
c_19_n_99270463_A_90_Ctr	8.11	15.328	7.262	0.7795	0.375	18.9863	15.328	0.24
c_19_n_99270428_A_90_Ctr	1.345	7.694	9.96	0.5261	0.375	13.6069	9.96	0.37
c_19_n_99274422_A_90_Otr	0.379	17.191	5.202	1.105	0.3125	4.9932	3.342	0.49
c_19_n_99274407_A_90_Otr	0.135	20.49	2.515	1.105	0.3125	4.3241	2.887	0.5
c_19_n_99274412_A_90_Otr	0.961	19.459	1.215	1.105	0.3125	4.3817	2.729	0.61
c_19_n_99274417_A_90_Otr	0.39	17.254	2.452	1.105	0.3125	5.1093	3.093	0.65
c_22_n_99270462_A_90_Otr	2.86	7.239	2.957	0.5	0.375	2.581	1.435	0.8
c_22_n_99270457_A_90_Otr	1.031	5.228	2.242	0.5	0.375	2.5575	1.14	1.24
c_19_n_99274402_A_90_Otr	0.164	8.367	1.007	1.105	0.3125	7.6059	3.151	1.41

Table 54 Aft Pylon Bulkhead and Connecting Parts Lowes Fatigue Margins

Detail Name	Fx	Fy	Fs	t	d	Sigma allowable	Sigma fatigue	Fatigue Margin
c_20_n_99270680_A_90_Otr	0.371	32.887	7.042	1.4799	0.375	5.7228	3.71	0.54
c_20_n_99270675_A_90_Otr	0.851	32.133	7.782	1.4799	0.375	4.8035	3.013	0.59
c_20_n_99270690_A_90_Otr	0.876	29.655	1.406	1.4799	0.375	7.2871	4.146	0.76
c_20_n_99270685_A_90_Otr	0.562	24.954	2.108	1.4799	0.375	5.5755	2.546	1.19
c_20_n_99269271_A_90_Otr	-0.22	6.551	8.093	1.4502	0.4375	18.6235	8.093	1.3
c_20_n_99269275_A_90_Otr	3.233	8.535	5.77	1.4502	0.4375	-0.3424	-0.106	2.23
c_20_n_99269267_A_0_Otr	-0.58	2.757	7.314	1.4502	0.4375	24.3016	7.314	2.32
c_20_n_99269259_A_90_Otr	0.48	5.055	4.663	1.4502	0.4375	-0.4499	-0.133	2.38
c_20_n_99269279_A_90_Otr	7.025	10.473	3.691	1.4502	0.4375	-0.0627	-0.016	2.92
c_20_n_99274141_A_90_Otr	0.453	18.944	4.598	0.5	0.3125	4.9324	1.245	2.96

Table 55 Lug Analysis Input Values

	Pu	α	a	D	t	W	Kbr	Kt	Ksb	Kaxu	Kaxy
Upper Link	289968	63	2.00	2.00	1.80	5.00	0.953	0.954	0.533	0.533	0.732
Lower Link	379683	11	2.00	2.00	2.10	3.96	0.951	0.964	0.816	0.816	0.74
Main Front Spar Fitting	183343	34	2.00	2.00	1.25	4.26	0.959	0.959	0.709	0.709	0.737
Lateral Front Spar Fitting	110201	69	1.43	1.31	1.25	2.85	0.956	0.956	0.799	0.759	0.829

Table 56 Lug Analysis Allowable Values

	Ftuax	Ftyax	Ftutr	Ftytr	Fbru	E
Upper Link	135000	125000	135000	125000	203000	1.69E+07
Lower Link	135000	125000	135000	125000	203000	1.69E+07
Main Front Spar Fitting	135000	125000	135000	125000	203000	1.69E+07
Lateral Front Spar Fitting	135000	125000	135000	125000	203000	1.69E+07

Table 57 Lug Analysis Yield Margins of Safety

	Paxy	Ptry	Kthy	Pthy	λ	Kfity	MSy
Upper Link	329175	326604	0.928	305616	1.11	1.15	0.24
Lower Link	415999	290763	0.945	393226	1.02	1.15	0.33
Main Front Spar Fitting	230313	180261	0.838	192966	1.07	1.15	0.28
Lateral Front Spar Fitting	169045	123088	0.722	122122	1.13	1.15	0.27

Table 58 Lug Analysis Ultimate Margins of Safety

	Paxu	Ptru	Kthu	Pthu	λ	Kfitu	MSu
Upper Link	388800	424979	0.996	387315	1.11	1.15	0.05
Lower Link	486000	371820	0.954	463786	1.02	1.15	0.05
Main Front Spar Fitting	270000	231658	0.871	235253	1.06	1.15	0.05
Lateral Front Spar Fitting	198427	158489	0.784	155499	1.13	1.15	0.08

Table 59 Angle/Channel Fitting Geometrical Inputs

	D	Dw	a	b	ta	tb	te
Fwd_Eng_Fitt_Bulkhead	0.75	1.1025	3.5	2.65	0.3	0.6	0.9770967
Aft_Eng_Fitt_Bulkhead	0.875	1.28625	4	4.75	0.3471385	0.414646	0.8121475
Upper_Link_Fitting	0.5	0.735	2.025	2	0.3683507	1.8	0.73

Table 60 Angle/Channel Fitting Allowable Values

	Ftu	Fty	Fsu
Fwd_Eng_Fitt_Bulkhead	134000	126000	87000
Aft_Eng_Fitt_Bulkhead	134000	126000	87000
Upper_Link_Fitting	134000	126000	87000

Table 61 Angle/Channel Fitting Section Values

	a/b	Cx	Cy	X	Y	A	Ixx	Iyy
Fwd_Eng_Fitt_Bulkhead	1.321	2.084	1.441	1.308	0.388	2.895	1.532	3.595
Aft_Eng_Fitt_Bulkhead	0.842	0.000	2.512	0.000	1.462	4.956	11.320	14.506
Upper_Link_Fitting	1.013	1.631	2.800	2.053	1.119	2.914	1.229	1.009

Table 62 Angle/Channel Fitting Wall Bending Margin of Safety

	P	Mx	My	fta	fbx	fby	ftu	λ	MS
Fwd_Eng_Fitt_Bulkhead	59687	38378.74	62844.44	20617.27	77957.44	12376.6	110951.3	1.15	0.05
Aft_Eng_Fitt_Bulkhead	67935	-170653	71331.75	13706.52	-38261.2	-2038.98	-26593.6	1.15	3.38
Upper_Link_Fitting	55822	-65236.3	93850.7	19156.49	-48104.5	23513.83	-5434.15	1.15	20.44

Table 63 End Pad Bearing Margin of Safety

	Ka	fbu	Fbu/Ftu	Fbu	λ	MS
Fwd_Eng_Fitt_Bulkhead	1.544234	96542.35	1.25E+00	1.68E+05	1.15	0.51
Aft_Eng_Fitt_Bulkhead	0.603557	62164.46	1.25E+00	1.68E+05	1.15	1.34
Upper_Link_Fitting	1.322759	138560.8	1.25E+00	1.68E+05	1.15	0.05

Table 64 Angle/Channel Fitting End Pad Shear Margins of Safety

	fsu	λ	MS
Fwd_Eng_Fitt_Bulkhead	29394.26	1.15	1.57
Aft_Eng_Fitt_Bulkhead	34501.04	1.15	1.19
Upper_Link_Fitting	55194.28	1.15	0.37

APPENDIX B

Table 65 Critical Load Cases By Component

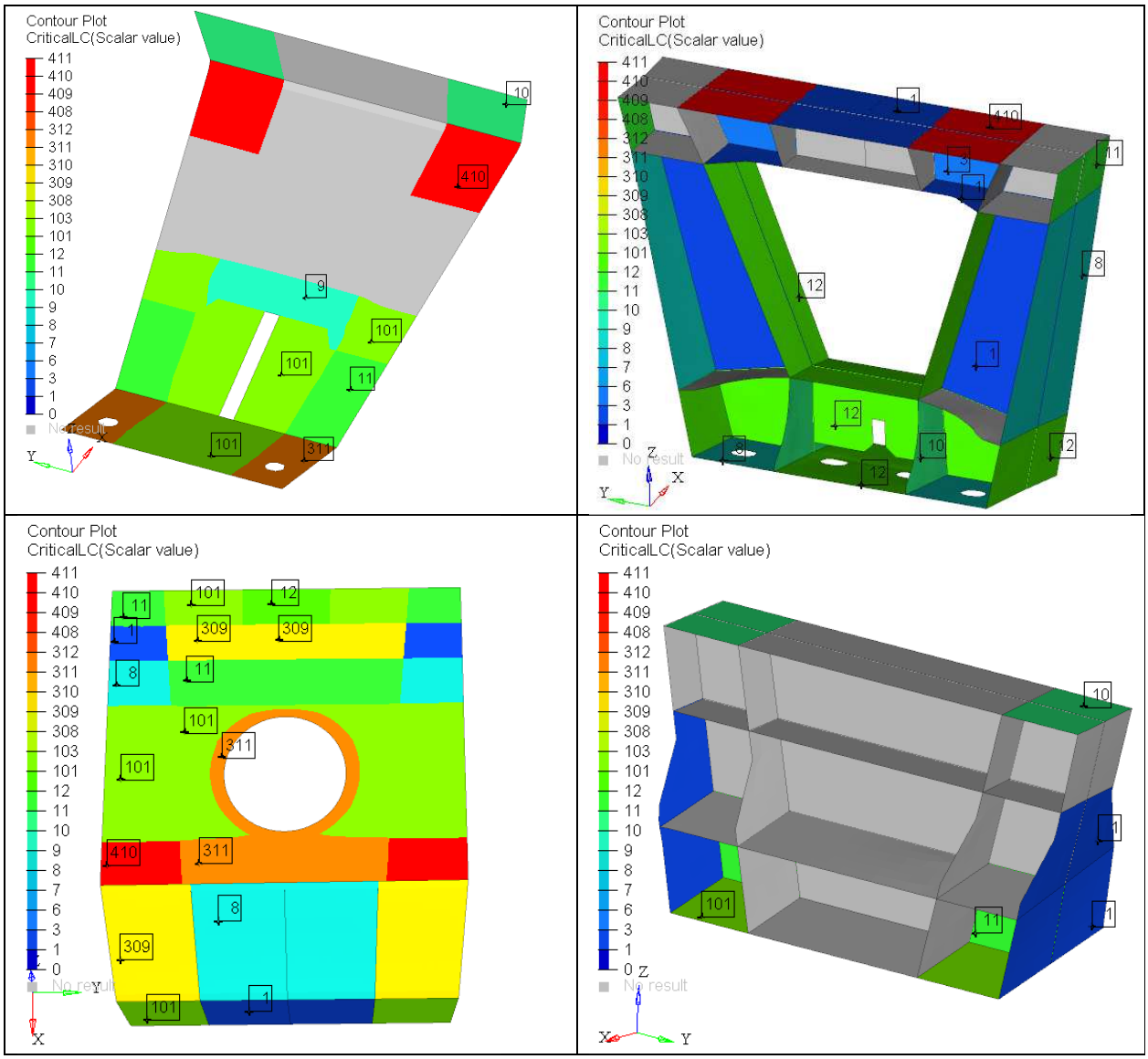

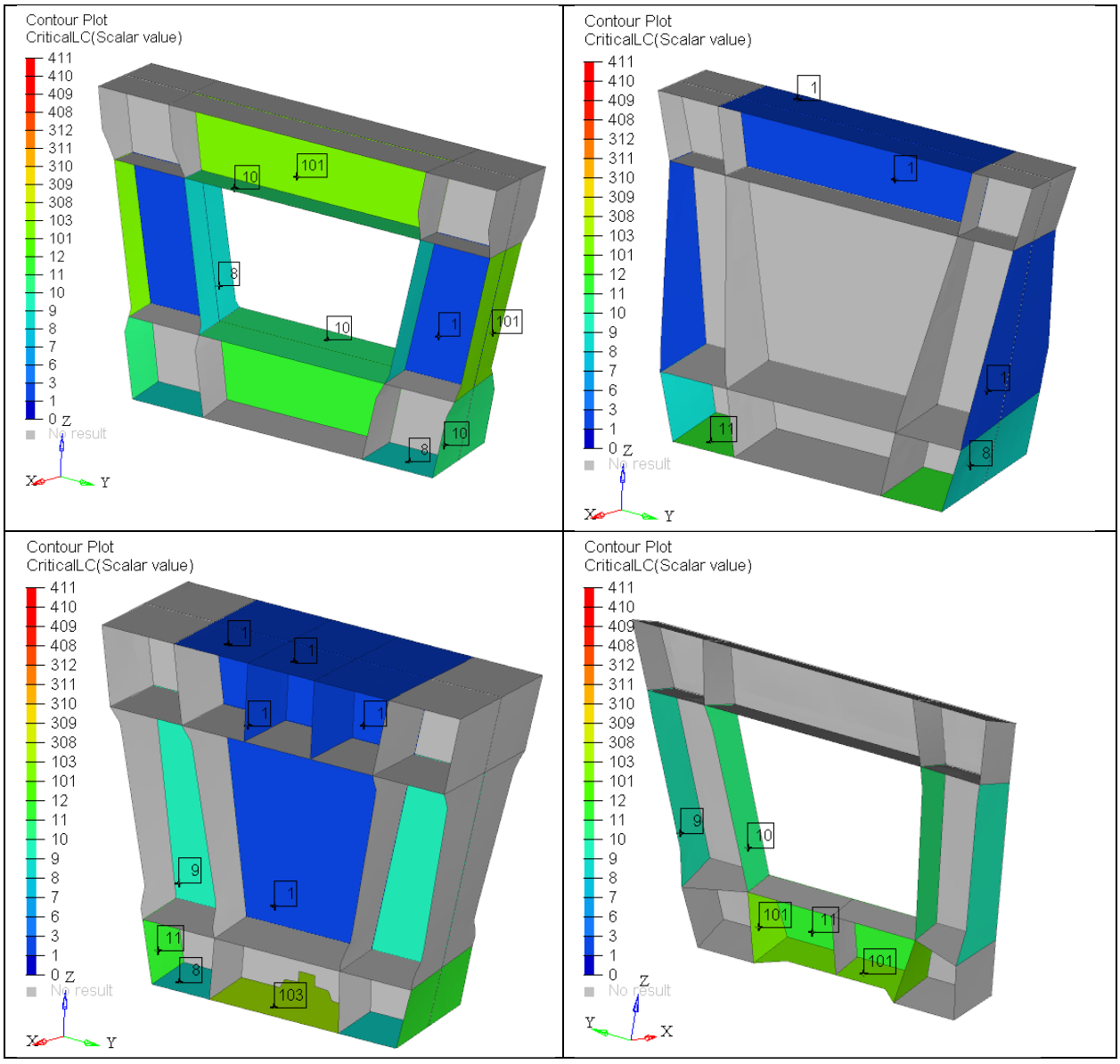
Contour Plot
CriticalLC(Scalar value)
411
410
409
408
312
311
310
309
308
103
101
12
11
10
9
8
7
6
3
1
0
Z
No result
X
Y
Contour Plot
CriticalLC(Scalar value)
411
410
409
408
312
311
310
309
308
103
101
12
11
10
9
8
7
6
3
1
0
Z
No result
X
Y
Contour Plot
CriticalLC(Scalar value)
411
410
409
408
312
311
310
309
308
103
101
12
11
10
9
8
7
6
3
1
0
Z
No result
X
Y
Contour Plot
CriticalLC(Scalar value)
411
410
409
408
312
311
310
309
308
103
101
12
11
10
9
8
7
6
3
1
0
Z
No result
Y
X

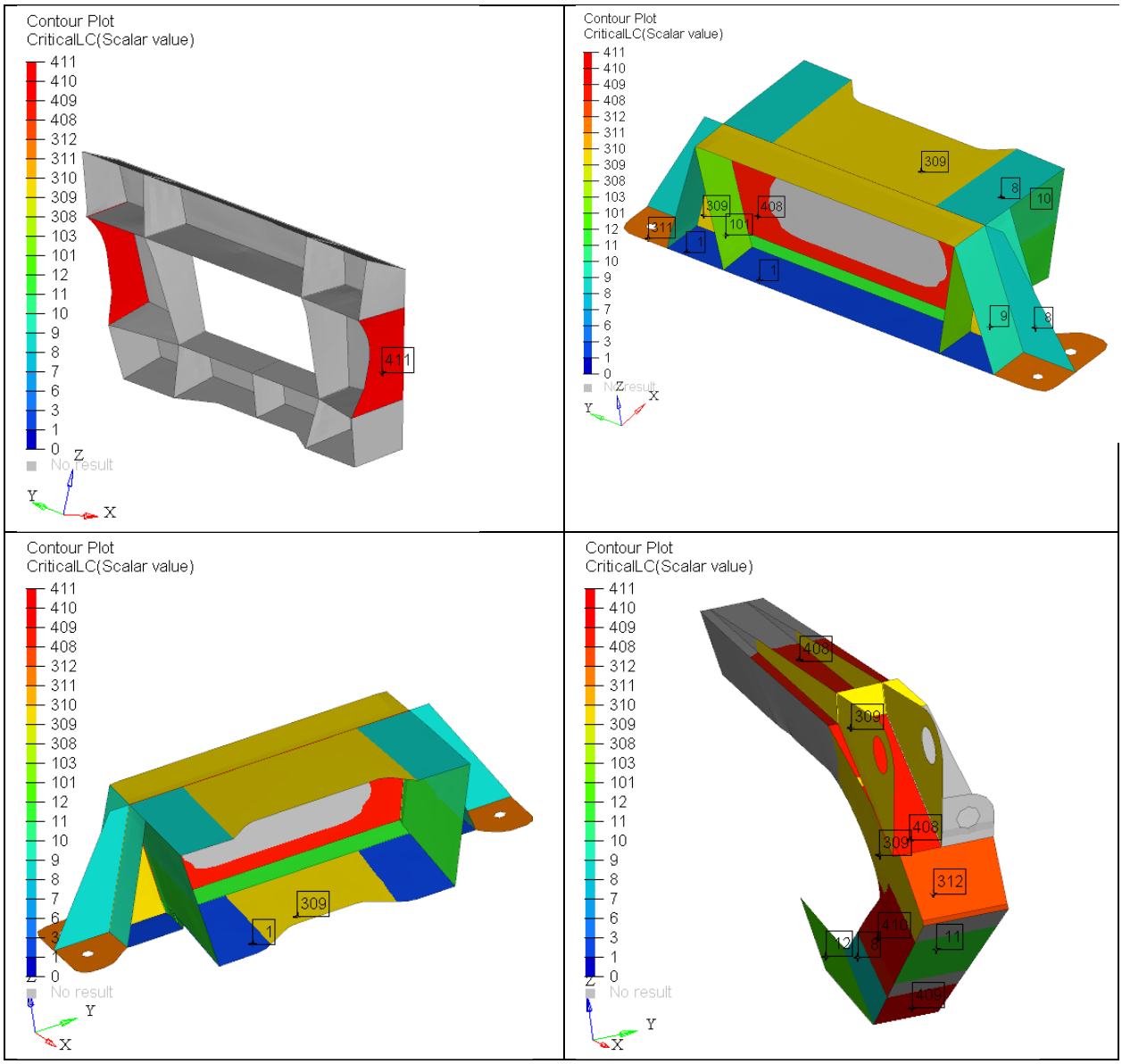
Contour Plot
CriticalLC(Scalar value)
411
410
409
408
312
311
310
309
308
103
101
12
11
10
9
8
7
6
3
1
0
No result
Z
Y
X
411
Contour Plot
CriticalLC(Scalar value)
309
8
10
309
408
411
101
1
1
9
8
Contour Plot
CriticalLC(Scalar value)
309
1
Contour Plot
CriticalLC(Scalar value)
408
309
408
309
312
410
11
409

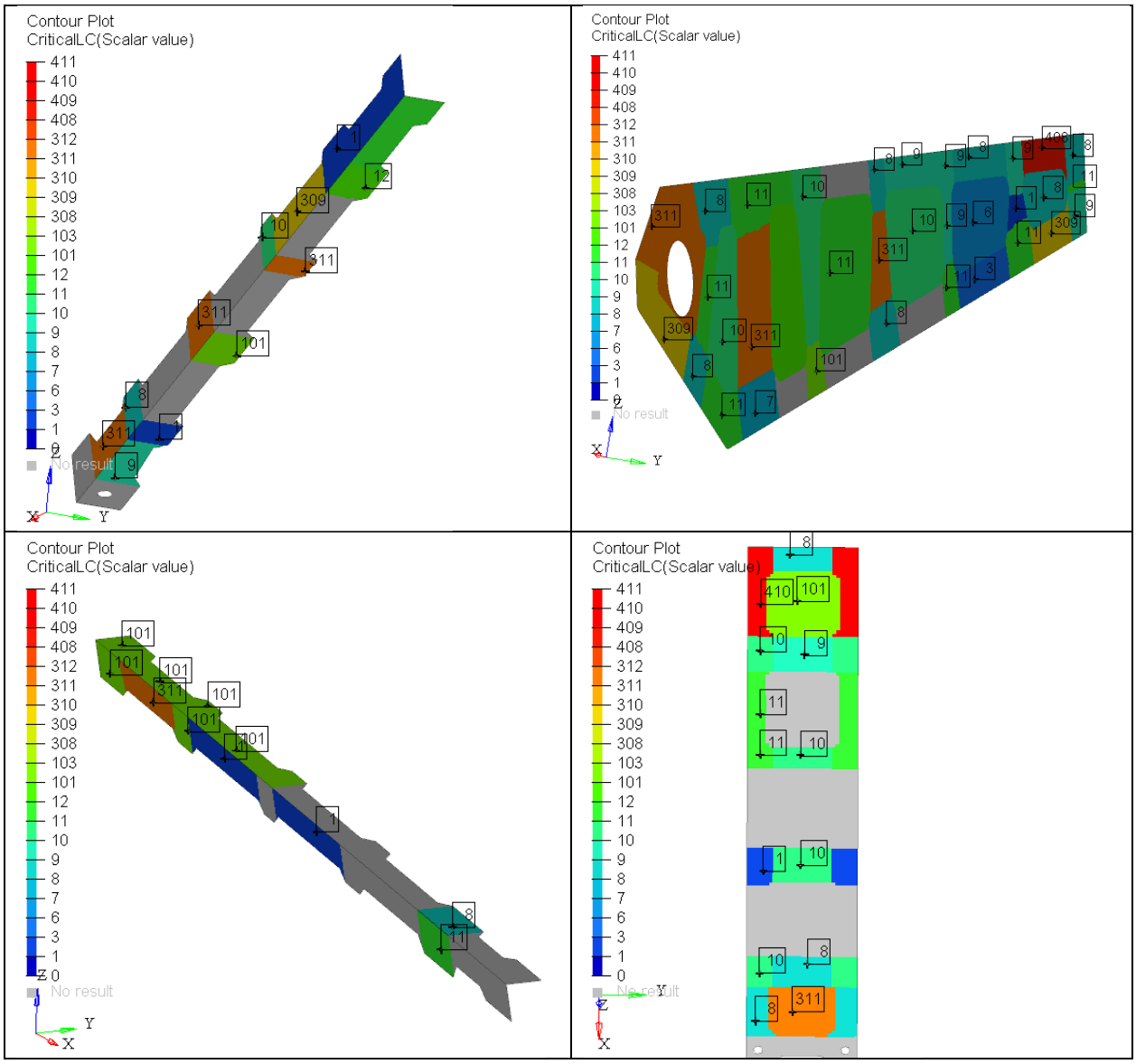
Contour Plot
CriticalLC(Scalar value)
411
410
409
408
312
311
310
309
308
103
101
12
11
10
9
8
7
6
3
1
0
No result
Contour Plot
CriticalLC(Scalar value)
411
410
409
408
312
311
310
309
308
103
101
12
11
10
9
8
7
6
3
1
0
No result
Contour Plot
CriticalLC(Scalar value)
411
410
409
408
312
311
310
309
308
103
101
12
11
10
9
8
7
6
3
1
0
No result
Contour Plot
CriticalLC(Scalar value)
411
410
409
408
312
311
310
309
308
103
101
12
11
10
9
8
7
6
3
1
0
No result

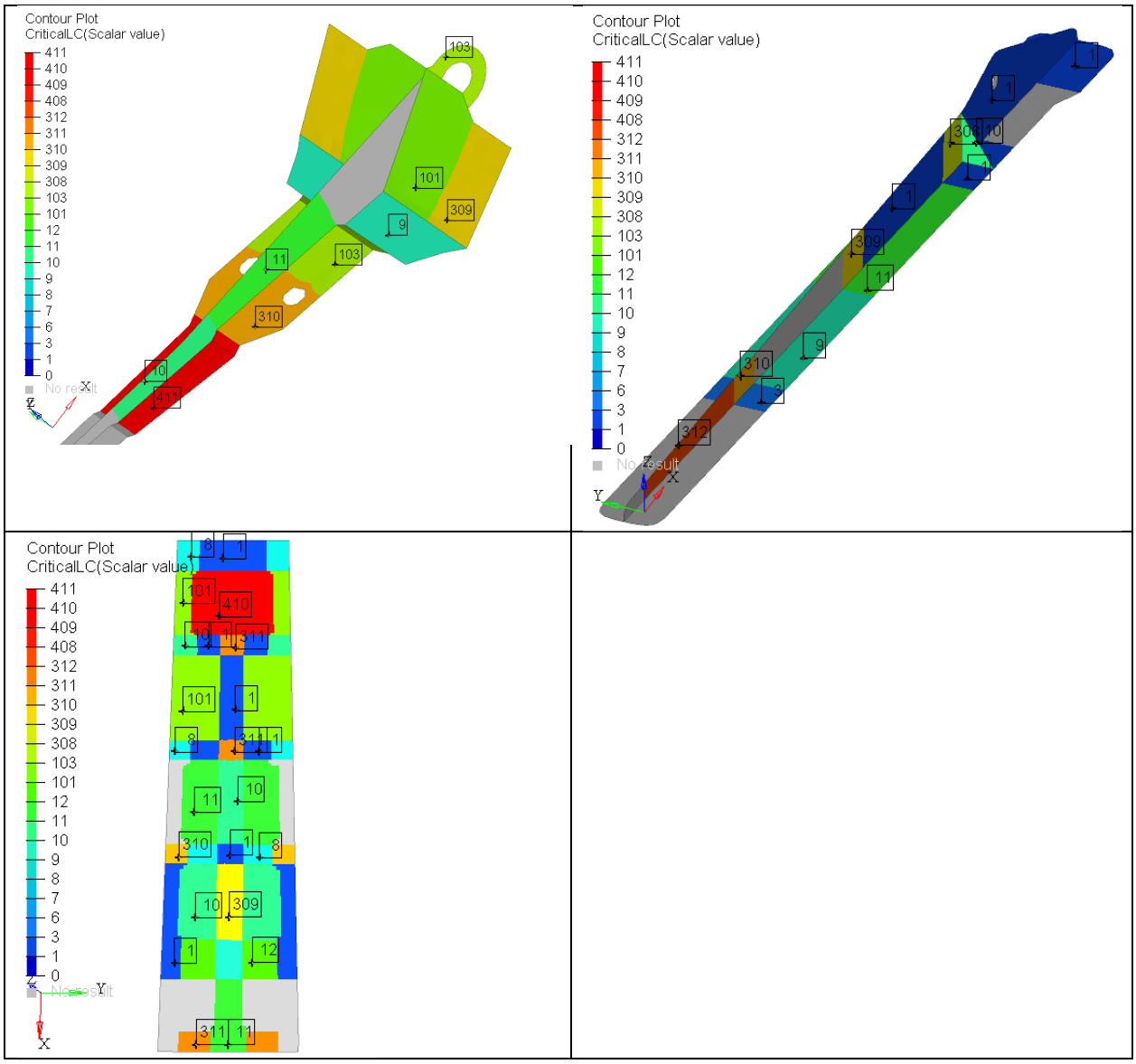
Contour Plot
CriticalLC(Scalar value)
411
410
409
408
312
311
310
309
308
103
101
12
11
10
9
8
7
6
3
1
0
No result
Contour Plot
CriticalLC(Scalar value)
411
410
409
408
312
311
310
309
308
103
101
12
11
10
9
8
7
6
3
1
0
No result
Contour Plot
CriticalLC(Scalar value)
411
410
409
408
312
311
310
309
308
103
101
12
11
10
9
8
7
6
3
1
0
No result

Table 66 Eigenvectors for the Stability Critical Load cases

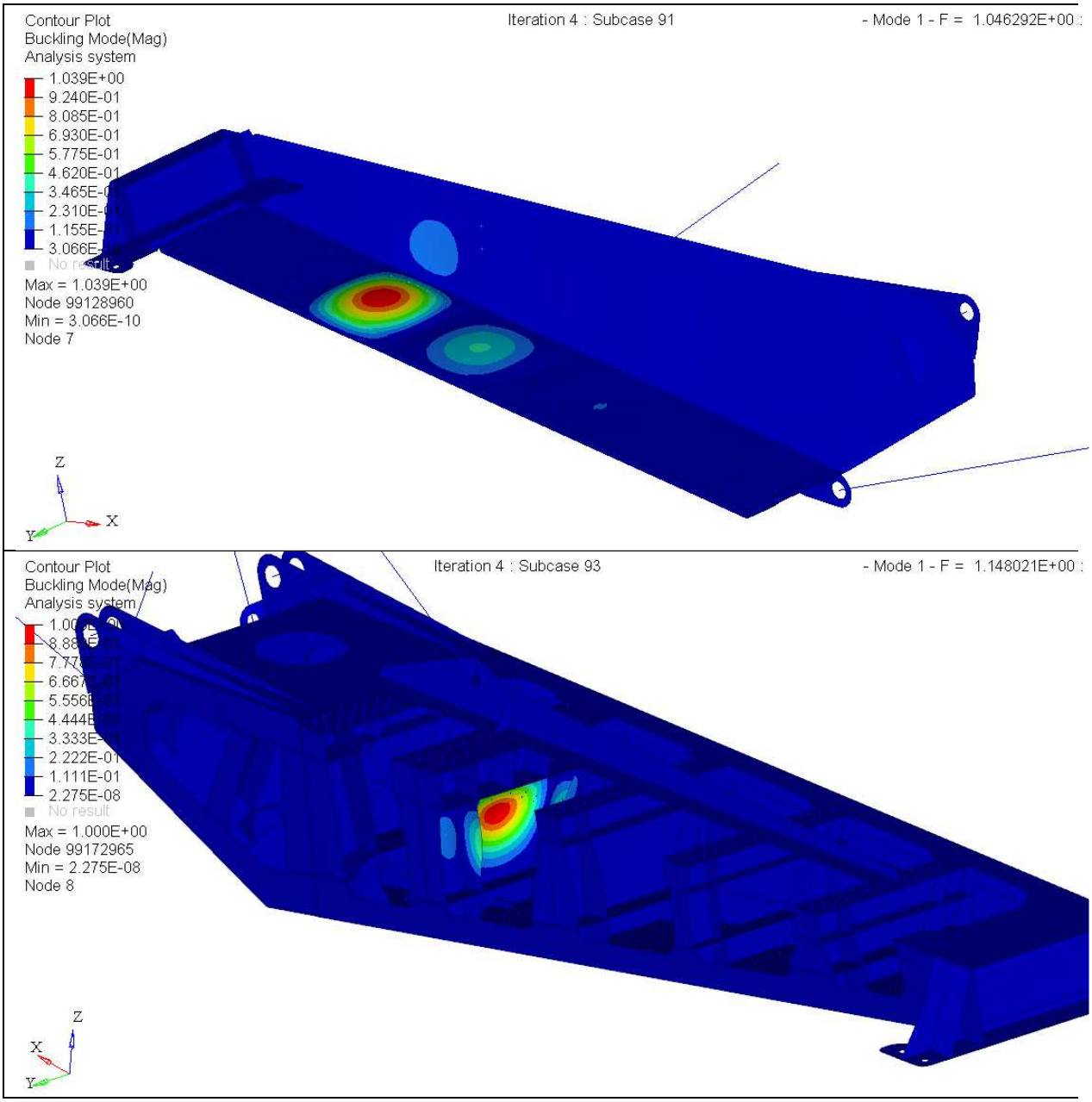

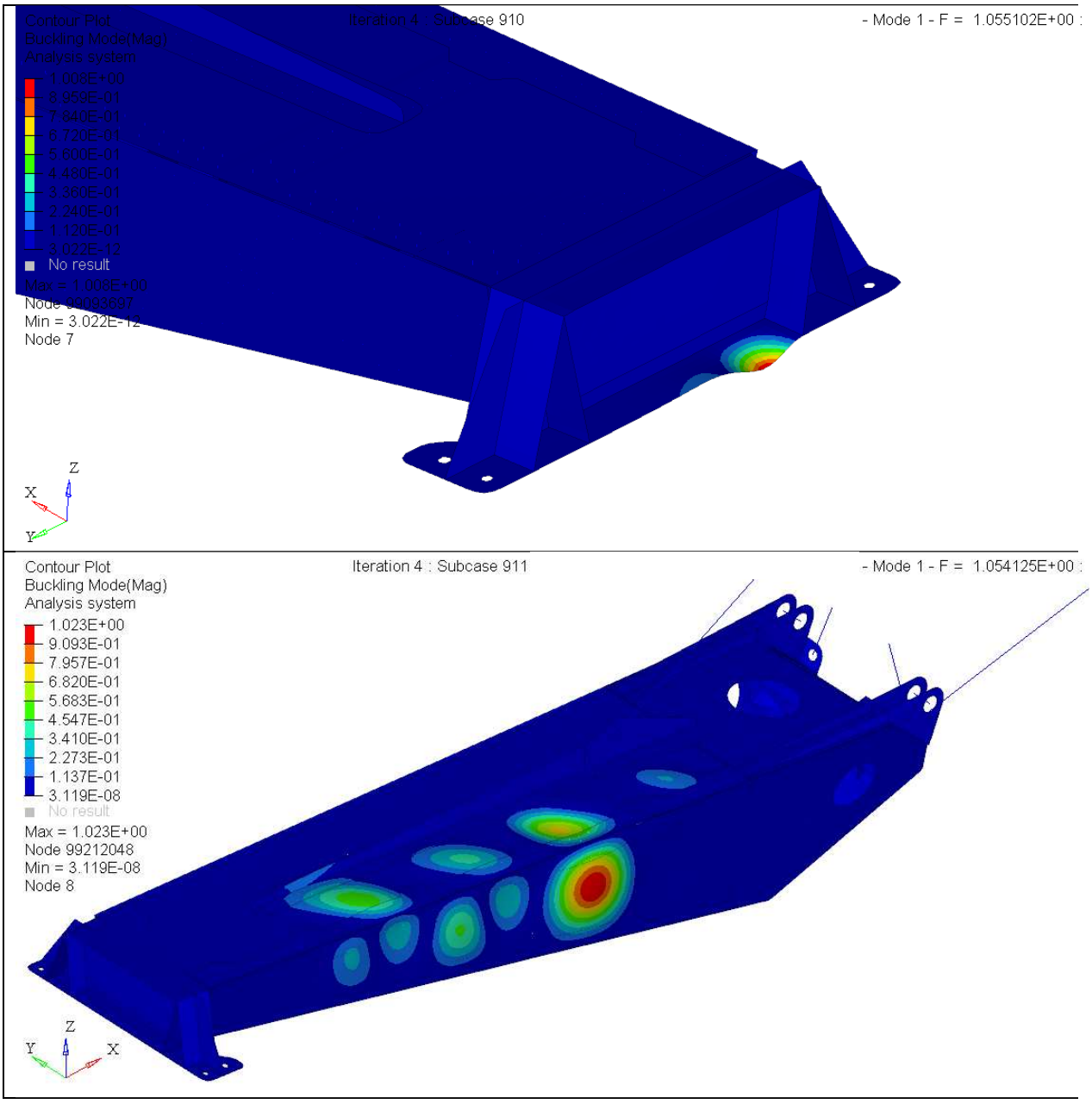
Contour Plot
Buckling Mode(Mag)
Analysis system
1.008E+00
8.959E-01
7.840E-01
6.720E-01
5.600E-01
4.480E-01
3.360E-01
2.240E-01
1.120E-01
3.022E-12
No result
Max = 1.008E+00
Node 94093697
Min = 3.022E-12
Node 7
Iteration 4 : Subcase 910
- Mode 1 - F = 1.055102E+00 :
Z
X
Y
Contour Plot
Buckling Mode(Mag)
Analysis system
1.023E+00
9.093E-01
7.957E-01
6.820E-01
5.683E-01
4.547E-01
3.410E-01
2.273E-01
1.137E-01
3.119E-08
No result
Max = 1.023E+00
Node 99212048
Min = 3.119E-08
Node 8
Iteration 4 : Subcase 911
- Mode 1 - F = 1.054125E+00 :
Z
Y
X

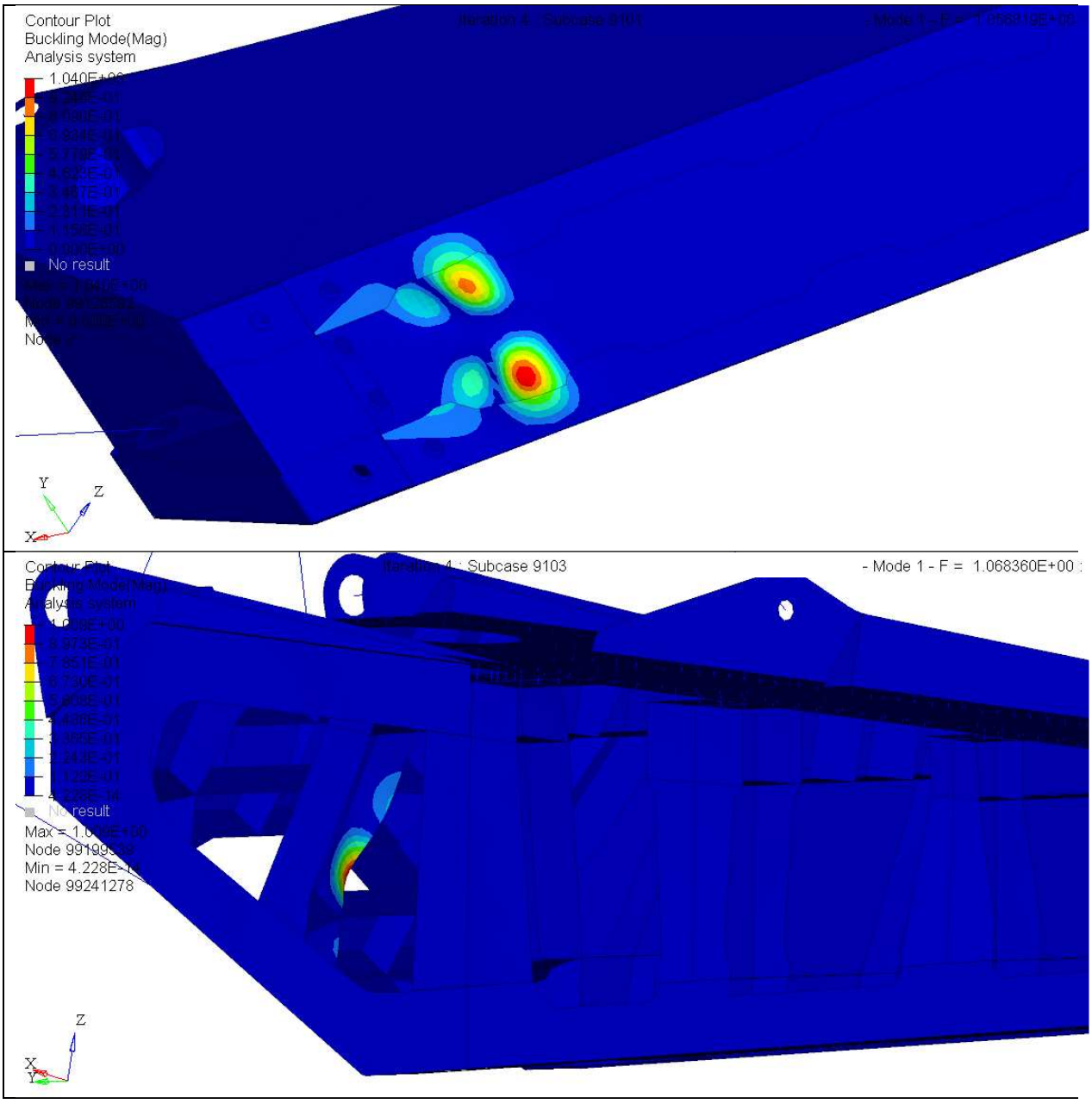
Contour Plot
Buckling Mode(Mag)
Analysis system
No result
Y
Z
X
Iteration 4 : Subcase 9103
- Mode 1 - F = 1.068360E+00
No result
Max = 1.000E+00
Node 99199
Min = 4.228E-14
Node 99241278
Z
X
Y

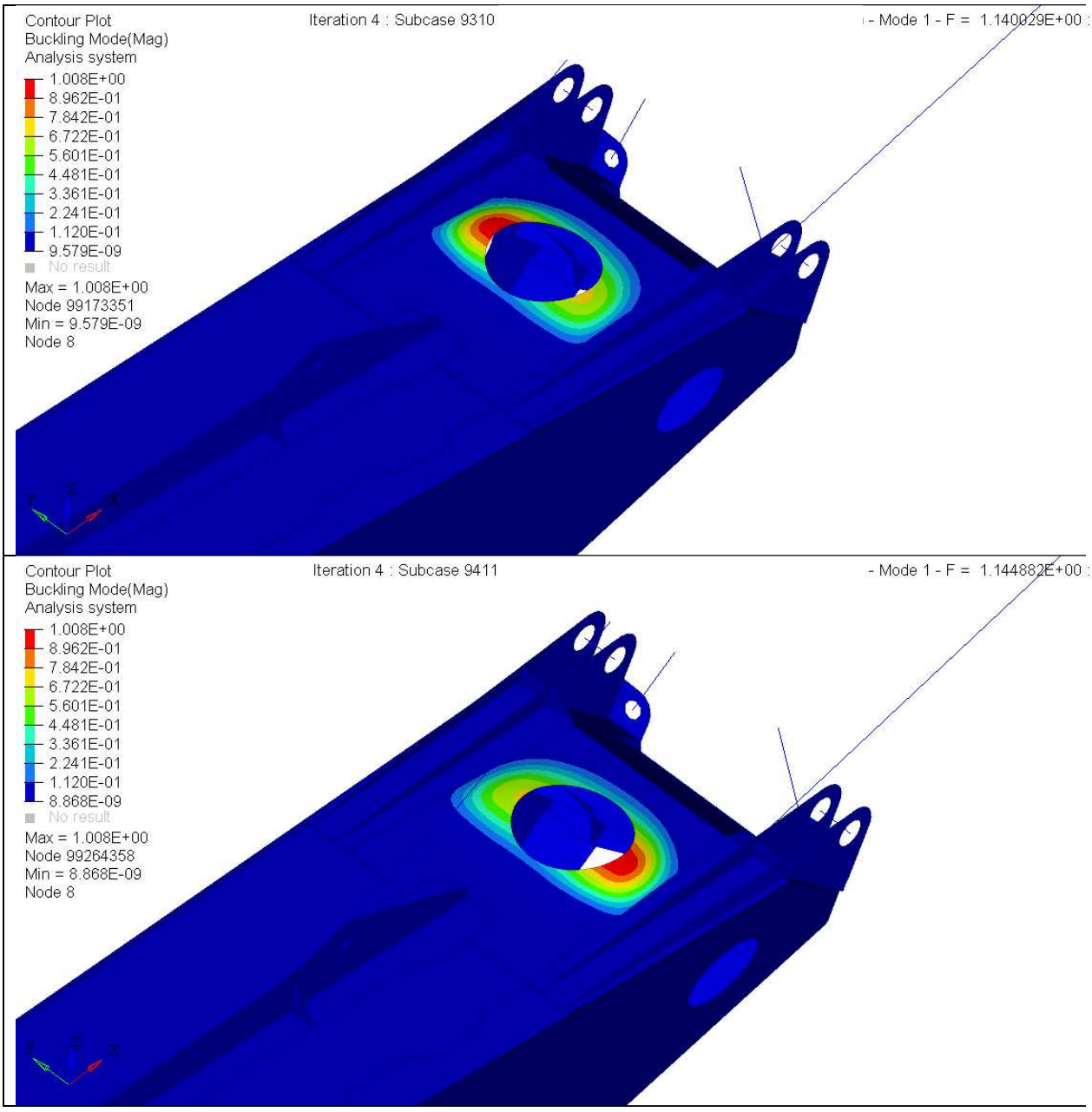
Contour Plot
Buckling Mode(Mag)
Analysis system
1.008E+00
8.962E-01
7.842E-01
6.722E-01
5.601E-01
4.481E-01
3.361E-01
2.241E-01
1.120E-01
9.579E-09
No result
Max = 1.008E+00
Node 99173351
Min = 9.579E-09
Node 8
Iteration 4 : Subcase 9310
- Mode 1 - F = 1.140029E+00 :
Contour Plot
Buckling Mode(Mag)
Analysis system
1.008E+00
8.962E-01
7.842E-01
6.722E-01
5.601E-01
4.481E-01
3.361E-01
2.241E-01
1.120E-01
8.868E-09
No result
Max = 1.008E+00
Node 99264358
Min = 8.868E-09
Node 8
Iteration 4 : Subcase 9411
- Mode 1 - F = 1.144882E+00 :

Table 67 Minimum Fastener Shear Margins of Safety

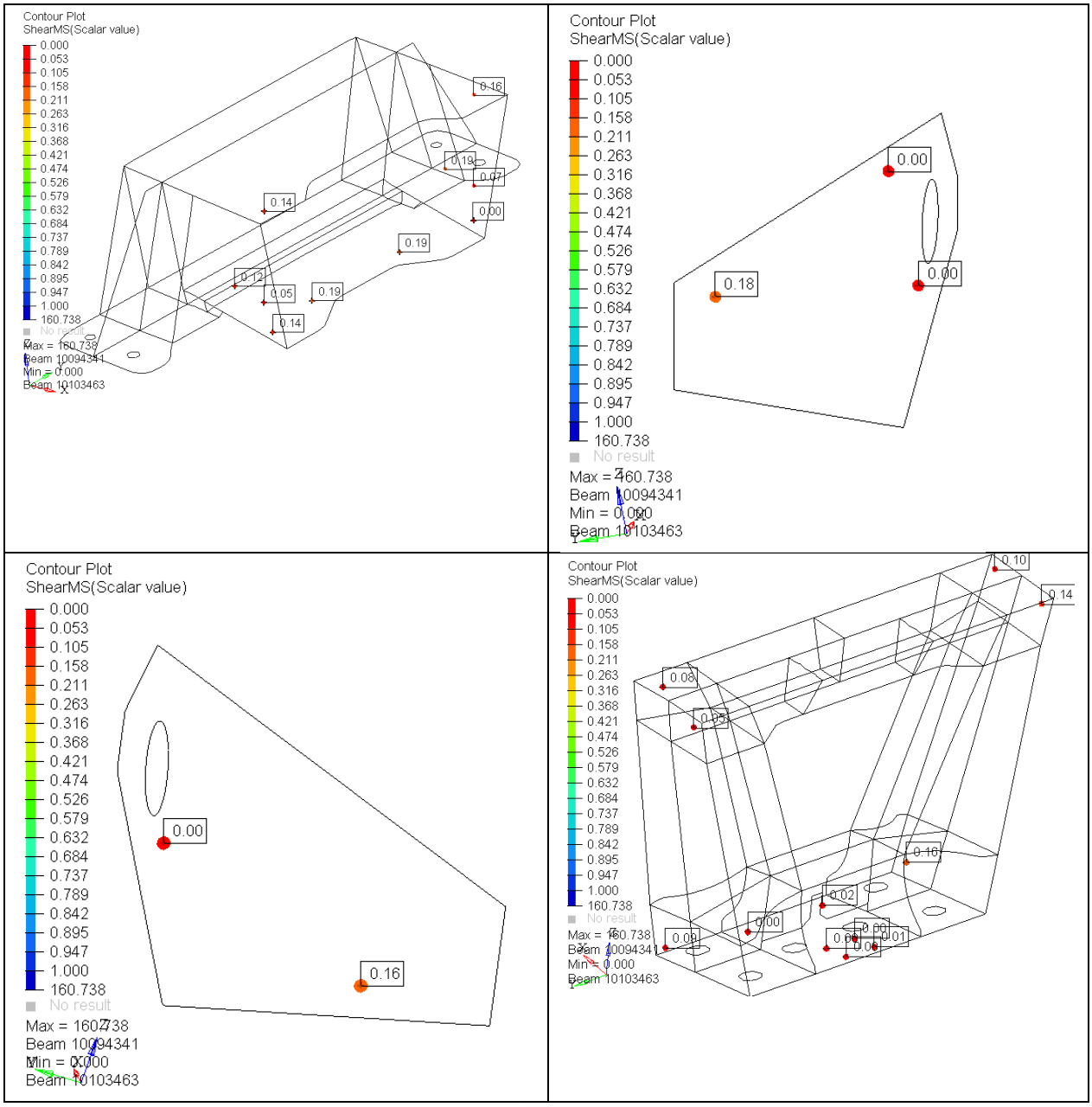

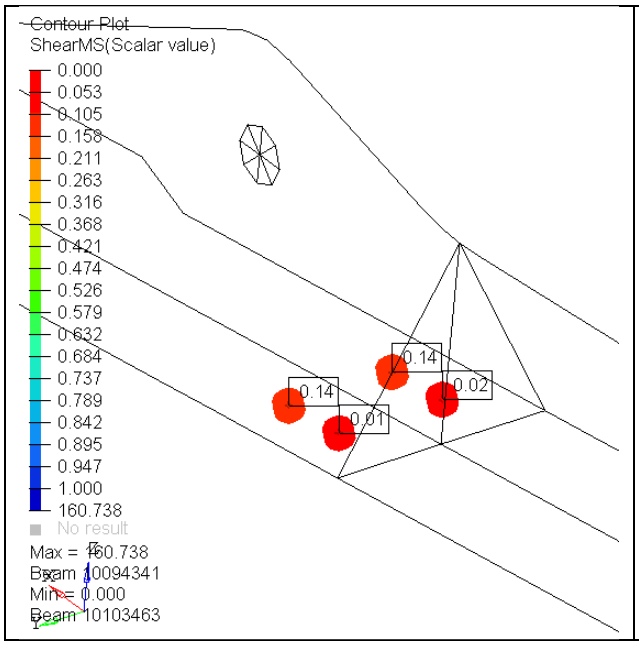
Contour Plot
ShearMS(Scalar value)
0.000
0.053
0.105
0.158
0.211
0.263
0.316
0.368
0.421
0.474
0.526
0.579
0.632
0.684
0.737
0.789
0.842
0.895
0.947
1.000
160.738
No result
Max = 160.738
Beam 10094341
Min = 0.000
Beam 10103463
0.14
0.14
0.02
0.01

Table 68 Minimum Bearing Stress Margins of Safety

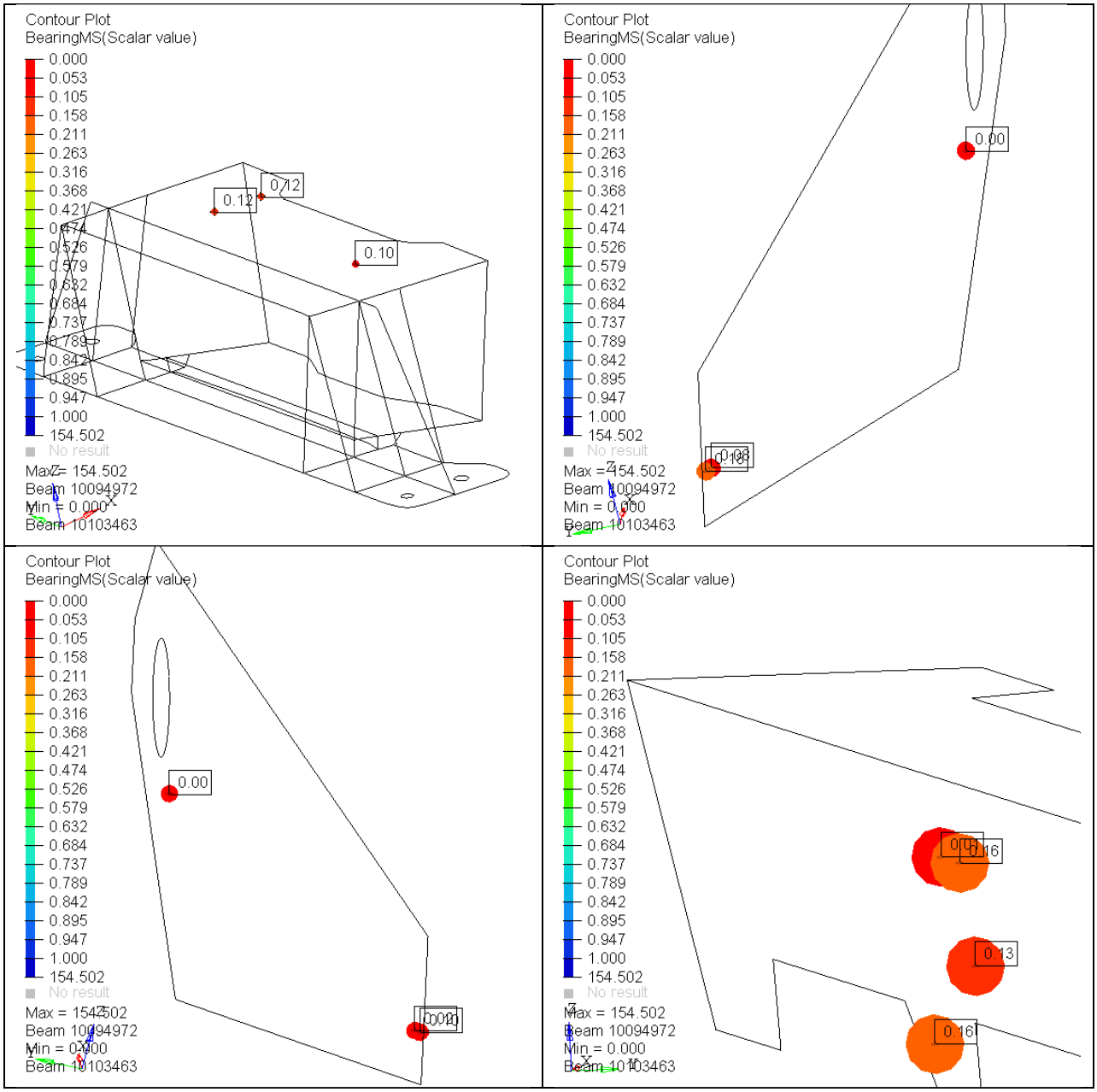

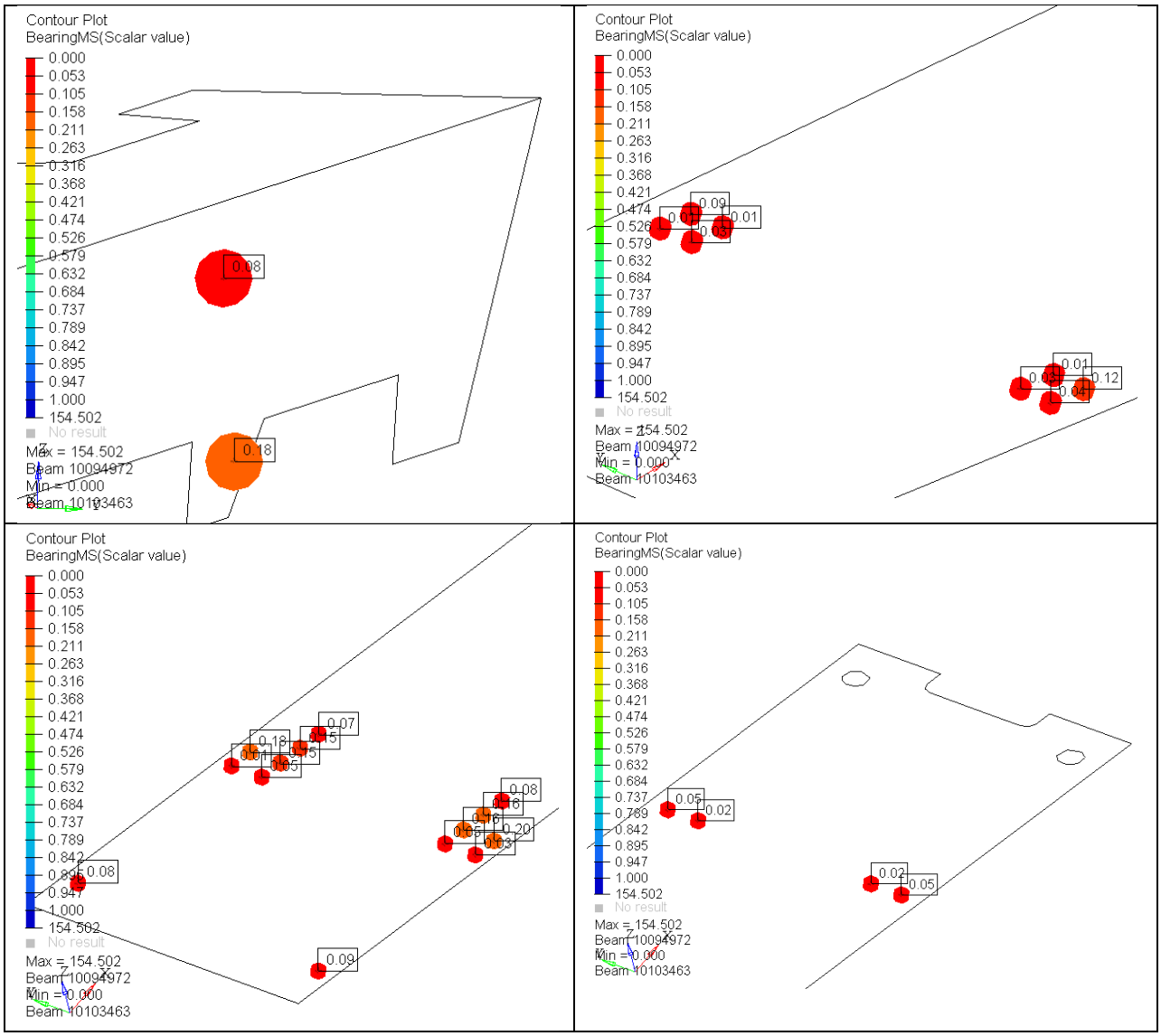
Contour Plot
BearingMS(Scalar value)
0.000
0.053
0.105
0.158
0.211
0.263
0.316
0.368
0.421
0.474
0.526
0.579
0.632
0.684
0.737
0.789
0.842
0.895
0.947
1.000
154.502
No result
Max = 154.502
Beam 10094972
Min = 0.000
Beam 10103463
0.08
0.18
Contour Plot
BearingMS(Scalar value)
0.09
0.01
0.03
0.12
Contour Plot
BearingMS(Scalar value)
0.07
0.18
0.08
0.20
0.08
0.09
Contour Plot
BearingMS(Scalar value)
0.05
0.02
0.02
0.05

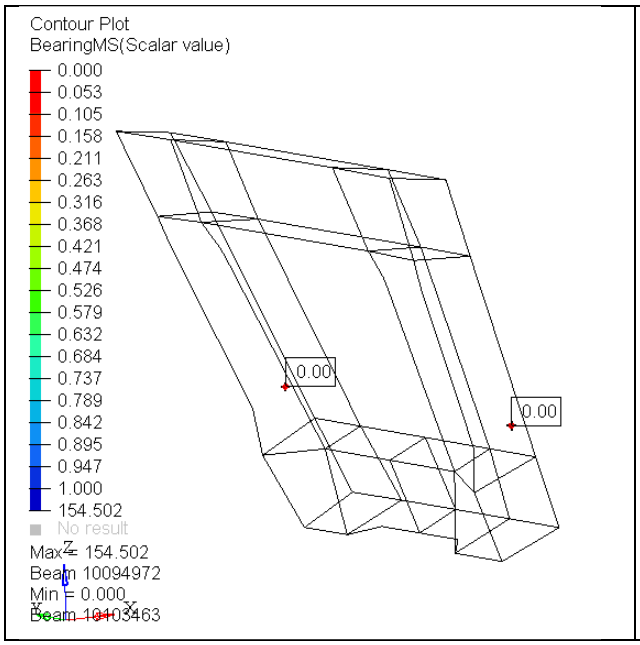
Contour Plot
BearingMS(Scalar value)
0.000
0.053
0.105
0.158
0.211
0.263
0.316
0.368
0.421
0.474
0.526
0.579
0.632
0.684
0.737
0.789
0.842
0.895
0.947
1.000
154.502
No result
Max = 154.502
Beam 10094972
Min = 0.000
Beam 10103463
0.00
0.00

Table 69 Fastener Joint Margins at the Forward Engine Fitting Bulkhead

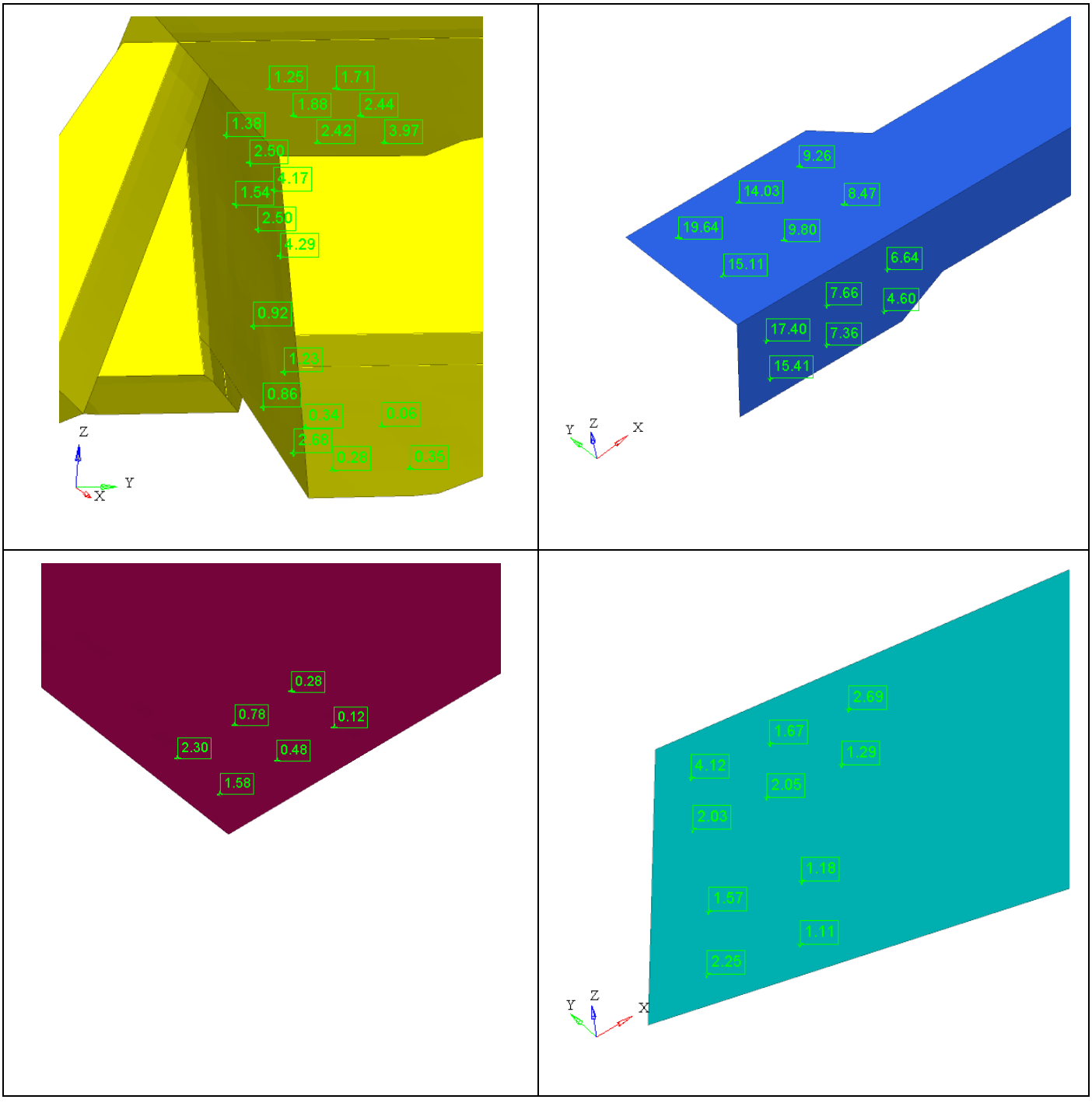

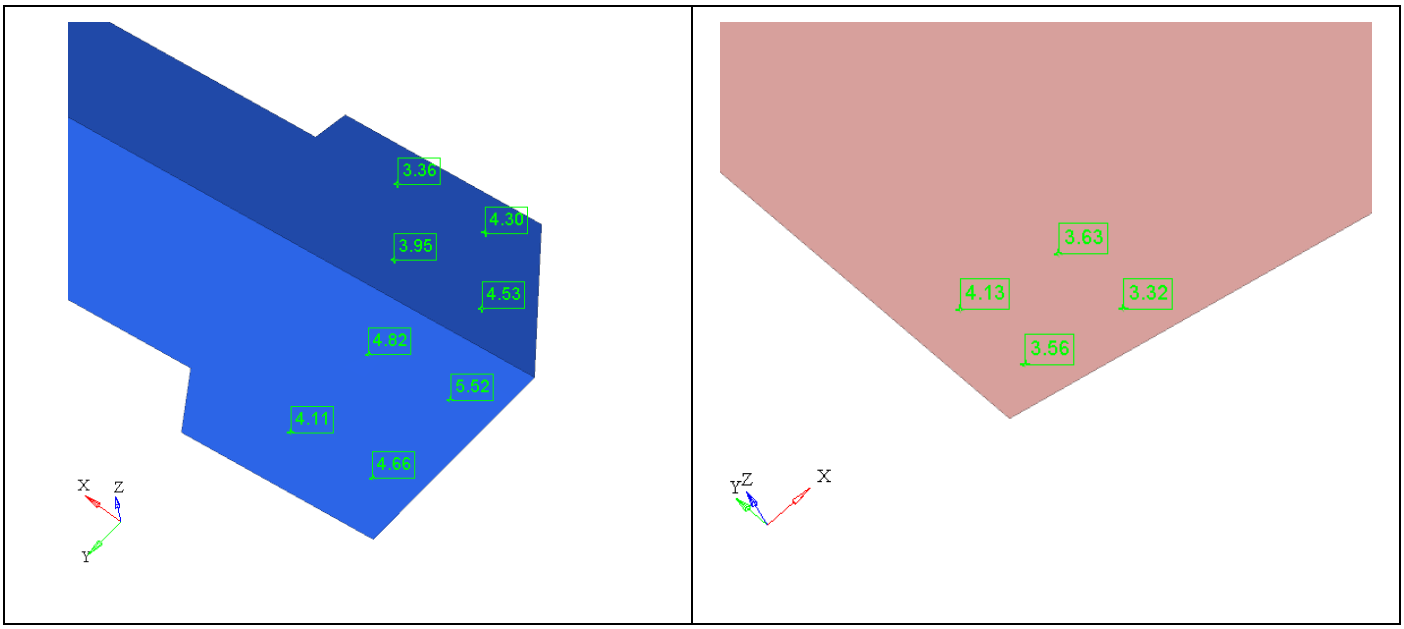

Table 70 Fastener Joint Margins at Frame1

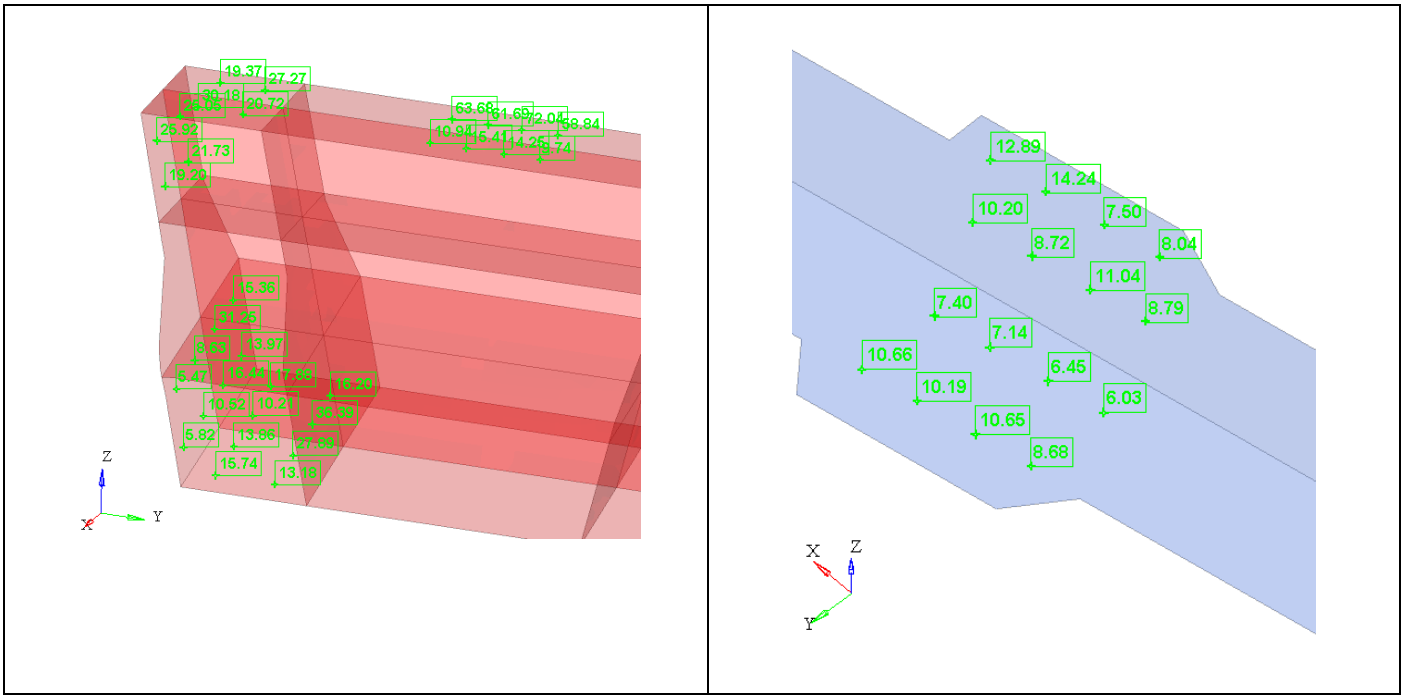

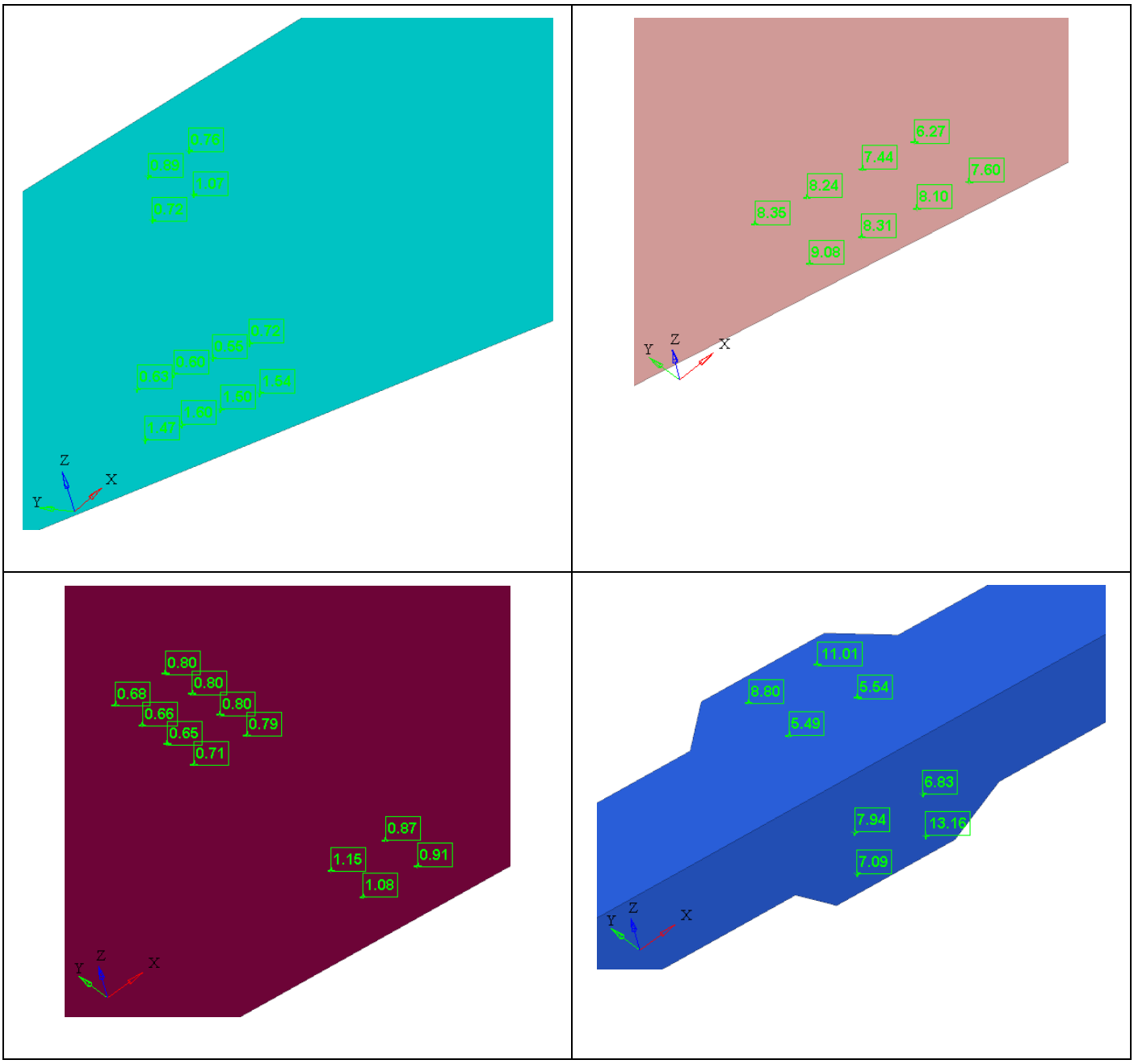
0.76
0.68
1.07
0.72
0.72
0.65
0.60
0.63
1.54
1.50
1.60
1.47
Z
X
Y
6.27
7.44
7.60
8.24
8.10
8.35
8.31
9.08
Y
Z
X
0.80
0.80
0.68
0.80
0.66
0.79
0.65
0.71
0.87
0.91
1.15
1.08
Y
Z
X
11.01
9.80
5.54
5.49
6.83
7.94
13.16
7.09
Y
Z
X

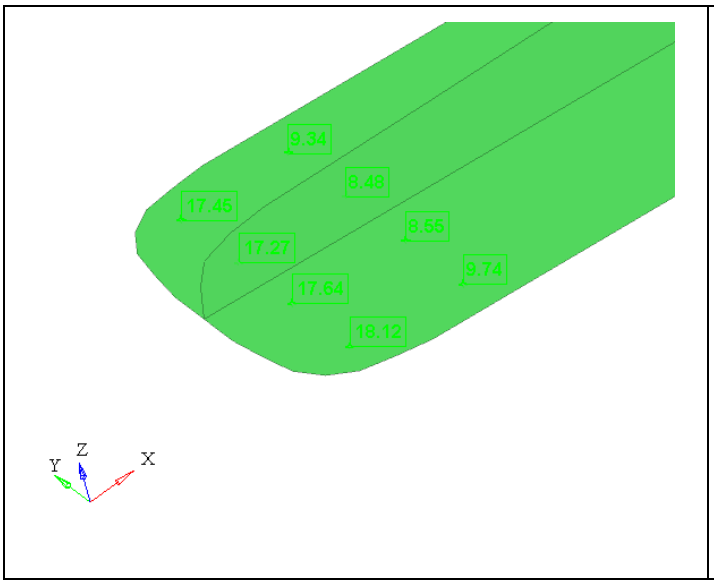

Table 71 Fastener Joint Margins at Frame2

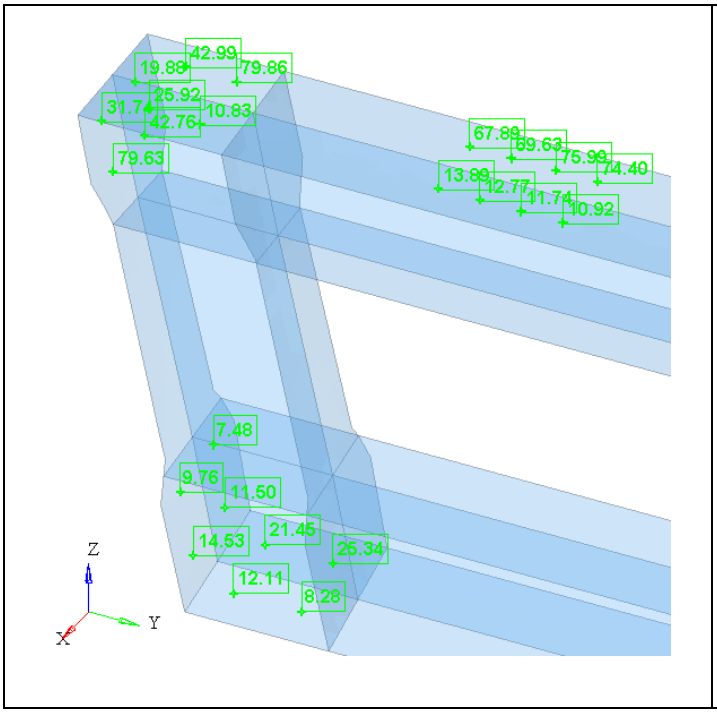

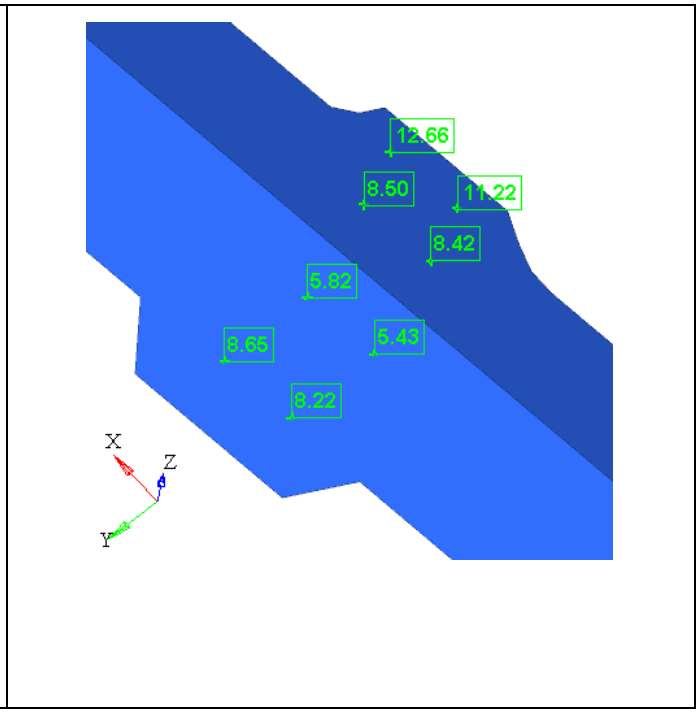

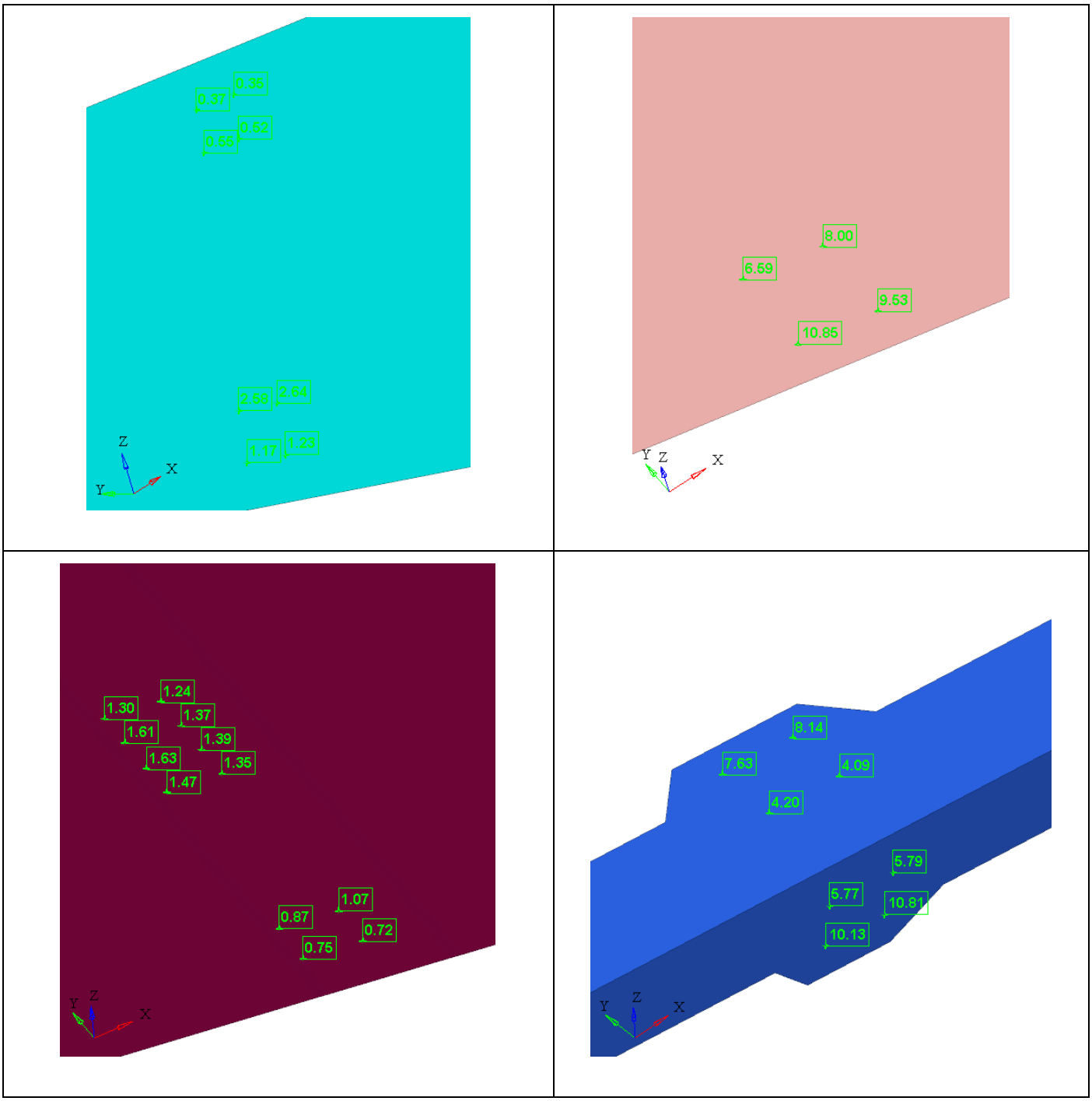
0.35
0.37
0.52
0.55
2.64
2.68
1.23
1.17
Z
X
Y
8.00
6.59
9.53
10.85
Y Z X
1.24
1.30
1.37
1.61
1.39
1.63
1.35
1.47
1.07
0.87
0.72
0.75
Y Z X
8.14
7.63
4.09
4.20
5.79
5.77
10.81
10.13
Y Z X

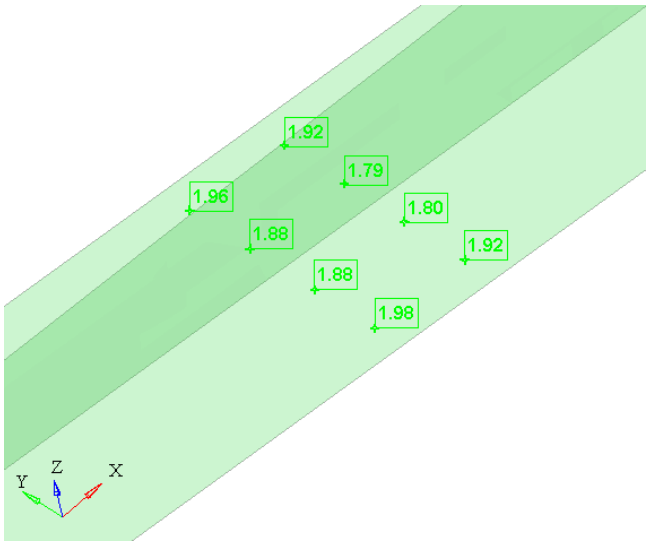

Table 72 Fastener Joint Margins at Frame3

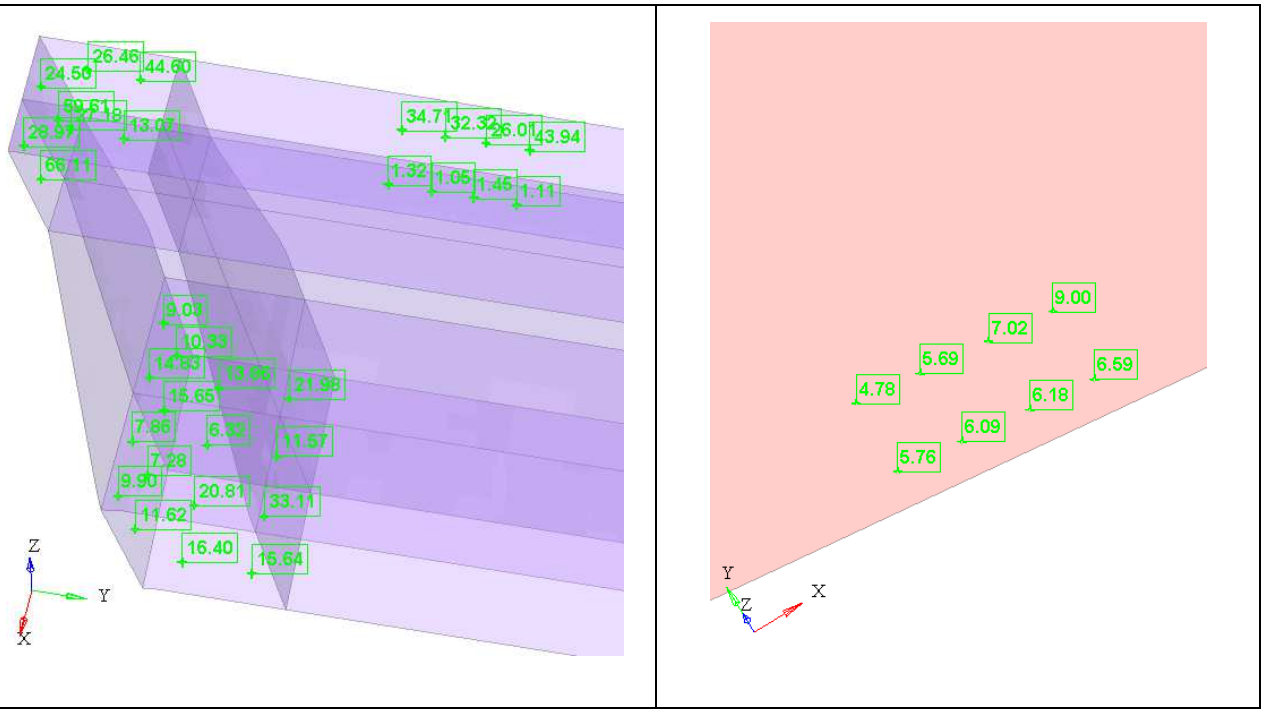

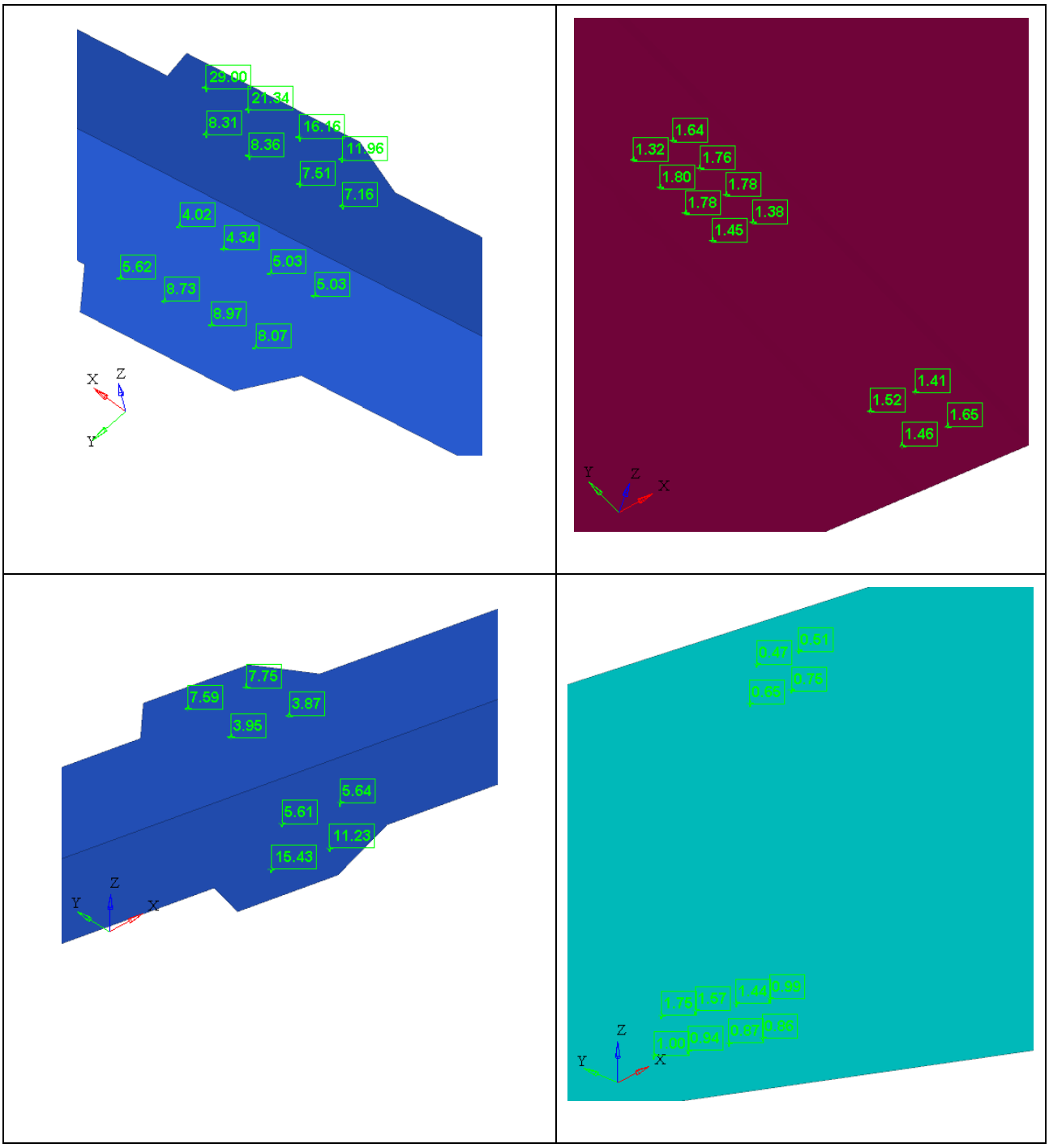
29.90
21.34
8.31
16.46
8.36
11.96
7.51
7.16
4.02
4.34
5.62
5.03
8.73
5.03
8.97
8.07
X
Z
Y
1.64
1.32
1.76
1.80
1.78
1.78
1.38
1.45
1.41
1.52
1.65
1.46
Y
Z
X
7.75
7.59
3.87
3.95
5.64
5.61
11.23
15.43
Z
Y
X
0.61
0.47
0.75
0.68
1.76
1.57
1.44
0.99
1.00
0.94
0.87
0.86
Z
Y
X

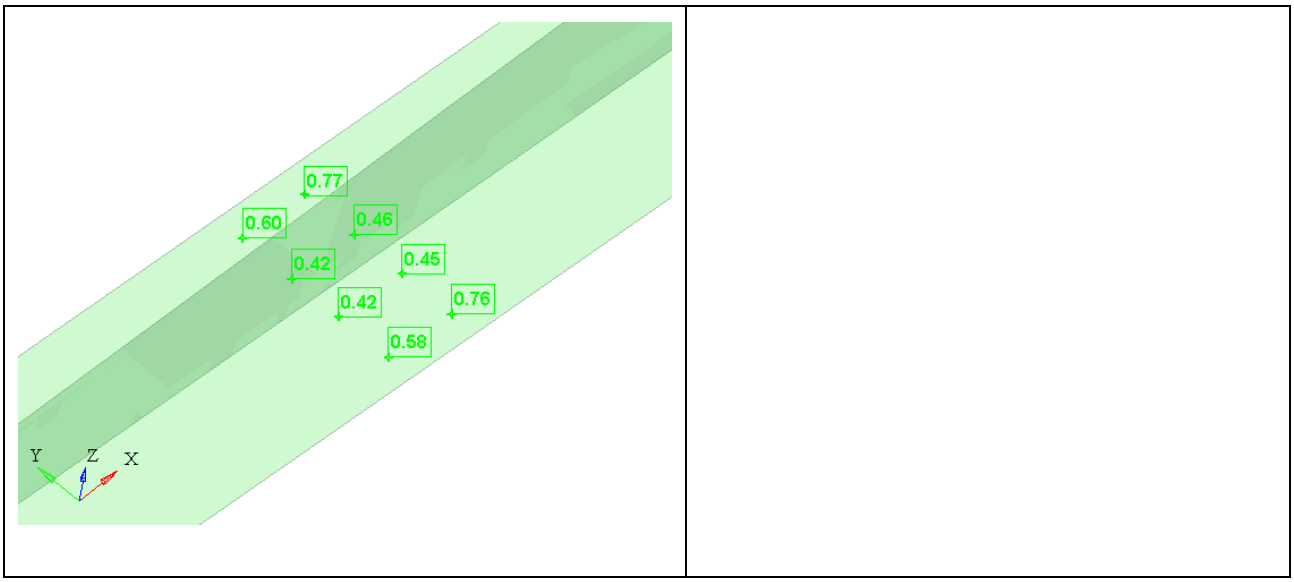

Table 73 Fastener Joint Margins at Frame4

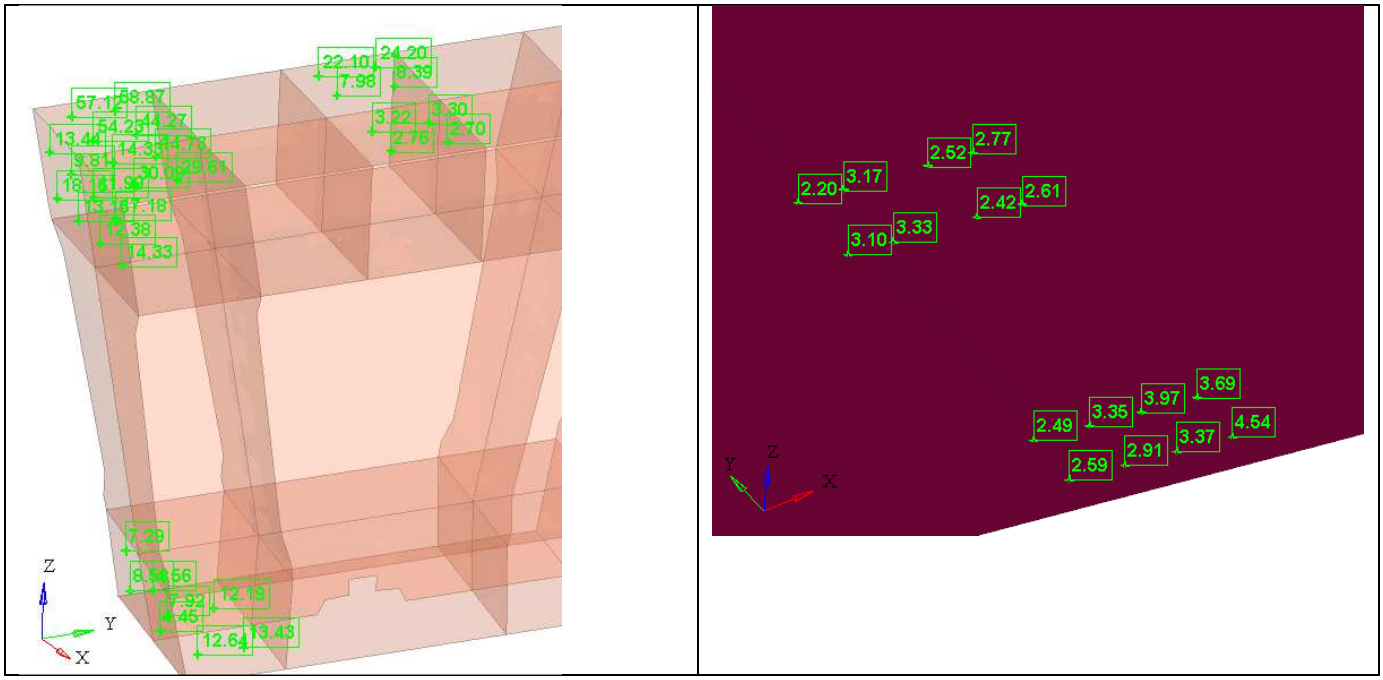

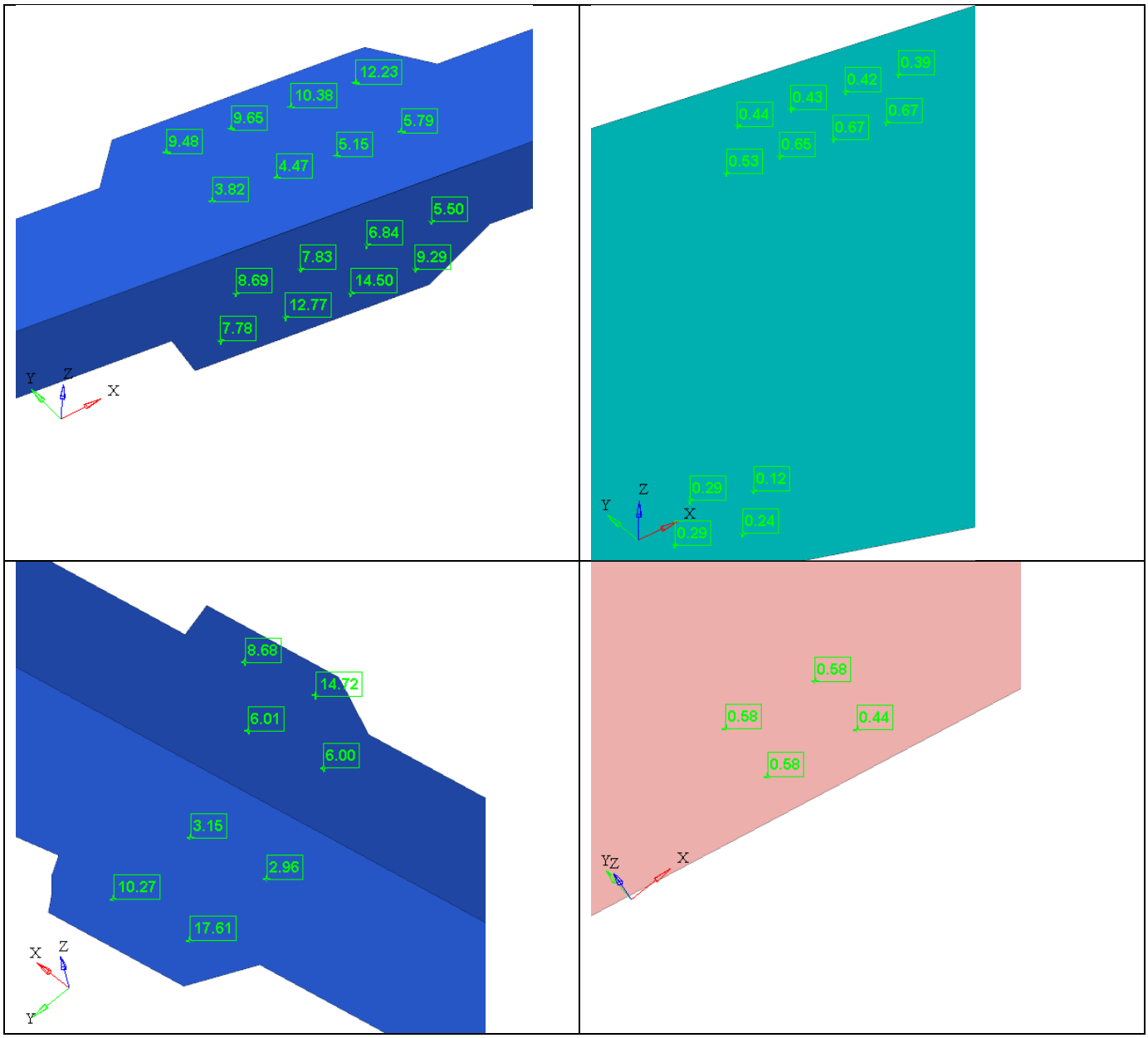
12.23
10.38
9.65
5.79
9.48
5.15
4.47
3.82
5.50
6.84
7.83
9.29
8.69
14.50
12.77
7.78
Y
Z
X
0.39
0.42
0.43
0.44
0.67
0.67
0.65
0.53
Z
Y
X
0.29
0.12
0.24
0.29
8.68
14.72
6.01
6.00
3.15
2.96
10.27
17.61
X
Z
Y
0.58
0.58
0.44
0.58
YZ
X

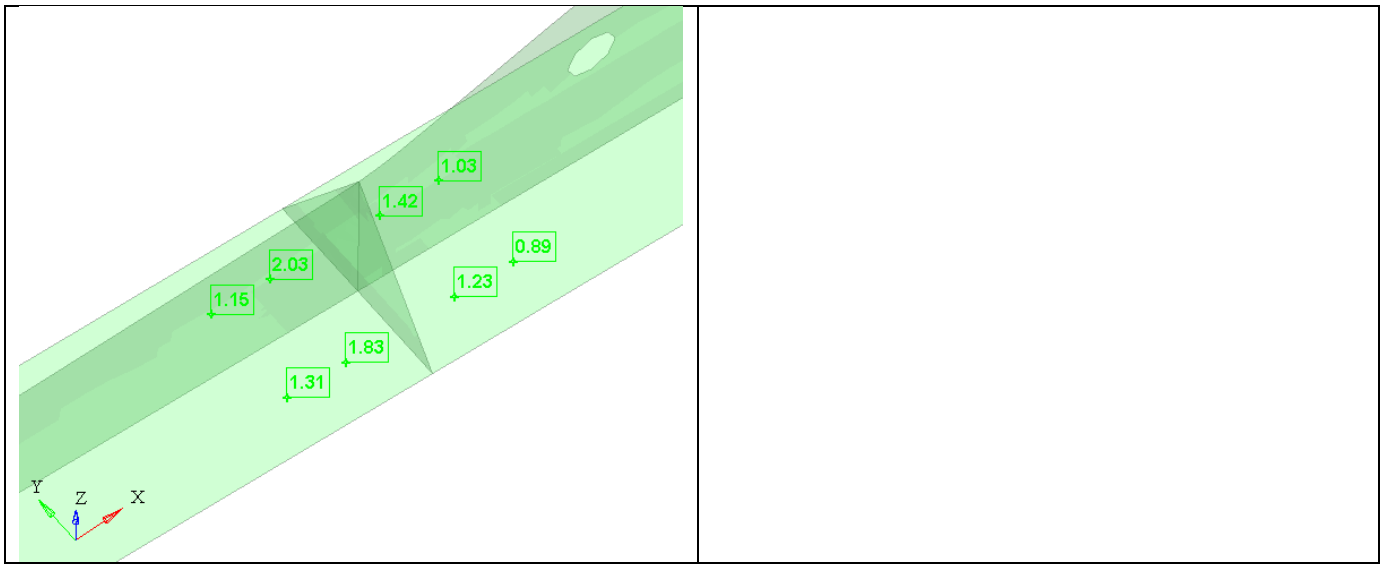

Table 74 Fastener Joint Margins at Frame5

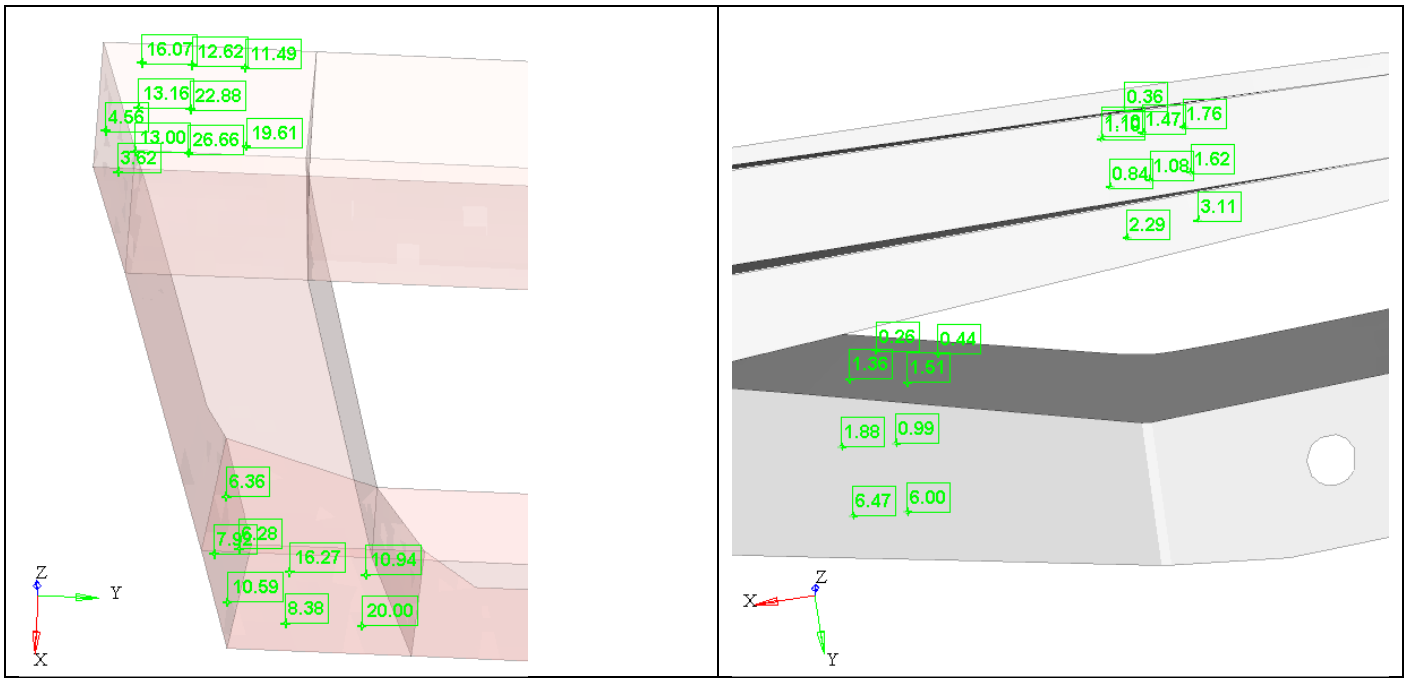

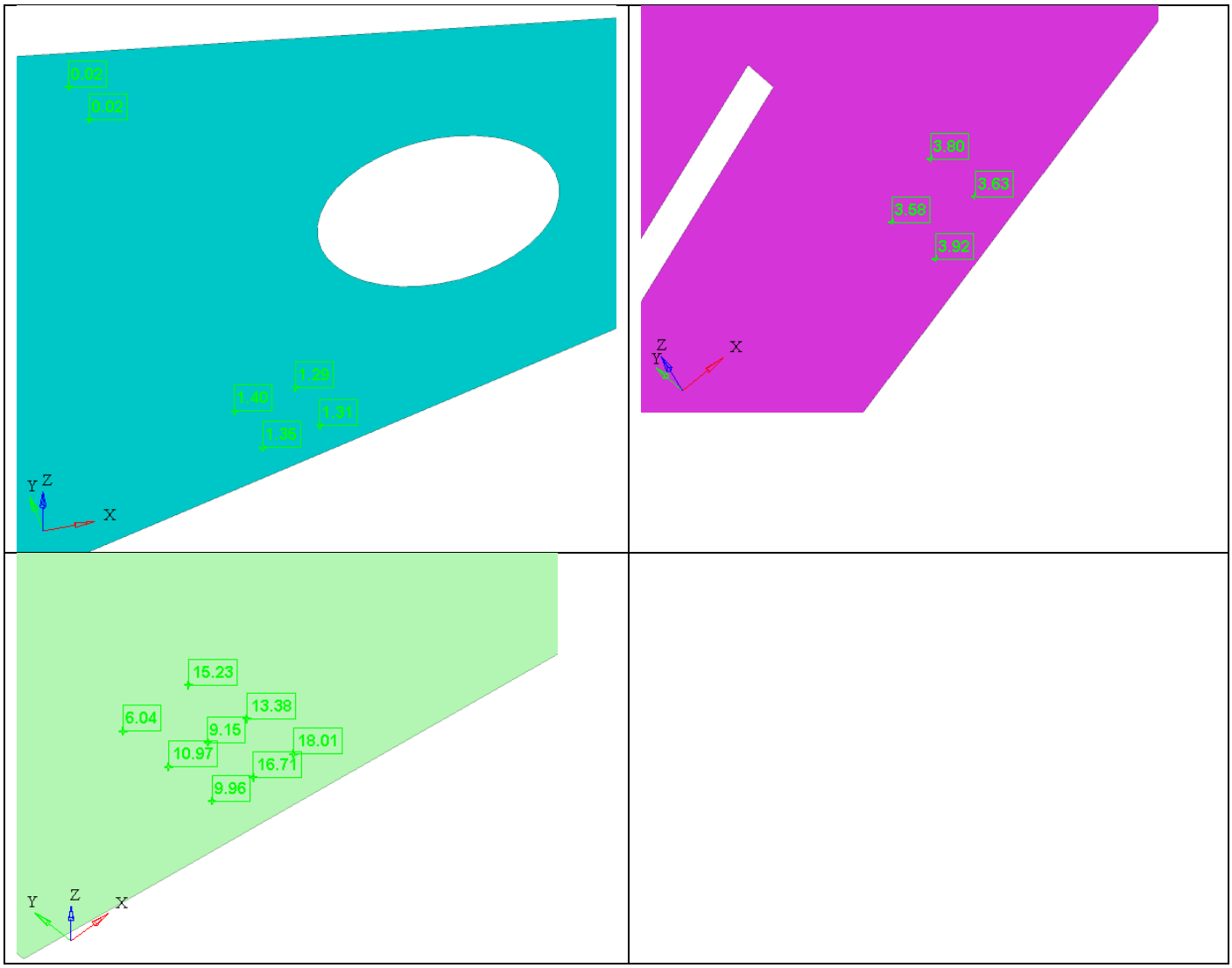
0.02
0.02
1.28
1.40
1.31
1.35
Y Z
X
3.80
3.63
3.58
3.92
Z
Y
X
15.23
13.38
6.04
9.15
18.01
10.97
16.71
9.96
Y
Z
X

Table 75 Fastener Joint Margins at Frame6

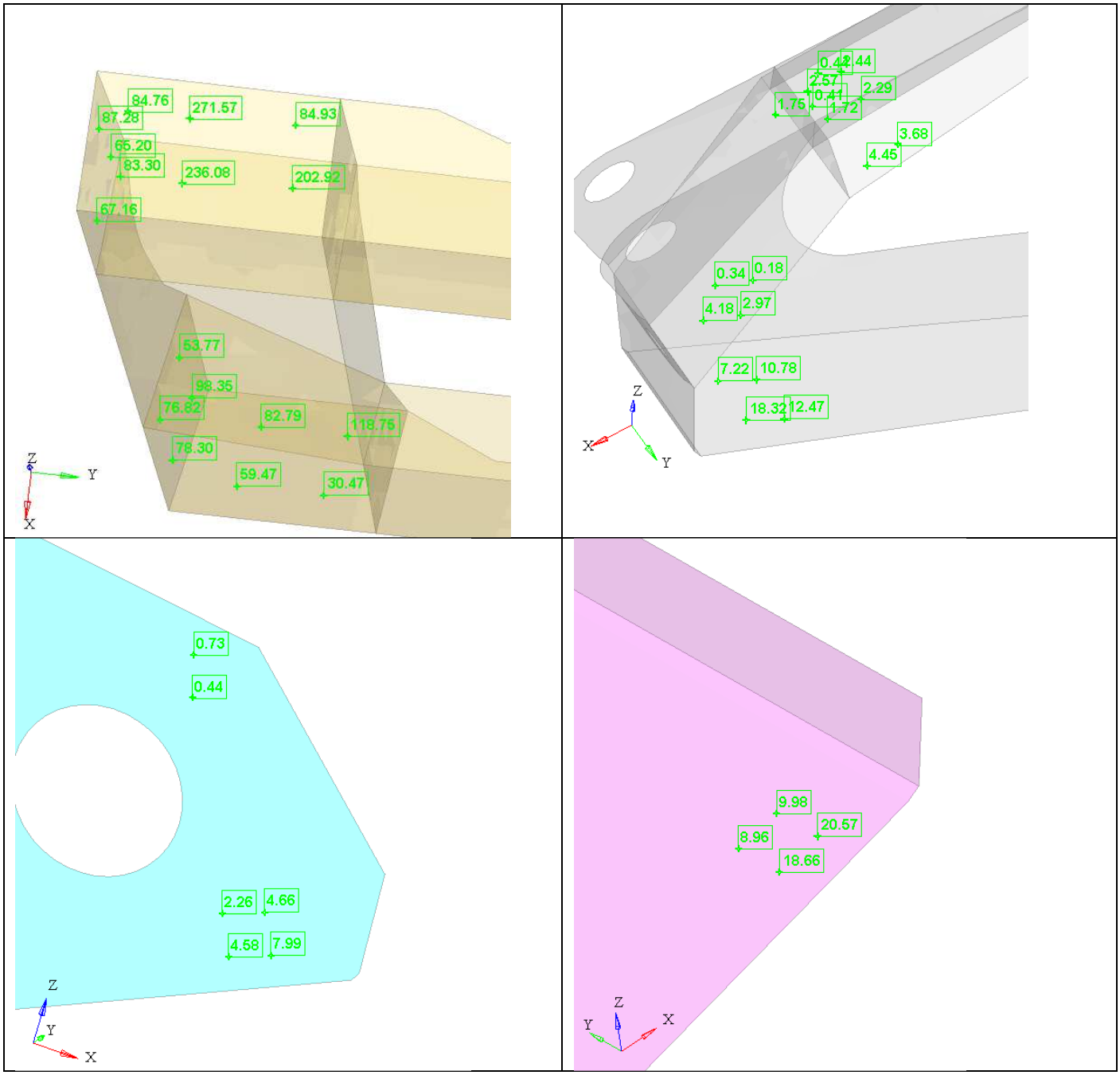

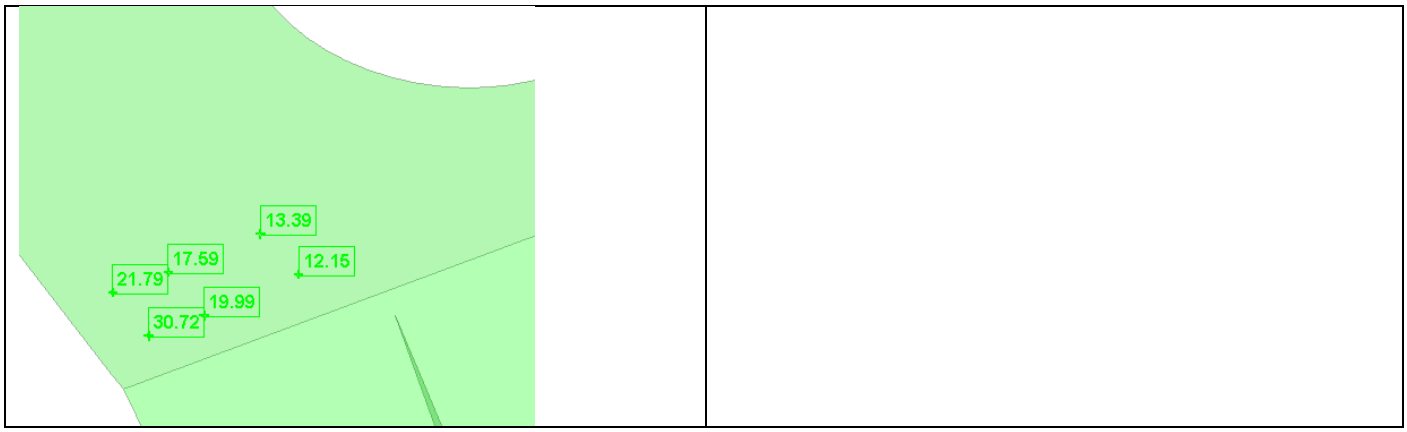

Table 76 Fastener Joint Margins at Aft Bulkhead

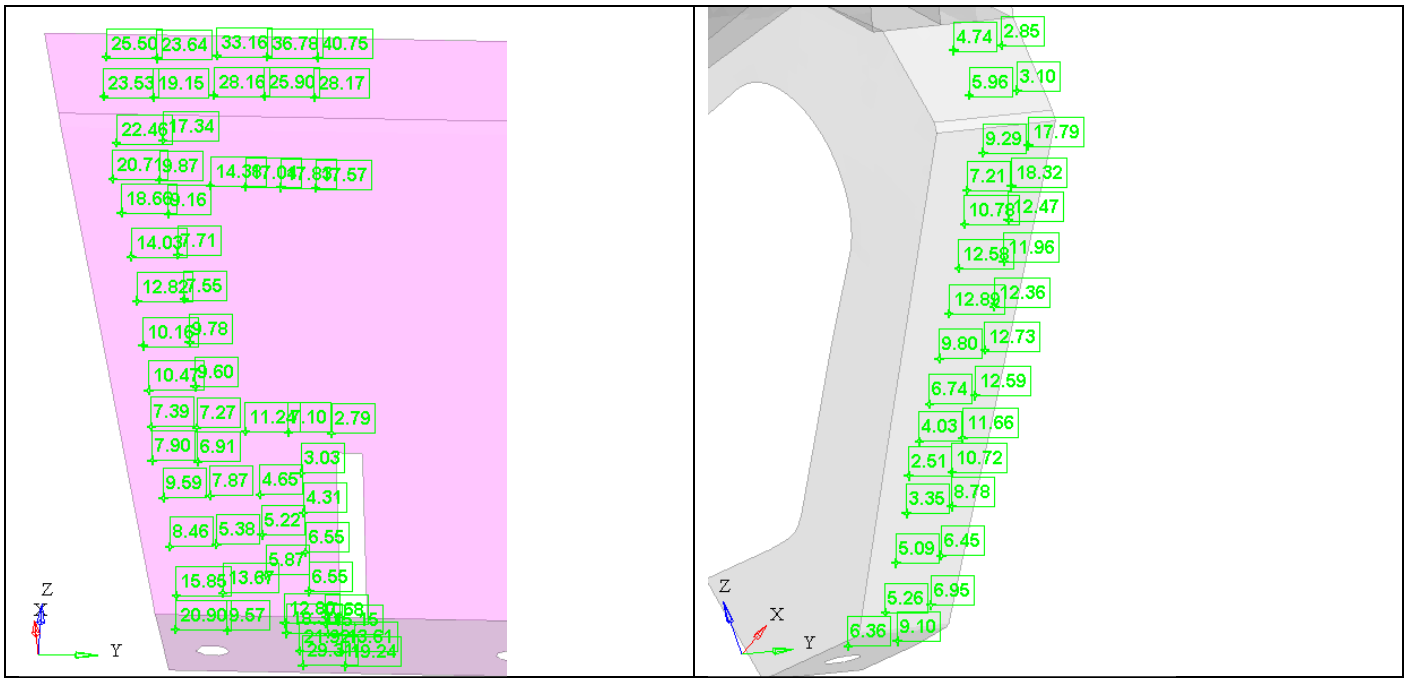

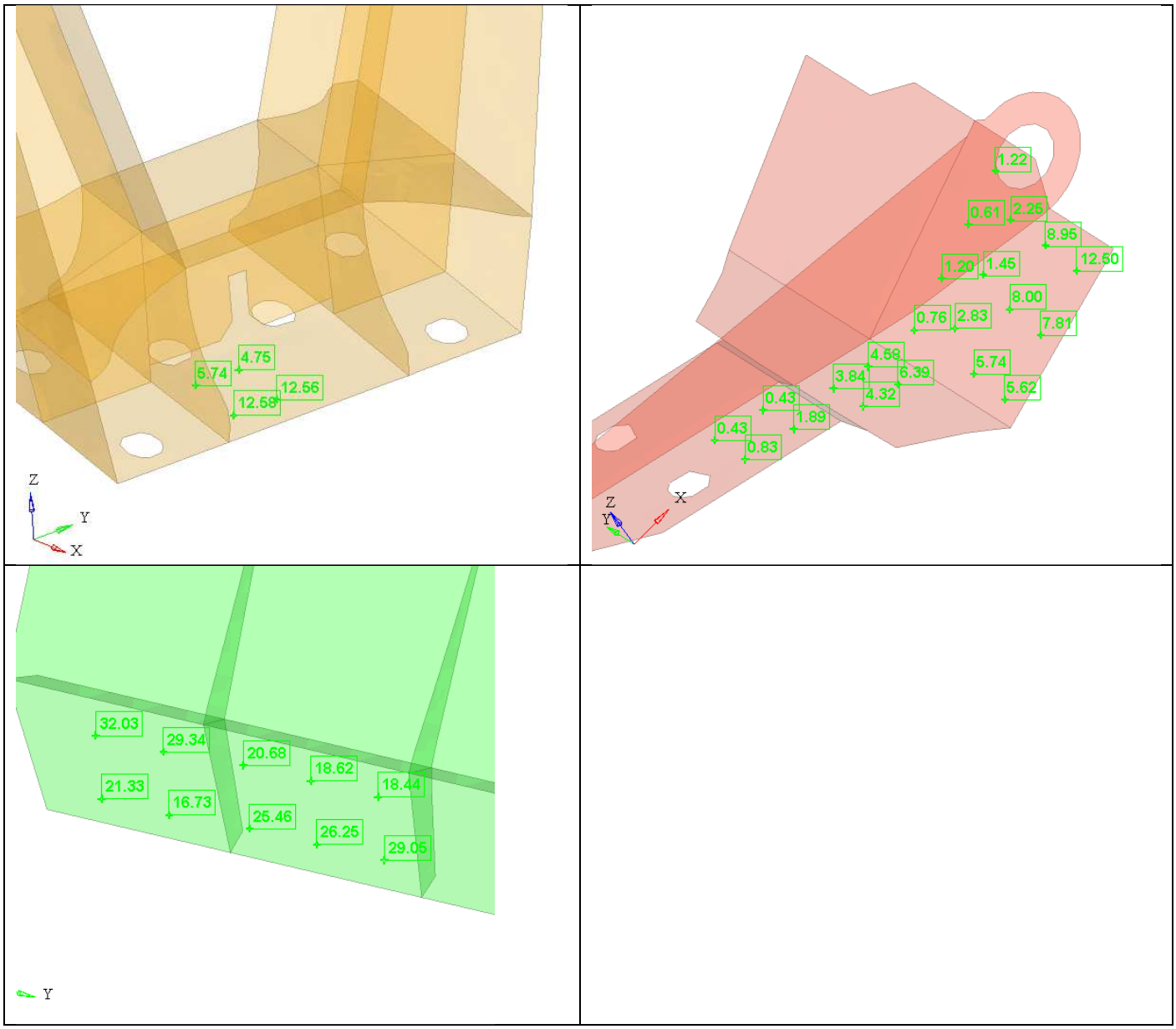
4.75
5.74
12.56
12.58
Z
Y
X
1.22
0.61
2.25
8.95
12.50
1.20
1.45
8.00
0.76
2.83
7.81
4.58
5.74
3.84
6.39
5.62
0.43
4.32
1.89
0.43
0.83
Z
Y
X
32.03
29.34
20.68
18.62
18.44
21.33
16.73
25.46
26.25
29.05
Y

Bibliography:

[A-Optistruct] Altair, “OptiStruct®” – a structural analysis and optimization code, https://altairhyperworks.com/product/OptiStruct

[ATSB2016] Australian Transport Safety Bureau, "Engine Pylon Carcking Involving Boeing 747-438, VH-OJT", Australian Transport Safety Report, AO-2016-148, 6 June 2016

[B1990] Barret, R.T., (1990). *Fastener Design Manual.* Cleveland, OH: NASA Reference Publication 1220, https://ntrs.nasa.gov/archive/nasa/casi.ntrs.nasa.gov/19900009424.pdf.

[B1973] Bruhn, E. F. (1973). *Analysis and Design of Flight Vehicle Strucures.* Indianapolis: Jacobs Publishing

[CK1986] Cazier, F., Jr., and Kehoe, M., Flight test of a decoupler pylon for wing/store flutter suppression”, AIAA Paper 1986-9730, 1986, 10.2514/6.1986-9730

[CMGR2018] Coniglio, S., Morlier, J., Gogu, C., and Remi, A., "Original Pylon Architecture Design Using 3D HPC Topology Optimization", AIAA Paper 2018-1388, doi: 10.2514/6.2018-1388

[DoD1998] Departmet of Defense. (1 DECEMBER 1998). *MIL-HDBK-5H*

[DS1982] Downing, S.D., Socie, D.F. (1982), “Simple Rainflow Counting Algorithms”, International Journal of Fatigue, Volume 4, Issue 1, January, 31-40.

[E2007] Estefan, J. A., “Survey of Model-Based Systems Engineering (MBSE)”, 2007, Incose MBSE Focus Group 25, http://www.omgsysml.org/MBSE_Methodology_Survey_RevB.pdf

[FXJ2017] Fang, Y-T., Xue, C.J., and Jiang, B.X., “Development of a Load Sensor for Aircraft Pylon Interface Load Measurement”, Journal of Aircraft, 2017, Vol.54: 336-345, 10.2514/1.C033003

[FSFAP,1995] Flight Safety Foundation, Accident Prevention, "Fractured Fuse Pin in Engine Pylon Results in Dragged Engine During B-747's Landing Roll-Out", Vol. 52, No. 3, March 1995, https://flightsafety.org/ap/ap_mar95.pdf

[FMS2012] Friedennthal, S., Moore, A., and Steiner, R., “Model-Based Systems Engineering”, in “A Practical Guide to SysML, The Systems Modeling Language”, Elsevier, 2012, ISBN 978-0-12-385206-9, doi: 10.1016/B978-0-12-385206-9.00002-8

[GM2004, Gantois, K., and Morris, A.J., "The multi-disciplinary design of a large-scale civil aircraft wing taking account of manufacturing costs", Structural and Multidisciplinary Optimization, 2004, , 28, pp. 31-46, DOI 10.1007/s00158-004-0427-7

[GMRG2019] Gilioli, A., Manes, A., Ringertz, U., and Giglio, M., “Investigation About the Structural Nonlinearities of an Aircraft Pylon”, Journal of Aircraft, 2019, Vol.56: 273-283, 10.2514/1.C034882

[GKB2009] Grihon, S., Krog, L., Bassir, D., “Numerical optimization applied to structure sizing at AIRBUS: A multi-step process”, International Journal on Simulation and Multidisciplinary Design Optimization, 2009, 3, pp. 432–442, doi: 10.1051/ijsmdo/2009020

[HG2002] Haftka, R.T., and Gurdal, Z., “Elements of Structural Optimization”, Third Edition, Kluwer Academic Publishers, 1992,, Chapter 10: Decomposition and Multilevel Optimization, ISBN 0-7923-1504-9

[HHH2008] Hansen, L.U., Heinze, W. and Horst, P., “Blended wing body structures in multidisciplinary pre-design”, Structural and Multidisciplinary Optimization, 2008, , Volume 36, Issue 1, pp 93–106, 10.1007/s00158-007-0161-z

[H2006] Haskins, C. (2006). INCOSE Systems Engineering Handbook: A Guide for System Life Cycle Processes and Activities. *International Council on Systems Engineering v.3*.

[ISC2003] Iuspa, L., Scaramuzzino, F., and Petrenga, P., “Optimal Design of an aircraft engine mount via bit-masking oriented genetic algorithms”, Advances in Engineering Software, 2003, Vol. 34, Issues 11-12, pp. 707-720, doi: 10.1016/S0965-9978(03)00100-5

[K2008] Kaufmann, M., "Cost/Weight Optimization of Aircraft Structures", Thesis, Stockholm, Sweden 2008, KTH School of Engineering Sciences, ISBN 978-91-7178-888-7, https://www.diva-portal.org/smash/get/diva2:13224/FULLTEXT01.pdf

[KZW2010] Kaufmann, M., Zenkert, D., and Wennhage, P., "Integrated cost/weight optimization of aircraft structures", Structural and Multidisciplinary Optimization, 2010, 41, pp. 325–334, DOI 10.1007/s00158-009-0413-1

[LSF1990] Livne, E., Schmit, L.A., and Friedmann, P.P., "Towards an Integrated Approach to the Optimum Design of Actively Controlled Composite Wings," Journal of Aircraft special issue on Multidisciplinary Optimization of Aeronautical Systems, Vol. 27, No. 12, December 1990, pp. 979-992.

[L1999] Livne, E., “Integrated Aeroservoelastic Optimization: Status and Progress”, Journal of Aircraft, Vol. 36, No. 1, January-February 1999, pp. 122-145.

[MO2011] Morten G. Ostergaard, A. R. (2011). Virtual testing of aircraft structures. *CEAS Aeronaut Journal*, 83–103.

[N1988] Niu, M. C.-Y. (1988). *Airframe Structural Design.* Los Angeles: Technical Book Company.

[RBFG2011] Remouchamps, A., Bruyneel, M., Fleury, C., and Grihon, S., “Application of a bi-level scheme including topology optimization to the design of an aircraft pylon”, Strucural and Multidisciplinary Optimization, 2011, Vol. 44, pp., 739–750, doi: 10.1007/s00158-011-0682-3

[WO1997] Wanhill, R.J.H., and Oldersma, A., "Fatigue and Fracture in an Aircraft Engine Pylon", NLR TP 96719, National Aerospace Laboratory, The Netherlands, 1997, https://core.ac.uk/download/pdf/80112240.pdf

[XXXT2012] Xue, C.-J., Xu, F.-J., Xu, Y., and Tan, W., “Structural Topology Optimization of a Pylon’s Mount Using Ant Colony Algorithms”, Journal of Aircraft, 2012, Vol. 49, pp. 724-734, 10.2514/1.C031612